Radiofluorination Methodology for Automated Chemistry

Christopher David Reed

Submitted in fulfilment of the requirements for the degree of Doctor of Philosophy

School of Chemistry – Newcastle University

June 2015

Dedication

In loving memory of Anthony William Reed.

Beloved Father, Husband and Grandfather.

May 22nd 1948 – September 12th 2013.

Declaration

The work described in this thesis was carried out in the School of Chemistry at Newcastle University during the period between October 2009 and July 2014 and is original except where acknowledged by reference.

No part of this work is being, or has been submitted for a degree, diploma or any other qualification at any other institution.

Acknowledgements

Firstly, I would like to thank Cancer Research UK and the EPSRC for funding this research and Newcastle University for providing me with the opportunity to perform it.

I would like to thank my supervisor, Dr Michael A. Carroll for his assistance, guidance and encouragement throughout the course of this work. I would also like to acknowledge his kindness, support and understanding of my situation during the final year of my studies. I would also like to thank my colleagues within the research group for their friendship and support.

I would like to thank Dr M. Probert and Dr R. Harrington for their assistance with crystallographic matters, Prof. W. McFarlane and Dr C. Wills for assistance with NMR spectroscopy, the EPRSC Mass Spectrometry Service, Swansea and Dr S. Boyer for elemental analysis.

I would also like to thank Prof. M. Green for his support and guidance throughout my time in the department, and the school office and workshop staff for their help and assistance.

Finally, I would like to thank my family, friends and fiancée for their kindness, patience and understanding, throughout my time at the university.

Abstract

Microfluidic technology has recently emerged as an invaluable tool in the development of PET radiochemical methods allowing the quantities of precursors/reagents/solvents to be significantly reduced thus facilitating timely isolation of the final radiolabelled product. [1-5] The Advion NanoTek microfluidic system has been used to optimise model reactions designed to evaluate the status of the system and validate investigations. It was noted that the use of conventional phase-transfer agent (Kryptofix® 222/K_2CO_3) causes blockages to the micro-channels wherein the radiochemical reactions take place. We have demonstrated that tetraethylammonium bicarbonate is a viable alternative to the traditional phase-transfer agent, for the radiosynthesis of [^{18}F]fluoroarenes, using a microreactor, via a key range of radiosynthetic strategies (Figure 1). Of particular benefit, in a microreactor, was the performance of tetraethylammonium bicarbonate where the occurrence of blocked reactors experienced with the conventional phase-transfer agent was eliminated thus dramatically increasing productivity.[6]

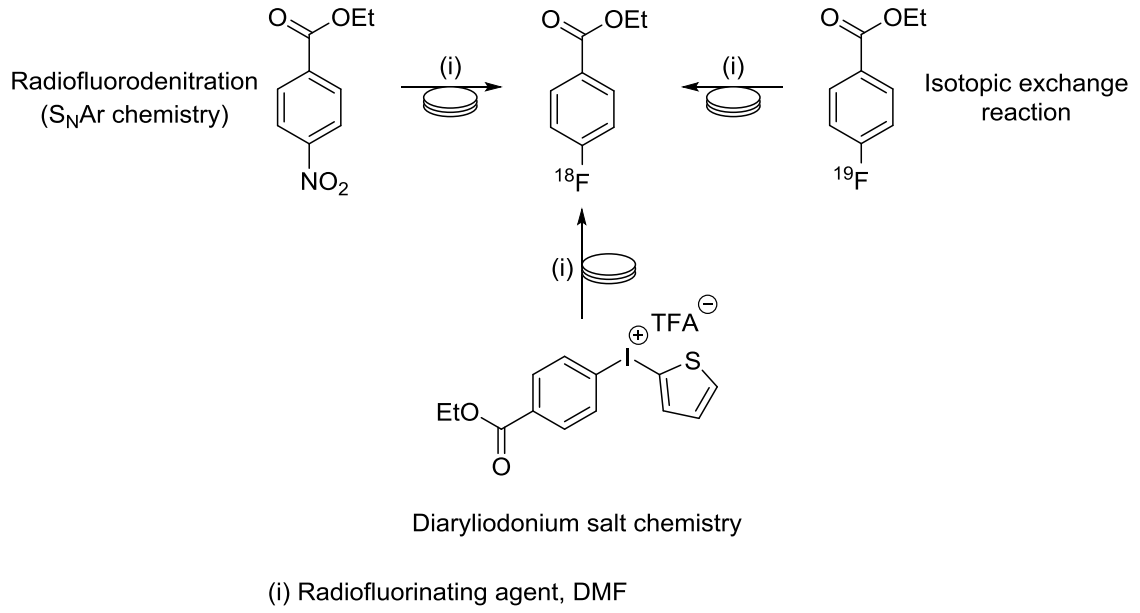

Figure 1: Key methods use to evaluate tetraethylammonium bicarbonate as a phase-transfer agent in the radiosynthesis of ethyl 4-[^{18}F]fluorobenzoate.

Various diaryliodonium salts have been synthesised via conventional methods and reacted with tetraethylammonium [^{18}F]fluoride, to generate ethyl 4- and 3-[^{18}F]fluorobenzoate with the synthesis of the 4-position regioisomer, generally, producing higher radiochemical yields. Excellent radiochemical yields and selectivity

were achieved for both isomers when using precursors bearing a 4-anisyl ring. The selectivity of the nucleophilic attack of [^{18}F]fluoride on a diaryliodonium salt has been clearly demonstrated using electron-neutral and electron-rich derivatives.

In addition, the Eckert & Ziegler Modular-Lab was used to generate a simple [^{18}F]fluoroarene from a diaryliodonium salt using tetraethylammonium [^{18}F]fluoride as the radiofluorinating agent. Radiochemical yields were low but comparable to those achieved when using the conventional phase-transfer agent, thus, proving that this new reagent may be used as a radiofluorinating agent in automated batch radiofluorinations.

References

1. H. J. Wester, M. Schottelius, P. A. Schubiger, L. Lehmann and M. Friebe, *PET Chemistry: The Driving Force in Molecular Imaging*, 2007. pp 271-287
2. G. Pascali, G. Mazzone, G. Saccomanni, C. Manera and P. A. Salvadori, *Nucl. Med. Biol.*, 2010, **37**, 547-555.
3. R. Bejot, A. M. Elizarov, E. Ball, J. Zhang, R. Miraghaie, H. C. Kolb and V. Gouverneur, *J. Labell. Compd. Radiopharm.*, 2011, **54**, 117-122.
4. P. W. Miller, *Journal of Chemical Technology & Biotechnology*, 2009, **84**, 309-315.
5. H. Audrain, *Angew. Chem. Int. Ed.*, 2007, **46**, 1772-1775.
6. C. D. Reed, G. G. Launay and M. A. Carroll, *J. Fluorine Chem.*, 2012, **143**, 231-237.

Abbreviations

18-crown-6	1,4,7,10,13,16-Hexaoxacyclooctadecane
Ar	Aryl
BM	Base module
Bz	Benzoyl
CA	Carrier-added
$CDCl_3$	Deuterated chloroform
CM	Concentrator module
d_6-DMSO	Deuterated dimethylsulfoxide
d_7-DMF	Deuterated *N,N*-dimethylformamide
DBU	1,8-Diazabicyclo[5.4.0]undec-7-ene
DC	Decay-corrected
DCM	Dichloromethane
DIB	Diacetoxyiodobenzene
Dioxane	1,4-Dioxane
DMF	*N,N*-dimethylformamide
DMP	Dess-Martin periodinane
DMSO	Dimethylsulfoxide
EAS	Electrophilic aromatic substitution
EI	Electron impact ionisation
h	Hours
HFIP	1,1,1,3,3,3-Hexafluoroisopropanol
IBX	2-iodoxybenzoic acid
IR	Infra-red
ISB	Iodosylbenzene
K222	4,7,13,16,21,24-Hexaoxa-1,10-diazabicyclo[8.8.8]hexacosane
L	Ligand(generic)
*m*CPBA	*m*-Chloroperbenzioc acid
MeCN	Acetonitrile
mp	Melting point
MS	Mass spectrometry
NCA	Non-carrier added

NDC	Non-decay corrected
NMR	Nuclear Magnetic Resonance
NTR	Non-target ring
Nu	Nucleophile
OAc	Acetate
OTf	Trifluoromethyl sulfonate (triflate)
OTs	*para*-tolylsulfonate (tosylate)
PTA	Phase-transfer agent
PTS	Phase-transfer system
QMA	Quaternary ammonium (resin)
RCIY	Radiochemical incorporation yield
RCP	Radiochemical purity
RCY	Radiochemical yield
RFA	Radiofluorinating agent
RM	Reactor module
RT	Room temperature
TBAF	Tetrabutylammonium fluoride
TFA	Trifluoroacetate
TFAH	Trifluoroacetic acid
TFE	2,2,2-Trifluoroethanol

Contents

1.1.1 List of Figures/Schemes/Tables/Images/Equations

1 Introduction

It is of great value to the drug discovery industry to be able to image and observe molecular events *in vivo* and in real-time in order to create detailed images of fundamental biochemical and physiological processes within living organisms. Such imagery is essential to the development of new approaches to the assessment of disease and the design of possible drug candidates. There is, therefore, a continuous need to create and develop imaging techniques to further improve selectivity, sensitivity, and tissue specificity.

1.1 Positron-emission tomography with fluorine-18

Imaging techniques such as Magnetic Resonance Imaging (MRI), X-rays and ultrasound typically provide sound structural detail but little or no information on events at a metabolic or molecular level. These imaging techniques therefore rely on structural abnormalities associated with a disease to provide a credible diagnosis. However, other techniques such as Positron-Emission Tomography (PET) and Single-Photon Emission Computed Tomography (SPECT) are able to image biological context in real-time and in living patients. These techniques use radioactive labels designed to be tissue or receptor specific to produce detailed pictures of the intended target.

1.1.1 Positron-emission tomography

Positron-Emission Tomography (PET) is a powerful, non-invasive molecular imaging technique used to gain valuable information on specific biological and pharmacological processes taking place in the human body. Positron-emitting radioisotopes (e.g. ^{15}O, ^{13}N, ^{11}C, ^{18}F) are incorporated into a biologically active molecule, allowing for the non-invasive imaging and quantification of pharmacological and biological processes whilst minimising the disruption to their pharmacodynamic properties. PET experiments can,

therefore, provide crucial information regarding the metabolism, biochemical mechanism, and receptor/enzyme interaction of potential drug candidates to the drug discovery and development industry. [1, 2]

PET is employed in both research and medicine, and currently being used extensively in clinical oncology, neurology and cardiology. Over 90% of PET scans performed today are used to gain oncological information. PET scans can be useful in diagnosis, staging and monitoring response to treatment of cancers such as Hodgkin's lymphoma, non-Hodgkin lymphoma and lung cancer. Other types of solid tumours have displayed strong uptake of established imaging agents, on a case-by case basis, which is especially useful in identifying secondary tumours or the reoccurrence of a highly active primary tumour which has been removed through surgery.

PET is used in neurology on the basis that areas of high radioactivity are associated with elevated levels of brain activity, which is correlated to cerebral blood flow. Oxygen-15 labelled water, can be used to achieve this but must be administered directly from a medical cyclotron, due to the 2-minute half-life of the isotope. Other mechanisms have been exploited to greater understand a variety of neurological disorders in neuropsychology, psychiatry, sterotatic surgery, and seizure focus, wherein there is greater uptake of imaging agents. Alzheimer's disease however, can be differentiated from other dementing processes as this disorder greatly decreases brain metabolism of both glucose and oxygen in tandem. The use therefore of an oxygen labelled imaging agent, alongside radiolabelled glucose can be used to make early diagnoses of this Alzheimer's disease.

PET has also developed as a clinical imaging technique for the quantitative assessment of myocardial perfusions and advanced coronary artery disease in cardiology. This is mainly thanks to the rapid growth of PET as an imaging modality in oncology, increasing the availability of PET instrumentation to imaging departments. Tracers labelled with Rubidium-82 can be used to measure blood circulation in the arteries of the heart, whilst radiolabelled glucose can be used to differentiate healthy cardiac tissue from damaged tissue, such as that generated by a heart attack.

Radiolabelled glucose has also been used to identify infection-associated inflammatory response to infectious diseases and has been shown to be a feasible technique for studying skeletal muscles during exercise, in musculo-skeletal studies.[3]

1.1.2 Positron emission

Positron Emission is a form of radioactive decay in which a positron and a neutrino are ejected from an unstable, proton-rich nucleus to produce a neutron. The positron emitted travels only a very short distance before colliding with an electron. Upon collision, the positron and the electron are annihilated to produce two γ-rays, each 511 keV in energy, which then travel at 180° to each other. In PET imaging studies, these γ-rays are detected by a 360° camera which uses a computer to construct a 3D image based on the sites of annihilation. Interference from background γ-radiation is negated as only pairs of γ-rays detected at 180° apart and of the corresponding energy are used to form the image. This mode of radioactive decay forms the basis for PET imaging (Image 2).

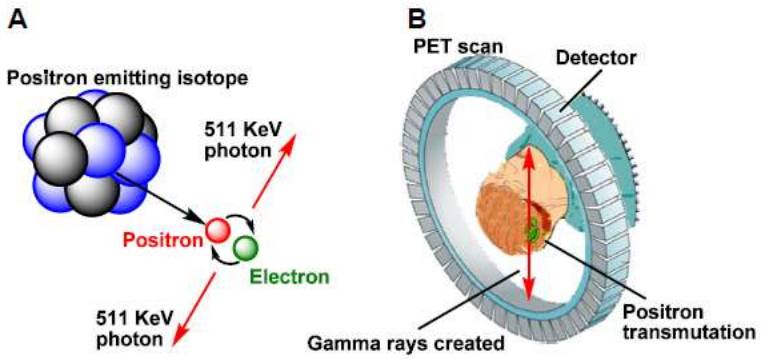

Image 2: (a) Positron and an electron annihilate producing two 511 keV photons travelling in opposite directions, (b) the coincidental photons are detected by the circular gamma ray detectors array of the PET camera. Taken from [4].

As well as positron emission, the same radioisotopes can also decay concurrently via electron capture (EC). This mode of decay occurs when an unstable, proton-rich nucleus captures an electron which then combines with a proton to produce a neutron. This also results in the release of γ-rays, however these γ-rays are not emitted at 180° to one another and can therefore be ignored in the imaging process. Fortunately, most of the commonly used positron-emitting radioisotopes decay predominantly via positron emission.

1.1.3 Radioisotopes in PET imaging

Positron emitting isotopes can be generated by particle accelerators called cyclotrons. These machines focus a beam of either protons or deuterons, of a required energy range, onto a target system specifically chosen to produce a particular radioisotope following a nuclear reaction (Table 1). There are many positron-emitting radioisotopes available to the radiochemist, some of which are low mass atoms found naturally in biomolecules. The use of these elements is favourable as exchanging for the radioisotope derivative imparts no effect on the biological activity of the molecule of interest.

Isotope	Half-life $t_{1/2}$ (min)	Positron Energy (MeV)	Mean Positron Range in water (mm)[5]	Nuclear Reaction	Target	Product	Decay Product	Decay mode PET:EC
^{11}C	20.4	0.96	1.03	$^{14}N(p, \alpha)^{11}C$	$N_2(+O_2)$ $N_2(+H_2)$	$[^{11}C]CO_2$ $[^{11}C]CH_4$	^{11}B	100
^{13}N	9.97	1.19	1.32	$^{16}O(p, \alpha)^{13}N$	H_2O H_2O+ EtOH	$[^{13}N]NO_x$ $[^{13}N]NH_3$	^{13}C	100
^{15}O	2.04	1.7	2.01	$^{15}N(d, n)^{15}O$	$N_2(+O_2)$	$[^{15}O]O_2$	^{15}N	100
^{18}F	109.7	0.64	0.64	$^{18}O(p, n)^{18}F$ $^{20}Ne(d, \alpha)^{18}F$	$[^{18}O]H_2O$ $Ne(+F_2)$	$^{18}F^-$ $[^{18}F]F_2$	^{18}O	97:3
^{68}Ga	67.7	1.90	2.24	$^{66}Zn(\alpha, 2n)^{68}Ge$ $^{68}Ge \rightarrow {}^{68}Ga$	^{66}Zn	^{68}Ge	^{68}Zn	89:11

Table 1: The most commonly used radionuclides in PET, showing their half-lives, the nuclear reactions for their production, target products, decay products and decay modes (N.B. EC = Electron Capture)

Unfortunately, many of these radioisotopes have half-lives short enough to present a synthetic challenge to the radiochemist. Ideally, the imaging agent should be synthesised, purified, analysed and formulated within three half-lives to ensure that sufficient radioactivity is administered to a subject undergoing a PET scan. This had necessitated the preparation of imaging agents in close proximity to the PET scanning facilities permitting the rapid transportation of an imaging agent to the scanning site. Modern radiochemistry facilities integrate radiochemistry laboratories, radioactivity generators, cyclotrons and PET scanning facilities in one convenient location. This has led to the development of compact or 'mini' cyclotrons able to generate the key radioisotopes such as carbon-11 and fluorine-18. These machines are considerably smaller than conventional cyclotrons and have only been made possible by advances in technology, target design, and software control. Additionally, "on-line" synthesis of imaging agents, wherein the radiotracer is synthesised on specially designed modules attached to the cyclotron, is also becoming more common.

When designing an imaging agent, the timescale of the biological process to be studied should be commensurate with the half-life of the isotope selected. A process with a

relatively long half-life, such as amino acid utilization (*e.g. S*-adenosyl methionine has a half-life of 100 min) would require an imaging agent bearing the fluorine-18 (109.7 min) or carbon-11 (20.4 min) radioisotope. A faster process, such as cerebral blood flow, may use a radionuclide with a much shorter half-life, such as oxygen-15 (2.04 min).

1.1.4 Fluorine in pharmaceuticals

Drug candidates containing one or more fluorine atoms are common throughout all fields of drug development (Figure 3). It has been estimated that up to 20% of pharmaceuticals prescribed or administered as part of a treatment strategy contain a fluorine atom.[6] The use of fluorine may induce a variety of useful properties into drug molecules, such as enhanced metabolic stability, selective reactivity, enhanced binding interactions, and changes to physical properties.

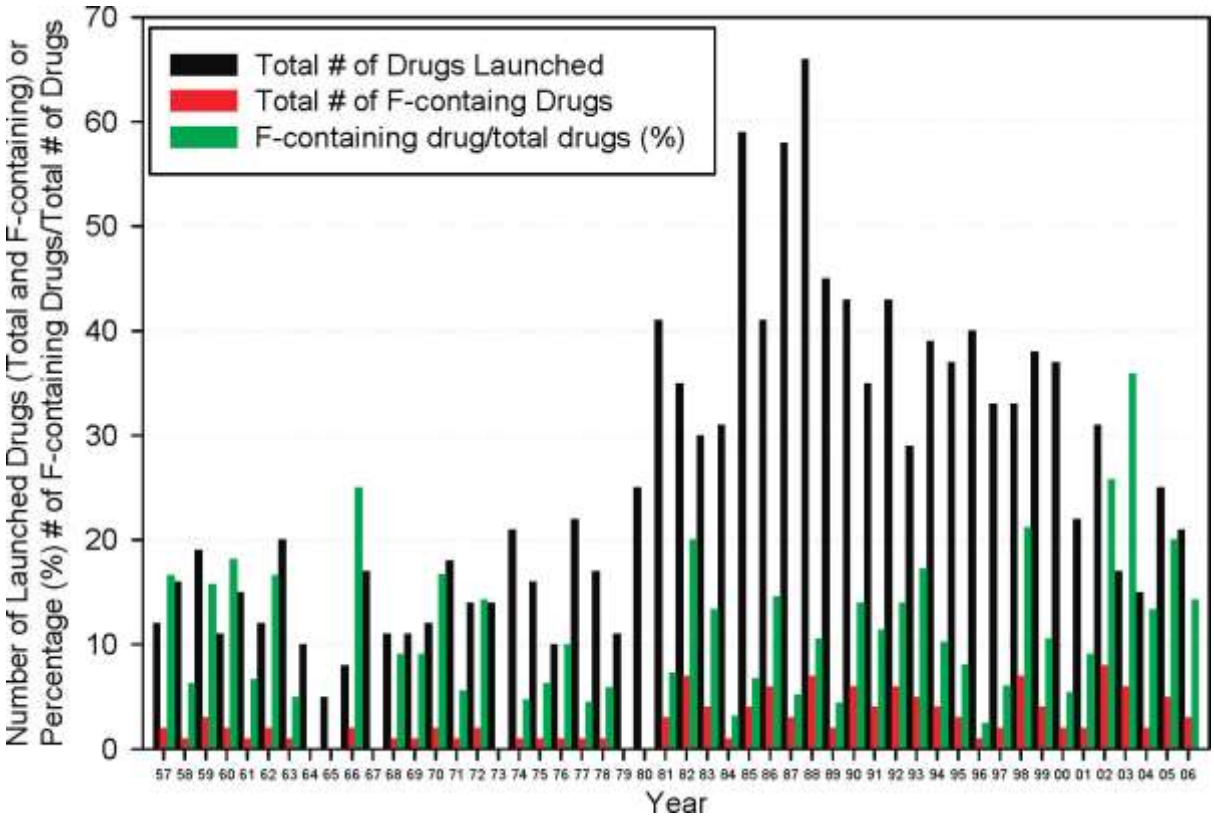

Figure 3: Graph to show drugs launched containing fluorine (1957-2006). Taken from [7].

Fluorine is small in size and the most electronegative element resulting in different reactivity between fluorinated compounds and the hydrocarbon counterpart have dominated design considerations. Fluorine also has a van der Waals radius and electronegativity similar to that of oxygen. These characteristics have allowed fluorine to be used as a substitute for either hydrogen or oxygen in numerous examples of drug design.

Element (X)	Van der Waals radius (Å)	Electronegativity (Pauling Scale)	Bond Length of C-X [Å]
Hydrogen	1.20	2.20	1.09
Oxygen	1.52	3.44	1.43
Fluorine	1.47	3.98	1.35

Table 2: Van der Waals radius, electronegativity and bond lengths to carbon of various atoms.

Trifluoromethyl groups have also been used as alternative to a range of other species including phenyl, *tert*-butyl, isopropyl and methyl groups. Despite their isosteric mimicry, fluoro and trifluoromethyl groups will undoubtedly have a profound effect on the physical and/or biological properties of a molecule. The strong electron-withdrawing nature of fluorine also has a profound affect on the acidity of neighbouring functional groups. Amines become less basic with both β- and γ- fluorine substitution. These inductive effects may even alter pK_a values with δ-substitution. This affect may even be cumulative with successive substitutions lowering pK_a. Pyridines, quinolines and anilines also experience a fall in basicity with the introduction of a fluorine substituent but these affects are attenuated by the aromatic nature of these compounds. Carboxylic acids, alcohols, heterocycles and phenols also become more acidic with fluorine substitution in adjacent positions.

Changes to pK_a values are an important consideration to lead optimisation studies as physiochemical properties (solubility, log *D*), binding affinities and absorption,

distribution, metabolism and excretion (ADME) become altered. Drugs associated with effective central nervous system (CNS) activity benefit from enhanced membrane penetration resulting from fewer positive charges, no negative charges and greater lipophilicity (cLogP, cLogD).

Aside from the inductive effects fluorine induces on neighbouring functionalities, fluorine substitution plays an important role in direct binding interactions. Lipitor (Atorvastatin) **1**, the biggest selling pharmaceutical worldwide, is a type 2 statin used to lower cholesterol (Figure 4).

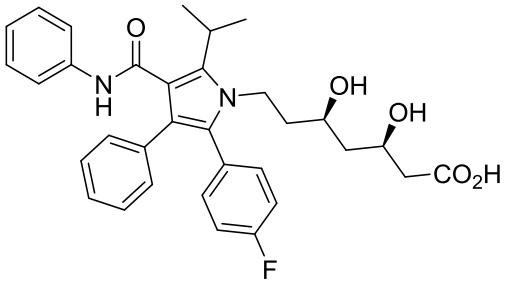

1

Figure 4: Lipitor (Avorvastatin)

The drug is prescribed to patients in order to reduce the amount of biosynthetic cholesterol produced by the patient, as well as to offset plaque accumulation and vascular constriction associated with increased blood pressure. The drug is a potent inhibitor of the enzyme 3-hydroxy-3-methylglutaryl-CoA reductase (HNG-CoA reductase) which is the rate-limiting enzyme of cholesterol biosynthesis in larger mammals. Atorvastatin, as well as other type 2 statins are all characterised by containing an essential fluorophenyl group. It has been proposed that this fluorophenyl group is stacked underneath the guanidinium group of Arg^{590}, resulting in a direct polar interaction between the arginine nitrogen ε atoms and the fluorine. This

is a major example of binding interactions determining the mode of action for a successful organofluorine drug.

The fluorination of drug molecules would be expected to produce a substantial effect upon the dipolar interactions. However, the change in binding potency of a fluorinated compound against the hydrocarbon parent is often quite small. In many examples, if direct bonding interactions are taking place then a mild effect on overall binding suggests that the effects on bipolar interactions are minimal. The fluorination of alkanes will decrease lipophilicity as the compound becomes more polar. However, the addition of fluorine or trifluoromethyl groups to aryl rings or to positions adjacent to a π-system or heteroatom containing functional group, increases lipophilicity and may strongly polarise the parent molecule. Fluorination may have only modest effects on the binding affinity as weak repulsive interactions are counterbalanced against the increase in hydrophobicity. The weak interaction could be a desirable outcome as a particularly labile site of metabolic oxidation can be blocked by fluorination without any major changes to target affinity. These qualities encourage the inclusion of fluorine into drug candidates, which is of major significance to the radiochemist as the fluorine-18 isotope becomes commonly used to radiolabel such compounds for non-invasive imaging using PET.

1.1.5 Fluorine-18 in PET imaging

Fluorine-18 is now considered to be the radionuclide of choice for PET imaging. Widespread use of the most commonly used PET tracer 2-[^{18}F]fluoro-2-deoxy-D-glucose ([^{18}F]FDG) **2** (Figure 5) which images areas of enhanced metabolism thereby improving diagnosis and evaluating the effectiveness of treatments in oncology, has spurred the global interest in PET studies.[8]

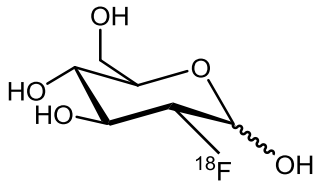

2

Figure 5: 2-[^{18}F]fluoro-2-deoxy-D-glucose **2** ([^{18}F]FDG)

The use of fluorine-18 has the following advantages:

- Fluorine-18 has a relatively long half-life (109.7 min) which allows sufficient time for multi-step synthetic labelling reactions and transportation of the radiolabelled product to the site of injection. This allows for multiple patients to be scanned from a single delivery at a PET centre.
- The positron emitted from fluorine-18 has a low positron energy (0.64 MeV). This means that the distance travelled by the positron is minimised before coming into contact with an electron. This short distance travelled from the point of emission to the site of γ-ray initiation, greatly improves the resolution of images and accuracy of detection. Compare this to oxygen-15, which has a positron energy of 1.72 MeV, allowing the positron to travel further from the site of emission and therefore increasing the uncertainty in the origin of the γ-rays.
- Fluorine-18 has a half-life relevant to the time scale of most biological processes. Other radioisotopes such as nitrogen-13 and oxygen-15 have half-lives so short that during the time taken between production and administration of the radiolabelled agent, its radioactivity has decreased to a level insufficient for accurate imaging.
- Fluorine-18 decays almost purely by positron emission (97%). This is important as decay via other means can produce unwanted side products, and requires a higher patient dose to obtain the same degree of data capture for the radiographer.
- Fluorine-18 decays to the form the harmless decay product, oxygen-18. This is vital as some positron emitting atoms decay to form products that emit harmful α or β particles. For example, copper-64 decays to forms nickel-64 and zinc-64.

- Fluorine may conveniently replace a hydrogen atom attached to carbon, however the fluorine atom is more isosteric to oxygen which has a similar bond length to carbon. The fluorine atom may therefore also substitute for a hydroxyl group and not disrupt the isoelectronics nor reduce the ability to form a hydrogen bond.[9]

Fluorine-18 also has the advantage of being to be produced in high levels of radioactivity. This has the following advantages:

- Multiple doses of an imaging agent can be administered per production run. The high levels of activity can be divided amongst several syntheses which are then, in turn, administered to patients.
- Higher levels of activity, combined with the convenient half-life also allow the imaging agents to be transported significant distances; from the location of isotope production to site of administration.
- The ratio of radioactivity to injection volumes is higher when large amounts of activity are generated. This is particularly important when injecting into small mammals for pre-clinical imaging.

1.1.6 Production of flourine-18

By far the most common reagent for electrophilic fluorination is $[^{18}F]F_2$ which can be obtained from the nuclear reactions of either $^{20}Ne(d, \alpha)^{18}F$, or $^{18}O(p, n)^{18}F$. It may be used as $[^{18}F]F_2$, which would limit the radiochemical yield (RCY) to 50%, or converted into the less reactive derivative acetyl hypofluorite ($[^{18}F]CH_3COOF$) reducing the maximum RCY even further. Due to the low specific activity (SA) of the $[^{18}F]F_2$, nucleophilic fluorine chemistry remains the dominant force in PET radiotracer production as this methodology leads to higher RCY and material yield (Figure 6).

Specific Radioactivity (SA):

Specific Radioactivity (Specific Activity) is the ratio of [^{18}F]fluoride ion radioactivity compared to its mass of carrier or total fluoride ion. SA is usually presented in GBq/µmol.

Radiochemical Yield (RCY):

The yield of a radiochemical reaction expressed as a fraction of the radioactivity originally present. If the RCY has accounted for the decay in radioactivity which has occurred during the radiosynthesis, then the term is 'decay corrected' radiochemical yield or RCY(DC). If not, then the term 'non-decay corrected' radiochemical yield or RCY(NDC) is used.

Radiochemical Purity (RCP):

The quantity of the desired radioactive compound expressed as a percentage of the total radioactive products present.

Figure 6: Key definitions used throughout radiochemistry

There are several possible ways to produce the fluorine-18 ion[10] but the most widely used method is from a cyclotron through the proton irradiation of ^{18}O-enriched water.[11] Small, compact cyclotrons are now capable of producing high activities of fluorine-18 from the nuclear reaction, ^{18}O(*p, n*)^{18}F, with typical production yields of 180mCi/µA at saturation of the target. The ABT Biomarker Generator will, generally, produce 1mCi/min during bombardment until saturation.[12] An advantage to this method is that the fluorine-18 is obtained as "non-carrier-added" (NCA). This means that the stable isotope is not required in order to obtain the radioisotope in a reactive form which is, therefore produced with a high SA ('carrier-added' or CA, denotes that a stable isotope has been added to aid the isolation of the target isotope). This is a vital characteristic of successful imaging agents as a low SA would mean that the target

would be saturated with non-radioactive fluorine ligands and so reduce any localised signal from the bound radioligand. Radioligands with high SA also allow for small mass doses to be injected into humans thereby reducing the chemical dose and the potential toxicity.

The [^{18}F]fluoride ion is obtained in [^{18}O]-H_2O making the ion unreactive due to its high degree of hydration. Most of the water must be removed in order to generate the reactive nucleophilic fluorine-18 ion. Usually, this ion is then solubilised in an organic solvent for impending reactions to take place. This is conventionally achieved by adsorption of [^{18}F]fluoride ion onto an ion exchange resin to allow for the recovery of the bulk of the [^{18}O]-H_2O.[13] This is followed by the elution of the [^{18}F]fluoride ion from the resin using a phase-transfer agent (PTA) such as Kryptofix®222/K_2CO_3 and dissolved in a small volume of solvent (*e.g.* 95:5 MeCN/H_2O). The water is then removed from this solution by repeated cycles of azeotropic evaporation with MeCN. The addition of a cryptand to the basic solution allows the potassium ion to become solubilised in a polar aprotic solvent, allowing for separation of the [^{18}F]fluoride ion which therefore increases in reactivity. After the drying step has removed the [^{18}O]H_2O, the [^{18}F]fluoride/PTA complex is then resolubilised in the reaction solvent. The vessel material is of important consideration as some of the fluorine-18 ion can become adsorbed onto the vessel wall.[14] It should be noted that this is a typical procedure only and variations can be made.

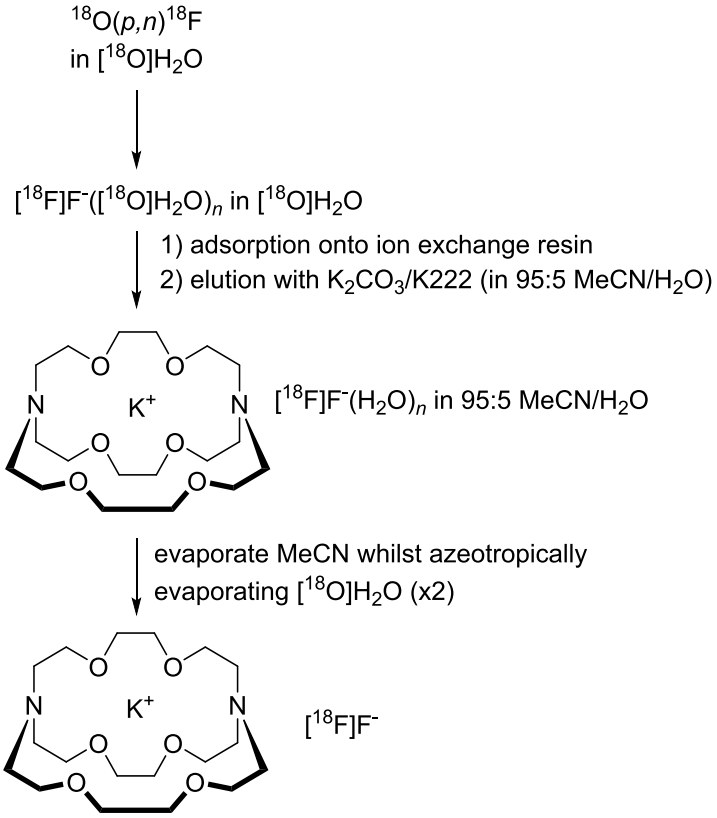

Scheme 1: Flowchart to show the preparation of the fluorine-18 ion

The above procedure is general but small variations can be made, for example, the base and the counterion are interchangeable. It is of great importance to separate the cation, thereby making the [^{18}F]fluoride as nucleophilic as possible. This also renders the fluoride ion prone to protonation hence why the majority of reactions using the [^{18}F]fluoride ion are conducted under weakly basic conditions. Unfortunately, this limits the availability of precursors as those used for labelling should not be a ready source of protons.

Although this is currently the leading method for labelling preparation, cyclotron produced [^{18}F]fluoride ions are still considered to be heavily laden with contaminants. These will arise from various sources throughout the procedure:

- Free radicals from the irradiated water.
- Other radionuclide from the bombardment process.

- Metal ions already present in the water.[15]
- Impurities delivered from ion exchange resin and through contact with other materials.
- Atmospheric carbon and others contaminants present on all equipment used.
- Impurities in the reagents/solvents.

The naked fluoride is virtually never obtained despite best attempts to dry or dehydrate. The complete removal is water is a difficult process which can also add possible impurities. Each step towards the dehydration of the [^{18}F]fluoride will serve to increase its nucleophilicity. Generally speaking, however, it only seems more important to ensure the [^{18}F]fluoride is as dry as possible when conducting more difficult reactions such as aromatic nucleophilic substitution reactions. Less rigorous drying may be required for water tolerant reactions such as aliphatic nucleophilic substitution reactions. Radiofluorination methods may even be conducted in water and also assist in preventing adsorption of fluorine-18 ions onto the vessel wall.

There have been several attempts made to purify the cyclotron produced fluoride ion including the conversion to [^{18}F]fluorotrimethylsilane **4**.[16, 17] This is then distilled out before being hydrolysed back to the fluorine-18 ion (Scheme 2).

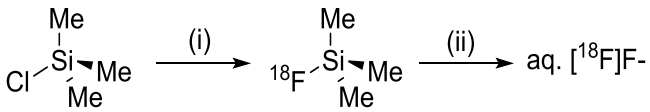

3 **4**

(i) aq.[^{18}F]F$^-$ (ii) H_2O

Scheme 2: Purification of the [^{18}F]fluoride ion from the conversion into fluorotrimethylsilane

1.2 Methods for labelling with the fluorine-18 ion

The vast majority of synthetic strategies to fluorine-18 labelling can be divided into two distinct groups: 1) direct fluorination, where the fluorine-18 isotope is introduced directly onto the target molecule of interest in one step; and 2) indirect fluorination, where the fluorine-18 isotope is first introduced onto a prosthetic group which is subsequently attached to the group of interest. These prosthetic groups are normally small [^{18}F]fluorinated alkyl or aryl groups which also contain reactive functionality. This second approach often requires a multi-step synthesis and is generally only used for labelling complex biological molecules which may not be able to tolerate the conditions imposed by direct fluorination methods.

Methods involving the fluorination may also be broken down into two clear categories: 'nucleophilic' using the fluorine-18 ion, and 'electrophilic' which generally uses [^{18}F]F_2 and derived reagents. Nucleophilic fluorination processes have dominated synthetic strategies in the past as greater selectivity and SA is achievable whilst the [^{18}F]fluoride is produced in larger quantities. Electrophilic [^{18}F]fluorinations are less favoured for several reasons:

1) they generally produce radiolabelled products with low SA due to the carrier-added method of [^{18}F]F_2 production,
2) the maximum RCY is 50%. The massive excess of F_2 means that it is extremely improbable that ^{18}F—^{18}F will be generated, and only ^{18}F—^{19}F will react with the precursor, hence the maximum RCY being 50%. Most of the fluorinating agent will be ^{19}F—^{19}F.
3) labelling with [^{18}F]F_2 is generally unspecific and can therefore lead to multiple [^{18}F]-labelled products.

However, there are strategies towards some of the most widely used PET agents that rely on electrophilic fluorine-18 reactions.[18, 19] For example, the first synthesis of the PET tracer [^{18}F]FDG **2** was completed using electrophilic fluorination.[20]

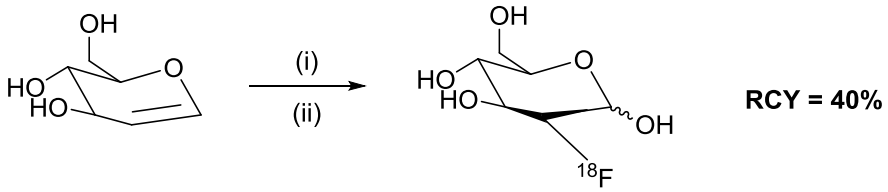

5 **2**

(i) [^{18}F]CH_3CO_2F, H_2O (ii) HCl

Scheme 3: Electrophilic [^{18}F]fluorination using acetyl [^{18}F]hypofluorite for the preparation of [^{18}F]FDG[20, 21]

Softer and more selective electrophilic fluorinating agents have recently been developed such as *N*-[^{18}F]fluorobenzenesulfonimide which is used to prepare and label fluorinated ketones and allylic fluorides. [22] However, this still requires additional synthetic steps and retains the low SA restriction even when high SA [^{18}F]F_2 is employed.

Whilst there now exists many different strategies to [^{18}F]fluorination, all methods suffer from inconsistent RCYs and SA. There are several reasons for this:

- The amount of [^{18}F]fluorine produced by a cyclotron is inconsistent. As the radioisotope is produced by bombarding a target with accelerated protons, varying proportions (approx. 1 in every 1800) protons interacts with [^{18}O]oxygen atoms to create fluorine-18 beam. This varies according to the general performance on the cyclotron.
- The output of cyclotrons will vary by age, manufacturer, maintenance and environment.
- Specific activity will differ across the same reactions types due to the varying degrees of contamination from fluorine-19, caused by the changes in the environment, equipment and reagents/solvents used.

- Trace but varying quantities of water and/or acid can vary the degree of reactivity of the fluoride. A greater volume of water will hydrate the fluoride ion and therefore reduce the 'hardness' of the nucleophile. The presence of acid will protonate the fluoride and produce, the less reactive, HF.
- As nano-quantities of fluorine-18 are used in reactions, they are, generally, very sensitive to small changes in the reaction conditions, thereby varying RCYs.

Despite these issues, the value of fluorine-18 chemistry for positron emission tomography significantly outweighs the drawbacks of the radiosynthetic methods.

1.2.1 Balz-Schiemann and Wallach reactions

One of the earliest methods to introduce fluorine-18 into a compound was the Balz-Schiemann approach (Scheme 4). In this procedure, an aryldiazonium tetrafluoroborate, **6** undergoes an fluorine-18 exchange to give aryldiazonium tetra[^{18}F]fluoroborate, **7** followed by a thermal decomposition to give the [^{18}F]fluoroarene, **8**.[23]

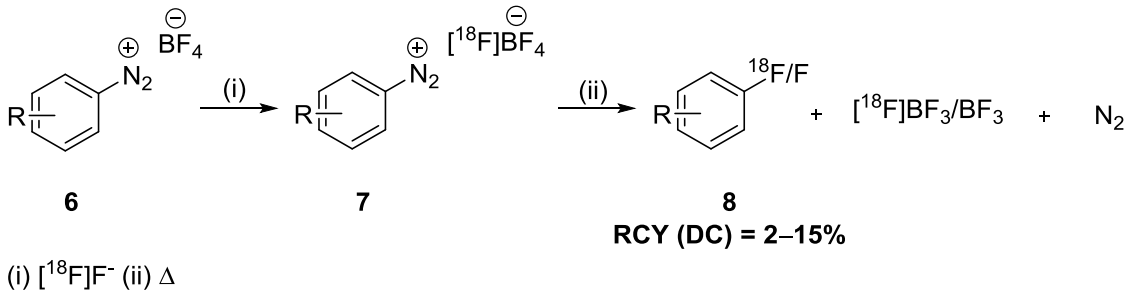

Scheme 4: The Balz-Schiemann reaction for the synthesis of [^{18}F]fluorarenes[23]

This approach has long been used to incorporate a fluoride ion into a position originally occupied by an aryl amino group. However, it carries with it one major disadvantage. Only one of the four fluorides on the tetrafluoroborate ion can possibly be the fluorine-18 isotope. This limits the SA of the radiolabelling process to 25% of the theoretical maximum as the result is more often the [^{19}F]fluorinated product. Using a non-fluorine containing counterion (*e.g.* aryldiazonium tetrachloroborate) helps avoid

the problem. However, this leads to significant transfer of the chloride which then requires separation from the desired fluoro compound which may prove difficult in the time required. Side reactions of the diazononium salt with residual water or other trace species also limit the capacity of the Balz-Schiemann approach.

The Wallach reaction also produces [^{18}F]fluoroarenes but by the acidic decomposition of a triazene precursor, **9** in the presence of the fluorine-18 ion (Scheme 5).[24]

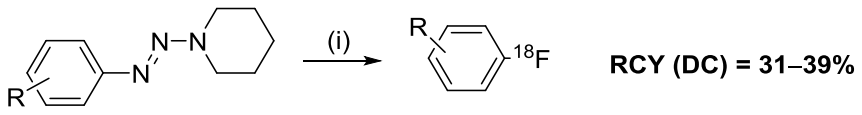

9 **10**

(i) [^{18}F]F$^-$, acid

Scheme 5: The Wallach reaction for the synthesis of [^{18}F]fluoroarenes[25, 26]

The reaction is considered to go via a diazonium salt intermediate, which may be obtained through protonation of the triazene. Attempts to optimise this reaction by varying the acid, solvent, and reaction stoichiometry have been made. Despite this, the reaction is still low yielding.

Balz-Schiemann and Wallach reactions are now rarely used in fluorine-18 radiolabelling due their low RCYs and the emergence of more successful alternatives.

1.2.2 Electrochemical radiofluorination

Electrochemical oxidative fluorination represents one approach towards the production of a fluoroarenes using a fluoride ion but without the need for strong activating groups to promote a nucleophilic exchange. By removing an electron from a phenyl ring, fluoride can easily react with the cation formed to generate an aryl radical. This intermediate can be further oxidised to produce an aryl cation which undergoes rearomatisation by loss of a proton to produce the fluoroarenes (Scheme 6).[27]

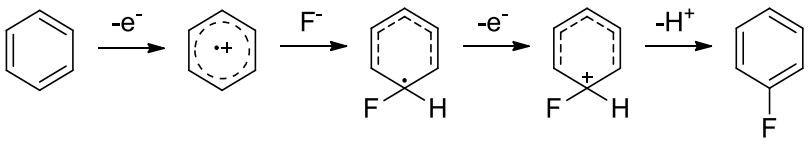

Scheme 6: EC_NEC_B Mechanism of electrochemical nucleophilic fluorination

Resichel and co-workers have used this process to generate fluorine-18 labelled amino acids.[28] Previous work form within the group found that fluorobenzene could be generated in a electrolysis cell, using $Et_3N.HF$ with MeCN as the electrolyte, in the presence of [^{18}F]fluoride.[29] This work was extended towards the synthesis of [^{18}F]fluorophenylalanine (Scheme 7).[28] The reaction showed a large degree of dependence upon the nature of the protecting groups at the amino and carboxylic functionality. Generally, however, RCYs were low with the best results (10.5 ± 2.5%) achieved using methyl and TFA groups (to protect the acid and amino functionality, respectively) temperatures of between -10°C and 0°C and using $Et_3N.3HF$ as the supporting electrolyte (Scheme 7). These conditions generated a carrier-added product and therefore a product low in SA (1.2 GBq/μmol). Despite these results, the short reaction times and efficient methodology leaves scope to pursue this 'mild fluorination' approach towards the generation of simple [^{18}F]fluoroarenes.

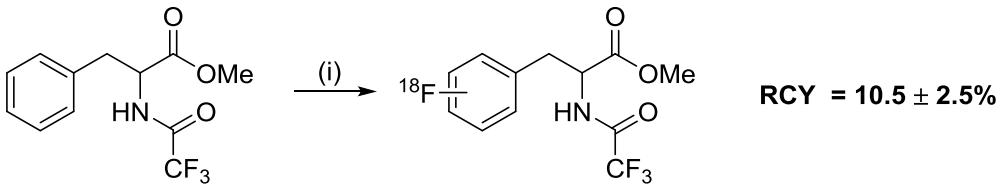

12 **13**

(i) $2e^-$, $-H^+$, [^{18}F]F^-

Scheme 7: Electrochemical radiofluorination of protected phenylalanine[28]

1.2.3 [^{18}F]Fluoride umpolung strategies

The major advantage of using the [^{18}F]fluoride compared to the electrophilic counterpart is that the nucleophilic specie can be produced in higher levels of SA.

Methods for oxidising the [^{18}F]fluoride to an electrophilic reagent would create opportunities to synthesise a large range of radiotracers inaccessible via conventional nucleophilic radiochemistry. Ritter and colleagues have reported the synthesis of a palladium-based electrophilic fluorinating agent derived from fluoride, which allows for the late-stage fluorination of aromatic targets (Scheme 8).[30] Previous work focussed on the electrophilic fluorination of palladium aryl complexes using F-TEDA.[31] Palladium(II) aryl complexes are oxidised which subsequently allow the formation of the aryl carbon-fluorine bond via reductive elimination from palladium (IV) aryl fluoride complexes. Careful consideration led to the design of a stable and highly fluorophilic complex, in a high oxidation state which allows for the transfer of a ligand to a nucleophile whilst undergoing reduction of the metal centre. Treatment of this complex with KF afforded the palladium fluoride complex in excellent yields and short reaction times. The authors propose that nucleophilic attack would only occur at the anti-bonding palladium-fluorine orbital ($\sigma^*_{Pd\text{-}F}$). No other LUMO lobe is available for nucleophilic attack because the aromatic ligands block the trajectories. Essentially, this is an S_N2 reaction at the fluorine atom with the palladium complex acting as a leaving group. The [^{18}F]Pd^{IV} complex was then synthesised from [^{18}F]KF/18-crown-6 in 10 min at RT before being combined with the palladium(II)-aryl and the mixture heated to 85 °C for 10 min. Three different, highly functionalised [^{18}F]aryl fluorides **17–19** could be accessed in RCYs (DC) ranging from 10–33% and in good SA (*ca.* 40 GBq/µmol).[30]

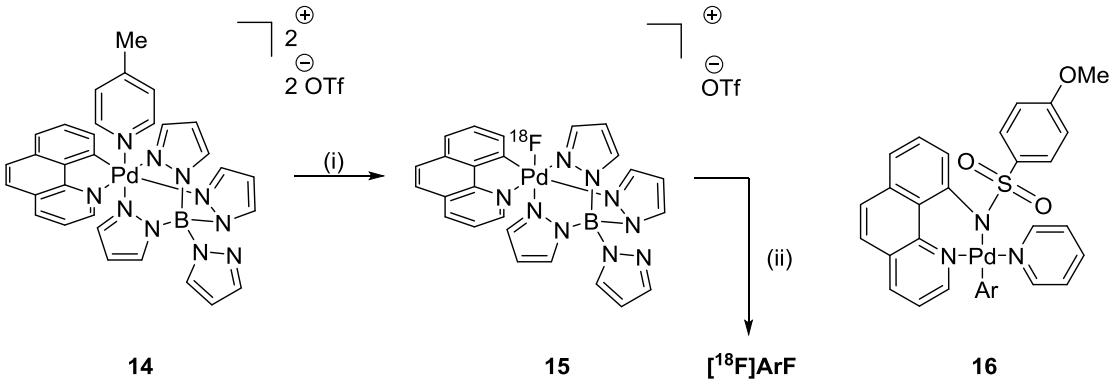

(i) [^{18}F]KF/[18]-crown-6, acetone, RT, 10 min (ii) **16**, acetone, 85 °C, 10 min

Products ([^{18}F]ArF):

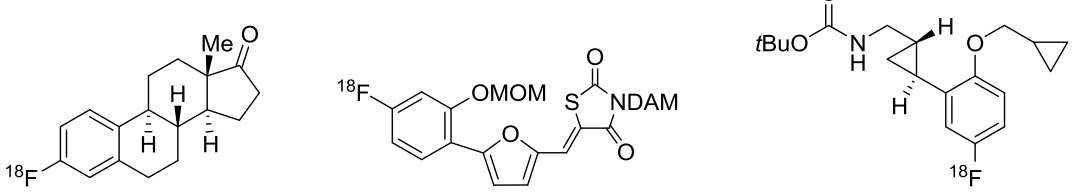

17
RCY (DC) = 33%

18
RCY (DC) = 10%

19
RCY (DC) = 18%

Scheme 8: Palladium-based electrophilic fluorinating agent derived from [^{18}F]fluoride, allowing for late stage radiofluorination of aromatic targets.[30]

1.2.4 Aryl umpolung strategies

Gouveneur and colleagues have reasoned that the coupling of phenol derivatives with [^{18}F]fluoride could be achieved via an aryl umpolung strategy, using an external reagent, to oxidise the phenolic entity to an electrophile.[32] Oxidation of the electron-rich aromatic compound creates an electrophilic species which undergoes attack by the fluoride ion and subsequent dearomatisation. Rearomatisation is achieved using an acid to afford the desired compound (Scheme 9).

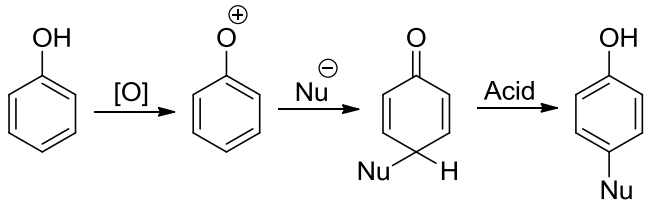

Scheme 9: Aryl Umpolung Strategy

4-*tert*-Butylphenol was synthesised as the electron-rich nature of this compound is representative of functionality present on some radiotracers used clinically. 4-

[^{18}F]Fluorophenol is also a versatile prosthetic group used in the indirect radiolabelling of more complex biomolecules. An optimised approach to the synthesis of 4-*tert*-butylphenol was used to radiolabel with [^{18}F]fluoride. The precursor is combined with tetra-n-butylammonium [^{18}F]fluoride ([^{18}F]TBAF) and trifluoroacetic acid (TFA) before the diacetoxyiodobenzene (DIB) is introduced. Rearomatisation using TFA gave the desired product in 21% RCY (DC). Using this optimised protocol, various 4-*tert*-butyl substituted phenols **20** were radiolabelled with RCYs (DC) of up to 32% being achieved.[32]

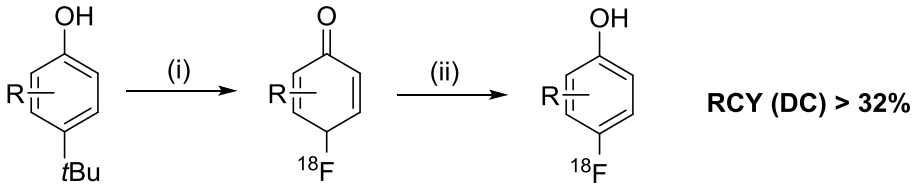

20 **21** **22**

(i) [^{18}F]TBAF, DIB, 1.5% TFA, CH_2Cl_2, RT, 10 min
(ii) 10% TFA, RT, 10 min

Scheme 10: One-pot oxidative fluorination[32]

This approach was proven to tolerate substitution at the *ortho* and *meta* positions of the aromatic substrate. The procedure is also rapid enough to allow for post-fluorination reactions to be performed without significant loss of activity. The promising result for the formation of 2-bromo-4-[^{18}F]fluorophenol **23** also prompted the authors to examine the scope for cross-coupling with phenylboronic acid via a Suzuki-Miyaura reaction (Scheme 11). 4-[^{18}F]Fluoro-2-phenylphenol **24** was achieved via this synthesis in > 95% RCY (DC) thereby potentiating the approach towards prosthetic group chemistry and expanding the range of possible targets.[32]

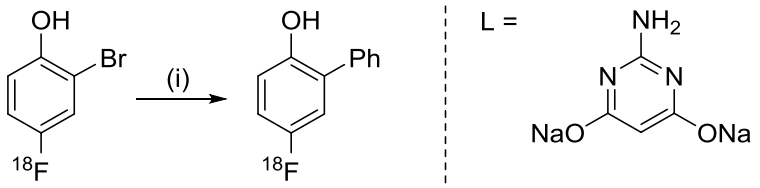

23 **24** **25**

RCY (DC) > 95 %

(i) $Pd(OAc)_2/L_2$, $PhB(OH)_2$ (ii) $MeOH/H_2O$ 70 °C

Scheme 11: Suzuki-Miyaura coupling post-radiofluorination[32]

1.2.5 Enzyme catalysed [^{18}F]fluorination

The use of enzymes to generate fluorine-18 labelled radiotracers under aqueous conditions, and at RT, is an attractive approach to the synthesis of potential imaging agents. They are also chemoselective and produce few side products. O'Hagan and co-workers have pioneered work in this field and first reported an example of the formation of a C-F bond by an enzyme (E.C.2.5.1.63) isolated from the bacterium, *Streptomcyes cattleya.*[33] The enzyme, now called fluorinase, was used to produce 5'-[^{18}F]fluoro-5'-deoxyadenosine (5'-[^{18}F]FDA) **27** from *S*-adenosyl-L-methionine (SAM) **26** (Scheme 12). Initial RCYs were low (*ca.* 1%) however, upon addition of a second enzyme, L-amino acid oxidase, the L-methionine by-product is consumed and equilibrium is shifted to favour the formation of 5'-[^{18}F]FDA resulting in RCYs > 90%. This process was used to generate 5'-[^{18}F]fluoro-5'-deoxyinosine (5'-[^{18}F]FDI) and 5'-[^{18}F]fluoro-5'-deoxy-D-ribose (5'-[^{18}F]FDR) in RCYs of up to 95% in < 2 h.

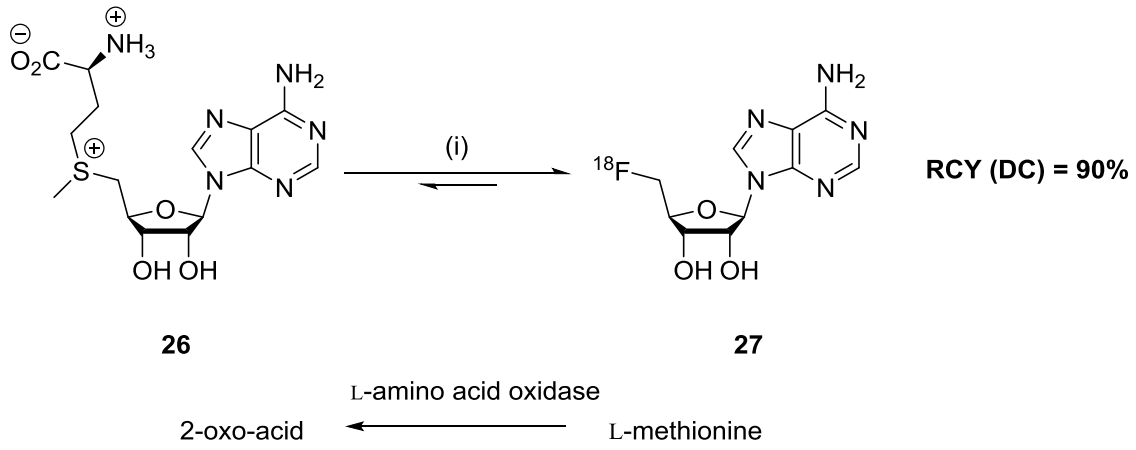

(i) [^{18}F]F$^-$, fluorinase, 35 °C, 1 h

Scheme 12: Radiosynthesis of 5′-[^{18}F]fluoro-5′-deoxyadenosine (5′-[^{18}F]FDA) using fluorinase[33]

These are highly efficient processes as a millimolar concentrations of enzyme (mM) can be used with picomolar concentrations of [^{18}F]fluoride ion, therefore the enzyme is present in considerable excess. More recently, an efficient synthesis of 5-[^{18}F]FDR has been accomplished by combining the fluorinase enzyme with a nucleoside hydrolase in a sequential one-pot reaction.[34] Good RCYs (DC) have been achieved and the stability of the enzyme demonstrated. Research into expanding the scope for this novel method of radiolabelling is on-going and may create diagnostic tools for future PET studies.

1.2.6 Nucleophilic aromatic substitution

Nucleophilic aromatic substitution is by far the most successful approach for introducing fluorine-18 into aromatic positions. This procedure uses nucleophilic [^{18}F]fluoride to displace a good leaving group. Typical leaving groups in order of increasing ability are: I<Br<Cl<F<NO_2≈N^+Me_3. The N^+Me_3 leaving group is particularly beneficial to the radiochemist, especially when used witht eh perchlorate, chloride or triflate counterions as separation of the labelled product from the precursor is facilitated by the large difference in charge. The disadvantage, however, in the

competing formation of [^{18}F]fluoromethane, a volatile radioactive compound which must heighten rigour in health and safety protocols in any radiochemistry laboratory.

Normally, the leaving group is *ortho* or *para* to at least one electron-withdrawing group. This is often necessary as nucleophilic aromatic substitution only works well on electron-deficient rings.

Nucleophilic aromatic substitution is used favourably by chemists for radiolabelling despite usually requiring harsh reaction conditions (high temperatures and polar organic solvents). This is because as most reactions are simple one-pot, one-step pathways capable of achieving high RCYs and high SAs. This also saves time which is crucial when working within a window of two to three half-lives. One such example is the synthesis of [^{18}F]haloperidol **29** which binds to a large number of neurotransmitter receptors (Scheme 13).[35]

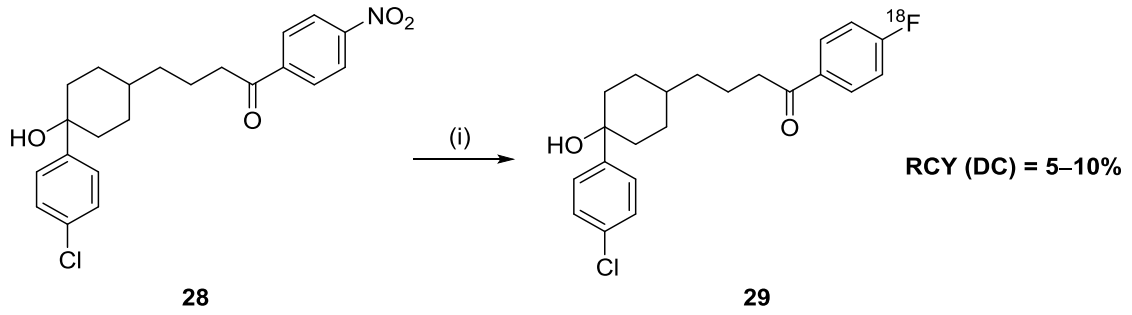

28 **29**

(i) [^{18}F]TBAF, DMSO, 145 °C, 30 min

Scheme 13: Direct synthesis of [^{18}F]haloperidol from the nitro precursor[35]

Only a very few examples exist of reactions with an electron-withdrawing group in the *meta*-position. The preparation of the mGluR5 radioligand, [^{18}F]FMTEB **31** is one of the few examples.[36, 37] However, only a very low RCY has been obtained (Scheme 14).

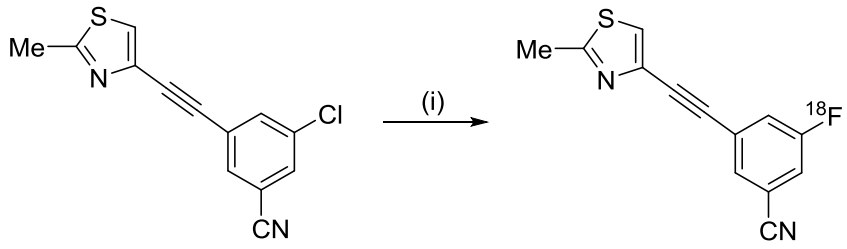

30 **31**

(i) K[^{18}F]F/K222, DMSO, microwaves

Scheme 14: The synthesis of [^{18}F]FMTEB[36]

1.2.7 Radiolabelling of triarylsulfoniums

A method for radiolabelling aromatic compounds with [^{18}F] fluoride has been developed based on the principles of nucleophilic aromatic substitution (S_NAr) using triarylsulfonium salts. This particular method is applicable to a various halogen-substituted aryl systems including non-activated and deactivated aryl rings, plus amides. Studies indicate that sulfonium salts have the potential to be optimised for labelling non-activated and deactiviated aryl rings that have Hammett σ_P substituted constants of greater than -0.170.

High radiochemical yields of [^{18}F]-4-fluoroiodobenzene from **X** represents a ready source of **X** for subsequent use in palladium catalysed C-C bond forming reactions.[38]

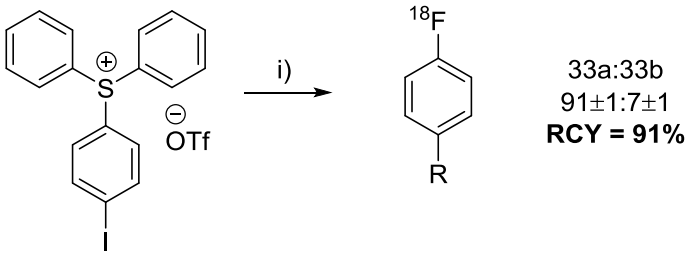

32

33a R = I
33b R = H

i) [^{18}F]KF/K222, MeCN, 80°C, 15 min

Figure 7: Radiosynthesis of [^{18}F]fluoro-iodo-benzene from a sulfonium salt.[38]

This approach to radiolabelling [^{18}F]fluoroarenes is relatively new but may have vast applications in the future of the radiosynthetic chemistry for PET imaging.

1.2.8 Indirect radiolabelling methods

The radiochemist faces a significant challenge in the radiofluorination of electron-rich arenes and macromolecules which may be not be appropriate to a direct, single-step labelling strategy. Such targets require the preparation of a reactive species bearing the fluorine-18 isotope (a prosthetic group) which is subsequently used to label the target compound and generate the desired imaging agent. These labelling agents may be aliphatic or aromatic and the target may be a small molecule or a large macromolecule, such as a peptide or protein.

1.2.8.1 Aliphatic prosthetic groups

An important group of labelling agents are the functionalised, straight-chain aliphatic [^{18}F]fluorides. These molecules are commonly prepared from the reaction of the [^{18}F]fluoride ion with α,ω-bi-functional precursors. Short-chain ω-[^{18}F]fluoroalkyl agents are the most common with [^{18}F]fluoromethyl bromide and 2-[^{18}F]fluoroethyl tosylate being the most frequently used. While tosylates are generally preferred for [^{18}F]fluoroethylation,[39] bromides appear to be more beneficial for [^{18}F]fluoromethylation. For example, Zessin and co-workers have reported the synthesis of the [^{18}F]fluoromethyl analogue of (+)-McN5652 ([^{18}F]FMe-McN) **36** as a new potential tracer for the serotonin transporter.[40] Cyclotron produced [^{18}F]fluoride was used to generate [^{18}F]bromofluoromethane from dibromomethane, using an automated synthesis platform. This [^{18}F]fluoromethylation agent was then combined with the thiolate presursor **35** to produce the desired target in a typically low RCY of 5% but in high SA. The initial radiofluorination step was performed in 25% RCY and

99% RCP. The radiotracer was then shown to be stable for 1 h in a 0.11 M sodium bicarbonate solution containing 50% propylene glycol (Scheme 15).

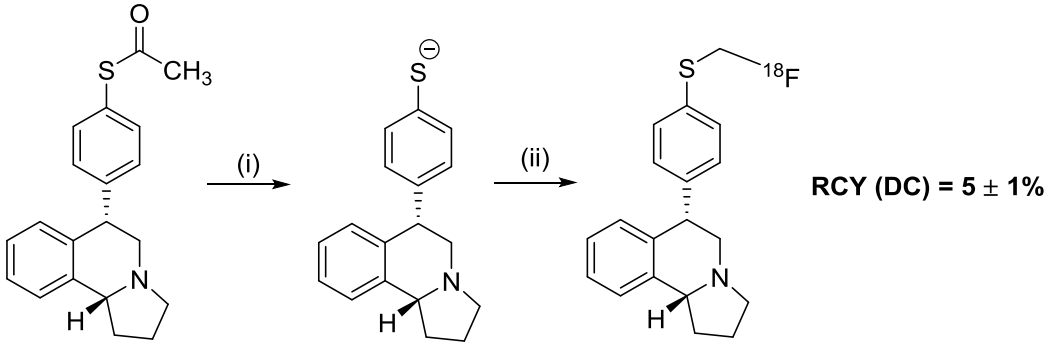

34 **35** **36**

(i) 0.3 M TBAH, MeOH, RT, 10 min (ii) [^{18}F]CH_2BrF, DMF, 40 °C, 1 min

Scheme 15: Radiosynthesis of (+)-trans-1,2,3,5,6,10b-hexayhdro-6- [4-[^{18}F]fluoromethylthio)phenyl]-pyrrolo-[2,1-a]iso-quinoline ([^{18}F]FMe-McN)[40]

[^{18}F]Fluoroethyl tosylate is far more reactive than the bromide derivative and may be produced and used *in situ* to generate radiotracers. This labelling agent has been applied to the synthesis of several radiotracers including, for example, 2-β-carbomethoxy-3-β-(4-chlorophenyl)-8-(2-[^{18}F]fluoroethyl)nortropane ([^{18}F]FECNT) **40** – a brain dopamine transporter (DAT).[41] 2-[^{18}F]Fluoroethyltosylate **38** was first prepared before being used to alkylate 2-β-carbomethoxy-3β-(4-chlorophenyl)nortropane **39** to generate the desired target in 21% RCY (Scheme 16). Excellent imaging results were achieved suggesting that this agent may be superior for mapping brain dopamine transporters in humans using PET.[41]

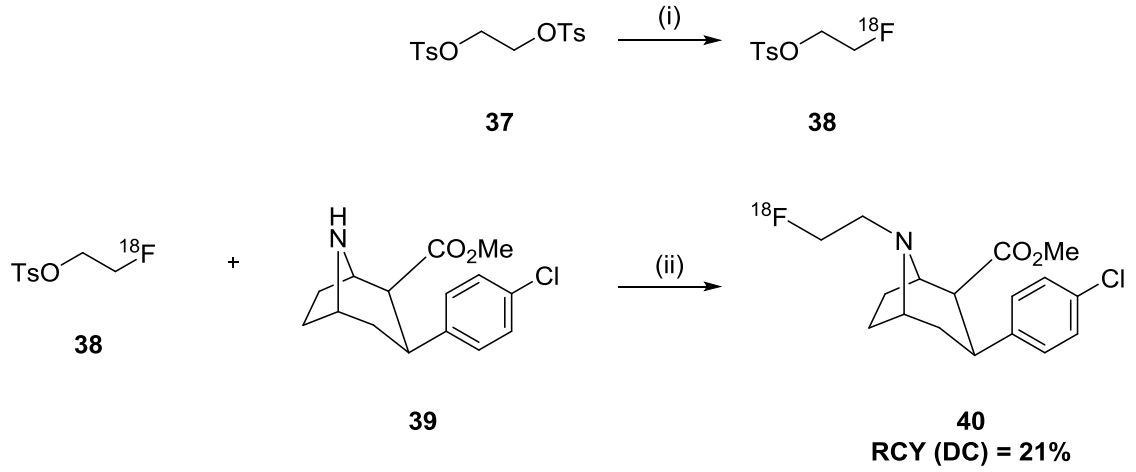

(i) [^{18}F]KF/K222, MeCN, 80 °C, 10 min (ii) DMF, 135 °C, 45 min

Scheme 16: Radiosynthesis of [^{18}F]FECNT[41]

[^{18}F]Fluoroethyl aryl sulfonates of higher reactivity, such as nosylate derivatives, have also been produced in this manner. Pike and coworkers investigated a series of novel [^{18}F]fluoroethyl derivatives bearing a less electron-rich aryl group, i.e. benzenesulfonyl, brosyl, nosyl, and 3, 4-dibromobenzenesulfonyl groups.[42] All reagents gave excellent RCYs (64–87%) of [^{18}F]FECNT in short reaction times. Results showed that these reagents offer high reactivity and straight-forward syntheses from stable precursors suggesting such agents (particularly 3,4-dibromobenzenesulfonate) should be considered as alternatives to [^{18}F]fluoroethyltosylate.[42]

1.2.8.2 Aromatic Prosthetic Groups

The lack of leaving groups required for nucleophilic substitution makes direct incorporation of fluorine-18 into peptides and proteins very difficult with only low levels of SA achievable. The harsh reaction conditions required of direct radiofluorination using [^{18}F]fluoride (high temperature, strongly basic) cause denaturation and decomposition of the sensitive biomolecules such as peptides, proteins, oligonucleotides and antibodies. The development of prosthetic groups for the radiolabelling of these biomolecules has, therefore, become widespread and could

emerge as a very important class of imaging agent. [^{18}F]Fluoroalkylating agents have, conventionally, been used in the indirect labelling of small, simple molecules whilst prosthetic groups prepared in a similar fashion for [^{18}F]fluoroamidation and [^{18}F]fluoroacylation are generally used to radiolabel biomolecules under mild reaction conditions.

1.2.8.3 Amine Reactive Prosthetic Groups

The formation of a stable amide bond between the amino group of a biomacromolecule and a prosthetic labelling agent presents an attractive strategy towards radiolabelling peptides and proteins. A vast number of potential prosthetic groups are, therefore, designed with the intention of coupling to proteins via an amino functionality present on an amino acid residue (*N*-terminus RNH_2 or lysine NH_2) or via an alkylamine linker. *N*-Succinimidyl-4-[^{18}F]fluorobenzoate ([^{18}F]SFB) **45** is one of the most commonly used prosthetic groups for labelling via acylation. Published radiosyntheses of [^{18}F]SFB have generally involved three steps in multiple vessels: (1) [^{18}F]fluorination of an appropriate aromatic precursor, (2) formation of the 4-[^{18}F]fluorobenzoate salt, and (3) conversion of the salt of [^{18}F]SFB.[43] However, more versatile approaches have recently been presented. For example, Tang and co-workers developed an efficient preparation based on a convenient, one-pot procedure consisting of [^{18}F]flourination of ethyl 4-(trimethylammoniumtriflate)benzoate **42**, saponification to generate the [^{18}F]fluorobenzoate salt **44** with tetrapropylammonium hydroxide, and conversion of the [^{18}F]fluorobenzoate salt to [^{18}F]SFB .[44] The resultant [^{18}F]SFB was used to label Avastin, an angiogenesis inhibitor used to treat various cancers, through [^{18}F]fluorobenzoylation of an amino residue.

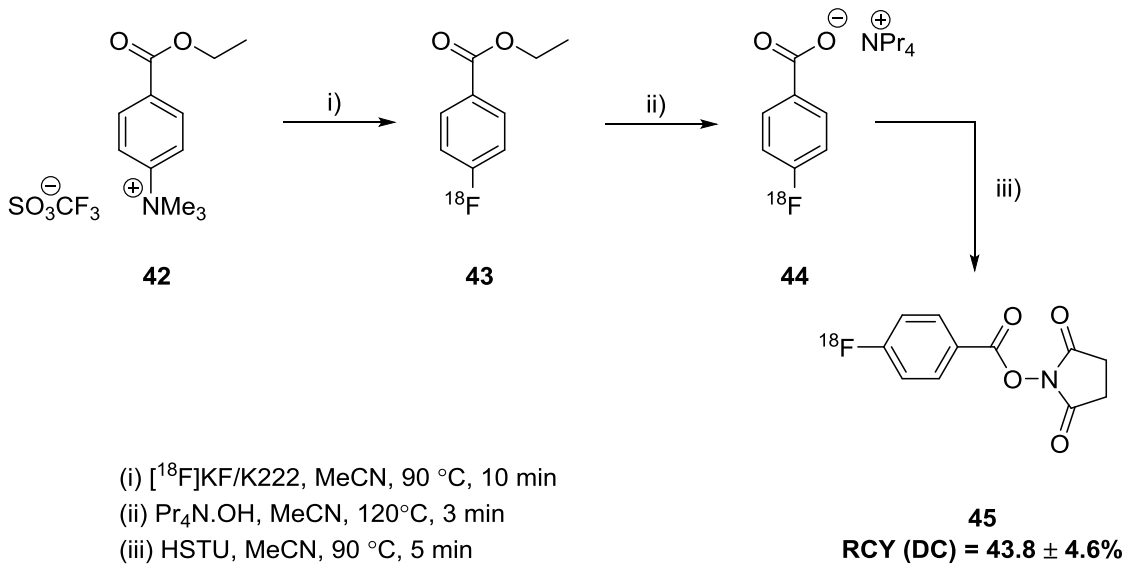

Scheme 17: Radiosynthesis of [^{18}F]SFB[44]

The drawback to this strategy lies in the difficulty in automating the process. Reducing the number of synthetic steps involved, helps circumvent this issue. Carroll and co-workers developed a single-step synthesis of [^{18}F]SFB using diaryliodonium salts (Scheme 18).[45] The required precursor **46** was subjected to [^{18}F]fluorination by reacting with [^{18}F]KF/K222 complex in DMF for 5 min at 130 °C and in a Pyrex reaction vial. RCYs of 23% were achieved.

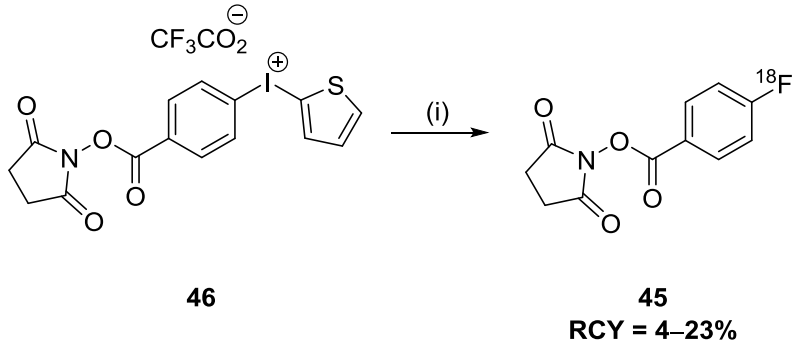

Scheme 18: Single-step radiosynthesis of [^{18}F]SFB[45]

There are other [^{18}F]fluorinated compounds which also serve as prosthetic groups, such as 4-[^{18}F]fluorophenacyl bromide **47**, *N*-succinimidyl-4-([^{18}F-fluoromethyl)benzoate **48**, 3-[^{18}F]-5-nitrobenzimidate **49**, methyl 2-[^{18}F]-

fluoropropionate **50**, 2-[^{18}F]fluoroacetic acid **51**, and *N*-succinimidyl-8-[4'-[^{18}F]fluorobenzyl)amino]suberate **52** (Scheme 19).

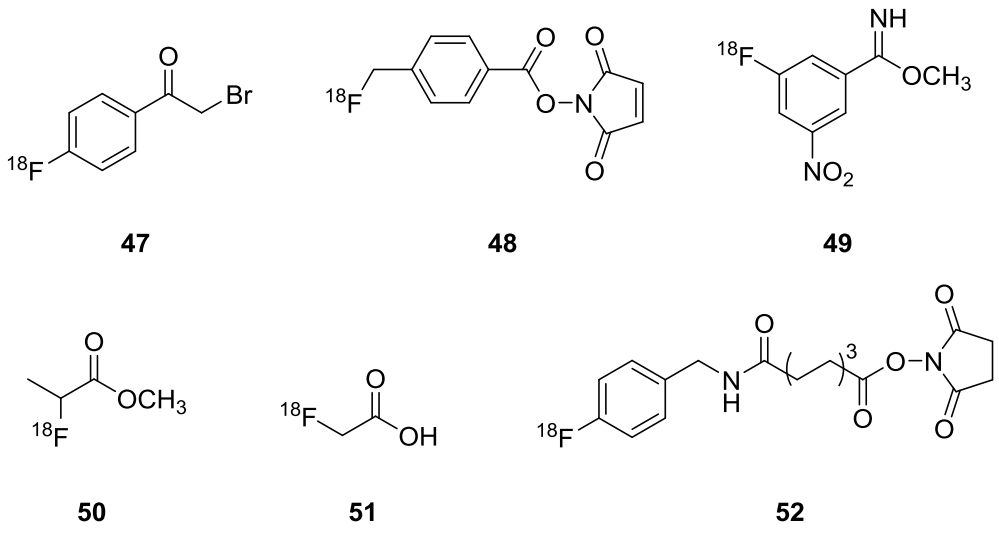

Scheme 19: Prosthetic groups for indirect labelling with fluorine-18

1.2.8.4 Thiol-Reactive Prosthetic Groups

The thiol group present in cysteine residues is also frequently targeted for the formation of conjugates with prosthetic groups. The rarity with which this residue is found allows for thiol reactive agents to modify biomolecules at specific sites and induce a means of high chemoselectivity. Due to its excellent selectivity, 1-[3-(2-fluoropyridin-3-yloxy)propyl]pyrrole-2,5-dione) ([^{18}F]FPyME) **55** is becoming an interesting alternative to more commonly used prosthetic groups. This [^{18}F]fluoropyridine-based maleimide reagent is used for the indirect labelling of proteins and peptides via selective conjugation with a thiol residue. de Bruin prepared [^{18}F]FPyME in 28–37% RCY in 110 min using a three-step strategy (Scheme 20).[46] Excellent chemoselectivity was observed upon comparing thiol and amino groups in a small hexapeptide before the prosthetic group was conjugated to 8-kDa proteins. Pleasingly, high yields of the conjugated end product were achieved in short reaction

times demonstrating the value of this thiol-selective, fluorine-18 reagent for the prosthetic labelling of peptides and proteins.

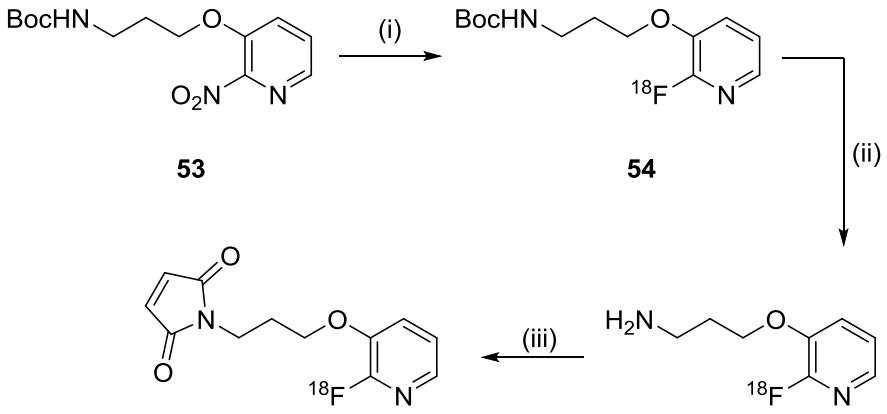

53 **54** **55** **56**

RCY (DC) = 19–41%

(i) [^{18}F]KF/K222, K_2CO_3, DMSO, 145 °C, 2–4 min (ii) TFA, CH_2Cl_2, 70 °C, 2–5 min
(iii) maleic anhydride, aq.sat. $NaHCO_3$, dioxane, vortex, RT, 10 min

Scheme 20: Radiosynthesis of [^{18}F]FPyME[46]

Wüest and coworkers have used [^{18}F]FDG **1** as a precursor for the synthesis of [^{18}F]fluorinated peptides and proteins.[47] The popular imaging agent was converted to [^{18}F]FDG-maleimidehexyloxime ([^{18}F]FDG-MHO) **58** using *N*-(6-aminoxyhexyl)maleimide **57** in 80% EtOH heated to 100 °C for 15 min (Scheme 21). RCYs of up to 69% were achieved, following radio-HPLC purification, in a total synthesis time of 45 min. The chemoselective conjugation of [^{18}F]FDG-MHO to thiol groups was investigated using the reaction with tripeptide glutathione (GSH) and the annexin A5 protein, which contains only one cysteine residue. Excellent RCYs were observed, even at low protein concentration levels, making [^{18}F]FDG-MHO a promising prosthetic group for chemoselective [^{18}F]labelling of thiol residues.[47]

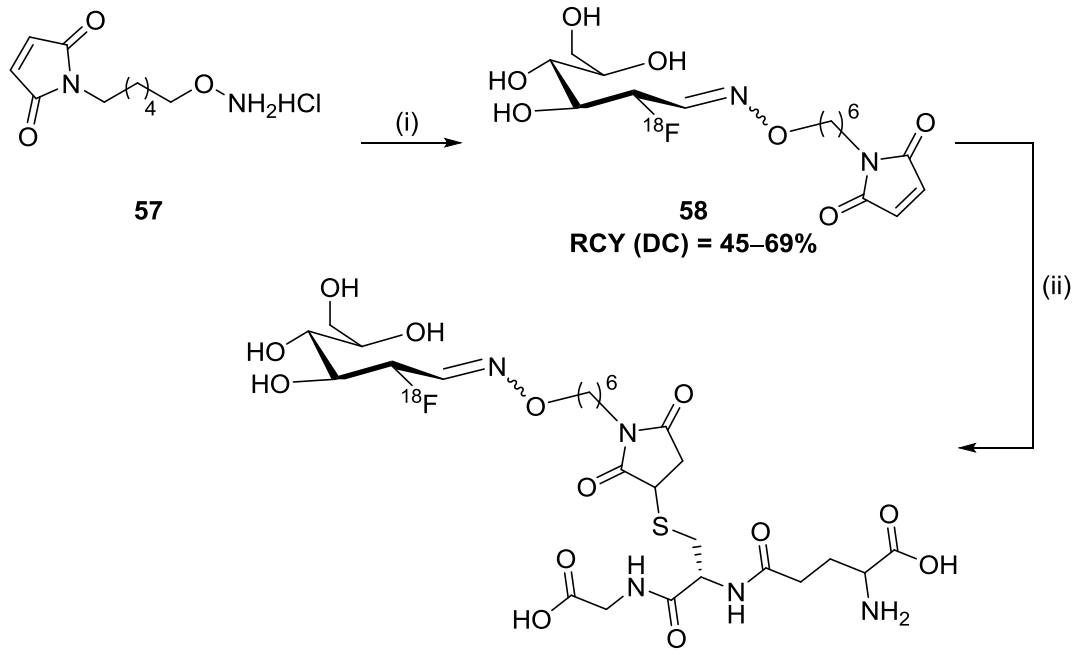

(i) [^{18}F]FDG, 80% EtOH, 100 °C, 15 min (ii) GSH, RT, 10 min, phosphate buffer (pH 7.2), 20 °C

Scheme 21: Radiosynthesis of [^{18}F]FGD-MHO followed by the radiolabelling of GSH[47]

1.2.8.5 Carboxylic Acid Reactive Prosthetic Groups

The formation of an amide using an [^{18}F]fluorinated amine to target an activated carboxylic acid group is another possible strategy towards indirect labelling of a biomolecule. However, there are restrictions which make this approach less popular than others. The target compound must, for example, bear an activated carboxylic group whilst not having free amine functionality which would promote inter- and intramolecular cross-linking. Protection of the free amine would be necessary and require a deprotection step thereby lengthening and complicating the total radiosynthesis. Despite this, Shai and colleagues used this approach to successfully label insulin in high specific radioactivity.[48] Cyclotron produced fluorine-18 was used to generate 4-([^{18}F]fluoromethyl)benzoylaminobutane-4-amine ([^{18}F]FMBAA) which was then coupled to a protected insulin derivative. A simple deprotection step was then

used to produce the final product which was found to retain the essential biological properties of native insulin.[48]

1.2.8.6 Other Prosthetic Groups

4-[^{18}F]Fluorobenzaldehyde ([^{18}F]FBA) was developed to exploit the efficient and chemoselective oxime formation possible between a hydrazone and aldehyde group. This simple [^{18}F]fluoroarene can be generated in a single-step and in high RCY to produce a prosthetic group with sufficient *in viv*o stability for chemoselectively labelling biomacromolecules under mild conditions. Jeong and co-workers have reported a novel and simple preparation of [^{18}F]FBA followed by successful conjugation with hydrazinonicotinic acid – human serum albumin conjugate (HYNIC-HSA) via hydrazine formation (Scheme 22).[49] Non-carrier added [^{18}F]FBA was prepared by the nucleophilic substitution of 4-trimethylammonium benzaldehyde triflate with [^{18}F]fluoride in the presence of tetrabutylammonium bicarbonate. The conjugation efficiency of HYNIC-HSA with [^{18}F]FBA was up to 90% which demonstrates that this simple [^{18}F]fluoroarene is an important prosthetic radiolabelling agent.[49]

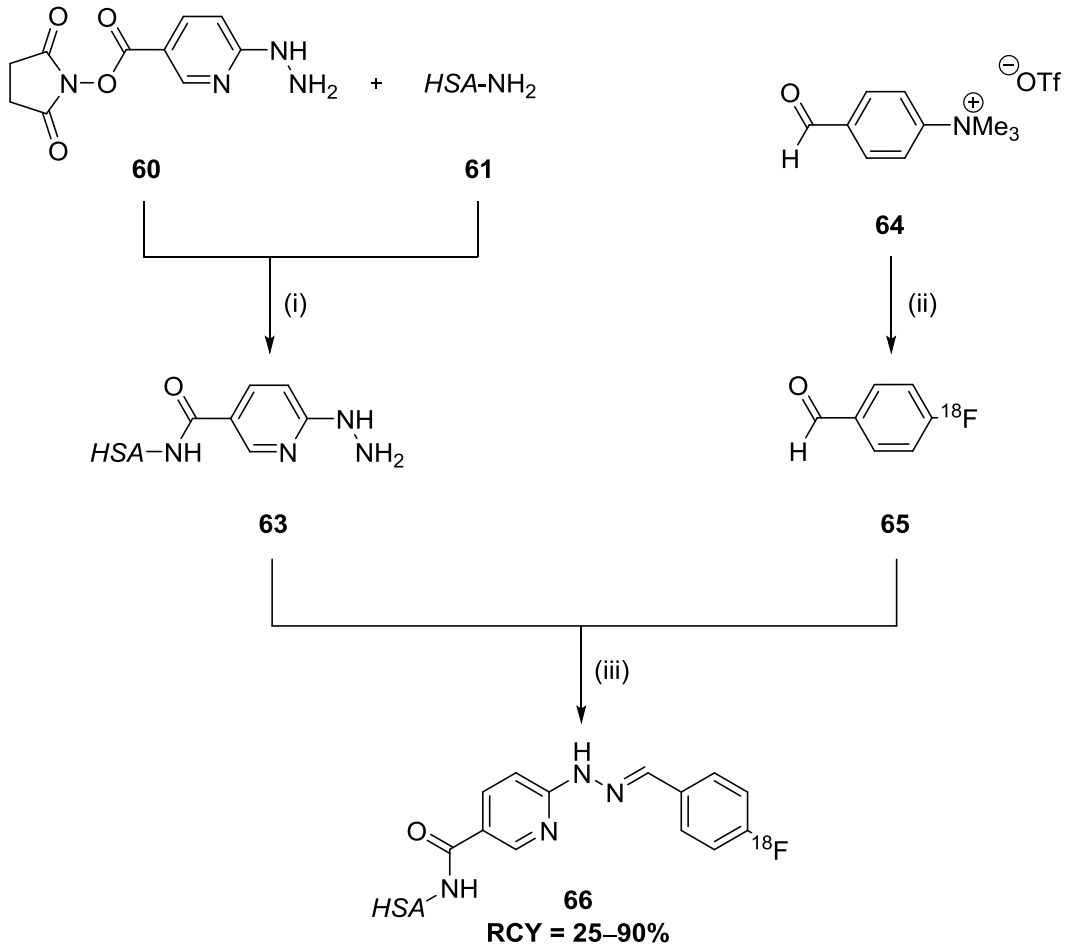

(i) Phosphate buffer (pH 7.5) DMSO, RT, 2 h (ii) [^{18}F]TBAF, DMSO, 100 °C, 6 min
(iii) Phosphate buffer (pH 7.5) RT, 30 min

Scheme 22: Radiosynthesis of fluorine-18 labelled HSA

Fluorine-18 labelled imidate esters react with proteins at lysine residues to form stable amidine bonds. Methyl 3-[^{18}F]fluoro-5-nitrobenzimidate has been prepared in a two-step reaction and found to be stable in borate buffered solution at room temperature with less than 10% hydrolysis over two hours.[50]

Isothiocyantes labelled with fluorine-18 react readily with amines to form thioureas. Fluorine-18 labelled isothiocyanates have been synthesised and conjugated to oligonucleotides, proteins and benzylamine.[51-53] Unfortunately, due to the low stability of [^{18}F]benzylfluorides, significant defluorination was observed as the conjugate was investigated *in vivo*.

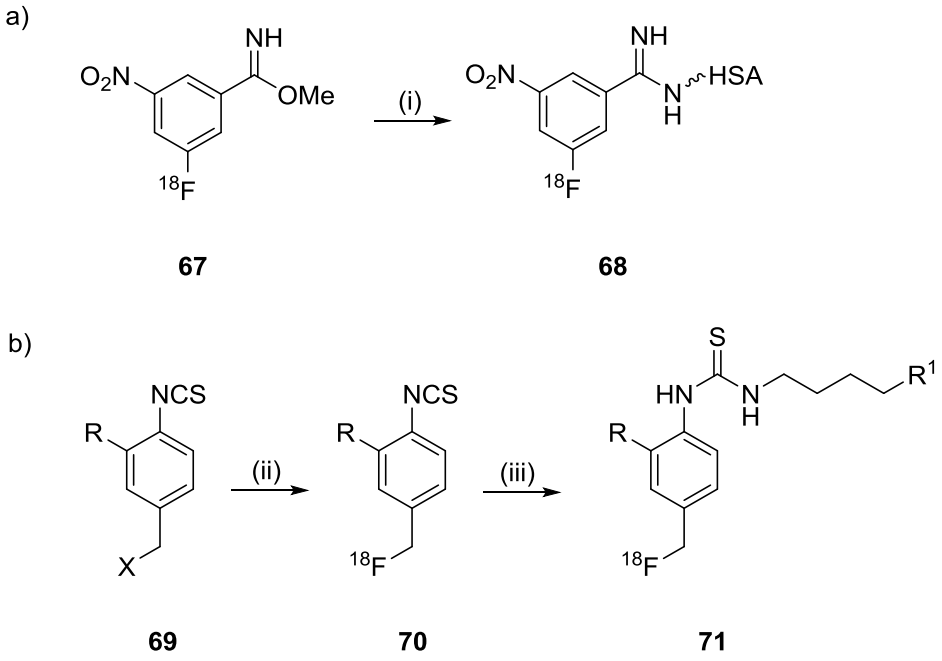

(i) H_2N~HSA, buffer (pH 8) (ii) $[^{18}F]F^-$ (iii) $H_2NC_4H_8R^1$

Scheme 23: (a) Radiolabelling through fluorine-18 imidate esters (b) Radiolabelling through fluorine-18 labelled isothiocyanates

1.2.9 Reactions with diaryliodonium salts

The severe limitation to typical aromatic nucleophilic substitution reactions with the $[^{18}F]$fluoride ion is the inability to label electron-rich arenes. Best attempts using the Balz-Schiemann and Wallach reactions have been inefficient. A new and improved method for the incorporation of $[^{18}F]$fluoride into arenes was introduced using diaryliodonium salts **72** (Scheme 24).[54] The advantage of this method is the applicability to both electron-rich and electron-deficient arenes.[55]

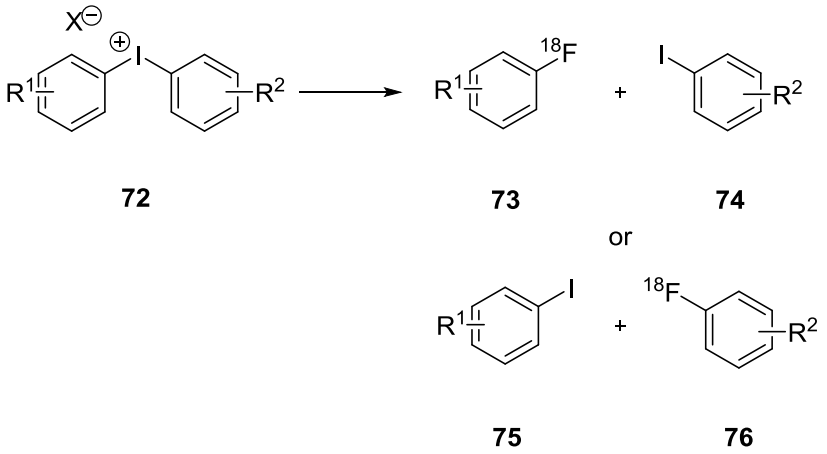

72 **73** **74**

75 **76**

Scheme 24: [^{18}F]Fluoride labelling of arenes through reactions of diaryliodonium salts with the [^{18}F]fluoride ion.

The regioselectivity of the reaction is determined by the stereoelectronic properties of the substitutents; generally, the more electron-deficient aromatic ring will selectively incorporate the fluoride nucleophile. However, an *ortho*-substituent on one of the aryl rings preferentially directs fluoride to that ring – the so-called "*ortho*" affect.[55-58] The RCYs of the radiofluorinated target can therefore be increased by the strategic modification of electronic and steric properties of the substitutents, and reaction conditions.[56] The benefits realised from utilising diaryliodonium salts in both direct and indirect radiofluorination chemistry, has been the motivation for their extensive use and practice within this research group and the PET radiochemistry community. For this reason, diaryliodonium salts warrant further discussion.

1.3 Iodine, hypervalency and diaryliodonium salts

Hypervalent iodine reagents were discovered in 1886 when German chemist, Conrad Willgerodt first prepared (dichloroiodo)benzene.[59] Willgerodt later went on the publish the first comprehensive book in this field in 1914[60] but it wasn't until nearly 60 years later when widespread interest in this class of compounds was established. Several reviews[61-65] and books[66, 67] were then published covering all aspects of hypervalent iodine chemistry, and now molecules of this type are widely used in organic synthesis.

Interest in this field has recently accelerated, partly due to developments in the application of diaryl-λ^3-iodanes in cross-coupling reactions[68-75] and their application in the synthesis of imaging agents for PET.[54, 76-81]Many more reviews have subsequently been published (Table 3), the most significant of which has been the Symposium-in-Print *Tetrahedron* issue dedicated to recent advances and applications of hypervalent iodine chemistry in concert with the 3rd International Conference on Hypervalent

Iodine Chemistry (ICHCI2010) compiled by Wirth and Quideau.[82] Herein this review is a brief summary of hypervalent iodine (III) compounds before focussing on diaryl-λ^3-iodanes and their application to the synthesis of imaging agents for PET.

Year	Authors	Title	Reference
1990	R.M. Moriarty K. Vaid	Carbon-carbon bond formation via hypervalent iodine oxidations	83
1994	O. Prakash N. Saini P.K. Sharma	Hypervalent iodine reagents in the synthesis of heterocyclic compounds	84
1996	P.J. Stang V.V. Zhdankin	Organic Polyvalent Iodine Compounds	85
1996	Y. Kita T. Takada H. Tohma	Hypervalent iodine reagents in organic synthesis: nucleophilic substitution of p-substituted phenol ethers	86
1997	T. Kitamura Y. Fujiwara	Recent progress in the use of hypervalent iodine reagents in organic synthesis. A review	87
1997	A. Varvoglis	Chemical Transformations induced by hypervalent iodine reagents	88
1999	T. Wirth U.H. Hirt	Hypervalent iodine compounds. Recent advances in synthetic applications	89
2003	P. Dauban R.H.Dodd	Iminoiodanes and C-N bond formation in organic synthesis	90
2004	H. Tohm Y. Kita	Hypervalent iodine reagents for the oxidation of alcohols and their application to complex molecule synthesis	91
2005	R.M. Moriarty	Organohypervalent Iodine: Development, Applications and Future Directions	92
2006	T. Wirth	Hypervalent iodine chemistry in synthesis: Scope and new directions	93
2006	R.D. Richardson T. Wirth	Hypervalent iodine goes catalytic	94
2007	N.R. Deprez M.S. Sanford	Reactions of hypervalent iodine reagents with palladium: mechanisms and applications in organic synthesis	95
2008	B.Olofsson	Diaryliodonium salts: A Journey from Obscurity to Fame	96
2009	T. Dohi Y. Kita	Hypervalent iodine reagents as a new entrance to organocatalysts	97
2011	M.S. Yusubov A.V. Maskaev V.V. Zhdankin	Iodonium Salts in Organic Synthesis	98

Table 3: Notable reviews of hypervalent iodine chemistry since 1990

1.3.1 Iodine and hypervalency

Molecules containing elements from groups 15-18 bearing more electrons in the valence shell than the octet are termed hypervalent molecules. Despite being commonly found in the monovalent form (oxidation state: -1) the large size and polarisablility of iodine, allows for hypervalency.[99] Hypervalent iodine molecules generally fall in to two classes of compounds; iodine (III) compounds, termed λ^3-iodanes according to IUPAC recommendations, and iodine (V) compounds or λ^5-iodanes (the lambda notation refers to non-standard bonding).

The iodine atom of λ^3-iodanes has a pseudotrigonal bipyramidal geometry with two heteroatom ligands in axial positions, whilst the least electronegative group and remaining lone pairs of electrons occupy the equatorial positions. This is true of every class of iodine (III) compound[67] – IL_3, RIL_2, R_2IL, and R_3I (L = heteroatom ligand, R = carbon atom ligand). In the hypervalent model, bonding in RIL_2 uses a non-hybridised 5p orbital in the linear L-I-L hypervalent bond (Figure 8). Two electrons from the doubly-occupied 5p orbital, and one electron from each of the ligands generate a 3-centre-4-electron bond (3c-4e or hypervalent bond).[100] These bonds are highly polarisable and are longer and weaker than the standard covalent bond. The remaining group is bound by a standard σ-covalent bond with $5sp^2$ hybridisation.[101, 102] Organo-iodine (III) compounds, termed organo-λ^3-iodanes, possess 10 electrons in the valence shell and hence are classed as hypervalent [10-I-3] species. (The electronic structures of hypervalent moieties are described in [N-X-L] format, in which N is the number of electrons associated with the central atom X, and L is the number of ligands bound.[103])

The iodine of the highly polarised L-I-L bond is strongly electrophilic. As the two lower energy orbitals (the bonding and non-bonding orbitals) of the three molecular orbitals produced by the 3c-4e bond are filled, partial positive charge develops on the iodine whilst partial negative charge develops on the axial heteroatom ligands. This is because the filled nonbonding orbital has a node about the central iodine atom.[66]

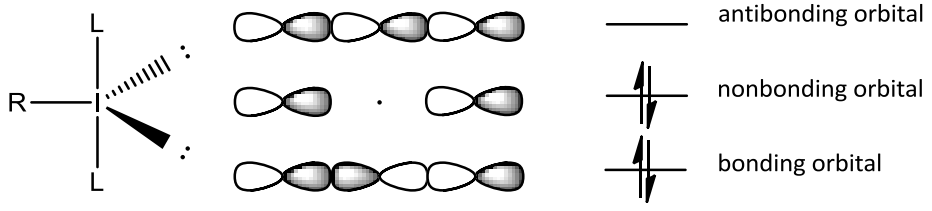

Figure 8. Pseudotrigonal bipyramidal geometry and molecular orbital of the 3c-4e bond.

Aryl λ^5-iodanes exist as a square pyramid structure with four heteroatom ligands in basal positions and an aryl group occupying the remaining apical position (Figure 9). Two orthogonal 3c-4e bonds allow the iodine to accommodate the heteroatom ligands whilst the apical, aryl group is bound via a hybridised 5sp orbital.[67]

Figure 9. Square pyramid geometry of the λ^3-iodane

Cyclic-λ^5-iodanes, such as IBX (2-iodoxybenzoic acid) and Dess-Martin periodinane (DMP) are commonly used as mild and highly selective oxidants of alcohols and amines. IBX can also effect the oxidative transformation of several other functional groups.[93] However, despite recent advances and rising interest, λ^5-iodanes continue to have few synthetic applications, when compared to the iodine (III) species. The chemistry of λ^5-iodanes has been far less developed, with the first comprehensive review of their synthetic application published only recently.[104] This report, therefore, will focus exclusively on the λ^3-iodanes.

1.3.2 Structure of organo-λ^3-iodanes

The pseudotrigonal bipyramidal geometry of the λ^3-iodanes, whilst in the solid state has been observed across all known organo-λ^3-iodanes published to date. Interestingly, this also includes dicyano(pentafluorophenyl)-λ^3-iodane, which despite the stability of the cyanide anion, exhibits bonding through the carbon for all three ligands and is therefore considered to be of the R_3I-type.[105]

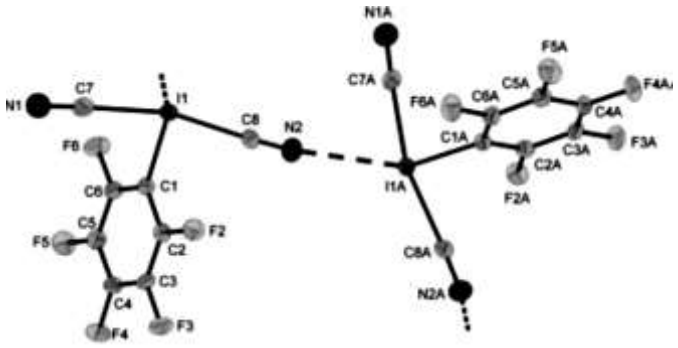

Figure 10: Molecular structure and intermolecular contacts of $PhF_5I(CN)_2$[105]

X-Ray crystallography and powder diffraction studies of the solid state structures have shown that most λ^3-iodanes exist as polymeric structures,[106-108] often including secondary bonding interactions,[107, 109] depending on the functionality of the compound. There is little consistency throughout the structures published so far with the formation of monomers,[108] dimers[110] and trimers[111] all possible. Bond angles around the L-I-L bonds have also varied, resulting in difficulty in identifying a trend within the solid state structures.

This observation is also true of the same compounds in solution, as many of the known λ^3-iodanes have shown to have one ligand with strong ionic character.[66] This is especially true of the diaryl-λ^3-iodanes (R_2IL). In polar solvents, cryoscopic and conductance measurements have revealed these compounds as having dissociated into the solvated iodonium ions and counterions.[67] Generalising the true structure of λ^3-iodanes in solution is avoided as the nature of the ligand,[112] concentration of solution[113] and type of solvent[112] into which the compound is dissolved, has bearing upon the structure adopted.

This argument has resulted in iodine (III) compounds often being referred to as “salts,” but this does not reflect the true structure of these species. For example, Ph_2ICl is called diphenyliodonium chloride because the I-Cl bond (3.06 Å) is longer than the

average covalent bond (2.56 Å).[114] However, X-ray crystal structure determination has found that Ph_2ICl has a trigonal bipyramid geometry with 10 electrons in the valent shell of the iodine atom (Figure 11).[115] This is contrasting to the tetrahedral geometry suggested by the term 'onium'. Onium salts, such as ammonium or phosphonium salts, include eight electrons in the valent shell of the positively charged atom and are not hypervalent. The valency shell of the iodine in Ph_2ICl has 10 electrons and is, therefore, hypervalent. [116] (Regardless of this, the terms 'diaryl-λ^3-iodane' and 'diaryliodonium salt' have been used interchangeably throughout the recent surge of interest in this research and, therefore, also within this report.)

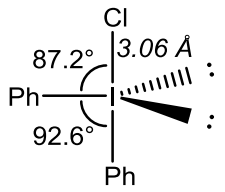

77

Chloro(diphenyl)-λ^3-iodane

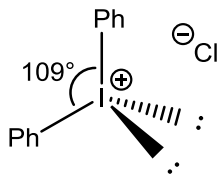

77

Diphenyliodonium chloride

Figure 11: Structure and bonding in chloro(diphenyl)-λ^3-iodane compared and theoretical structure of diphenyliodonium chloride[115]

1.3.3 Reactivity of organo-λ^3-iodanes

The versatility of organo-λ^3-iodanes has encouraged their employment in diverse synthetic strategies. These compounds have the ability to react via a multitude of different possible mechanisms, some of which have received far greater attention than others, due to their involvement in more significant syntheses within organic chemistry.

1.3.3.1 Ligand Exchange

One of the most important modes of reaction involves an exchange of ligand on the iodine atom, whilst leaving the oxidation state (III) unchanged. This process, termed a

'ligand exchange', has been intensely studied but elucidation of a detailed mechanism is ongoing. Heteroatom ligands of organo-λ^3-iodanes are readily displaced by nucleophiles via either an associative or dissociative mechanism (Figure 12).[63] There is considerable evidence to support the associative approach whilst experimental results supporting the dissocative pathway are limited.[113] The iodine atom of $ArIL_2$ **78** is electrophilic and reacts with a variety of nucleophiles as they attack the C-I σ*-orbital resulting in the immediate formation of a *trans*-tetracoordinated iodate **79**. This intermediate then isomerises to form the *cis*-iodate with elimination of the heteroatom ligand to produce a new aryl-λ^3-iodane **80**.

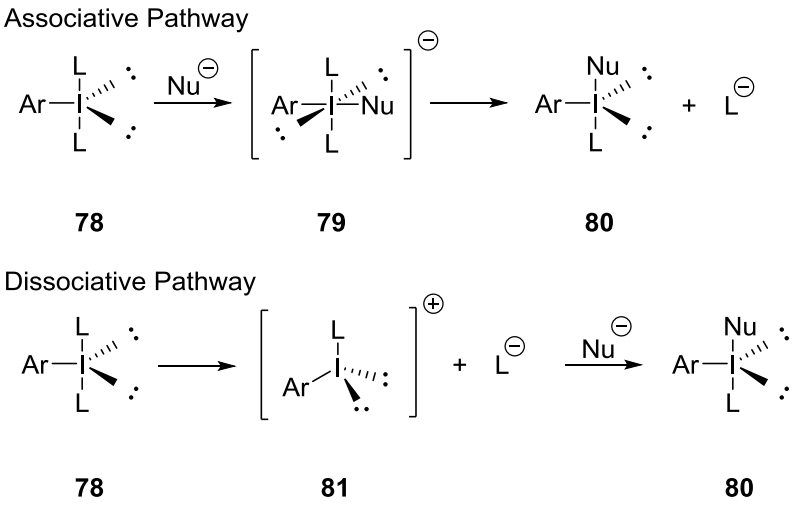

Figure 12: The two possible mechanistic pathways, associative and dissociative, for ligand exchange reactions[66]

1.3.3.2 Reductive elimination and hypernucleofugality

Another key mode of reactivity involving organo-λ^3-iodanes, is the reductive elimination of the hypervalent iodine species to the monovalent iodide, with loss of a heteroatom ligand (Figure 13). This is often observed in reactions of aryl-λ^3-iodanes.[117] The driving force behind this process lies in the hypernucleofugality of the aryl-λ^3-iodanyl group. A hypernucleofuge must present two features: a) leaving group ability greater than that of a 'superleaving group' such as a triflate (OTf) and, b) hypervalent

character.[117] Reduction of the hypervalent iodine to the univalent iodide of normal valency is the origin of the very high leaving group ability of the λ^3-iodanyl group. An increase in entropy is also observed as the single hypervalent specie generates three molecules on degradation. The λ^3-iodanyl group is eliminated with simultaneous reduction to an iodoarene and concomitant elimination of the heteroatom ligand (Figure 13).

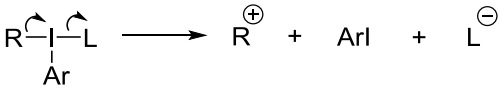

82

Figure 13: Process of reductive elimination[66]

1.3.3.3 Pseudorotation of λ^3-iodanes

Organo-λ^3-iodanes are configurationally unstable and undergo facile interconversion of stereoisomers due to the large size of the iodine atom. The apical heteroatom ligands can mutually exchange sites via repeated pseudorotation (Ψ) about the iodine atom. The isomerisation by which the apical ligands exchange with the equatorial ligands through the bending of bonds is referred to as 'Berry-pseudorotation'.[118] The two apical bonds move concertedly to become equatorial bonds through a square-based pyramid intermediate structure (Figure 14). This process is of vital importance to the reactivity of λ^3-iodanes as, in the ground state, the most electron-rich or sterically demanding substituent is forced to occupy the equatorial position.[119] The result is a distinct difference in reactivity between the equatorial and axial substituents.[119] This process has particular bearing on the selective ligand coupling of attacking nucleophiles with the substituents of asymmetric diaryl-λ^3-iodanes.

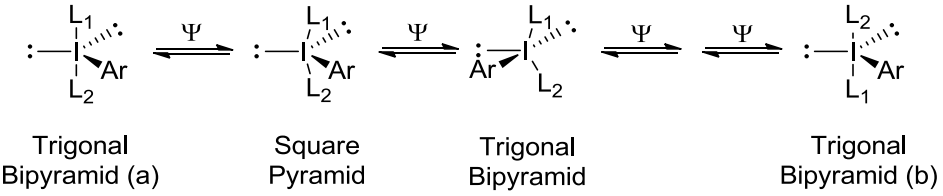

Figure 14: Pseodorotation about the iodine of organo-λ^3-iodane **78**

1.3.3.4 Ligand Coupling

The term 'ligand coupling' was introduced by Oae to describe the intermolecular coupling of two ligands bound to a hypervalent atom.[120] The mechanism still lacks full understanding due to facile stereomutation of the trigonal bipyramid structure by Berry pseudorotation and rapid intermolecular ligand exchange reactions.[66] Studies into the thermolysis of diaryl(halo)-λ^3-iodanes have been shown to yield a mixture of iodoarenes and haloarenes, as the halogen will always attack the *ipso* carbon of the neighbouring aryl groups.[121-123] This reaction mechanism has formed the theoretical basis of the selectivity in the [^{18}F]fluorination of both electron-rich and electron-deficient arenes from the reactions of diaryl-λ^3-iodanes with nucleophilic [^{18}F]fluoride.[54] This is the reasoning behind our interest in the diaryl-λ^3-iodane class of compounds and, hence, the focus of this review.

1.3.4 Synthesis of diaryl-λ^3-iodanes

The earliest preparations of diaryl-λ^3-iodanes were reported in the late nineteenth century by Hartmann and Meyer.[124] At the time, these compounds were considered obscure and for many years, little investigation was made towards developing new and efficient synthetic strategies. Vast improvements in preparations were made decades later when the popularity of these compounds increased. Innovation towards new, efficient methods has continued today as the potential application of hypervalent iodine compounds expands further.

The most common strategies towards diaryl-λ^3-iodanes typically involve two steps. Initially, an aryl iodide specie is oxidized to the iodine (III) equivalent using an inorganic oxidant whilst in the presence of an acid. Following this, a ligand exchange reaction takes place with an arene or organometallic reagent. A key feature of this second step is the electrophilic aromatic substitution (EAS) of the arene by the iodine (III) species, which commonly takes place in the presence of an acid, which then generates the counterion. Regioselectivity is often achieved by employing lithiated, stannylated, silylated aryls and aryl boronic acids. Anion exchange reactions will often be performed to create a more diverse range of counterions or to allow more facile isolation of products.

1.3.4.1 Development of conventional synthetic strategies towards diaryl-λ^3-iodanes

Masson and co-workers made initial gains towards the synthesis of diaryl-λ^3-iodanes in the 1930s.[125] They discovered that diaryliodonium salts could be prepared from reacting iodic acid with a range of aromatic compounds in the presence of sulfuric acid. Significant advancements were made by Beringer and co-workers in the 1950s and 60s, who produced an extensive series of publications on both the synthesis and reactivity of diaryliodonium salts.[122, 126-141] Their approach concentrated on the coupling of arenes with hypervalent iodine species, in the presence of an acid, to yield symmetrical and unsymmetrical diaryliodonium salts, bearing both electron-withdrawing and electron-donating groups (Scheme 25). As expected from EAS reactions, the activating and deactivating nature of the substituents influenced both the reactivity and the yields. Sulfuric acid was required for the synthesis of salts bearing electron-withdrawing substrates[135] whereas the reagent combination of acetic

anhydride and trifluoroacetic acid was found to be most efficient for those with electron-donating groups.[133]

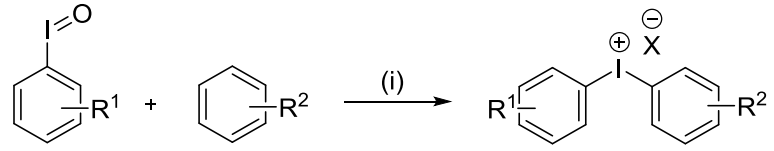

83 **84** **72**

(i) H_2SO_4, or AcOH, Ac_2O, H_2SO_4

Scheme 25: Beringer synthesis of diaryliodonium salts

Regiospecific control in the synthesis of diaryl-λ^3-iodanes was first achieved by Koser and co-workers in the synthesis of diaryliodonium tosylates **87**, generated from the reaction of hydroxy(tosyloxy)iodobenzene (Koser's reagent) with aryl(trimethyl)silanes **85**.[142] It was found that the phenyliodinations proceed with initial cleavage of the carbon-silicon bond, thereby creating regiochemical control, regardless of other substituents (Scheme 26).[142] The regiospecific formation of aryl(2-furyl)iodonium tosylates, has also been achieved, following this approach.[143]

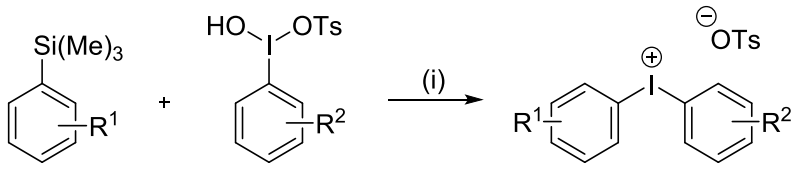

85 **86** **87**

(i) MeCN, Δ

R^1	R^2	Yield
H	H	46%
2-Me	H	42%
3-Me	H	63%
4-Me	H	29%
H	4-Me	30%
2-Me	4-Me	59%
3-Me	2-Me	58%
4-($SiMe_3$)	H	49%
3-($SiMe_3$)	H	24%
4-4'-($SiMe_3$)phenyl	H	27%

Scheme 26: Regiospecific synthesis of symmetrical and unsymmetrical diaryliodonium salts from Kosers reagent and aryl(trimethyl)silanes

Koser later found that the direct condensation of [hydroxy(tosyloxy)iodo]arenes with electron-rich arenes, such as thiophene, can be achieved without the presence of an activating group.[144]

Following this work, Ochiai and colleagues reported the synthesis of diphenyliodonium tetrafluoroborate **89** from the reaction of phenyl(trimethyl)silane **88** with boron trifluoride-activated iodosylbenzene (ISB).[145] ISB is less reactive than Koser's reagent towards nucleophiles and requires activation by a strong Lewis acid. Boron trifluoride-activated ISB is reactive enough towards the nucleophilic attack of **88** to afford the iodine (III) specie (Scheme 27).

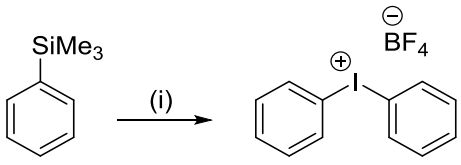

88 **89**

(i) PhIO, BF_3-Et_2O, RT, 21 h
(ii) $NaBF_4$

Scheme 27: Ochiai synthesis of diphenyliodonium tetrafluoroborate from BF_3-Et_2O activated ISB

In 1992, Kitamura *et al* found that ISB could also be activated towards ligand exchange reactions with arenes by using triflic acid.[146] Yields were later improved by using DIB

instead of ISB, thus creating the highly reactive [$PhI(OAc)_2 \cdot 2TfOH$] species *in situ*. Subsequent reactions with electron-rich arenes gave the diaryliodonium triflates in good yields and high *para*-selectivity.[147] Substituted diacetoxyiodoarenes have also been used, thereby generating a range of functionalised unsymmetrical diaryliodonium salts.[148] The approach was also used in the generation of TMS-substituted salts, which serve as synthetically useful agents in the production of benzyne adducts (Scheme 28).[149]

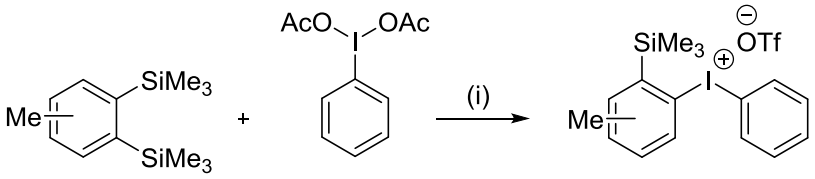

90 **91** **92**

(i) TfOH, CH_2Cl_2, ° 0 C to RT

Scheme 28: Kitamura synthesis of (trimethylsily)-substituted diaryliodonium salts

In efforts to further improve the yield of reactions with phenylsilanes, Stang and co-workers found that the corresponding arylstannanes show increased reactivity towards iodine(III) compounds, due to the decrease in strength of the C-Sn bond. Aryl(cyano)iodonium triflates **95**, prepared in two steps from the aryl iodide **93a** by oxidation with pertrifluoroacetic acid and subsequent reaction with Me_3SiCN were found to react with tributyltin derivatives under mild conditions and in good yields (Scheme 29).[150]

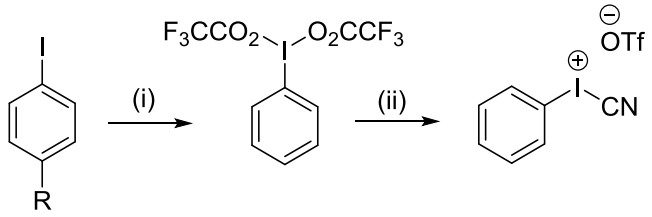

93a (R=H) **94** **95**
93b (R=OMe)

(i) CF_3CO_3H, CH_2Cl_2, -78 °C to RT
(ii) TMSOTf, Me_3SiCN, CH_2Cl_2, RT

Scheme 29: Stang synthesis of aryl(cyano)iodonium triflates

Pike and co-workers have extended this work to include the reaction of Koser's reagent with arylstannanes **96** to produce, both substituted and unsubstituted, diaryliodium tosylates **87** (Scheme 30).[151] This approach was reapplied to form the heteroaromatic diaryl-λ^3-iodanes in excellent yield.[152]

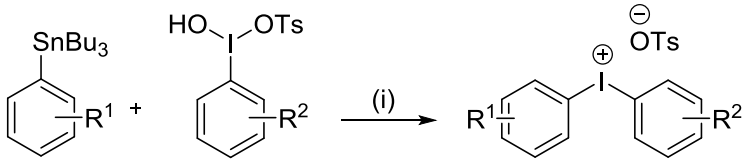

96 **86** **87**

(i) CH_2Cl_2

Scheme 30: Pike synthesis of diaryliodonium tosylates from arylstannanes

Ochiai and co-workers reported a direct, regioselective synthesis of diaryliodonium tetraarylborates from diacetoxyiodoarenes, via the transfer of an aryl group from the corresponding alkali metal tetraarylborate.[153] The tetrafluoroborate salts could be also be obtained following an anion exchange. Following this, the use of vinyl- and arylboronic acids and esters was also successful in generating both symmetric and unsymmetric diaryliodonium tetrafluoroborates via a boron trifluoride catalyzed boron-iodane exchange reaction. Products were reported in excellent yields and with high regioselectivity.[154]

The use of arylboronic acids was initially developed by Widdowson and colleagues.[155] Previous work from within the group involved the regioselective preparation of diaryliodonium salts using aryl-trialkylstannanes as intermediates. However, work turned to the corresponding arylboronic acids for two reasons. Firstly, organotin compounds are toxic and, therefore, use within the group as intermediates in the production of biomolecular imaging agents was undesirable. Secondly, electron-rich aryltrialklystannanes are susceptible to protolysis which creates difficulties upon purification and formation of the diaryl-λ^3-iodane. Treatment of the arylboronic acid with DIB in the presence of triflic acid gave the diaryliodonium triflate whilst reaction with Koser's reagent gave the equivalent tosylate. High yields were achieved before the general applicability of the procedure was tested with heteroaryl boronic acids. Against these reagents, it was found that Koser's reagent allowed for the relatively facile purification of the tosylate salts when compared to the corresponding triflate.[155] Using a similar method, aryltrifluoroborates have been shown to react with aryliodine difluorides to give diaryliodonium tetrafluoroborates.[156]

1.3.4.2 Novel syntheses of selected diaryl-λ^3-iodanes

Stang and co-workers have also developed a novel form of diaryl-λ^3-iodanes, constituting conformationally rigid, tetranuclear macrocyclic ring systems termed, molecular boxes.[157-159] These species have vast potential as anion hosts,[160] and in molecular electronics,[161] nanoscale technology[162] and may also provide insight into non-covalent bonding.[163, 164] The 'T-shaped' geometry of λ^3-iodanes, with approximate 90° bond angles, allow for the formation of novel macrocyclic tetraiodonium salts. The reaction of 4,4'-bis(trimethylsilyl)biphenyl **98** with a bisiodonium triflate **97** in CF_3CO_2H, followed by slow addition of Me_3SiOTf gave the cyclotetraaryltetraiodonium salt **99** in

good yield (70%) (Scheme 31a).[157] Hybrid iodonium-platinum (or palladium) cationic tetranuclear macrocyclic boxes have also been synthesised, some of which have included a chiral biphosphine ligand bound to the metal **100** (Scheme 31b).[157, 158]

a)

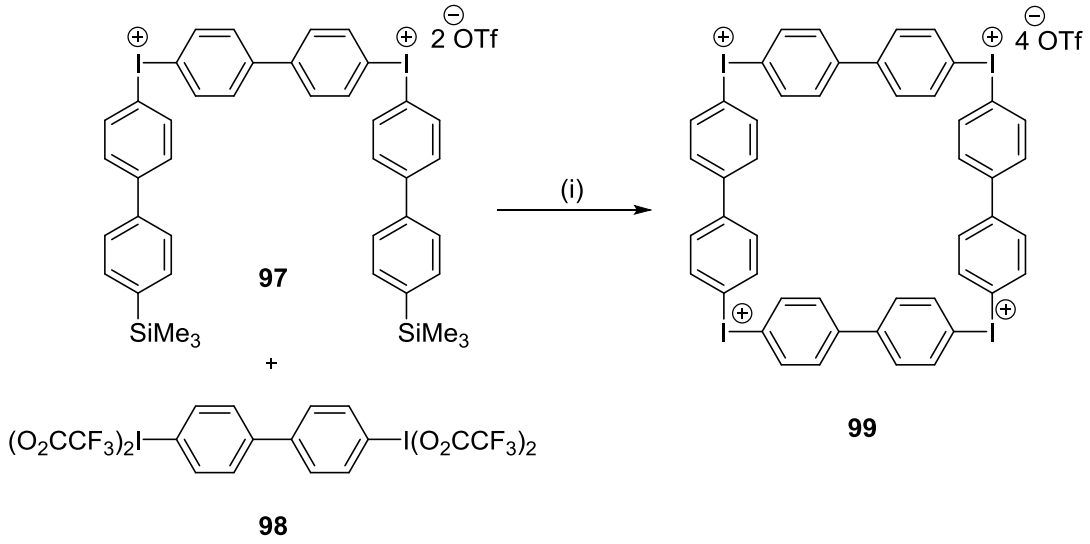

(i) Me_3SiOTf, CH_2Cl_2

b)

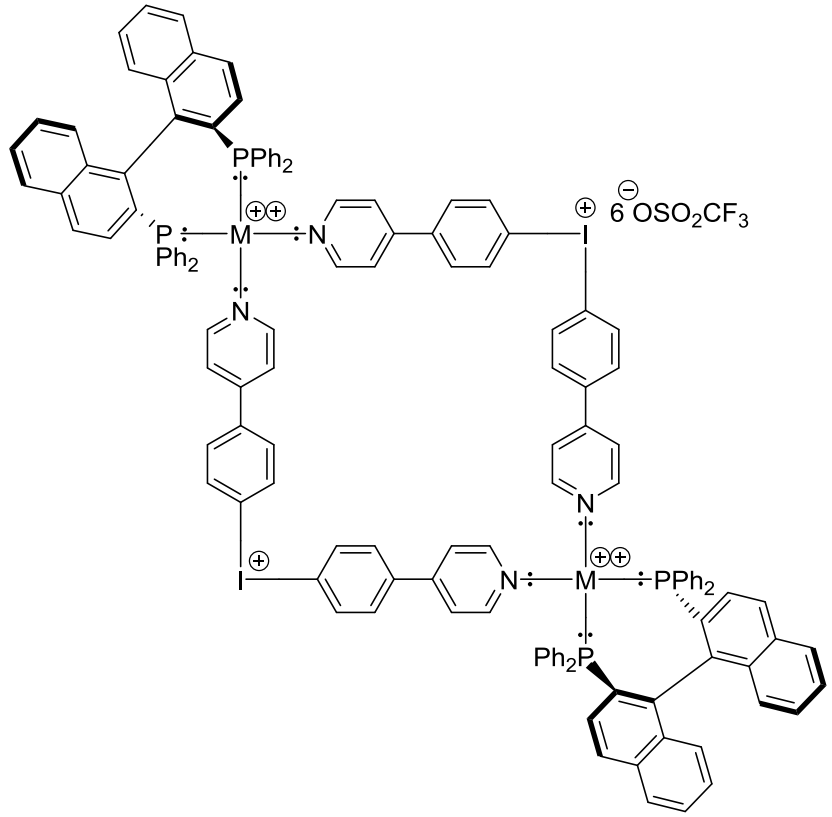

100a M = Pd, 91%
100b M = Pt, 71%

Scheme 31:Diaryl-λ^3-iodanes in the synthesis of molecular boxes[157, 158]

The first synthesis of chiral diaryliodonium salts was achieved by Ochiai and collegues in 1999.[165] Tetraphenylstannane was used in the presence of boron trifluoride etherate, to convert two chiral precursors *i.e.* 2-(diacetoxyiodo)- **101** and 2,2'-bis(diacetoxyiodo)-1,1'-binaphthyls[166] into chiral tetrafluoroborate salts **102** (Scheme 32). Substituted derivatives were also synthesised to in order to achieve the asymmetric α-phenylation of cyclic β-keto esters.

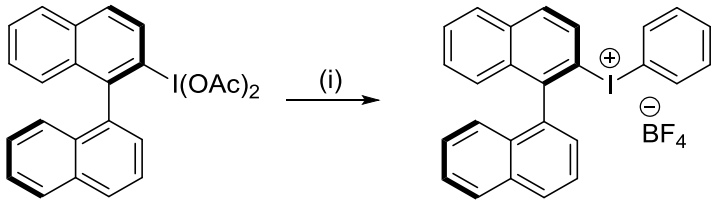

101 **102**

(i) Ph_4Sn, $BF_3.Et_2O$, DCM, RT

Scheme 32: Ochiai synthesis of diaryl-λ^3-iodanes

Using a similar approach, Zhdankin recently reported the synthesis of chiral, benziodazole-derived phenyl- **104** and alkynyliodonium salts, in which nitrogen acts as a ligand attached to the iodine atom (Scheme 33).[167]

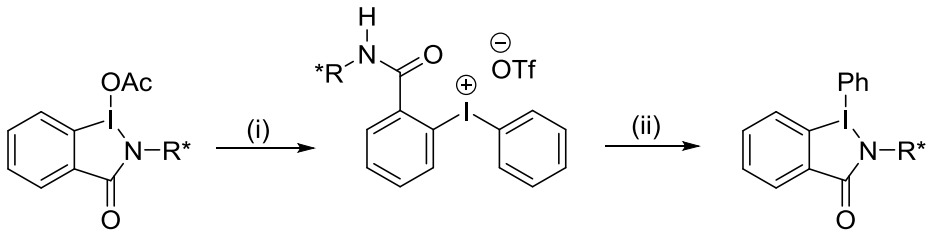

103 **104** **105**

103a/104a/105a R = (*S*)-$CH(CH_3)CO_2CH_3$
103b/104b/105b R = (*S*)-CH(*i*-Pr)CO_2CH_3

(i) $PhSnBu_3$, TMSOTf (ii) $NaHCO_3$

Scheme 33: Zhdankin synthesis of N-functionalized benziodazoles from chiral diaryl-λ^3-iodanes

Most synthetic strategies towards diaryl-λ^3-iodanes involve the use of an acid or acidic media. This limits the use of substrates to those which do not contain acid-sensitive substituents. Beringer and Nathan introduced the synthesis of diaryl-λ^3-iodanes under basic conditions in 1969.[168] Both aryl- and heteroaryliodonium chlorides were synthesised in fair to excellent yields from the reaction of the appropriate aryllithium **107** with the iodonium transfer agent, *trans*-(chlorovinyl)iodonium dichloride **106** (Scheme 34a).[168, 169] This compound, prepared from the reaction of iodine trichloride with acetylene, is very unstable, highly reactive and not commercially available.[168] However, the synthetic application of this approach remains highly valuable as both symmetrical and unsymmetrical salts bearing acid-sensitive substrates can be obtained in a regiospecific manner.[169] Bis(heteroaryl)iodonium chlorides **110**, previously difficult to obtain under acidic conditions, have also been successfully prepared from this iodonium-transfer procedure (Scheme 34b).[170, 171] These compounds may be readily converted to the corresponding triflate salts via reaction with trimethylsilyl triflate.

a)

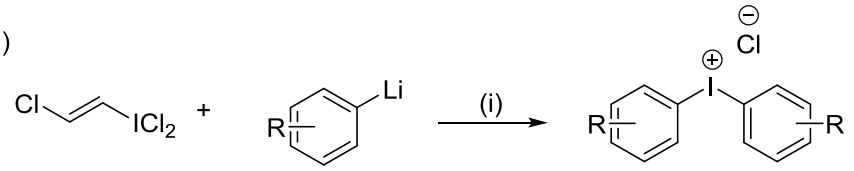

106 **107** **108**

(i) Et_2O, -78 °C to RT

b)

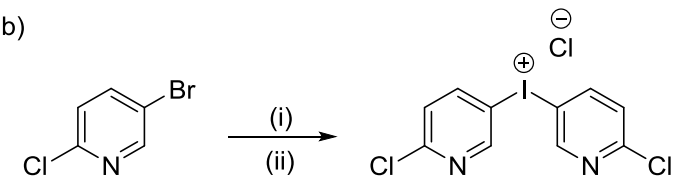

109 **110**

(i) BuLi, Et_2O, -78 °C, 40 min (ii) **106** -78 °C to RT, 4 h

Scheme 34: Reactions of aryllithium reagents with *trans*-chlorovinyliodoso dichloride

1.3.4.3 Recent developments

Vast progress has been made recently in the one-pot, direct synthesis of iodonium salts from arenes with either iodine or aryl iodides in the presence of an oxidant. This approach obviates the isolation of unstable iodine (III) species leading to greater substrate scope whilst reducing reaction times and increasing efficiency.

Significant gains in this field have been recently reported by Olofsson and co-workers. *m*-Chloroperbenzioc acid (*m*CPBA) was previsously identified as an efficient oxidant in the formation of diacyloxyiodoarenes from aryl iodides. It was then envisioned that the same reagent could be employed in the oxidation of aryl iodides to form diaryliodonium salts directly. Treatment of iodobenzene with *m*CPBA and trific acid with excess benzene afforded diphenyliodonium triflate (Scheme 35a).[172] Triflic acid was used to activate the oxidant whilst simultaneously forming the salt. This operationally simple procedure yielded both symmetrical and unsymmetrical salts bearing electron-rich, electron-deficient and heteroatom arenes. Unfortunately, this approach was unsuccessful in synthesising symmetric salts from either very electron-rich or very electron-deficient arenes. However, success was achieved in the synthesis of pyridyl(aryl)iodonium salts, previously only obtainable under basic conditions.

This scope of this method was tested further in attempts to also omit the isolation of aryl iodide species and synthesise the reagents *in situ*, directly from iodine. Diphenyliodonium tosylate was, again, formed in high yield from the reaction of benzene with iodine, *m*CPBA and TfOH in either 10 min (at 80 °C) or alternatively, 22 h at RT (Scheme 35b). Despite a greater scope of products attainable from the use of aryl iodides, the direct synthesis from iodine was further investigated. The latter approach

was found to be efficient in the preparation of iodonium salts bearing alkyl and halogen substituents, exemplified by the synthesis of bis(4-tert-butyl-phenyl)iodonium triflate. Large amounts of reagent were required, however, a 78% yield was achieved in just 45 min.[173]

Following this work, a direct, one-pot reaction yielding electron-rich and symmetrical and unsymmetrical diaryliodonium salts was developed. Toluenesulfonic was used instead of triflic acid resulting in the formation diaryliodonium tosylates in good yields (Scheme 35c). An in situ anion exchange was also developed, allowing for access to the equivalent triflate salts.[174] The same method was successfully reapplied to the direct synthesis of the triflates from iodine, instead of the aryl iodides (Scheme 35d).[174]

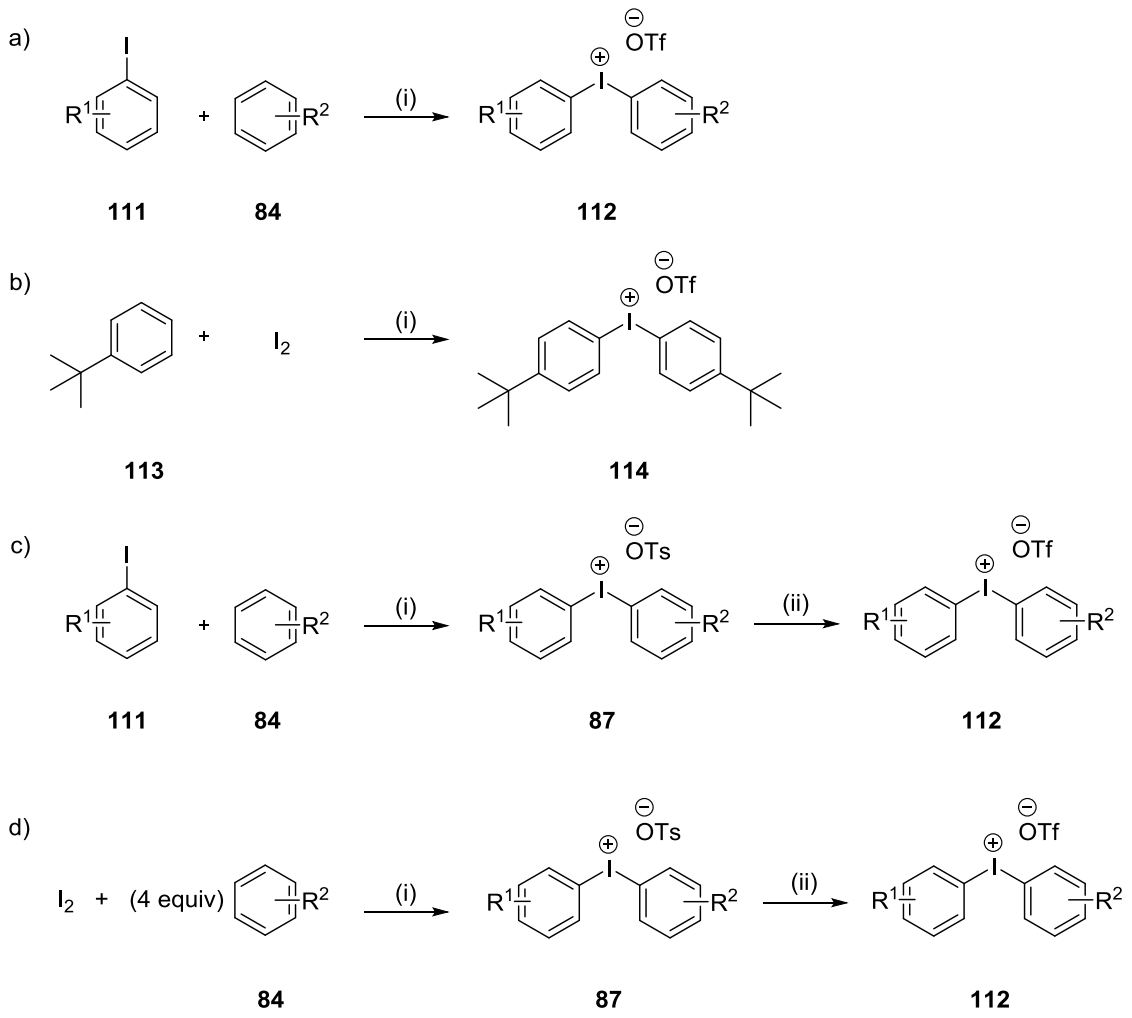

a) (i) *m*-CPBA TfOH, CH_2Cl_2, b) (i) *m*-CPBA (3 equiv.) TfOH (5 equiv) CH_2Cl_2
c) (i) *m*-CPBA, TsOH, CH_2Cl_2/TFE (ii) TfOH, d) (i) *m*-CPBA, TsOH, CH_2Cl_2/TFE (ii) TfOH

Scheme 35: Development of a one-pot synthesis of diaryliodonium salts from the Olofsson group.[172-174]

Recently, the nature of the oxidants employed in these direct, one-pot strategies has received further attention. Conventional routes towards diaryliodonium salts have realised high-yielding and facile syntheses of diaryl-λ^3-iodanes from aryl iodides and the corresponding aromatic partners using stoichiometric amounts of organic and inorganic oxidants. However, large quantities of these reagents frequently result in high levels of toxic by-products and waste material. This is of vital consideration when preforming large scale reactions of this type. The environmentally benign urea-hydrogen peroxide has recently been employed as an oxidising agent in the formation of diaryliodonium triflates[175] and trifluoroacetates.[176] Peracetic acid (PAA) has also

been used with fluoroalcohols, in the synthesis of both unsymmetrical and symmetrical diaryliodonium tosylates and triflates.[177] High yields and short reaction times were achieved from various aryl iodides, except for those bearing an electron-rich moiety, when combined with an electron-rich aromatic partner.

The use of fluoroalcohols in the generation of diaryliodonium salts is a recent development, introduced by Kita and colleagues. A direct condensation route to diaryl-λ^3-iodanes, from reactions of various arenes with Koser's reagent, in both 2,2,2-trifluoroethanol (TFE) and 1,1,1,3,3,3-hexafluoroisopropanol (HFIP) has also been reported (Scheme 36).[178] Both solvents were shown to exert a positive effect upon the efficiency of the dehydrative condensation of hypervalent iodine reagents towards aromatic and heteroaromatic compounds. Short reaction times and high yields were achieved under mild conditions from a variety of electron-rich and unsubstituted aromatic compounds. The high polarity and low nucleophilicity of these solvents allow for the stabilisation of the cationic intermediates proposed to be involved in these reactions.[179]

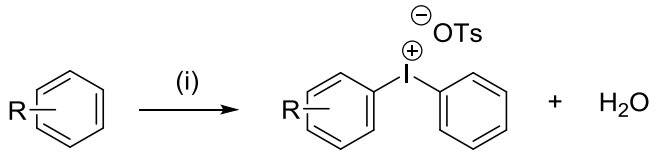

84 **115**

(i) PhI(OH)OTs, TFE or HFIP, RT

Scheme 36: Direct dehydrative approach to diaryliodonium(III) salts in fluoroalcohol solvents[179]

1.4 Radiofluorination of diaryliodonium salts

Diaryliodonium salts have been known to react with nucleophiles in arylation reactions for many years. However, it wasn't until 1982 that van der Puy first explored the use of

diaryliodonium salts to generate aryl fluorides.[180] Since then, these synthetically useful species have become of significant importance to the development of radiolabelled arenes for use in PET. Many studies into the mechanism of the reaction have been conducted. Those presented herein this report are selected examples which best represent the most significant aspects of the process.

1.4.1 Mechanism of nucleophilic substitution of diaryliodonium salts

The ability of diarylhalonium ions to arylate nucleophiles effectively and under mild conditions has been known for many years. However, mechanisms for polar reactions of diarylhalonium salts with nucleophiles remained unclear and an explanation for the so-called "*ortho*" affect (Section 1.2.9) was unaccepted. The ease with which electron-rich species undergo coupling to a nucleophile suggested a mechanism other than direct nucleophilic substitution. In 1992, Grushin and co-workers proposed a "turnstile mechanism" (Figure 15) to rationalise many of the anomalous facts associated with the reactivity of diaryliodonium salts with nucleophiles.[181]

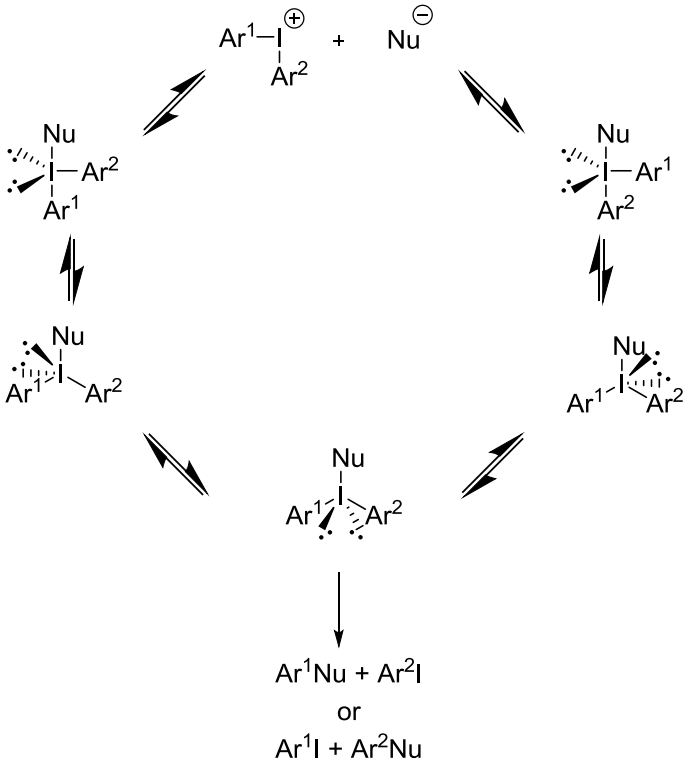

Figure 15: Turnstile mechanism proposed by Grushin.[181]

By investigating the reactivity of halonium derivatives of the quasi-aromatic inorganic systems, greater understanding of the mechanism of the reaction between diaryliodonium salts and nucleophiles was achieved. The nucleophile attacks the positively charged iodine atom of the iodonium cation **116** to form a trivalent intermediate following ligand exchange of the counterion. Rapid Berry-pseudorotation occurs between intermediates, which leads to two differing transition states **117** and **118**. These transition states undergo a ligand coupling to collapse via reductive *syn*-elimination to form two pairs of possible products **121** and **122** or **123** and **124**. The "*ortho*" affect is explained as the resulting relief of steric strain in the transition state due to the more bulky group aryl substituent occupying an easily attacked equatorial position. The predominant conformation places the *ortho*-substituted aryl ligand and the two lone pairs (or 'phantom' ligands) in the equatorial positions. Ligand coupling leads to the *syn*-reductive elimination and the transfer of the attacking nucleophile to

the *ortho*-substituted aryl ring. In the absence of *ortho*- substituents, the favoured transition state places the most electron-rich ring in the axial position to stabilise the positive charge on the iodine. This results in the formation of the major products wherein the nucleophile is selectively incorporated onto the more electron-deficient ring which, therefore, adopts the equatorial position.[182]

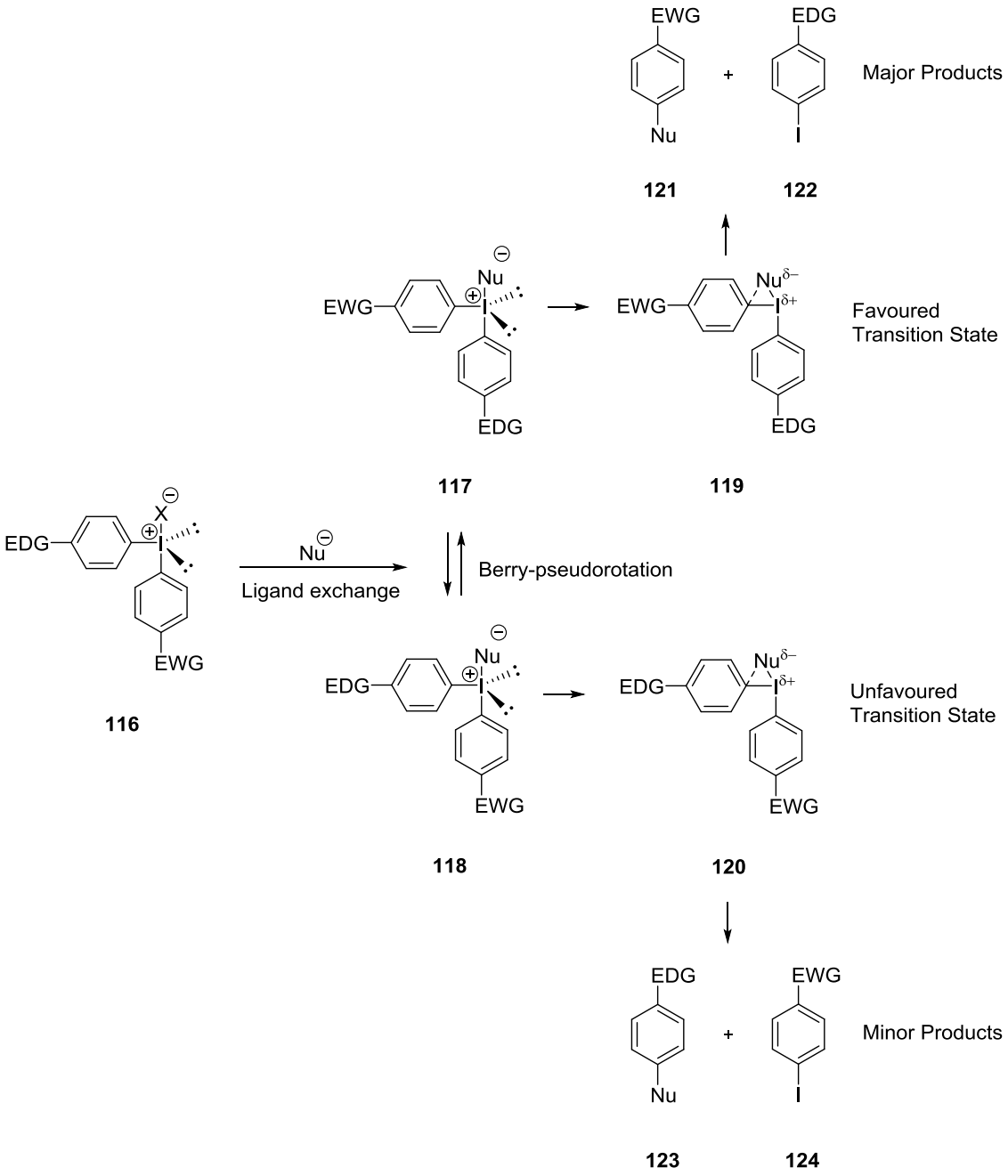

Scheme 37: General mechanism for the attack of nucleophile on a diaryliodonium salt[183]

The "*ortho*" affect is the dominant influence as *ortho*-substituted aryl ligands have been shown to couple to the nucleophile despite being the more electron-rich of two aromatic rings.[57]

1.4.2 Regioselectivity in reactions of diaryliodonium salts with fluoride

This understanding of the mechanism of nucleophilic attack on a diaryliodonium salt has been used to influence the regioselectivity of the aromatic substitution process. Modifying the electronic and steric properties of the substitutents may be used to maximise the yield of the desired products. This is essential when using fluorine-18 which can only be produced in nano-molar quantities forcing radiosynthetic precursors into a vast excess. Pike and colleagues first reported a study on the synthesis of [^{18}F]fluoroarenes from the reaction of cyclotron-produced [^{18}F]fluoride ion with diaryliodonium salts (Scheme 38).[54] A range of diaryliodonium salts bearing various substituents were reacted against NCA [^{18}F]fluoride in MeCN and at 85 °C inside a sealed and pressurised glassy-carbon vessel.

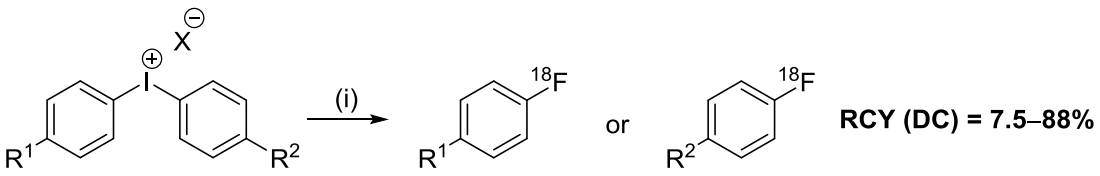

125 **126** **127**

R^1 = H, OMe
R^2 = H, Me, Cl, OMe
X = Cl, OTs, Br, TFA

(i) [^{18}F]KF/K222, MeCN, 110 °C, 35 min or 85 °C, 40 min

Scheme 38: Pike radiosynthesis of various [^{18}F]fluoroarenes[54]

Generally, the reactions proceeded with attack on the most electron-deficient ring. However, the presence of large substituents altered the regioselectivity of the reaction by promoting the [^{18}F]fluorination of the more bulky but electron-rich ring. For

example, the reaction of 2,4,6-trimethylphenyl(phenyl)iodonium triflate with the [^{18}F]KF/Kryptofix®222, gave 2,4,6-trimethyl[^{18}F]fluorobenzene as the sole fluorinated product, along with the iodobenzene byproduct. However, the authors reported that the critical factor appears to be the bulk at the *ortho*-position and that a single *ortho*-substituent is enough to induce incorporation of the nucleophile on the substituted ring. This is in-keeping with the turnstile mechanism proposed by Grushin (Section 1.4.1).[181] In further studies, combining an *ortho*-substituted ring with an electron-rich ring was shown to be a simple means of regiocontrol in [^{18}F]fluorinating diaryliodonium salts.[148] Reactions wherein the diaryliodonium salts were substituted with a 3- or 4- alkoxy group on one ring and alkyl groups on the other gave only the alkyl[^{18}F]fluoroarenes when fluorinating using [^{18}F]fluoride (Scheme 39).

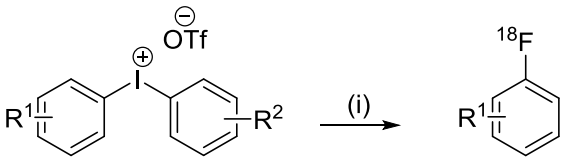

128 **129**

(i) [^{18}F]CsF, MeCN, 85 °C, 40 min

R^1	**R^2**	**RCY (DC) (%)**
2-CH_3	4-OCH_3	64
3-CH_3	4-OCH_3	66
2,4,6-CH_3	4-OCH_3	67
3,5-CH_3	4-OCH_3	45
4-$(CH_3)_3CCH_2$	3-OCH_3	66

Scheme 39: Pike syntheses of [^{18}F]fluoroarenes from unsymmetrical diaryliodonium salts. In all cases, the [^{18}F]fluoroarene **129** was the sole [^{18}F]fluorinated product.

Heteroaryl ligands have also been found to direct the attacking the fluoride nucleophile to the target ring of a heteroaryl(aryl)iodonium salt. Carroll and co-workers used various heteroaromatics and benzoheteroaromatics as the non-target ring (NTR) to demonstrate the fluorination of arylheteroaryliodonium salts.[152] The work confirmed predictions made by computational techniques used to deduce the outcome of the fluorination of heteroaryl(aryl)iodonium tosylates. It was found that simple heteroaromatics (furan, thiophene and *N*-methylpyrole) promote the incorporation of fluoride onto the electron-deficient phenyl ring to produce fluoroarene. Coenen and coworkers then used the 2-thienyl group to direct the radiofluorination of various arenes using NCA [^{18}F]fluoride.[184] The 2-thienyl group is electron-rich and less sterically demanding than a phenyl ring which allows the introduction of [^{18}F]fluoride onto less electron-rich arenes, such as anisole, in one convenient step (Scheme 40).

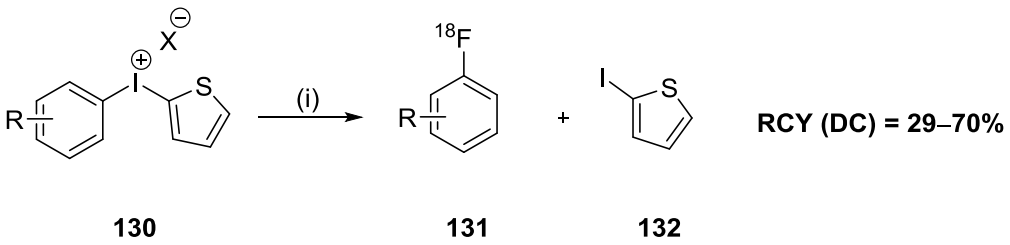

130 **131** **132**

R = 4-OBn, 4-OMe, 4-Me, H, 3-OMe, 4-Cl, 4-Br, 4-I, 2-OMe
X = OTf, OTs, Br, I

(i) [^{18}F]KF/K222, DMF, K_2CO_3 130 °C, 40 min

Scheme 40: Regioselective nucleophilic fluorination of 2-thienyl(aryl)iodonium salts[184]

When the target ring was also electron-rich (relative to benzene) the best results were achieved using 2-methoxyphenyl(2-thienyl)iodonium bromide which afforded 2-methoxy-[^{18}F]fluorobenzene in 60% RCY within 20–30 min. The authors reported that only the desired [^{18}F]fluoroarenes were produced with no evidence of a

radiofluorinated side-product. This in contrast to the later work of Carroll and co-workers, who also carried out a detailed study of nucleophilic fluorination of aryl(thienyl)iodonium salts.[185] By analysing the crude reaction mixture of diaryliodonium salt reactions by GC-MS, multiple products were detected (Scheme 41) strongly suggesting that the process may not be as selective as previously reported. Fluorination of 2-thienyl(phenyl)iodonium tosylate revealed the generation of the iodoaryl products and those resulting from nucleophilic attack of the counterion on the iodonium cation.

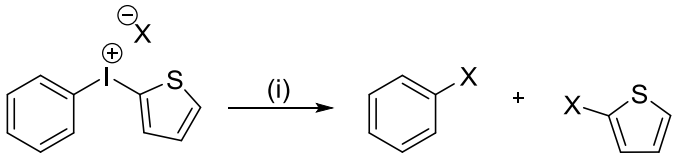

133 **134** **135**

X = F, I, OTs

(i) CsF, DMF, 130°C, 1.5 h

Scheme 41: Multiple products generated from the fluorination of 2-thienyl(phenyl)iodonium tosylate.[21]

Radiofluorination of 2-thienyl(phenyl)iodonium tosylate was clearly shown to produce [^{18}F]2-[^{18}F]fluorothiophene as well as [^{18}F]fluorobenzene. Previous reports describing no production of 2-fluorothiophene were conducted in open vessels at elevated temperatures and may therefore be misleading and the apparent absence is most likely due to the high volatility of 2-fluorothiophene (boiling point 82 °C) which may be lost during work-up/analysis. The authors also found that 2-fluorothiophene can be very difficult to detect by HPLC and GC, having the tendency to co-elute with other fluoroarenes or the injection solvent. The compound is also unstable and has limited UV activity making detection by TLC both difficult and inconsistent.

Due to the difficulties associated with the use of the 2-thienyl aromatic ring, alternative electron-rich species have been used to synthesise target [^{18}F]fluoroarenes. Fluoropyridines have found increasing applications in PET as radiolabelling with fluorine-18 can be readily achieved in the 2- and 6- positions via nucleophilic aromatic substitution. However, fluorine may be labile in this position thereby reducing the potential applications of the imaging agent. The 3-labelled regioisomer is considerably more difficult to synthesise via the same approach but may benefit from enhanced metabolic stability. Carroll and coworkers used 4-methoxyphenyl(heteroaryl)iodonium salts **136** and **138** to generate 3-[^{18}F]fluoropyridine **137** and 3-[^{18}F]fluoroquinoline **139** in good RCYs (55–63% and 22–25%, respectively) (Scheme 42).[78] The authors found that the desired products were the only fluorinated compounds produced and, therefore, the use of 4-methoxyphenyl as the NTR provided sufficient selectivity for the process.

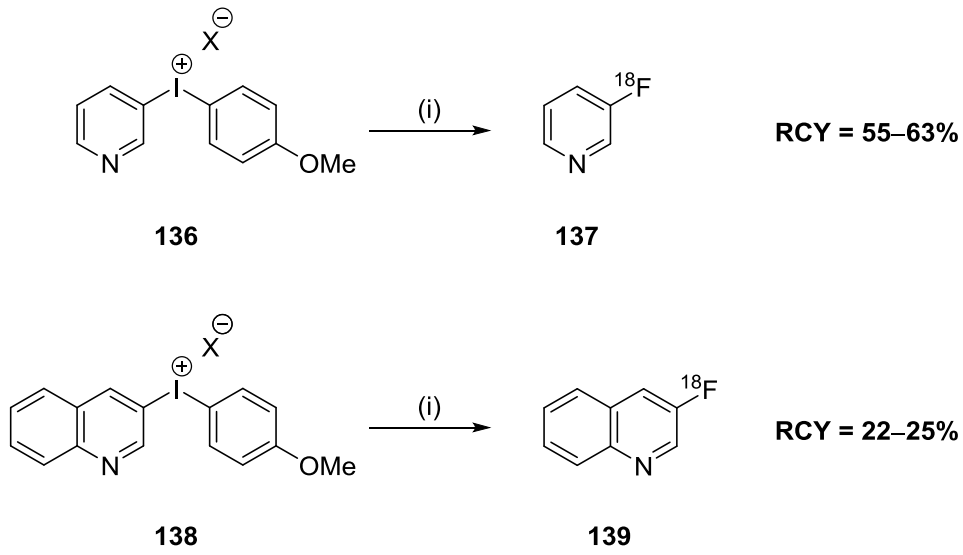

X = OTs or OTf

(i) [^{18}F]KF/K222, Δ, 30 min

Scheme 42: Preparation of 3-[^{18}F]fluoropyridine and 3-[^{18}F]fluoroquinoline.[78]

Pike and colleagues have also, more recently used the 4-methoxyphenyl ring to produce a range of substituted [^{18}F]fluoroarenes from the corresponding tosylates using a microreactor.[186] Excellent yields were recorded when performing reactions in DMF with 0.25% H_2O at 150 °C for 181 s. The rapid reaction times and temperatures are made possible by the use of a microfluidic device which combines reagents under high pressure through micro-sized channels. Interestingly, the work also showed that fluorinations of diaryliodonium salts were achievable in good yields in the presence of a large amounts of water and without the use of a cryptand to prepare the [^{18}F]fluoride.[186]

1.4.2.1 The "Ortho" Affect

As described earlier (Sections 1.2.9 and 1.4.1) the incoming nucleophile will preferentially be incorporated onto the aryl ring bearing a bulky *ortho*-substituent.[57, 58] Pike and co-workers were first to report the application of the "*ortho*" affect in the radiofluorination of simple arenes.[55] Through a detailed study involving the fluorination of various diaryliodonium salts, the regioselectivity was shown to be controlled by electronic factors and by the bulk of *ortho*-substituents on the rings, with the latter being the dominant factor. Generally, reactions proceeded by attack on the most electron-deficient ring, however, the introduction of steric bulk altered the regioselectivity with nucleophilic attack favouring the ring bearing a substituent in the *ortho*-position. A single *ortho*-substituent was shown to be sufficient to induce attack on that ring.[55]

This principle has been extensively studied by Pike and co-workers, again, using a microreactor to rapidly synthesise *ortho*-substituted [^{18}F]fluoroarenes from reactions with diaryliodonium salts.[80] The diaryliodonium salt (2-methylphenyl)(phenyl)-

iodonium, bearing either the bromide, chloride, iodide or tosylate ions were reacted with NCA [^{18}F]fluoride, in different solvents at temperatures of up to 200 °C and reaction times of up to 4 min. Each salt produced higher RCYs when using DMF as opposed to either MeCN containing a small proportion of water (1.5%) or, for one particular salt, anhydrous MeCN. The bromide and tosylate salts produced almost quantitative incorporation of [^{18}F]fluoride whereas incorporations were significantly lower using the iodide and chloride. Most importantly, in all reactions, [^{18}F]fluorotoluene was the major radioactive product and [^{18}F]fluorobenzene was the minor radioactive product with selectivity ranging from 2.00 to 3.00. These results strongly support the "*ortho*" affect hypothesis and that a simple methyl substituent can induce strong selectivity. In order to gain further understanding, the study was extended to a broader range of diaryliodonium salts bearing different *ortho*-substituents. Radiofluorination of each salt was performed using either CA or NCA [^{18}F]fluoride in either anhydrous or "wet" DMF. Conditions for each reaction were optimised to produce impressive RCYs ranging from 51% to 95% (Scheme 43).

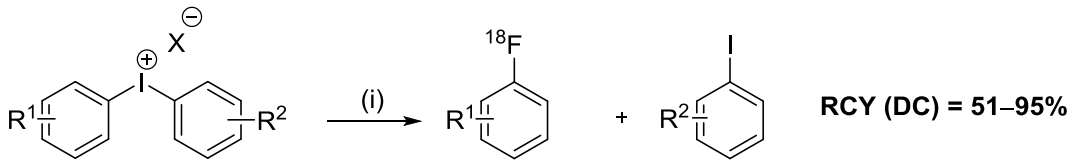

140 **141** **142**

R^1 = 2-H, 2-Me, 2-OMe, 2-Br, 2,6-di-Me, 2,4,6-tri-Me
R^2 = 2-H, 2-Me, 2-OMe, 2-Et, 2-^{i}Pr, 2-Me, 2,4,6-tri-Me
X = Cl, OTs

(i) CA/NCA [^{18}F]KF/K222, DMF or DMF with 0.25% H_2O, 110 °C to 190 °C, 188 s or 236 s

Scheme 43: Pike radiosynthesis of various *ortho*-substituted diaryliodonium salts[80]

From the selectivity values produced, the authors were able to deduce that the power of *ortho*-substituents to impart an "*ortho*" affect was in the following order: 2,6-di-Me

> 2,4,6-tri-Me > Br > Me > Et ≈ ^{i}Pr > H > OMe. Interestingly, an *ortho*-methoxy substitutent failed to induce any selectivity as 2-[^{18}F]fluoroanisole was consistently the minor radioactive product, across the study. This shows that the "*ortho"* affect is not purely related to substituent bulk, as suggested by previous studies which have focused on *ortho*-alkyl substituents. The authors propose that the selectivity may be enhanced by the presence of one or more hydrophobic groups (*e.g.* methyl) thus creating a lipophilic microenvironment in which the attacking [^{18}F]fluoride ion can act as a powerful nucleophile. The fluoride weakens the aryl carbon-iodine bond before attacking the locally lipophilic *ortho*-substituted ring. Substituents with a positive inductive effect (*e.g.* methoxy) oppose this process, whilst substituents with a negative inductive effect (*e.g.* bromide) reinforce it. These are important factors to consider when determining the product selectivity of such reactions.

By applying the "*ortho*" affect, DiMagno and coworkers have found that even exceptionally electron-rich arene rings can be fluorinated with high regioselectivity by the reductive elimination reaction of 5-methoxy[2.2]paracyclophan-4-yl-iodonium salt **143** (Scheme 44) .[187] The authors sought to investigate a potential aryl substituent which would result in the stereoelectronic control of unidirectional reductive emilination (SECURE) from diaryliodonium salts. They hypothesied that if the mechanistic assumption of a concerted reductive elimination process is adopted, then selective destabilisation of the transition state requires significant steric congestion above and/or below the aromatic ring and little steric congestion in the plane of the ring. This was achieved using the [2.2]paracyclophane moiety which induces severe, out-of-plane steric congestion resulting in the ability to control the nucleophile incorporation of the even exceptionally electron-rich arenes (Scheme 44). By

combining the steric and electronic effects, the selectivity of the reductive elimination step has been enhanced. However, complex synthetic prodecures are required to generate the salts bearing the [2.2]paracyclophane rings. This is especially taxing when the target ring is highly functionalised.

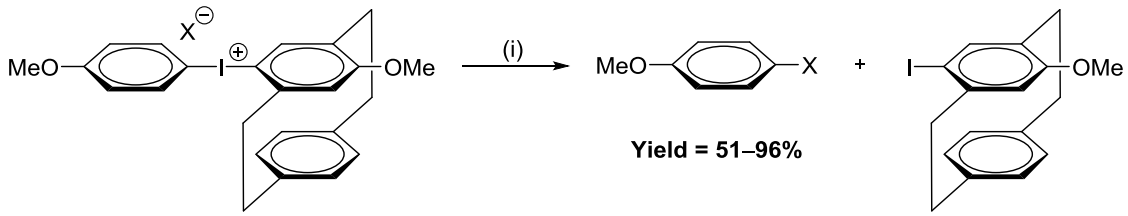

143 **144** **145**

X = N_3, OAc, OPh, SCN, SPh

(i) TBA/NaX, MeCN, 45–80 °C

Scheme 44: Anisole functionalisation by thermal decomposition[187]

1.4.2.2 Mechanistic Studies

Togni and coworkers have tried to gain a greater understanding of the factors which govern the selectivity of the reductive elimination reactions involving a diaryliodonium salt and a nucleophile.[188] The stationary points of the reaction pathway of a diaryliodonium salt bearing a phenyl and anisyl ligand attacked by a bromide nucleophile were calculated using density functional theory (DFT).

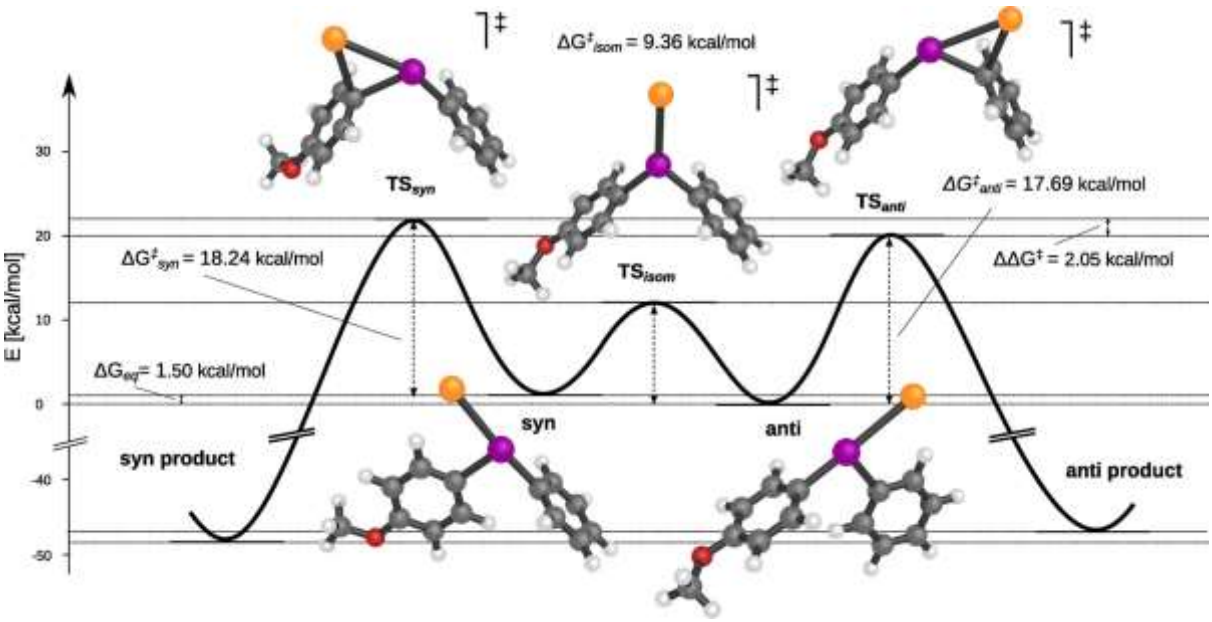

Figure 16: Reaction profile of bromo-4-methoxyaryl-phenyl-iodane giving the relative barrier heights ΔG‡ and their absolute differences ΔΔG‡ expressed in terms of Gibbs free energy. Stationary points of the structures are also included. Taken from [188].

As depicted in the diagram, the reaction of the diaryliodonium salt with the nucleophile leads to two T-shaped iodane isomers (TS_{syn} and TS_{anti}) which are connected by a Y-shaped transition state (TS_{isom}). The ensuing *ipso*-attack of the bromide leads to incorporation into either the anisyl of phenyl ring. The reductive elimination process begins with one of the two possible iodane isomers. The energy barrier to isomerisation is small leading to a fast equilibrium between species which is followed by the rate-determining reductive elimination steps to yield the products. The selectivity, therefore, is determined by the difference in energy of the barriers to reductive elimination between the two possible iodane transition states. This is representative of the Curtin-Hammett principle.

The selectivity predicted for the reaction depicted (Figure 16) was in qualitative agreement with the experimental result. The calculated barrier leading to the phenylbromide was 2.05 kcal/mol lower in energy, showing that this product is favoured, which is reflected in the experimental ratio of the products (9:1).

As the hypervalent iodine bond is clearly involved in both possible reductive elimination reactions, the authors hypothesised that the properties of this bond are likely to influence the selectivity observed. The partial charges of the *ipso*-atoms were obtained from a natural population analysis and used to the compare the polarity of the 3c-4e bond in the *syn*- and *anti*-isomers. The partial charge on the iodine atom was close to +1.0 in both isomers and is compensated by the negative partial charges on the ligand *ipso*-atoms in the 3c-4e bond. The relevant difference in the polarity of the 3c-4e bond was found to lie in the *ipso*-carbon atom of the aryl ligands. Upon discovering this, the authors investigated the relationship between the polarity of the 3c-4e bond and the outcome of the reductive elimination step. A plot of the partial charge differences between the *ipso*-carbon atoms against the corresponding theoretical selectivity ($\Delta\Delta G‡$) revealed that the greater the difference between the partial charges of the *ipso*-carbons, the more pronounced the selectivity (Figure 17). Experimental selectivity was found to confirm these predictions. There were, however, several cases which did not follow this trend. Further investigation revealed that these instances involved aryl ligands bearing bulky substituents further demonstrating the role steric hindrance plays in the selectivity of this reaction. Furthermore, the authors also noted that the polarity of the 3c-4e bond corresponds to the experimental Hammett σ-parameters associated with that directing group.

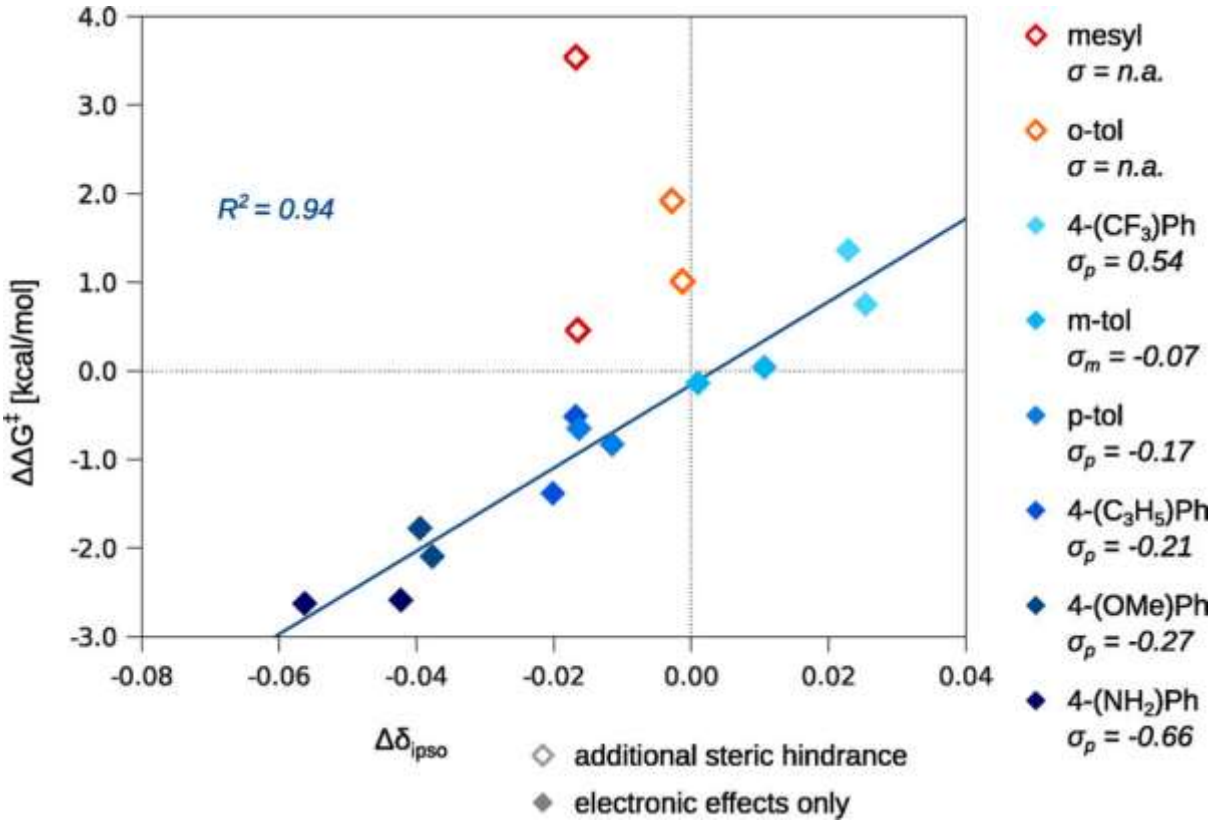

Figure 17: Theoretical selectivity $\Delta\Delta G\ddagger$ for the functionalization of a phenyl group using different directing groups (X = N_3 or Br) plotted against the natural charge differences of the ipso-carbon atoms of the aryl ligands in the 3c-4e bond. For each group, the Hammett σ-parameters are also shown. Taken from [188].

1.4.2.3 Evidence to support the formation of bridged dimers and trimers

Carroll and co-workers have found, through computational chemistry studies on crystal structures of dialkynyl iodonium fluorides, that R_2I-F is expected to form a stable dimer involving a novel unsymmetrical bridge.[189] The reactivity of this dimer is similar to that of the corresponding monomeric units. Interestingly, this dimer formation provides a previously unconsidered, low energy pathway for interconversion of the aryl groups, which shows that the specificity of these reactions is purely transition state controlled.

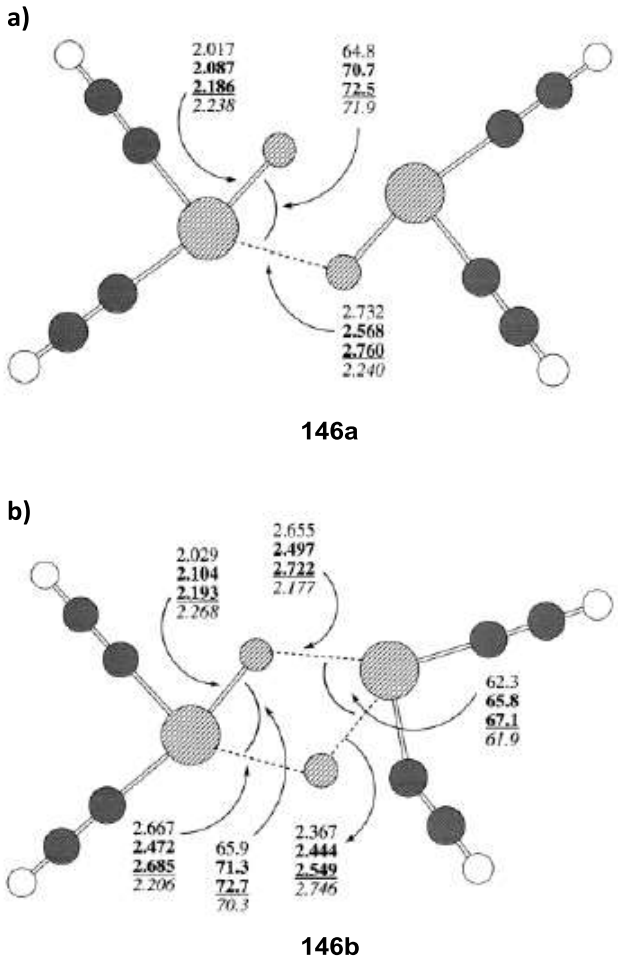

Figure 18: Geometry (distances in Å and angles in degrees) for (a) the ground state and (b) the transition state of dialkynyl iodonium fluoride. Taken from [189].

Due to the relatively large values for the dimerisation enthalpies, this work was extended to investigate higher oligomers.[190] Results based on both the enthalpies and estimated entropies and the derived free energies revealed that large concentrations of trimeric reactants may be possible in the gas phase and, most interestingly, in polar organic solvents such as MeCN. The structure of the trimer is in contrast to the dimer, in that it may be purely symmetrical.

This may also suggest an entirely entropically-controlled pathway for axial-equatorial interconversion of the ligands. The authors suggest, therefore, that the monomer-based "turnstile" mechanism proposed by Grushin[181] (Section 1.4.1) may have a competing pathway. The authors have also proposed that the transition state for

disproportionation to R-I and R-F derived from this trimer displays unusual coordination around the reacting fluorine, which suggests enhanced stabilisation via this pathway. This stable transition state would therefore become a competitive reaction species. This becomes particularly important in fluorine-18 reactions where the fluoride is present in minute quantities compared to other counterions, which may participate in these cyclic structures.[190]

Pike and coworkers have conducted mechanistic studies which support the formation of bridged dimers in less polar organic solvents, where most reactions involving diaryliodonium salts are conducted.[191] Previous studies have shown that diaryliodonium salts are fully dissociated in aqueous or polar media[122] whilst existing as anion-bridged dimers held together by iodine-halogen bonds in solid-state structures.[115, 192] The X-ray structure of an unsymmetrical diaryliodonium salt, 2-methylphenyl(2-methoxyphenyl)iodonium chloride **147** (Figure 19) was determined and shown to have a conformational dimeric structure with the hypervalent iodine as a stereogenic centre in both conformers. Quantum chemical calculations suggested that **147** exists as dimers in MeCN due to the strong secondary bonding interaction between the iodine and Cl atoms in the two enantiomeric forms. This arises from the I-Cl bond which is primarily ionic due to the bond length being 0.64 Å longer than in solid $PhICl_2$ (2.46 Å). These calculations appear consistent with LC-MS data which showed that dimeric and tetrameric anion-bridged clusters were present in dilute organic solution. The authors have suggested that reactions of similar compounds with nucleophiles may require dissociation of the dimers or tetramers to promote the replacement of chloride ions with fluorine-18 and therefore produce the desired compounds.

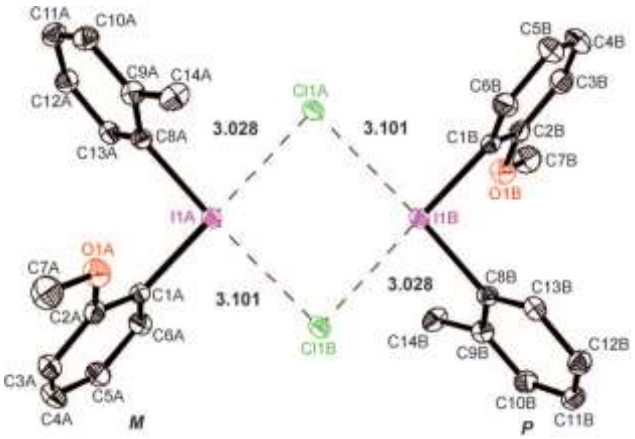

147

Figure 19: X-ray crystal structure of dimeric 2-methylphenyl(2-methoxyphenyl)iodonium chloride **147**, represented in an ORTEP drawing. Some bond distances are given. Iodine atoms A and B represent to two conformational monomers M and P, respectively. Taken from [191].

1.4.2.4 Evidence to support nucleophilic aromatic substitution

It has been suggested that the reaction mechanism may involve nucleophilic aromatic substitution, a theory which has been investigated by Coenen and co-workers who used different substituted aryl(2-thienyl)iodonium salts to systematically vary the electron-density of the target ring and study the mechanism of nucleophilic fluorination.[184] Investigating the effect of substitution patterns of the target ring against RCYs clearly demonstrated the gain in RCYs induced by the "*ortho*" affect. Yields were considerably higher than para- and meta- substituted target rings with the latter generating the poorest yields. An optimum precursor concentration of 25 mmol/L was suggested for working with aryl(2-thienyl)iodonium salts. A more detailed insight into the influence of electronic character on the nucleophilic radiofluorination was obtained by comparing aryl(2-thienyl)iodonium bromides with substituted phenyl rings of differing electron densities. As expected, the RCY generally increased with a decrease of the electron density, the exception being the *ortho*-methoxy derivative. Plotting the reaction rates of the radiofluorinations against Hammett substituent constants of the groups present on the target ring, reveals a linear relationship

corresponding to the inference of an S_NAr mechanism for the nucleophilic fluorination on aryl(2-thienyl)iodonium salts. The authors also found that DMF was the best solvent, which was to be expected as polar, aprotic solvents promote S_NAr reactions. The optimal temperature was 130 °C with higher temperatures producing lower yields, most likely due to the thermal decomposition of the precursors.

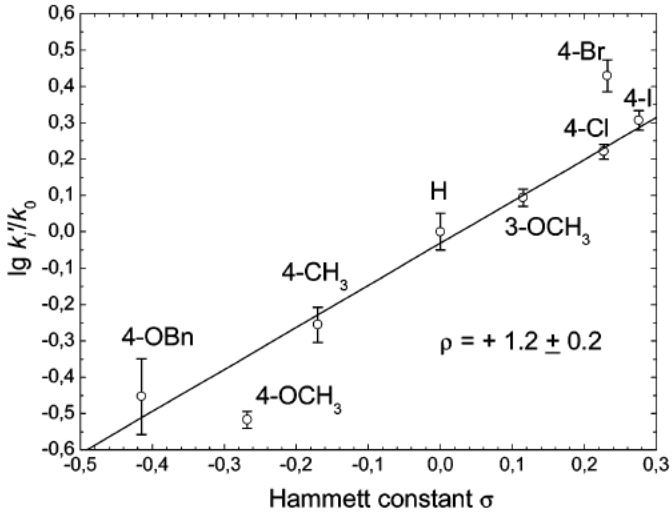

Figure 20: Hammett diagram for the radiofluorination on substituted aryl-(2-thienyl)iodonium bromides (130 °C in DMF). Taken from [184].

As *ρ* (the reaction constant) is positive, the reaction is favoured by electron-withdrawing groups, which is also in accordance with the S_NAr hypothesis. However, it was noted that due to the high reactivity of *ipso*-aryl carbon, the fluorination reaction has a low sensitivity to substituent effects in the *para*-position.[184]

Pike and colleagues have studied the radiofluorination of diaryliodonium tosylates under aqueous and cryptand-free conditions. Salts with strong electron-withdrawing substituents in either *para* or *ortho* position gave moderate yields of the desired [^{18}F]fluoroarenes. These reactions, therefore, strongly resemble S_NAr reactions of non-hypervalent substrates. Various *meta*-substituted salts were also tested, RCYs did not increase with Hammett values and a mixture of weak electronic and steric effects are

believed to be in effect. Interestingly, the authors also found that moderate RCYs were achievable when the reaction solvent had a water content of up to 28% and whilst no cryptand was used to prepare the nucleophilic fluoride.[186]

1.4.2.5 Evidence to support a free radical reactivity

The use of free radical scavengers have been shown to promote the reproducibility of RCYs achieved from the radiofluorination of diaryliodonium salts. Carroll and co-workers had observed a large variation in the outcome of these reactions, especially when using particularly electron-rich precursors.[193] Diaryliodonium salts are known to undergo various reaction pathways (Section 1.3.3) which include homolytic fission of the aryl iodine bond generating aromatic radicals that may initiate undesired chemistry. During initial scoping studies on the crude reaction mixture of the fluorination process, a selection of protonated products (*e.g.* anisole) and biaryl materials were shown by GC-MS analysis to be present in large amounts. In order to reduce the potential for the homolytic pathway to generate such unwanted products by *in situ* generated radicals, a range of radical scavengers were tested. The authors found that the use of a radical scavenger significantly improved the reproducibility of the fluorination process, especially when using 2,2,6,6-tetramethylpiperidine 1-oxidanyl (TEMPO). Interestingly, the material yields of the fluoroarene products also were substantially increased whilst zero loss to the selectivity of the process was observed. This work strongly promotes the suggestion that a homolytic reaction pathway is prevalent during the fluorination process, and that using a free radical scavenger reduces the variability of reaction results and promotes reproducibility.

Other groups have had mixed results. Pike and co-workers studied the nucleophilic fluorination of diaryliodonium tosylates in the preparation of *meta*-substituted arenes

bearing either electron-donating or electron-withdrawing substituents. The authors found that high and consistent RCYS were obtained in the absence of TEMPO (up to 93% RCY (DC)). However, when this investigation was translated to the radiosynthesis of more complex 3-[^{18}F]fluoro-1-[(thiazol-4-yl)ethynyl]benzenes, the presence of TEMPO improved reaction yields (up to 2.5-fold greater) whilst retaining product selectivity. The authors commented that the benefit of adding TEMPO may depend on the structure of the diaryliodonium salt precursor and the consequent susceptibility to radical induced decomposition. Diaryliodonium salts are known to be photosensitive[194] and have been used as photoinitiators in polymerisiation reactions.[96] The microreactor used in this work conducts reactions in the dark thereby potentially suppressing photolytic decomposition of the precursors. However, upon scaling-up the reactions to activities suitable for imaging studies, TEMPO had no effect upon reactions conducted using the microreactor. Upon repeating experiments in an automated batch reactor, yields were improved when in the presence of TEMPO. These varied results show that the benefit of using free radical scavengers is as yet unexplained and further investigation into the presence of a homolytic reaction pathway is needed.

1.4.2.6 Effect of counterion

The anion used in diaryliodonium salts is known to strongly effect the reaction outcome with the highest RCYs arising from the use of inorganic anions. These ions induce an effective ion-pair separation in polar solvents[113, 122] but it has also been shown that dimeric and trimeric structures are possible in salts bearing these counterions in polar solvents.[189, 190] A fully dissociated iodonium cation is favourable for nucleophilic attack by fluoride, however, anions with high nucleophilicity compete with the attacking nucleophile. Conversely, organic counterions are less reactive but

exhibit a more pronounced covalent character which induces steric and electronic effects local to the iodine centre. A preliminary step becomes necessary in which the attacking fluoride must exchange with the organic counteranion before it can form a trigonal-bipyramidal transition complex by which the proposed "turnstile" mechanism proceeds. Coenen studied the RCYs obtained by reacting [^{18}F]fluoride with 2-methoxyphenyl(2-thienyl)iodonium salts in DMF at 130 °C whilst varying the counterion.[184] The results showed that the bromide derivative gave the highest yield, proving the aforementioned hypothesis, whilst tosylates produced the lowest. Triflates produced surprisingly high RCYs, surpassing those of iodide, possibly due to the exceptional leaving group ability. The triflates also showed the fastest reaction kinetics with tosylates, once again, producing the poorest results. The authors proposed that these findings suggested the incomplete dissociation of diaryliodonium salts, even when using the inorganic counterions. NMR studies on the cations revealed the degree of dissociation. In the case of fully dissociated iodonium salts, the $^{1}H_{ortho}$ shifts of the cations would be identical, regardless of the nature of the anion. However, clear differences in chemical shifts were observed across all anions, especially between bromide and tosylate ions. This variation in proton shift and the RCYs produced promote the suggestion of a non-fully dissociated reaction pathway and that the degree of dissociation and, hence, the RCYs depends upon the nature of the counterion.[184]

These results are in accordance with previous work by Pike and Aigbirhio which also included the study of both inorganic and organic counterions (bromide, chloride, triflate, trifluoroacetate).[54] In this case, however, the highest RCYs were achieved when using the trifluoroacetate anion, which is thought to be the ideal counterion as it

is not strongly nucleophilic but sufficiently stable to reduce the covalent nature of the bond to iodine thereby lowering the steric and electronic effect in the process. Previous work from within this research group on the fluorination of diaryliodonium salts has also shown that trifluoroacetate was highly compatible with the preparation of complex polyfunctional iodine (III) species and that higher chemical purity is achieved when synthesising salts bearing this counterion.[195]

1.4.2.7 Effect of solvent

The solvent used in the radiofluorination of diaryliodonium salts has a large effect on the RCY. In the majority of cases, an S_NAr reaction requires an aprotic, polar solvent such as DMSO, MeCN or DMF. However, DMSO has been found to be inappropriate for fluorinations of diaryliodonium salts and produced very poor RCYs. This is attributed to the low reduction potential of DMSO causing redox processes between iodine(III) species and solvent molecules. The S-O bond also favours a $S^+—O^-$ polarisation, distinct nucleophilicity and therefore, a strong solvation of cations, which lowers their reactivity. There is also evidence that DMSO affects diaryliodonium cations in such a way that the oxygen atom partially neutralises the positive charge of the iodine(III) centre.[196, 197] It is most likely that a combination of these factors contributes to the general unsuitability of DMSO as a solvent for the fluorination of diaryliodonium salts. Coenen and colleagues achieved no labelling reaction when attempting to radiosynthesise 1-bromo-4-[^{18}F]fluorobenzene using *bis*-(4-bromophenyl)iodonium bromide in DMSO.[184] However, upon changing the solvent to either DMF or DMF/dioxane, RCYs (DC) dramatically increased up to 65%. These results are in accordance with the work of Wüest who also found DMF to be the superior solvent upon radiosynthesising 4-[^{18}F]-fluoroiodobenzene from 4,4'-diiododiphenyliodonium

salts with various counterions.[198] Both Wüest and Coenen have found that using MeCN produced disappointing results which is surprising as many other groups have found this solvent to be beneficial to the reaction.[55, 152, 199] More recently, Pike and coworkers made a direct comparison between DMF, MeCN and MeCN with 1.5% H_2O, using a microreactor to synthesise *ortho*-substituted [^{18}F]fluoroarenes from reactions of [^{18}F]fluoride with various diaryliodonium salts.[80] The results clearly identified DMF as the superior solvent with greater RCYs achieved regardless of substituents or counterions present. It should be noted, however, that this study was conducted using a microfluidic device, wherein the viscosity of the solvent has a significant effect upon the outcome of the reaction. Regardless of this, DMF is generally accepted as the solvent of choice for the [^{18}F]fluorination of diaryliodonium salts and has been adopted by many research groups.[200-203]

DiMagno has also found, perhaps counterintuitively, that fluorination of arenes can be achieved in excellent yields when fluorinating diaryliodonium salts in non-polar solvents such as toluene and benzene.[204] Through advanced NMR studies on the reaction of diaryliodonium salts with anhydrous tetramethylammonium fluoride, it was reported that selectively of the nucleophilic fluorination and the yields of products can be optimised by varying the reaction conditions. The low polarity solvents are shown to suppress competing side reactions whilst precipitating inorganic salts which may catalyse ligand exchange, electron transfer and disproportionation reactions. Interestingly, it was also found that excellent conversion to the fluoroarenes can be achieved when the total concentration of fluoride is very small, as is the case when using the fluorine-18 radioisotope to generate potential PET radiotracers.

1.4.3 Radiofluorination of diaryliodonium salt precursors to generate imaging agents

One of the most significant imaging syntheses of a PET imaging agent from a diaryliodonium salt precursor, is the Wirth's synthesis of [^{18}F]-L-DOPA, a vital radiotracer in the diagnosis of Parkinson's disease and other neuroendocrine tumours. Several stable but complex diaryliodonium halides were synthesised before reacting with NCA [^{18}F]fluoride. Optimal conditions were found when using either MeCN or toluene, as the fluorination solvent. The electron-rich anisyl group was used as the NTR to achieve low RCYs of <1% (based on HPLC analysis). The disappointing yields mean that the current conditions require further optimisation, however, this is still a significant synthesis due to the vast application of the target radiotracer.[205]

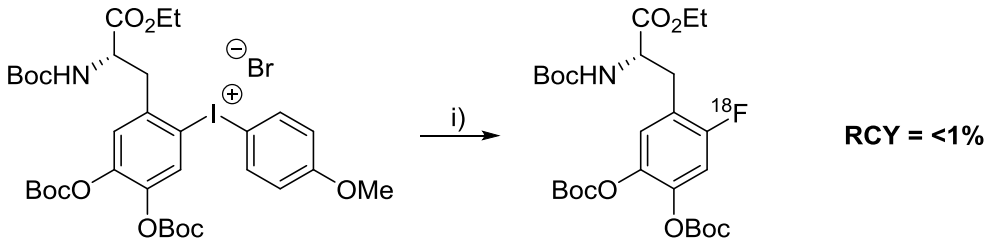

i) [^{18}F]KF/K222, K_2CO_3, TEMPO (0.7 mol%), MeCN/DMSO (2:1), 30 min

Figure 21: Radiosynthesis of [^{18}F]-L-DOPA from a diaryliodonium salt.[205]

Few applications to the preparation of specific radiotracers from diaryliodonium salts have been as successful as Zhang's preparation of [^{18}F]DAA1106, a PET ligand for imaging peripheral-type benzodiazepine receptors in the brain.[206] The corresponding diaryliodonium tosylate precursor was synthesised in excellent RCYs before reacting with NCA cyclotron-produced [^{18}F]fluoride to afford the desired product (Scheme 45).

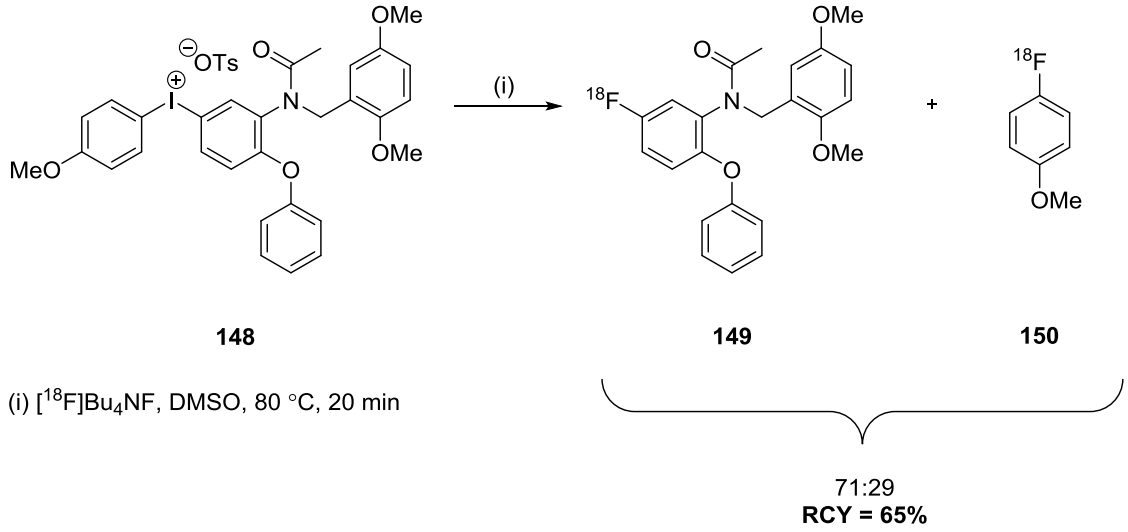

Scheme 45: Radiosynthesis of [^{18}F]DAA1106[206]

Simple diaryliodonium salt compounds were also synthesised and used as model compounds to optimise reaction conditions. Various solvents were tested with the most promising results obtained when using DMSO. This is interesting as DMSO has been found to be inappropriate for reactions of this type.[184] The conventional PTA, Kryptofix®222/K_2CO_3, was replaced by tetrabutylammonium bicarbonate ($Bu_4N.HCO_3$) which improved the efficiency of the reaction. The results clearly demonstrated the selectivity of the reaction with excellent RCYs achieved when using the electron-rich anisole as the NPR. The analogous phenyliodonium salt gave the desired product in only 3% RCY.

Katzenellenbogen and colleagues reported the radiosynthesis and biological evaluation of two [^{18}F]fluorinated analogues of the PPAR agonist, farglitazar (Scheme 46).[207] Radiosynthesis of **151** was achieved in 35% RCY using [^{18}F]CsF as the [^{18}F]fluorinating agent. Interestingly, good yields of the desired compound were achieved when using the phenyliodonium tosylate whilst employing the more electron-rich anisole and thienyl derivatives afforded no desired product. These potential PET imaging agents have been used for the diagnosis of vascular disease and breast cancer and were both

shown to be metabolically stable. However, tissue distribution studies showed that target tissue uptakes were non-specific and disappointingly low. These compounds, therefore, are unlikely to be suitable for effective imaging of breast cancer or vascular disease.[207]

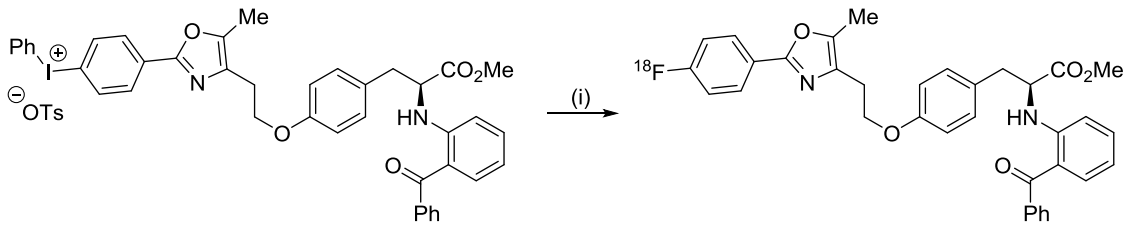

150 **151**
RCY (DC) = 35%

(i) (a) [^{18}F]CsF, DMF, 130 °C, 10 min (b) 0.5 M LiOH, 80 °C, 10 min

Scheme 46: Radiosynthesis of fluorine-18 labelled analogue of farglitazar

Kim and co-workers have used diaryliodonium tosylate precursors **152** to develop fluorine-18 labelled 2-aryl-6-benzothiazoles **153**.[208] These compounds could prove to be potentially useful PET probes for imaging β-amyloid plaques, which seemingly play an important neuropathological role in Alzheimers disease. A range of precursors were synthesised via conventional pathways before being tested unders various conditions. Higher yields were obtained using microwave heating and in the presence of TEMPO. Short reaction times, high SAs and RCPs were also achieved. Electron-rich NTRs were again used successfully to direct the radiofluorination to the benzothiazole ring with best results obtained when using the 3-thienyl derivative.[208]

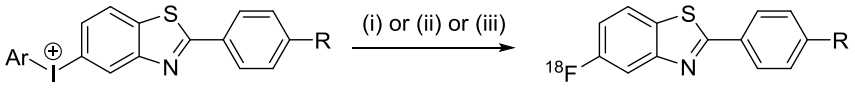

152 **153**

152a R = NO_2, Ar = Ph
152b-f R = NCH_3Boc,
Ar = Ph, 4-anisyl, 4-toluyl, 2-thienyl, 3-thienyl
152g R = $N(CH_3)_2$, Ar = Ph

153a R = NH_2
153b R = $NHCH_3$
153c R = $N(CH_3)_2$

(i) (a) [^{18}F]nBu_4N, MeCN, TEMPO, MW (100 W) 6 min; (b) $SnCl_2$, EtOH, 90 °C, 10 min for **153a**; (ii) (a) [^{18}F]nBu_4NF, MeCN, TEMPO, MW (100 W), 6 min or 130 °C, 10 min; (b) EtOAc/HCl (v/v = 3:1), 75 °C, 10 min for **153b**; (iii) [^{18}F]nBu_4NF, MeCN, TEMPO, MW (100 W), 6 min for **153c**.

Scheme 47: Radiosynthesis of 2-aryl-6-[^{18}F]fluorobenzothiazoles[208]

Kim and coworkers have, again, used the diaryliodonium tosylate precursor **154** to develop a highly efficient synthesis of [^{18}F]flumazenil **155**, an important radiopharmaceutical agent for the assessment of central benzodiazepine receptor concentration (cBZR) in the brain (Scheme 48).[209]

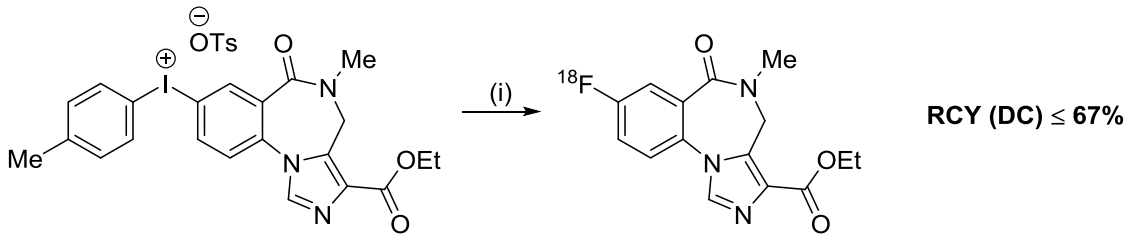

154 **155**

(i) [^{18}F]KF/K222, K_2CO_3 TEMPO, DMF, 150 °C, 5 min

Scheme 48: Radiosynthesis of [^{18}F]flumazenil[209]

PET studies targeting this biomarker have been used to quantitatively evaluate cBZR in epilepsy,[210] panic disorders,[211] the evaluation of cortical damage to the brain following an acute stroke,[212, 213] as well as other conditions.[214, 215] Carbon-11 labelled flumazenil ([^{11}C]FMZ) has proved to be very useful in such studies but the short half-life of the radioisotope restricts administrations to one or two patients per cyclotron-production of radioactivity. The fluorine-18 labelled derivative has a similar uptake pattern and allows for extended PET studies due to the longer half-life of the radioisotope. Many

research groups have attempted to synthesise **155** from the nitro precursor via nucleophilic substitution, but RCYs have been disappointingly low (3–10%).[216, 217] Kim and colleagues have drastically improved yields by adopting the diaryliodonium salt approach.[209] It was found that the stability of the diaryliodonium salt under basic conditions at high temperatures is an important factor in the fluorination process. Stability studies revealed that the more electron-rich diaryliodonium tosylates had lower stabilities, and that, therefore, 4-methylphenyl-mazenil iodonium tosylate was the most attractive precursor for the efficient production of **155**. Using optimised conditions, studies were extended to large scale production, employing a commercially automated device to obtain the desired product in excellent yields and in short reaction times. High SAs and reproducible yields were also achieved using the automated equipment.

More recently, Selivanova and coworkers have radiolabelled a novel and potent inhibitor of matrix metalloproteinases MMP2/MMP9 **157** (Scheme 49).[218] The activity of these proteases is elevated under many pathological conditions including atherosclerotic plaque rupture. Gelatinases MMP2 and MMP9 are of particular interest in oncology because of their implication in angiogenesis, cancer cell proliferation and metastasis. The aim of the study was to image these active inhibitors, *in vivo*, using radiolabelled (*R*)-2-(4-(4-fluorobenzamido)phenylsulfonamido)-3-(1*H*-indol-3-yl)propanoic acid which showed the best binding properties in vitro.[218]

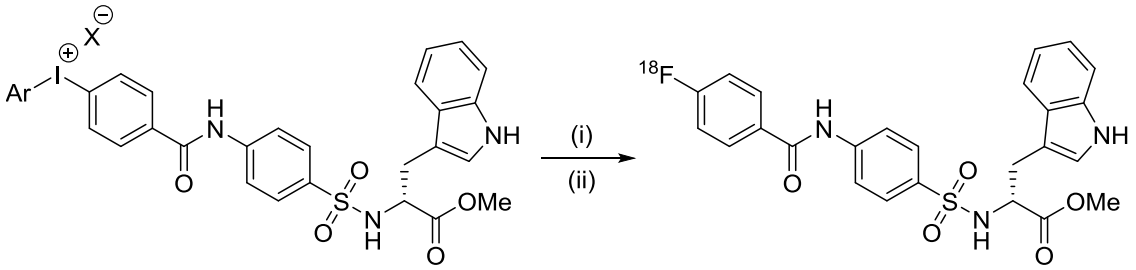

156 **157**
RCY (DC) = 20%

Ar = 4-anisyl, 2-thienyl
X = TFA, OTs, OTf, Br, ClO_4
(i) [^{18}F]F^-, Ca_2CO_3, DMF, H_2O, 130 °C, 3 min (ii) NaOH, 100 °C, 10 min

Scheme 49: Radiosynthesis of a high affinity probe for imaging matrix metalloproteinases 2 and 9.[218]

Radiolabelling was achieved in one-step from NCA [^{18}F]fluoride using the corresponding diaryliodonium salt precursors **156**, followed by deprotection of the carboxylic acid functionality. In optimising reaction conditions, different counterions were tested when using either 4-anisyl or 2-thienyl as the NTR. It was found that RCYs were higher when reaction times were shorter. Reactions either did not occur or gave disappointing yields when anhydrous solvents (MeCN, DMF, DMSO) were used. Higher yields were achieved using trace amounts of water. The authors suggest that traces of water catalyse the formation of the intimate ion-molecule pair (where the molecule is the NTR) making the target aromatic ring positively charged and susceptible for nucleophilic attack. Ionising solvents such as water may reduce the energy required for heterolytic bond cleavage, thereby favouring this pathway over the homolytic. The authors also found that the use of free radical scavengers did not improve RCYs, thereby supporting the heterolytic bond dissociation argument. In general, the precursor bearing anisole leaving group, gave better RCYs than that bearing the 2-thienyl group, thus, further optimisation of the reaction was performed using the 4-anisyl derivative. The influence of the counterion was evaluated and found to induce significant effect on RCYs. When using the heavily functionalised diaryliodonium salts,

RCYs were highest when using inorganic counterions and decreased in the following order: perchlorate > bromide > tosylate > triflate. This may be because the bulkier organic anions have more covalent character and hinder solvolysis of an iodonium salt, limiting the formation of an intimate ion-molecule pair. The target compound was reproducibly synthesised and formulated for *in vivo* application in 10–20% RCY (DC) with excellent specific radioactivities (> 90 GBq/μmol) and RCP (> 95%). Pleasingly, **157** also showed excellent in vivo stability in wild-type mice and shows strong promise as a suitable tracer for oncological and atherosclerotic imaging.[218]

Raffel and colleagues have also used diaryliodonium salts to develop a new cardiac sympathetic radiotracer with kinetic properties advantageous for quantifying regional nerve density in PET.[219] Initial attempts to generate 4-[^{18}F]fluoro-*m*-hydroxyphenethylguanidine (4-[^{18}F]FMHPG) **159** (Scheme 50) from the di-*N,N*'-Boc-protected guanidine precursor **158** showed zero incorporation despite varying reaction solvent and sources of [^{18}F]fluoride. The addition of water and the presence of TEMPO also had no effect.

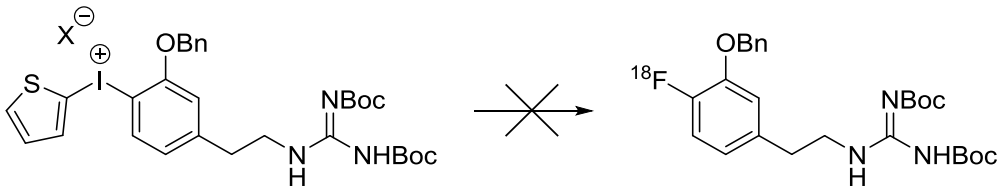

158 **159**

X = Br, OTs

Scheme 50: Attempts to synthesise 4-[^{18}F]FMHPG in one step from the corresponding diaryliodonium salt precursors

The authors proposed that, as diaryliodonium salts may decompose under harsh, basic conditions, the guanidinyl group might be causing a disturbance to the [^{18}F]fluorination reaction. To test this, the di-*N,N*'-Boc-protected guanidylethyl group of the iodonium

precursor **158** was replaced with an *N*-Boc-protected aminoethyl group **160** and used to generate *N*-Boc-3-benzyloxy-4-[^{18}F]fluoro-*m*-tyramine **161** in RCYs of up to ~45 % when using DMF with trace amounts of water in the presence of TEMPO (Scheme 51). In order to achieve the following deprotection and guanylating steps, a commercially available automated radiofluorination system was used. *N,N'*-Bis-(tert-butoxycarbonyl)-5-chloro-1*H*-benzotriazole-1-carboxamidine was proven to be the best guanylating agent. RCYs of the desired final product averaged 7 ± 3% (DC) and in 99% RCP. Good SAs were also achieved (1.2 ± 0.3 Ci/µmol).

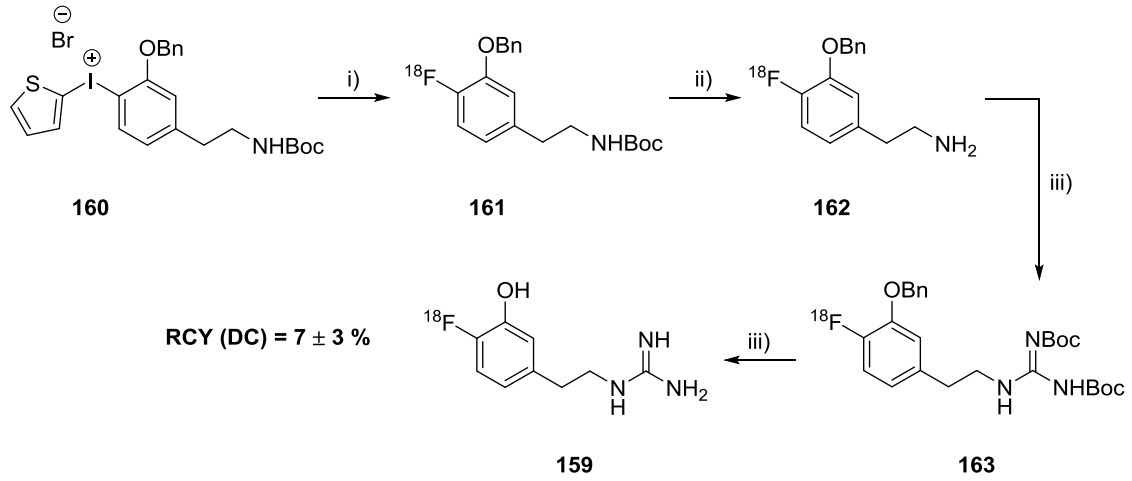

(i) [^{18}F]CsF, TEMPO, DMF, H_2O, 150 °C, 25 min, (ii) 1.0 N HCl, 100 °C, 10 min
(iii) *N,N'*-Bis-(*tert*-butoxycarbonyl)-5-chloro-1*H*-benzotriazole-1-carboxamidine, DIEA/MeCN, 45 °C, 15 min
(iv) 1.0 N HBr, 120 °C, 15 min

Scheme 51: Radiosynthesis of [^{18}F]FMHPG[219]

The authors noted that RCYs of the radiofluorination step were significantly lower following conversion to the automated radiofluorination system. This exemplifies the challenges the radiochemist must face when translating conventional chemistry to more complex platforms required for automated radiochemical procedures. Despite this, yields were sufficient for microPET imaging studies in rhesus macaque monkeys to take place. Biological evaluations were highly encouraging and suggest that this agent is capable of providing accurate and robust quantitative measures of regional cardiac

sympathetic nerve density in human subjects. If this is the case, then **159** could have important implications in diseases associated with cardiac sympathetic dysfunction, including sudden death, heart failure, cardiac arryhythmias and diabetic autonomic neuropathy. There may also be a clinical role as a diagnostic imaging agent for localising adrenergic tumours, such as neuroblastoma and pheochromocytoma, using PET.[219]

1.4.4 Radiofluorination of diaryliodonium salt precursors to generate prosthetic groups used in PET imaging

Diaryliodonium salts have also been used to produce prosthetic groups for the indirect labelling of biological targets. Pike and co-workers used a microfluidic device to study the nucleophilic fluorination of diaryliodonium tosylates **164** in the preparation of *meta*-substituted arenes bearing either electron-withdrawing (Table 4) or electron-donating (Table 5) substituents.[199] By using this platform, reaction temperatures beyond the boiling point of the solvent were possible and shown to increase RCYs. Initially, MeCN was used in the trial reactions as the [^{18}F]fluoride ion is readily solubilised in the presence of the K^+ and Kryptofix®222. However, the RCY of *m*-[^{18}F]fluoroanisole from the corresponding 2-thienyl salt was greatly improved when changing to DMF suggesting that the outcome of the reaction may be dependent upon the choice of solvent used. The authors noted that impressive results have been obtained previously when [^{18}F]fluorinating *ortho*-substituted diaryliodonium salts in DMF. However, the effect of solvent was not studied in this work and the majority of reactions were performed in MeCN. Generally, highest RCYs were achieved when NTRs were 3-MeC_6H_4, 4-$MeOC_6H_4$, 2-thienyl, or 5-Me-2-thienyl groups.

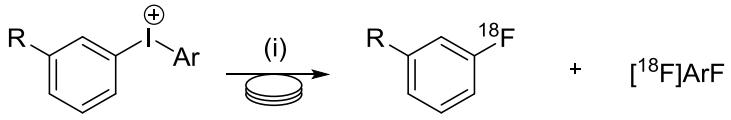

164 **165** **166**

(i) [^{18}F]KF/K222, MeCN, 130 °C to 190 °C, 146 s to 236 s

R	Ar	Time (s)	Temp (°C)	RCY (%)	RCY Ar[^{18}F]F (%)	Total RCY (%)
-CN	3-CNC$_6$H$_4$	189	160	55		55
-CN	Ph	146	130	25	< 1	26
-CN	4-OMeC$_6$H$_4$	146	130	82	11	93
-CN	3-MeC$_6$H$_4$	189	160	76	5	81
-CN	2-thienyl	189	160	58	2	60
-CN	5-Me-2-thienyl	189	180	78	1	79
-NO$_2$	4-OMeC$_6$H$_4$	191	130	58	7	65
-NO$_2$	2-thienyl	140	130	31	4	35
-NO$_2$	5-Me-2-thienyl	189	160	37	2	39
-CF$_3$	4-OMeC$_6$H$_4$	189	190	53	< 1	54
-CF$_3$	2-thienyl	236	180	66	0	66
-CF$_3$	5-Me-2-thienyl	189	190	57	0	57

Table 4: RCYs (DC) of *m*-[^{18}F]fluoroarenes from the NCA radiofluorination of diaryliodonium tosylates bearing an electron-withdrawing substituent in the *meta*-position.[199]

R	Ar	Time (s)	Temp (°C)	RCY (%)	RCY Ar[^{18}F]F (%)	Total RCY (%)
-Me	Ph	236	160	12	15	27
-Me	4-OMe	236	180	47	5	52
-Me	2-thienyl	236	190	26	< 1	27
-Me	2-thienyl	236	200	82	0	82
-OMe	Ph	236	150	87	6	93
-OMe	2-thienyl	314	200	9	1	10
-OMe	4-OMeC$_6$H$_4$	236	180	36	1	37

Table 5: RCYs (DC) of *m*-[^{18}F]fluoroarenes from the NCA radiofluorination of diaryliodonium tosylates bearing an electron-donating substituent in the *meta*-position[199]

Wüst and co-workers developed a novel approach to radiolabelling more complex molecules via transition-metal mediated cross-coupling reactions, using 4-[^{18}F]fluoroiodobenzene **168** generated from 4,4'-diiododiphenyliodonium salts **167**.[198]

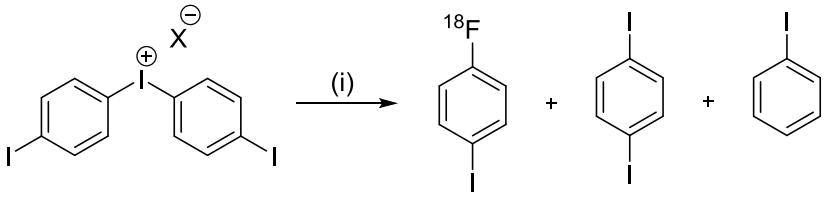

167 **168** **169** **93**

RCY (DC) = 13–70%

X = Cl, OTf, OTs

(i) [^{18}F]KF/K222, DMF, 120 °C, 40 min

Scheme 52: Radiofluorination of 4,4'-diiododiphenyliodonium salts to generate precursors for transition-metal mediated cross-coupling reactions[198]

Various counterions were tested in synthesising **168**, with the tosylate and triflate precursors producing the most reproducible results compared to the chloride anion. Different solvents were also tested with DMF producing the highest results whilst MeCN and DMSO generated far lower yields. Microwave heating did not improve RCYs but did drastically reduce reaction times – a critical consideration to radiochemical syntheses when incorporating short-lived radioisotopes. To reduce the duration of the purification process, solid-phase extraction techniques were used as opposed to slightly more conventional HPLC methods. In all fluorination experiments, however, the formation of diiodobenzene **169** and iodobenzene **93** was observed, originating from the thermal decomposition of the iodonium salt. These by-products could not be removed by SPE and therefore, acted as competitive ligands in subsequent cross-coupling reactions. Despite this **168** was successfully used in the Stille coupling approach towards the radiosynthesis of two potential radiotracers for monitoring COX-2 expression via PET **171** and **173** (Scheme 53).[220]

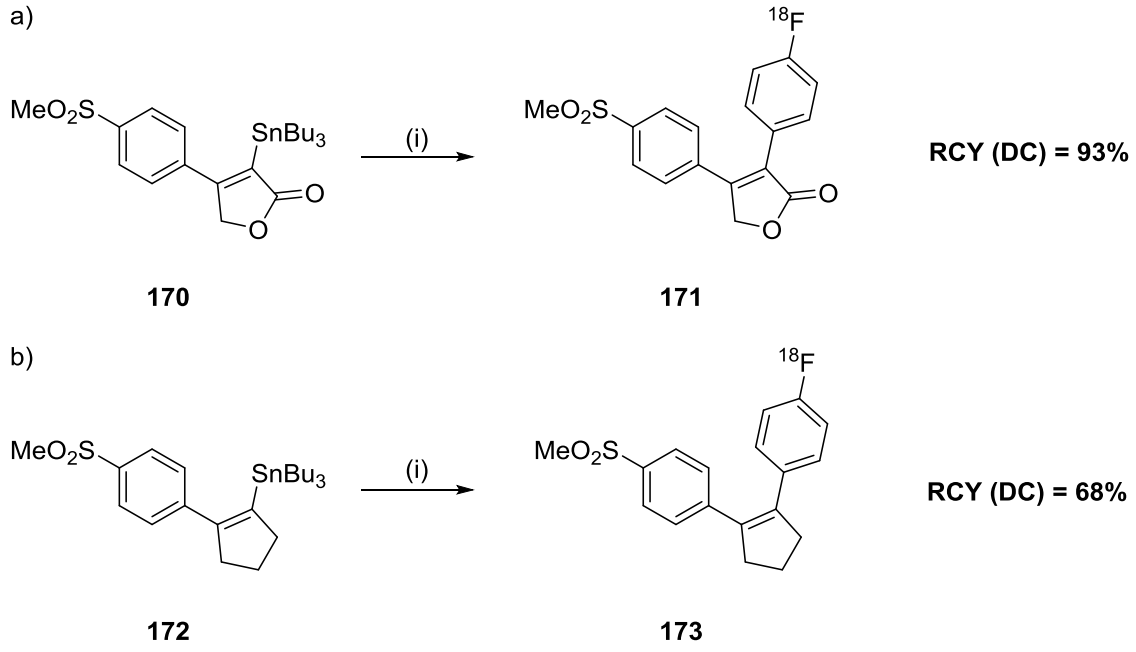

(i) **168**, Catalyst system

Scheme 53: Radiosynthesis of potential radiotracers for monitoring COX-2 expression via Stille Cross-coupling using 4-[^{18}F]fluoroiodobenzene[220]

Optimised reaction conditions were applied to achieve compounds **171** and **173** in RCYs of up to 93% and 68% respectively, based on 4-[^{18}F]fluoroiodobenzene. Wüst has also used this approach to synthesise 5-(4-[^{18}F]fluorophenyl)-2-deoxy-uridine **176** (Scheme 54).[221] Radiolabelled nucleosides have attracted significant interest due to the central role nucleosides and nucleotides play in biological systems. SPE techniques from previous studies were improved upon to completely remove the 1,4-diiodobenzene by-product and provide chemically and radiochemically pure **168** for the cross-coupling reactions.

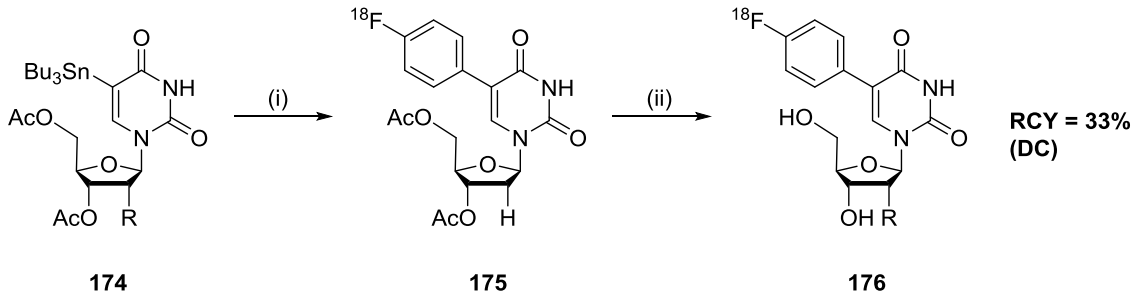

(i) **168**, $Pd_2(dba)_3$/CuI/$AsPh_3$, DMF/dioxane (ii) 1 M KOH

Scheme 54: Radiosynthesis of 5-(4'-[^{18}F]fluorophenyl)-2'deoxy-uridine via a Stille cross-coupling reaction[221]

Griffiths and colleagues reported the first synthesis of fluorine-18 radiolabelled lapatinib **182** (Scheme 55) - a potential radiotracer for PET imaging of ErbB1/ErbB2 tyrosine kinase activity, using *meta*-[^{18}F]fluorobenzaldehyde **178** as the radiofluorinating synthon.[77] Fluorination of phenyl(3-formylphenyl)iodonium bromide **177** using anhydrous [^{18}F]CsF in a microwave and in the presence of TEMPO afforded the **178**. This was immediately converted to the corresponding alcohol **179** by treating with aqueous $NaBH_4$ before being converted to *meta*-[^{18}F]fluorobenzylbromide **180** by reaction with triphenylphosphine dibromide. This was then coupled to the lapatinib precursor **181** to produce **182** in 8–12% RCY (NDC) in 140 min.

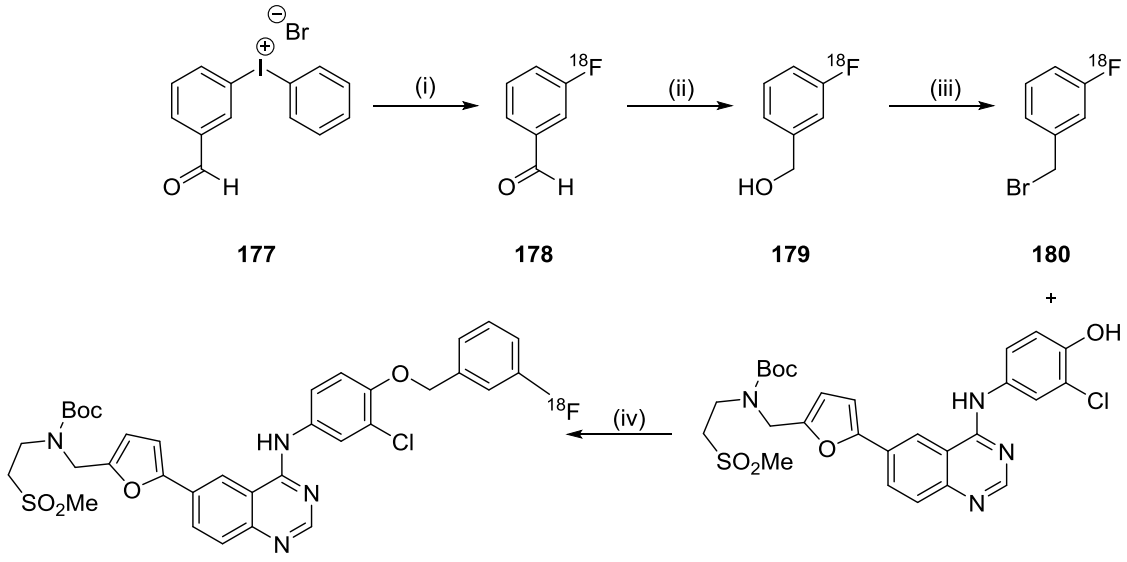

(i) [^{18}F]CsF, TEMPO, DMF, 110 °C, 5 min (ii) $NaBH_4$ DMF with H_2O (iii) PPh_3Br_2, DMF
(iv) a) K_2CO_3, DMF, 110 °C, 10 min b) TFA. 100 °C, 10 min c) 6 N NaOH

Scheme 55: Radiosynthesis of [^{18}F]lapatinib **182**[222]

Pike has developed a rapid, single step synthesis of azido **185** or azidomethyl **187** bearing [^{18}F]fluoroarenes from reactions of diaryliodonium salts with NCA [^{18}F]fluoride (Scheme 56).[200] These fluorine-18 bearing synthons have great potential in "click"

chemistry and increase the scope of possible radiotracers. By using a microfluidic device, previously poorly accessible [^{18}F]-labelled "click" synthons were generated in good RCYs and in short reaction times using diaryliodonium salts bearing the 4-anisyl NTR **184** and **186**. Interestingly, the radiosynthesis of **187** was achieved under "wet" conditions thus obviating the drying of cyclotron-produced [^{18}F]fluoride ion and therefore enhancing the practicality of the method whilst reducing total reaction times. The use of the microfluidic device also allowed for reaction temperatures to be greatly extended beyond the boiling points of the reaction solvents, thereby further improving RCYs.

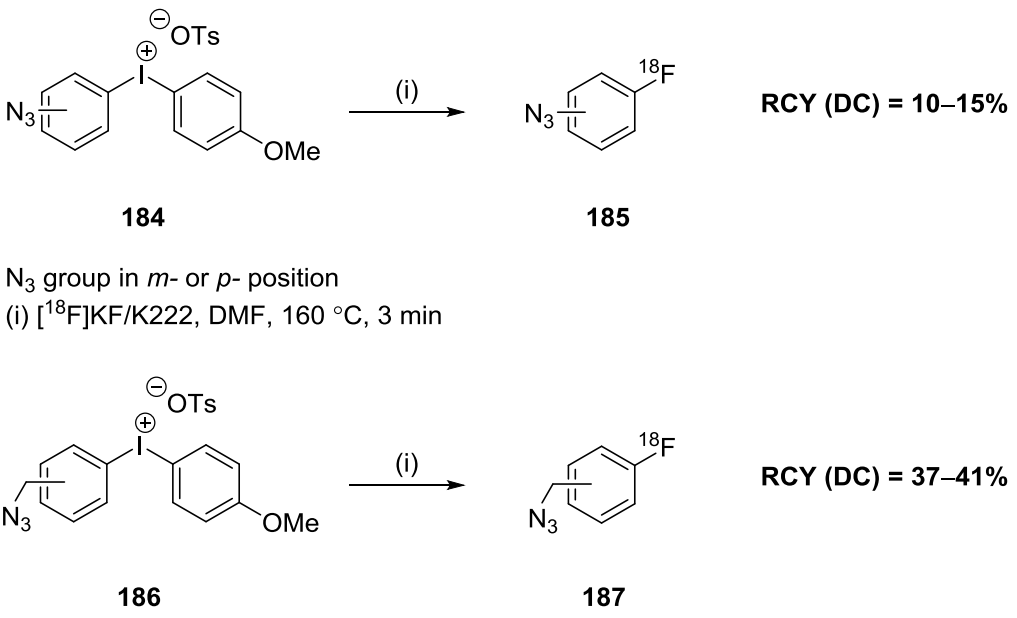

Scheme 56: Radiosynthesis of azido- and azidomethyl-substituted [^{18}F]fluoroarenes[200]

More recently, Pike and Chun have generated a range of fluorine-18 bearing prosthetic groups from various functionalised diaryliodonium salts, to expand the scope for producing structurally complex yet valuable, PET radiotracers.[203] RCYs (DC) varied with position of functional group, choice of electron-rich aryl ring and choice of counteranion. Under optimised conditions, fluorine-18 labelled fluorobenzaldehydes,

fluorobenzylhalides, fluorobenzoic acid esters and fluorophenyl ketones were obtained selectively in 40–73%, 20–55%, 46–89% and 81–98% RCYs, respectively. The use of microfluidic device, again, drastically reduced reaction times thereby allowing for high-throughput of experiments and the rapid optimisation of reaction conditions. Reaction temperatures of up to 200 °C were applied when DMF (boiling point = 153°C) was the solvent. Experiments in which the use of DMF and MeCN could be compared directly showed that considerably higher RCYs were obtained when using the former solvent. However, the authors noted that since the products of these reactions are synthons, then the reaction conditions for the following steps, and hence the solvent required, should be given great consideration. The NTRs varied across the study with higher RCYs generally resulting from those precursors bearing (2,4,6-trimethoxy)phenyl ring partners. Complete selectivity for the desired radioactive product was only observed, however, when using 2-thienyl and 5-methyl-2-thienyl as the NTRs. There was no observable difference between the use of chloride or tosylate anions and that the manner in which the anion influences the RCYs of these reactions remains unclear.[203]

1.5 Summary

As discussed above, Imaging techniques such as Magnetic Resonance Imaging (MRI) X-rays and ultrasound typically provide sound structural detail but little or no information on events at a metabolic or molecular level. Positron-Emission Tomography (PET) is a powerful, non-invasive molecular imaging technique used to gain valuable information on specific biological and pharmacological processes taking place in the human body. Positron-emitting radioisotopes are incorporated into a biologically active molecule, allowing for the non-invasive imaging and quantification of pharmacological and biological processes whilst minimising the disruption to their pharmacodynamic properties. Fluorine-18 is now considered to be the radionuclide of choice for PET imaging due to the convenient half-life, low positron energy and high degree of decay via positron emission. Widespread use of the most commonly used PET tracer [^{18}F]FDG **2,** which images areas of enhanced metabolism thereby improving diagnosis and evaluating the effectiveness of treatments in oncology, has spurred the global interest in PET studies. Nucleophilic fluorine-18 chemistry remains the dominant force in PET radiotracer production as the [^{18}F]fluoride can be produced in high SA.

A target arene may be radiolabelled with fluorine-18 via many different methods, of which nucleophilic aromatic substitution is the most common. The major drawback to this approach, however, lies in the difficulty to radiolabel electron-rich arenes. The reactivity of diaryliodonium salts provides access to [^{18}F]fluoroarenes which were previously inaccessible via conventional methodology.[54] These hypervalent molecules have been used extensively to generate potential imaging agents either via direct radiolabelling methods or via the generation of fluorine-18 labelled prosthetic groups (Section 1.2.8).

The regioselectivity of the reaction involving nucleophilic attack of [^{18}F]fluoride is determined by the stereoelectronic properties of the substituents; generally, the more electron-deficient aromatic ring will selectively incorporate the fluoride nucleophile, with particular consideration for the electron-density at the *ipso* carbons of vital importance.[188] However, an *ortho*-substituent on one of the aryl rings preferentially directs fluoride to that ring – the so-called "*ortho*" affect.[55-58] The RCYs of the radiofluorinated target can therefore be increased by the strategic modification of electronic and steric properties of the substituents, and reaction conditions.[56] However, there may be many other factors at play as evidence exists to support competing reaction mechanisms possibly involving a homolytic pathway (Section 1.4.2.5) and conventional nucleophilic aromatic substitution (Section 1.4.2.4). It has been shown that the configuration of the transition state is crucial to the outcome of the reaction with the attacking fluoride showing preference for the aryl group found in the equatorial position during the transition state.[152]

The counterion of the precursor, as well as the solvent in which the fluorination takes place, also have bearing upon the outcome of the reaction, with DMF and MeCN found to be the superior solvents.[184] Several counterions have been used, however, the trifluoroacetyl anion has been found to show good thermal stability (*c.f.* triflates) whilst allowing for facile synthesis of salts bearing this counterion (Section 1.4.2.6). Despite being studied extensively, a complete and conclusive description of the nucleophilic fluorination of diaryliodonium salts has not been widely accepted.

Given current understanding of this research field, herein this project, we aimed to generate a range of ethyl [^{18}F]fluorobezoates from various diaryliodonium salt precursors using advanced radiosynthesis techniques. In doing so, we aim to further

understand the mechanism the radiofluorination of these species, thereby aiding the potential production of future imaging agents to be used in PET studies.

2 Results and Discussion

2.1 Synthetic Chemistry

2.1.1 Aims

Previous work within this research group has focussed on the use of diaryliodonium salts to synthesise all regioisomers of ethyl [^{18}F]fluorobenzoate **188a-c** (Figure 22) compounds which were previously difficult to prepare due to the limitations of nucleophilic aromatic substitution chemistry.[223]

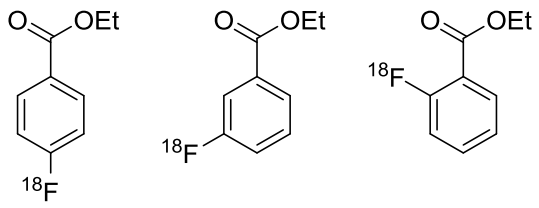

Figure 22: Regioisomers of ethyl [^{18}F]fluorobenzoate

The ethyl [^{18}F]fluorobenzoates are desirable targets as the ester functionality may be converted to several other chemically useful functional groups for the purposes of indirect radiolabelling.

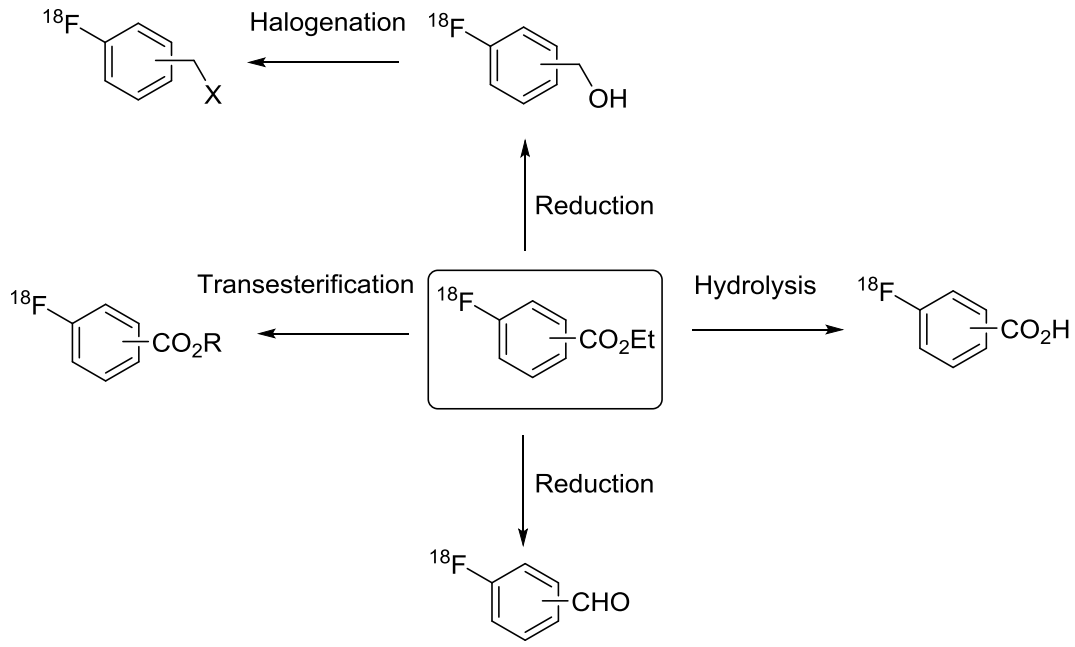

Scheme 57: Ester functionality provides access to various other functional groups

Each regioisomer may also serve as a prosthetic group and contribute to structure-activity relationship (SAR) studies thus providing important biological information on the pharmacodynamics of the imaging agent. Most importantly, ethyl 4-[^{18}F]fluorobenzoate **188a** also serves as a precursor to [^{18}F]SFB, which is the most versatile prosthetic group for the incorporation of fluorine-18 into peptides, proteins or antibodies.

In previous work, diaryliodonium trifluoroacetates **189** were used to obtain the fluorine-19 isotopomers **188d-f** in high selectivity and in excellent yields (Table 6).

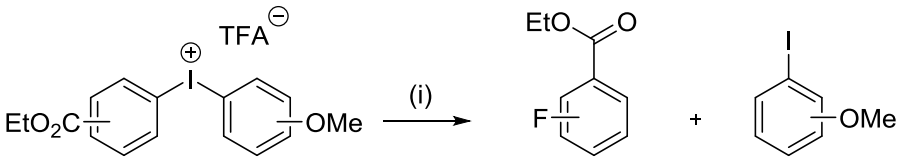

189a-f **188d-f** **190a-b**

(i) CsF, TEMPO, MeCN, DMF, 130 °C, 1.5 h

Compound	Regioisomer	Anisyl derivative	Yield of ethyl fluorobenzoate (%)	Selectivity of the reaction (ethyl fluorobenzoate: iodoanisole)

189a	2-I	2'-OMe	16	**188f**	1	:	0	**190b**
198	2-I	4'-OMe	29	**188f**	1	:	0	**190a**
189c	3-I	2'-OMe	49	**188e**	11	:	1	**190b**
195	3-I	4'-OMe	70	**188e**	1	:	0	**190a**
189e	4-I	2'-OMe	81	**188d**	1	:	0	**190b**
192	4-I	4'-OMe	74	**188d**	1	:	0	**190a**

Table 6: Synthesis of all regioisomers of ethyl fluorobenzoate[224]

The fluorine-18 derivatives have been synthesised previously but in non-optimised RCYs (~20%).[224] Before being used to radiolabel a biologically active molecule, RCYs must be improved and it is this aspect that forms the initial focus of this research project.

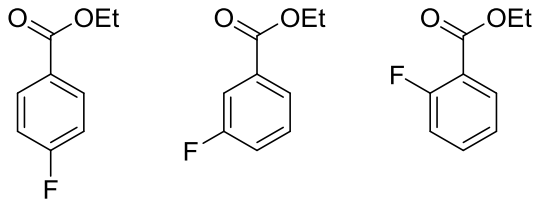

188d **188e** **188f**

Figure 23: Regioisomers of ethyl fluorobenzoate

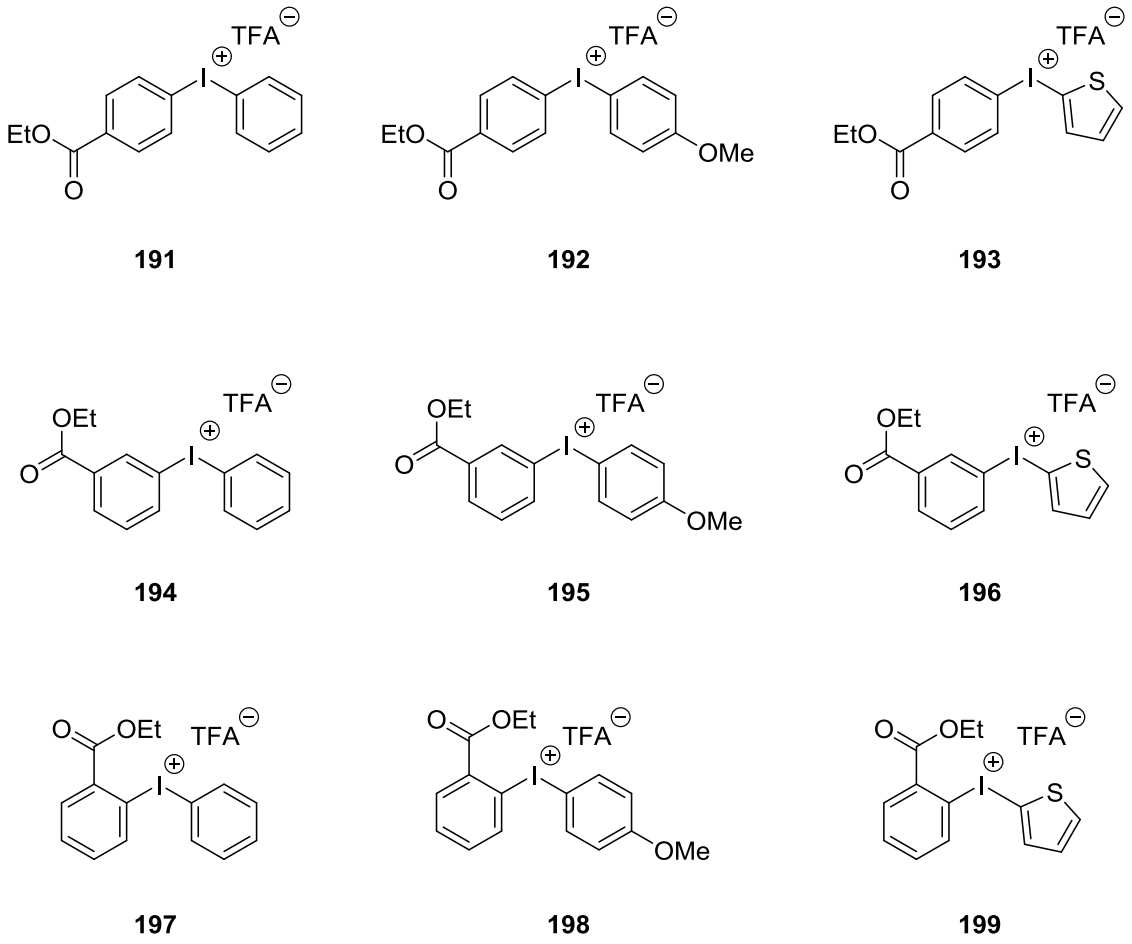

191 **192** **193**

194 **195** **196**

197 **198** **199**

Figure 24: Diaryliodonium salt precursors to be the initial target compounds of the project.

The traditional approach towards the synthesis of diaryliodonium salts which would serve as precursors to the ethyl fluorobenzoates (Scheme 58) was undertaken. The electron-rich 4-anisyl and 2-thienyl groups were chosen as the NTRs in order to promote the formation of the desired targets by directing the fluorination to the electron-deficient, ester-bearing ring. The phenyl group is also electron-rich, relative to the ethoxycarbonylphenyl group and so was also included in the study. Trifluoroacetates were to be used as counterions as previous work had suggested that these species limit the formation of by-products derived from the counterion acting as a competing nucleophile (*c.f.* Br, OTs) whilst exhibiting improved thermal stability compared to triflates.

The initial focus was to synthesise the appropriate aryl stannanes which would be combined with diacetoxyiodoarenes to form the target precursors (Scheme 58).

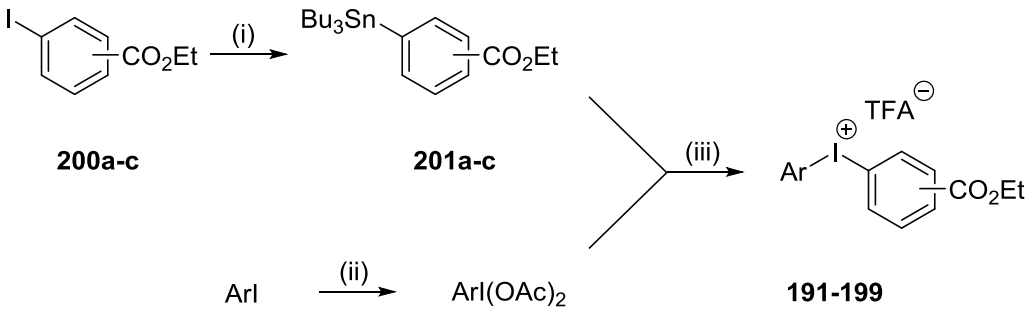

93 (Ar = phenyl) **204** (Ar = phenyl)
202 (Ar = 4-anisyl) **205** (Ar = 4-anisyl)
203 (Ar = 2-thienyl) **206** (Ar = 2-thienyl)

(i) (a) *n*BuLi, diethyl ether (b) Bu_3SnCl (ii) $NaBO_3.4H_2O$, AcOH, 50 °C, 6–8 h
(iii) DCM, TFAH, -30 to RT, 18 h

Scheme 58: Synthetic route to diaryliodonium trifluoroacetates

2.1.2 Formation of tributylstannyl substituted ethyl benzoates

As the preferred precursor to the target diaryliodonium salts are ethyl (tri-n-butyltin)-benzoates, the primary intention was to synthesise compounds **201a-c**. The most common procedure for the transformation of aryl halides to the corresponding arylstannanes is via the formation of an organometallic (Grignard,[225] lithium,[226] zinc[227]) reagent followed by the reaction with a trialkytin chloride. Alternatively, a palladium catalyst may be used with an excess of hexabutylditin to form functionalised stannanes from the corresponding aryl halides.[228] For this project, initial attempts were made using *n*BuLi in a halogen-metal exchange reaction followed by the addition of tri-n-butyltin chloride to form ethyl 4-(tri-n-butyltin)benzoate **201a** (Scheme 59).

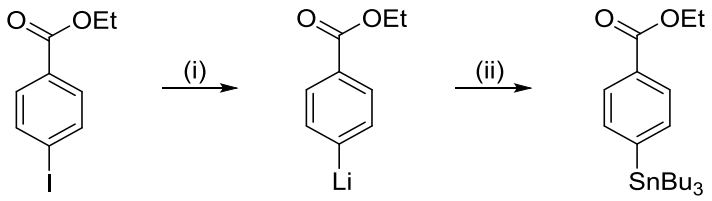

200a **207** **201a**

(i) (a) *n*BuLi, diethyl ether (ii) Bu_3SnCl

Scheme 59: Metal-halogen exchange reaction followed by addition of $SnBu_3Cl$ to form the stannane

Unfortunately, no stannane was produced despite numerous attempts over a range of temperatures and reaction times, evidenced by ^{1}H-NMR and HPLC. We propose that this is most likely due to the sensitivity of the ester substituent which may be prone to attack from the nucleophilic butyl group resulting in ketone formation, also evidenced by crude ^{1}H-NMR. At low temperatures (–100 °C) and over varying reaction times, with various equivalents of *n*BuLi, zero stannane could be observed. Taking into account that even the most effective modifications would still only produce disappointing yields, this approach was dismissed and the search for a simple, reproducible process which would not require the use of an expensive palladium catalyst, was undertaken.

It was noted that organozinc species could be used in conjunction with the appropriate transition-metal catalyst to create a range of polyfunctional compounds.[229, 230] The preparation of organozinc compounds from aromatic halides requires mild conditions when the aromatic ring bears sensitive functional groups such as esters. Suitable reaction conditions for the synthesis of aromatic organozinc species were reported by Kazmierski and colleagues.[231] Aromatic halides were converted to the corresponding aromatic organozinc species using acid activated zinc, in the presence of a cobalt (II) halide catalyst (Scheme 60).

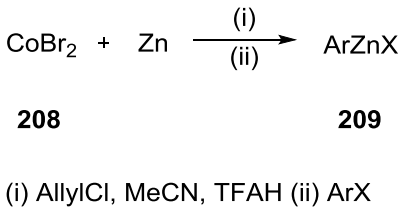

Scheme 60: Preparation of organozinc species

The catalytic cycle (Scheme 61) is first initiated by the reduction of Co(II)Br_2 **208** by zinc dust which has been previously activated by TFAH. The resulting Co(I)Br then undergoes an oxidative insertion into the aryl halide bond to afford the trivalent cobalt complex ArCo(III)Br_2. This is then reduced to the ArCo(II)Br species by the excess of zinc. The catalytic cycle is completed by the transmetallation reaction between ArCo(II)Br and the $ZnBr_2$ formed in the two previous steps. This gives the ArZnBr product and regenerates **208**.[232]

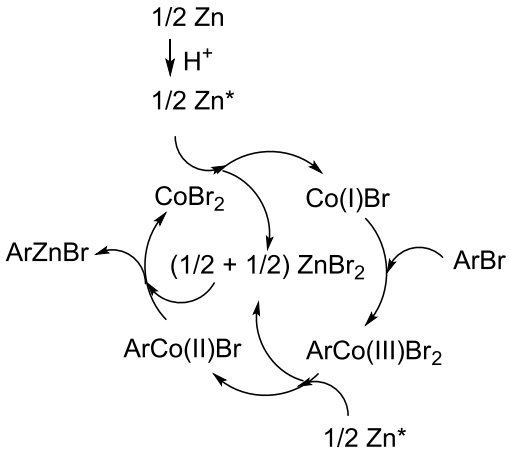

Scheme 61: Catalytic cycle to show production of ArZnBr[232]. Zn* = activated zinc.[232]

To avoid the formation of alternative products (ArH and Ar-Ar) a 5 min preliminary step is introduced using a catalytic amount of allyl chloride. The allyl chloride is fully converted into propene, 1,5-hexadiene and the addition product of the allylzinc species in MeCN, establishing the catalytic cycle. Previously, PhBr was used to reduce the production of ArH by being converted to PhH. It was found however, that a higher proportion of PhBr tends to slow down the reaction and produce a significant amount

of PhZnBr. It was deemed, therefore that PhBr is not reactive enough to act as an additive in this reaction. Allyl chloride was the most beneficial as it is fully converted to the compounds mentioned above, all fully separable from the aromatic products. Different durations of the preliminary steps were attempted but it was found that a 5 min preliminary step was sufficient, after testing in a one-step reaction.

The quantity of the catalyst used was reduced but when using 5% of $CoBr_2$, compared to 10%, the reaction was significantly slower. For this reason, the proportion of allyl chloride was increased compared to that of the catalyst by bringing up to 3 equiv. versus $CoBr_2$. With this, the reaction proceeded rapidly.

Gosmini and colleges have extended this work by investigating the synthesis of functionalised arylstannanes using a method for organozinc preparation (Scheme 62).[233] This approach does not require an expensive palladium catalyst but still produces high and reproducible yields under mild conditions. The ArZnBr species (Scheme 61) undergoes a transmetallation reaction with Bu_3SnCl to form the arylstannane **209**.

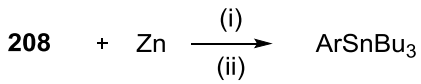

(i) AllylCl, MeCN, CF_3CO_2H
(ii) ArX, Bu_3SnCl, 50 ^oC

Scheme 62: Gosmini et al preparation of aryl stannanes from aryl halides[233]

Zinc dust and $CoBr_2$ **208** were introduced to a dry reaction vessel which was then filled with N_2. MeCN, allyl chloride and a catalytic amount of TFAH were then added and the reaction stirred for 5 min. The ethyl iodobenzoate **200a-c** and tributyltin chloride were

then added simultaneously and the reaction stirred at 50 °C for 1 h to give good yields (Table 7).

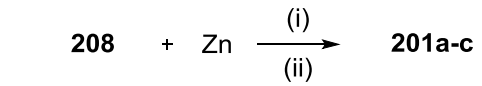

(i) AllylCl, MeCN, CF_3CO_2H (ii) **200a-c**, Bu_3SnCl, 50 ^oC

Isomer	Reaction Time (h)	Average Yield	n =
Ethyl 2-(tri-n-butylstannyl) benzoate **201a**	1	53	3
Ethyl 3-(tri-n-butylstannyl) benzoate **201b**	1	56	4
Ethyl 4-(tri-n-butylstannyl) benzoate **201c**	1	67	13

Table 7: Results of stannylation using cobalt (II) bromide and zinc dust. 'n' is the total number of syntheses.

It is not practical to either store or isolate the intermediate organozinc species **210a-c**, therefore the addition of tri-n-butyltin chloride is performed immediately following the formation of the organozinc species **210**. The nucleophilic carbon attacks the electrophilic tin eliminating the chloride leaving group, generating a penta-coordinate stannyl intermediate where the C-Zn bond is then broken to give the stannane **201a-c** and ZnICl (Scheme 63).

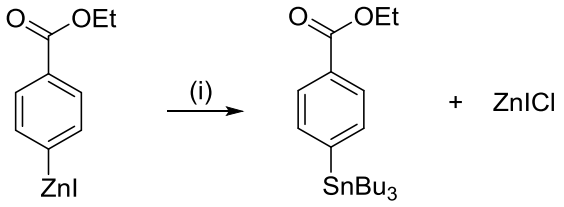

210 **201a**

(i) $SnBu_3Cl$

Scheme 63: Arylstannane formation from aromatic organozinc species

The differences in yield (Table 7) are small suggesting that neither electronic nor steric affects greatly influence the outcome of the reaction. Overall, the yields of the stannanes were pleasing due to the robustness of the reaction, short reaction times and no need of an expensive palladium catalyst or hazardous butylithium reagents.

A major difficulty in the preparation of pure organostannanes lies in their purification. The tributyltin compounds are viscous oils or liquids with very high boiling points. When working on a microscale, fractional distillations are impractical. In normal phase chromatographic purification, organostannanes often elute with the solvent front on silica gel, even with a non-polar eluant such as hexane, unless there are also polar functionalities present in the molecule. In addition, unsaturated organostannanes are sensitive to acid (including silica gel) and protio-destannylation is often observed during chromatographic purification.[234] To address these issues, purification of organostannanes was achieved using reverse phase flash chromatography (C-18 cartridge).[235] This method developed by Farina, requires the stannanes to be loaded onto the stationary phase in a 1:1 mixture of DCM and MeCN before eluting with MeCN only. However, loading in pure MeCN was found to be equally effective. By using an automated flash chromatography system, crude stannanes **201a–c** could be rapidly purified in a reproducible manner.

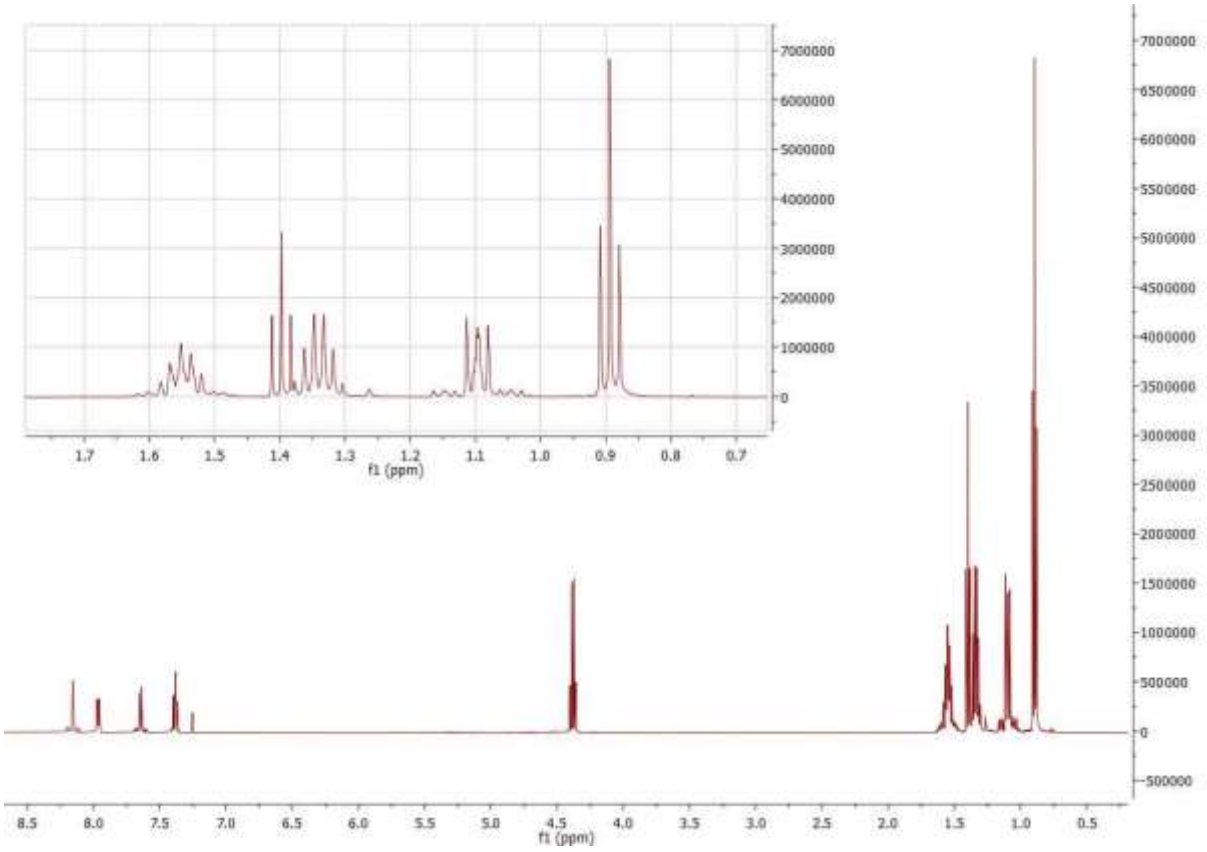

Figure 25: ^{1}H-NMR of **201c** with expansion of n-butyl region

2.1.3 Formation of diacetoxyiodoarenes

Diacetoxyiodoarenes are an important class of chemicals best prepared directly from iodoarenes and peroxyacids. Diacetoxyiodo-derivatives are readily formed upon oxidation of iodoarenes with hydrogen peroxide, in acetic acid and acetic anhydride.[236]

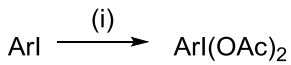

211 **212**

(i) H_2O_2, AcOH, Ac_2O

Scheme 64: Formation of diacetoxyiodoarenes using hydrogen peroxide, acetic acid and acid anhydride

An alternative approach which avoids the application of the potentially explosive, unstable, and highly concentrated hydrogen peroxide utilises sodium perborate.[237] M^{c}Killop and Kemp conducted a survey on the use of sodium perborate for the oxidation of functional groups and found that sodium perborate in acetic acid is a

highly effective reagent for the oxidation of many different functional groups but most importantly, iodoarenes to diacetoxyiodoarenes.[238] They found that the choice of solvent is an important consideration as simple oxidations are accomplished with ease in acetic acid, whilst attempts using alternative acids such as propionic acid were unsuccessful. This approach was adopted for the synthesis of diacetoxyiodoarenes throughout the project.

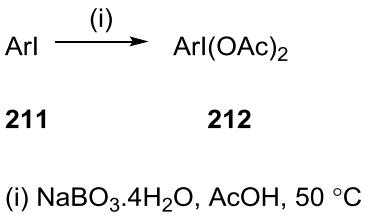

Scheme 65: Formation of diacetoxyiodoarenes from corresponding iodoarenes using sodium perborate

When used in water, sodium perborate releases hydrogen peroxide, but the new solution is not a simple mixture of hydrogen peroxide and sodium borate. It has been shown using NMR and Raman spectroscopy that when in dilute solution, an equilibrium containing peroxoborate anion **217** is established. These peroxoborate species are able to produce the hydroperoxide anion **216** at a much lower pH than when using hydrogen peroxide directly.[238] The ability of the tricoordinate boron **215** to accept hydroxyl ion from the hydroperoxide intermediate **218** and act as a leaving group, is also a driving force in this reaction.

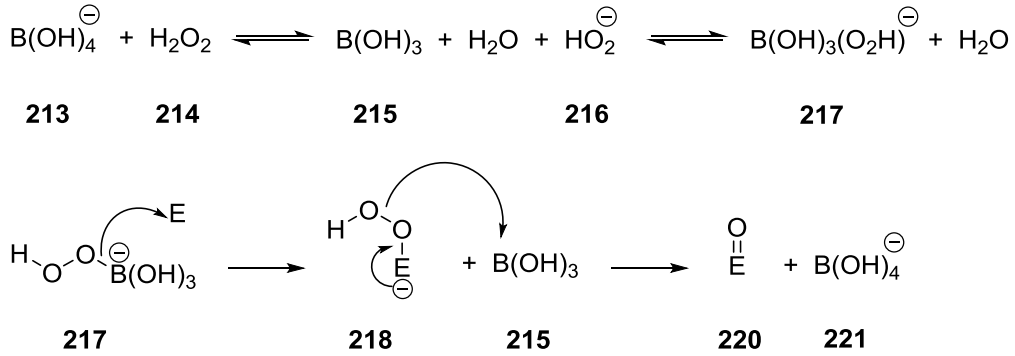

E = Electrophile

Scheme 66: Reaction pathway to show oxidation process using hydrogen peroxide and a perborate

When using sodium perborate with acetic acid, a more powerful oxidising species may be formed. Generally, sodium perborate does not dissolve freely to any significant extent but does so here by reacting first with the acetic acid solvent. This leads to the formation of the peracetic acid, which may be responsible for the oxidising properties of sodium perborate. There is also good evidence, however, for the production of an intermediate peroxy species **226** which most likely contains a B-OOAc species, a more powerful oxidising agent.[238]

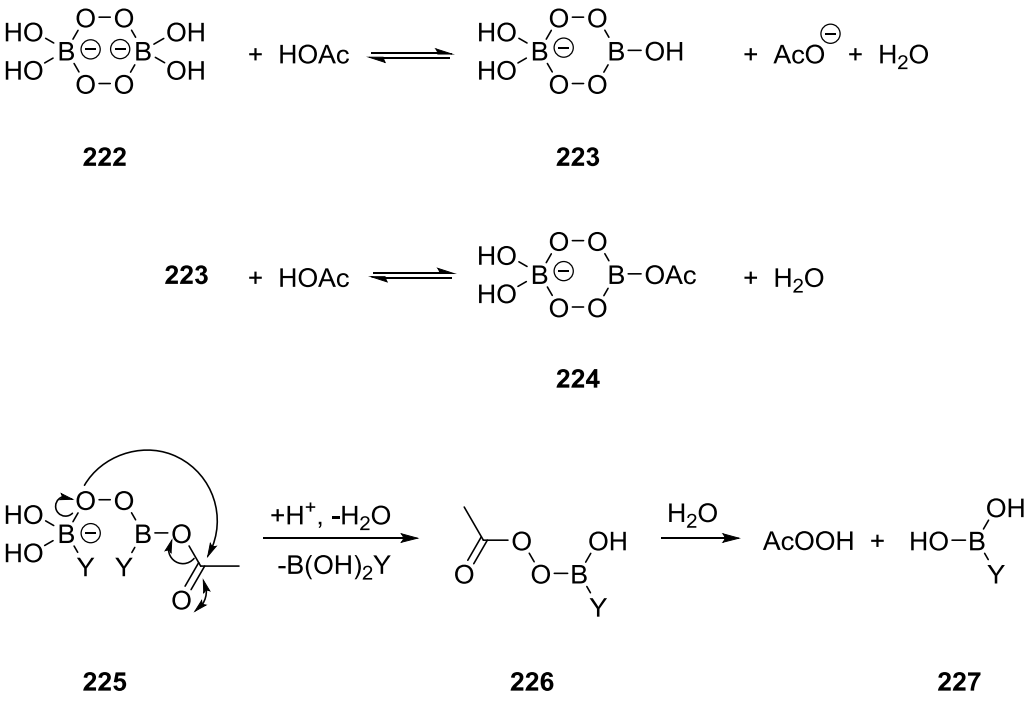

Scheme 67: Proposed formation of peracetoxyboron complex from perborate and acetic acid

Diacetoxy-4-iodoanisole **205** was prepared from the addition of sodium perborate tetrahydrate to a solution of 4-iodoanisole **93b** in glacial acetic acid. The mixture was heated to 50 °C and stirred for 5–8 h, by which time, the starting material had been consumed, according to TLC analysis.

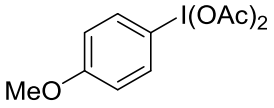

205

Yield = 40%

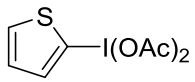

206

Yield = 40%

Figure 26: Isolated yields of diacetoxyiodoarenes

The maximum Isolated yields of the diacetoxyiodoarenes obtained was only ~40% which may be due to the low thermal stability of the final products. The electron-rich nature of the aryl groups reduces the stability of the hypervalent iodine species and promotes the decomposition process which returns the starting materials, which were, occasionally, difficult to separate from the desired diacetoxyiodoarenes. Only minor modifications to the procedure were made in attempting to elevate yields as optimisation of this reaction was not the focus of the project (*N.B.* Diacetoxyiodobenzene **204,** DIB, was purchased from fine chemicals suppliers and used as received).

2.1.4 Formation of diaryliodonium salts

The formation of diaryliodonium salts was based on the Shah-Pike-Widdowson synthesis of functionalised unsymmetrical diaryliodonium salts.[148] Diacetoxyiodoarenes were reacted with 2 eq. of trifluoroacetic acid giving the intermediate complex, [ArI(OAc)$_2$-2CF$_3$CO$_2$H]. These complexes were then treated *in situ* with the stannylated ethyl benzoate, at –30 °C, before being allowed to warm to

room temperature overnight to give the desired products. The diaryliodonium trifluoroacetates were obtained by crystallisation from petroleum ether:diethylether:DCM.

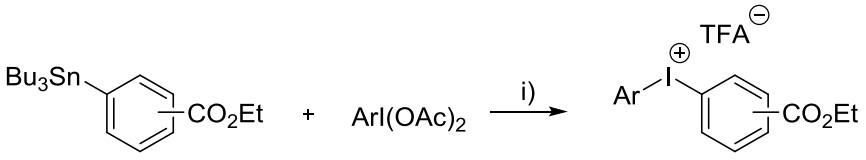

201a-c **204-206** **191-199**

(i) $NaBO_3.4H_2O$, TFAH, DCM,–30°C to RT, 18 h

Compound	Position of ester functionality	Ar	Yield (%)	Appearance
191	para-	phenyl	56	White crystals
192	para-	4-anisyl	73	White crystals
193	para-	2-thienyl	68	White solid
194	meta-	phenyl	56	White crystals
195	meta-	4-anisyl	55	White crystals
196	meta-	2-thienyl	56	White solid
197	ortho-	phenyl	Trace (by NMR)	N/A
198	ortho-	4-anisyl	Trace (by NMR)	N/A
199	ortho-	2-thienyl	Trace (by NMR)	N/A

Table 8: Yields and appearances of target iodonium salts

Having iodonium salts **191–196** available, the focus of the work moved to the fluorination of the diaryliodonium salts.

2.1.4.1 Crystal structure of diaryliodonium salts

There is evidence to suggest that λ^3-iodanes exist as polymeric structures in the solid state.[106-111] It was decided, therefore, that the solid state structure of the diaryliodonium salts **191–196** should be investigated. Using a solvent layering technique, material suitable for X-ray crystal analysis of **191–196** was produced. Compounds **191–193** were shown to exist exclusively in the monomer form, whilst compounds **194-196** clearly showed the presence of dimeric, trimeric and tetrameric

forms with the dimer dominating the crystal formation. This strongly suggests that secondary intermolecular bonding interactions exist on compounds **194-196**. This may affect the outcome of fluorination reactions as the nucleophile may be obstructed from attacking the iodine centre. Berry-pseudorotation is also proposed as being integral to the mechanism of fluorination. The formation of rigid oligomers may prevent the ligands from freely rotating about the iodine centre thus hindering the ligand coupling and formation of the fluoroarene.

It can also be clearly seen from the crystal structures that, as discussed earlier (Section 1.3.2) the most electron-rich aryl groups occupy the equatorial position to stabilise the positive charge of the iodine induced by the hypervalent bond. This can be seen clearly for compounds **192 and 194–196**. Interestingly, crystal structures of **191** and **193** both show the more electron-rich groups occupying the axial position. This arrangement is less preferred than that of the electron-rich in the equatorial position as this group is not able to stabilise the hypervalent bond by donating electron-density towards the electron-deficeint iodine centre whislt in the axial position. However, as discussed (Section 1.4.2.2) it is the arrangement of the transition state which is important to the fluorination process and not the arrangement of the ground state.[189]

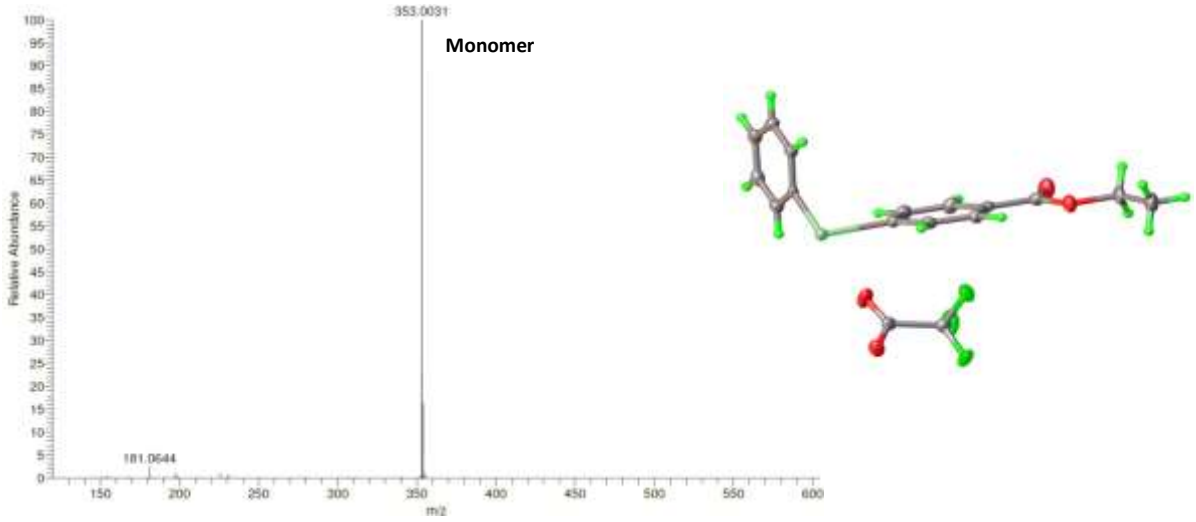

Figure 27: MS spectra and crystal structure (monomer) of **191**

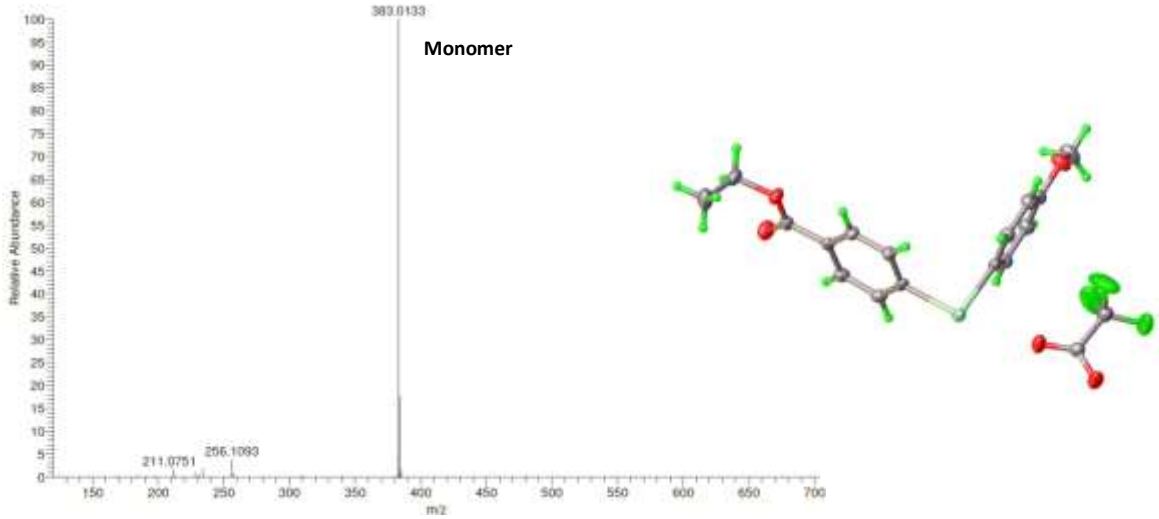

Figure 28: MS spectra and crystal structure of **192**

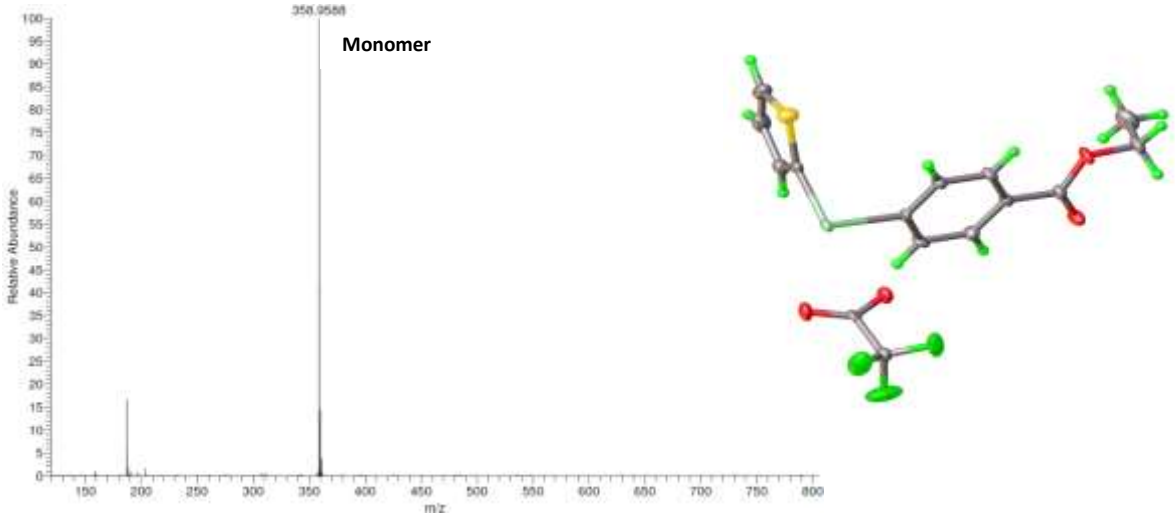

Figure 29: MS spectra and crystal structure (monomer) of **193**

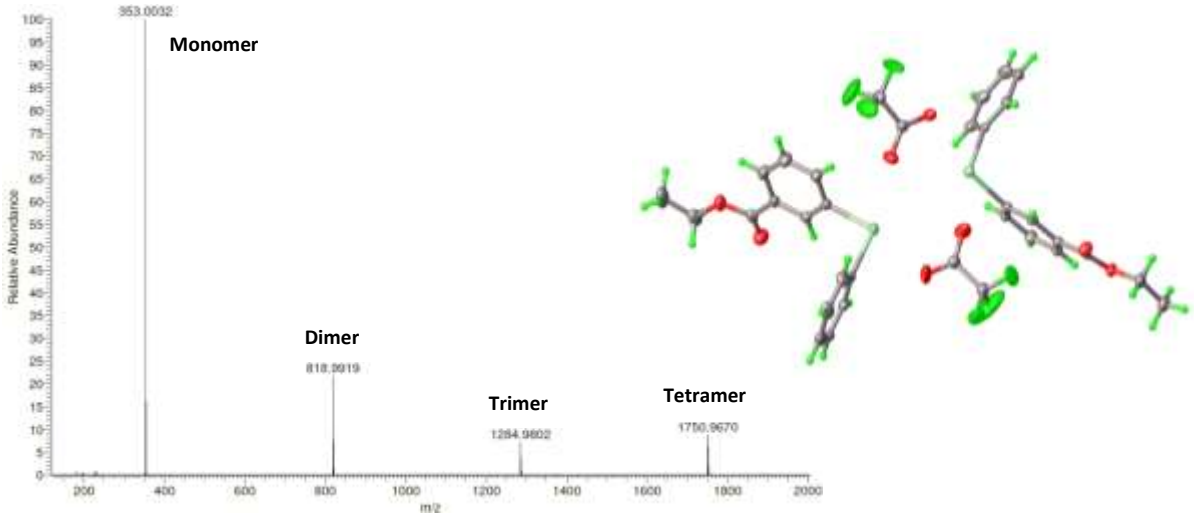

Figure 30: MS spectra and crystal structure (dimer) of **194**

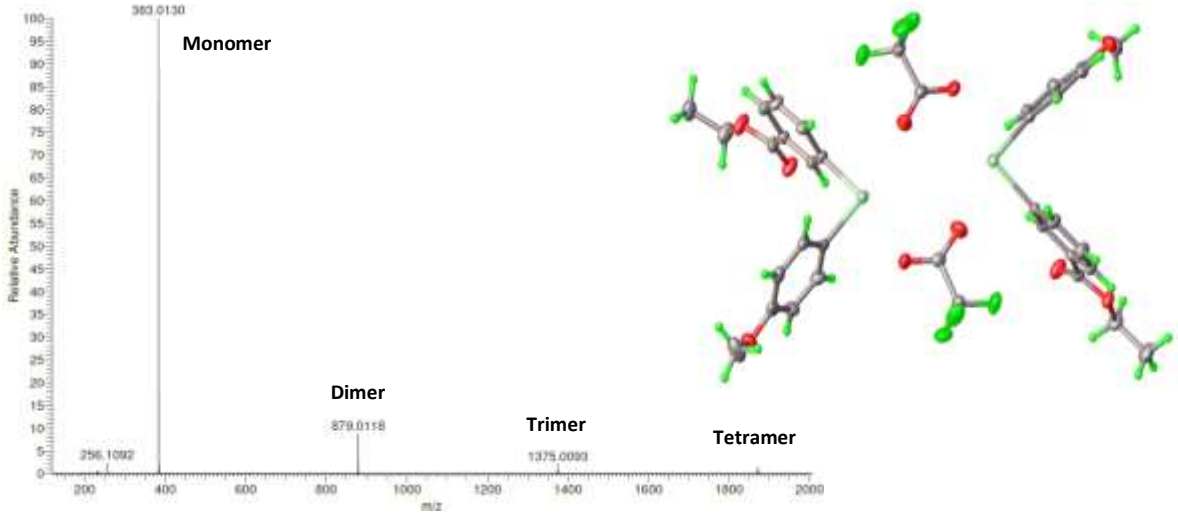

Figure 31: MS spectra and crystal structure (dimer) of **195**

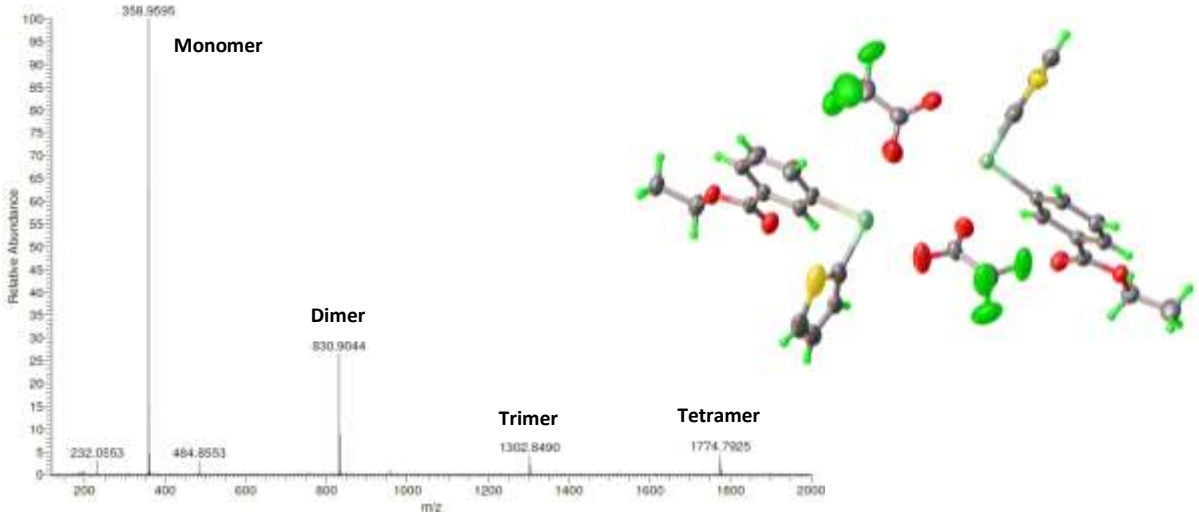

Figure 32: MS spectra showing oligomeric structures and crystal structure (dimer) of **196**

2.1.5 Fluorination of diaryliodonium salts

Before experimenting with [^{18}F]fluoride, fluorination of the diaryliodonium salts was performed using CsF in dry *N, N*-dimethylformamide in order to investigate the selectivity of the reaction (Scheme 68).

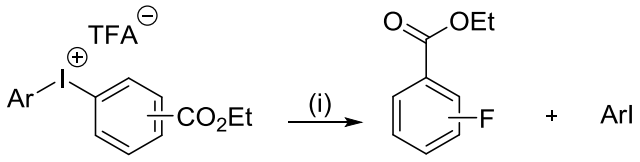

191-196 **188d-e**

(i) CsF, DMF, 130 °C, 1.5 h

Scheme 68: Fluorination of diaryliodonium salts **191-196**

As discussed earlier (Sections 1.2.9 and 1.4.1) the reaction most likely proceeds via a "turnstile mechanism", incorporating a reductive elimination step, following the dissociation of the anion to give the diaryliodonium cation.[181] Momomeric iodine cations are quite flexible and are therefore able to interconvert through different conformations. By doing so, the ligands rapidly interchange through positions relative to the anion, which is secondarily bonded to the pivotal hypervalent iodine atom.[189] The nucleophilic fluoride must attack the *ipso*-carbon atom in the ring which is equatorial, from an apical position. The fluoride therefore attacks either of the two interconverting isomers to produce two different transition states that yield different fluorinated products. The ratio of fluorinated products then depends entirely upon the difference in free energies of the two transition states. This would be assuming that the fluorination reaction follows the Curtin-Hammett principle which states that the relative amounts of products formed from two different conformations of substrate are independent of the relative amounts of the conformations and depend solely upon

the difference in the free energy of the transition states, provided that the rates of the reaction are considerably slower than the rates of conformational interconversion.[148]

Where there are no *ortho*-substitutents present and therefore no "*ortho* affect" (Section 1.4.2.1) is exerted, the nucleophilic fluoride is incorporated into the most electron-deficient ring.[184]

Compounds **191–196** were fluorinated using CsF in DMF at 130 °C for 1.5 h under N_2 (Scheme 68). Samples were taken (0.3 mL) rapidly cooled to RT, diluted with d_7-DMF (0.4 mL) and analysed by ^{19}F-NMR in order to observe the selectivity of the reaction. Upon fluorinating **191-193,** peaks corresponding to the formation of ethyl 4-fluorobenzoate (δ –107.32 ppm in d_7-DMF) were observed in each instance (Figure 33). No peaks corresponding to the fluorinated NTR were observed (Table 9). This is in accordance with the proposed selectivity of the reaction. The large peak found in each spectrum (–76.61, –75.44, and –75.48) correspond to fluorine of the TFA anion of the diaryliodonium salt.

Fluorinated Compound	**NTR**	**Non-desired product**	**^{19}F-NMR δ of non-desired product (ppm)**
191	phenyl	fluorobenzene	–114.18
192	4-anisyl	4-fluoroanisole	–125.61
193	2-thienyl	2-fluorothiophene	–136.74

Table 9: Table to show ^{19}F-NMR chemical shifts of non-desired fluoroarenes

Upon fluorination **194–196,** using the same method, peaks corresponding to the formation of ethyl 3-fluorobenzoate (δ –113.67 ppm in d_7-DMF) were observed in each instance. Again, peaks corresponding to the fluorinated NTR were not observed, further demonstrating the selectivity of the reaction.

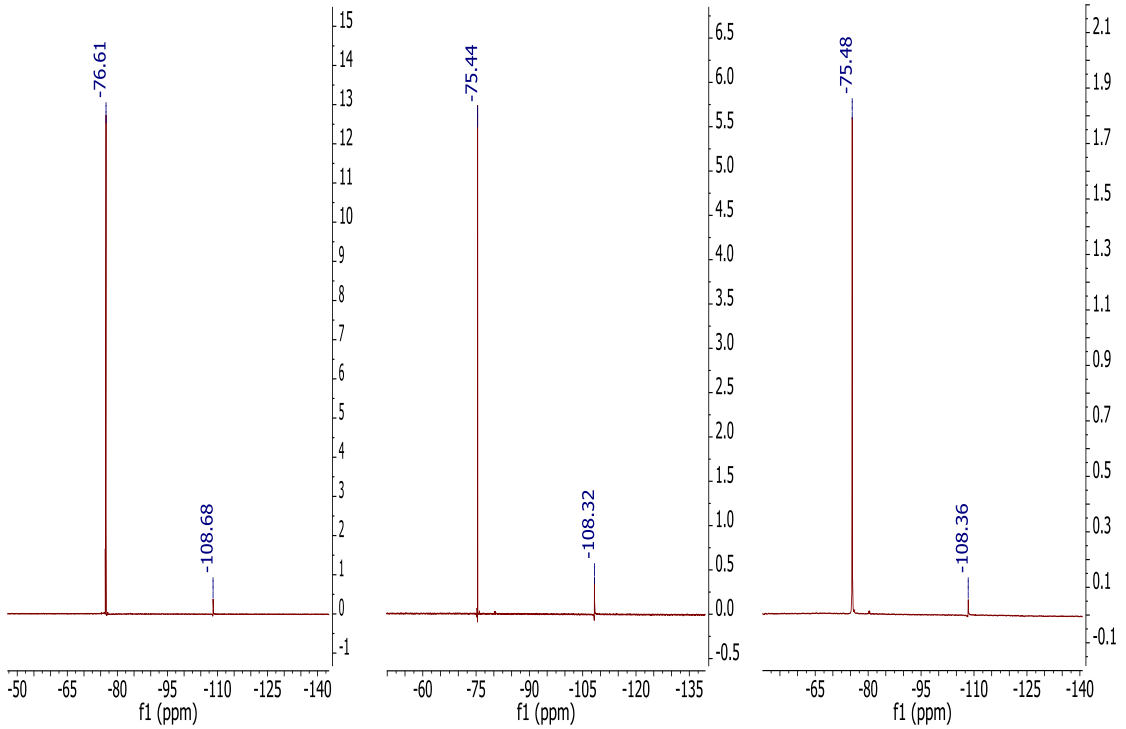

Figure 33: ^{19}F-NMR to show the formation of ethyl 4-fluorobenzoate from diaryliodonium salts using CsF - from **191** (left) from **192** (middle) from **193** (right)**.**

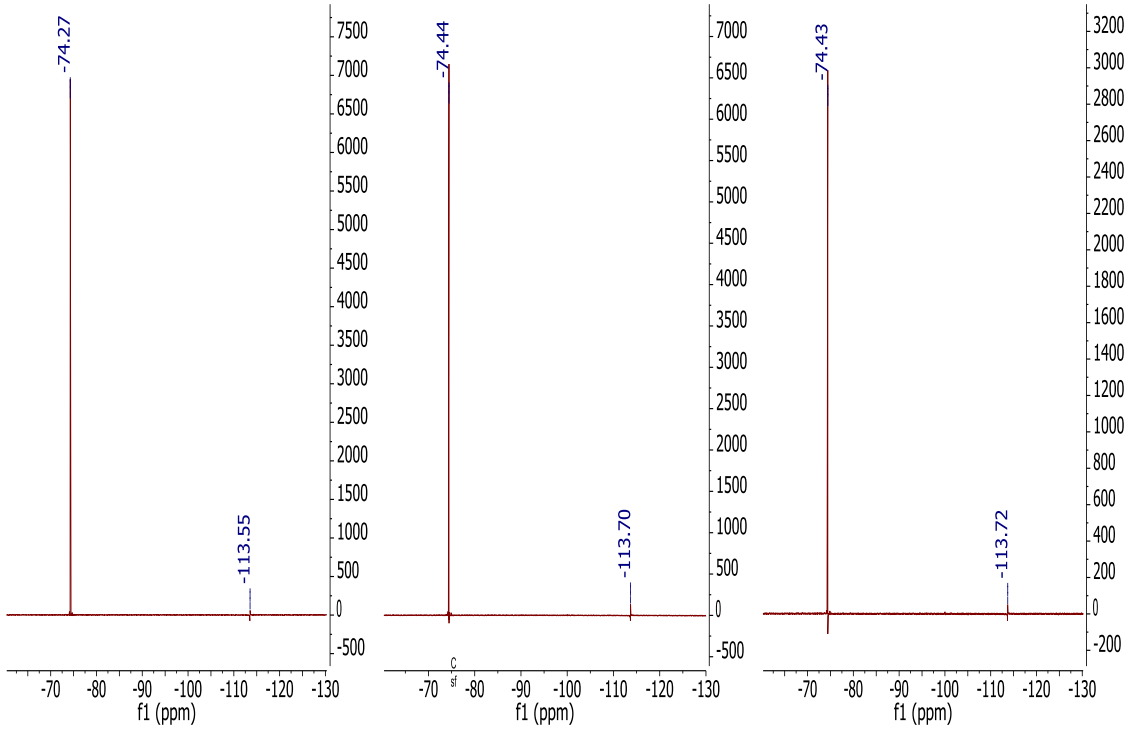

Figure 34: ^{19}F-NMR to show the formation of ethyl 3-fluorobenzoate from diaryliodonium salts using CsF - from **194** (left) from **195** (middle) from **196** (right).

2.1.6 Syntheses of trifluoroacetyl(2-ethoxycarbonylphenyl, aryl)-λ^3-iodanes

As shown earlier (Section 2.1.4) only trace amounts of the trifluoroacetyl(2-ethoxycarbonylphenyl, aryl)-λ^3-iodanes **197–199** could be generated using the traditional approach. It could be seen from crude ^{1}H-NMR that reasonable amounts of the diaryliodonium salts had been produced, however, there were significant challenges in attempting to purify the product. Many different solvents were used in attempting to purify by crystallisation but the low yields prevented the formation of solid, producing only an oil containing a mixture of starting material, product and unwanted side-products. Flash chromatography (DCM:MeOH) resulted in the transesterification of the ester functionality resulting in a mixture of the desired compounds and the methyl ester derivatives. This was confirmed by HMQC NMR. Changing the composition of the mobile phase (DCM:EtOH) frequently resulted in co-elution of the product with unwanted side-products. Attempts to synthesise the corresponding tosylates using *m*-CPBA,[76, 186] with the intention of generating the trifluoroacetates by anion exchange, were very low yielding.

As diaryliodonium salts **191–196** were available for [^{18}F]fluorination reactions, with the selectivity of the process having been confirmed, focus of the project moved to the radiofluorination of diaryliodonium salts.

2.1.7 Conclusion

An unconventinonal approach, obviating the use of hazardous organolithium reagents and expensive palladium cataylsts, has been successfully used to generate all regiosisomers of ethyl (tri-n-butylstannyl)benzoate in good yields and short reaction times. A simple but effective method of chromatography has aided the isolation of the desired stannanes in very high purity. These compounds were combined with

diacetoxyiodoarenes to produce the 4- and 3- regioisomer diaryliodium salts. These compounds demonstrate the regioselectivity of the reaction with fluoride, which targets the electron-deficient ring to produce only the desired fluoroarenes, as evidenced by ^{19}F-NMR. Crystal structures for the 4- and 3-regioisomers have also been determined, which highlight the presence of higher order materials in addition to the monomeric species.

2.2 Microfluidic Radiochemistry

For nearly 50 years, PET has been used to investigate a range of medical conditions in oncology, neurology, psychiatry, and cardiology. There have been over 1500 biologically active compounds bearing positron emitting isotopes described in the literature.[239] However, one tracer, [^{18}F]fluorodeoxyglucose, accounts for over 90% of all clinical PET scans due to its broad applicability and availability. Other radiotracers, with greater specificity, have the potential to generate greater understanding of differing medical conditions but their use has, so far, been restricted to specialist facilities.

Central to the radiopharmaceutical synthesis is the rapid and efficient incorporation of a radioactive isotope into a molecule of interest followed by immediate purification and formulation. This can pose a significant challenge to the radiochemist, especially when using short-lived positron emitting isotopes such as fluorine-18. Radiolabelling must occur in the final stages of the synthetic sequence which may involve multiple processes concluding with a deprotection step. Furthermore, as radiotracers must be produced as pharmaceutical grade materials, purification and reformulation must be considered when planning a radiosynthetic strategy. Large quantities of starting radioactivity may be required to compensate for decay, inefficient incorporation and losses during purification and dose preparation. Conventional laboratory methods are not suitable for radiochemistry practices as they involve personal exposure to radiation and are often time-consuming. Automated or robotic equipment capable of controlling chemical reactions is required to ensure that the radiochemist can be separated from positron emitting isotopes by lead shielding and therefore, protected from harmful gamma-rays. This equipment is also capable of reducing the timescale of

such processes whilst conveying the necessary degree of reproducibility required of a routine production schedule.

PET radiolabelling methods are also carried out on a small scale due to the minute amounts of radioisotope produced by modern cyclotrons. This creates further challenges such as radioisotope preconcentration, side reactions, product purification, and product analysis.

2.2.1 Aims

Recently, there has been great interest within the PET community in the potential benefits of microfluidic technology.[240] The popularity of microfluidic devices has dramatically increased as it has become increasingly apparent that these synthetic chemistry platforms bear features which overcome some of the challenges presented by radiochemical syntheses. This methodology, coupled with the strict control of the reaction parameters, also has the potential to enhance selectivity for the desired transformation over by-product generation, improve radiochemical yields (RCYs) and thus facilitate the purification of the target radiopharmaceutical. In addition, the high degree of reproducibility inherent to this approach is essential for the routine production of PET imaging agents. A critical advantage of microfluidic systems, in PET radiochemistry, when compared to conventional batch platforms, is that they enable multiple reactions to be conducted from a single batch of radioisotope allowing a degree of process optimisation not typically associated with short-lived radioisotopes. For this reason, a microfluidic device was adopted to investigate the radiosynthesis of ethyl [^{18}F]fluorobenzoates from diaryliodonium salts **191-196**.

2.2.2 Microfluidics

Microfluidic devices or microfluidic chips are small devices with an internal network of micron-sized channels (typically 10–300 μm) capable of performing, controlling and processing miniaturised chemical process in a continuous-flow manner.[241-243] Most microfluidic devices also incorporate mixing units, a heat source and a pumping system to control fluid or gas flow. Devices may be constructed from various materials whilst flow is generally induced by either mechanical syringes, diaphragm pumps or via an electric field to induce electrokinetic flow.

In microfluidic technology fluids are forced to flow in micro-channels, creating an environment different from fluid flow in bulk systems, which is closer to the molecular level than conventional flask-based chemistry. This is the principle of miniaturisation and is responsible for the significant reduction of reaction times in microfluidics. The time required for a single molecule to react from reagent to product through a transition state is in the range of 10^{-14} – 10^{-13} s, while the time required for all the molecules in a flask to react generally ranges from minutes to hours (10^{2} – 10^{4} s). The size of molecules is in the range of 10^{-10} – 10^{-9}m, whilst the size of a flask ranges from 10^{-2} – 10 m, which means that there is clear correlation between the size of the reaction environment and the reaction time (Figure 35).[244]

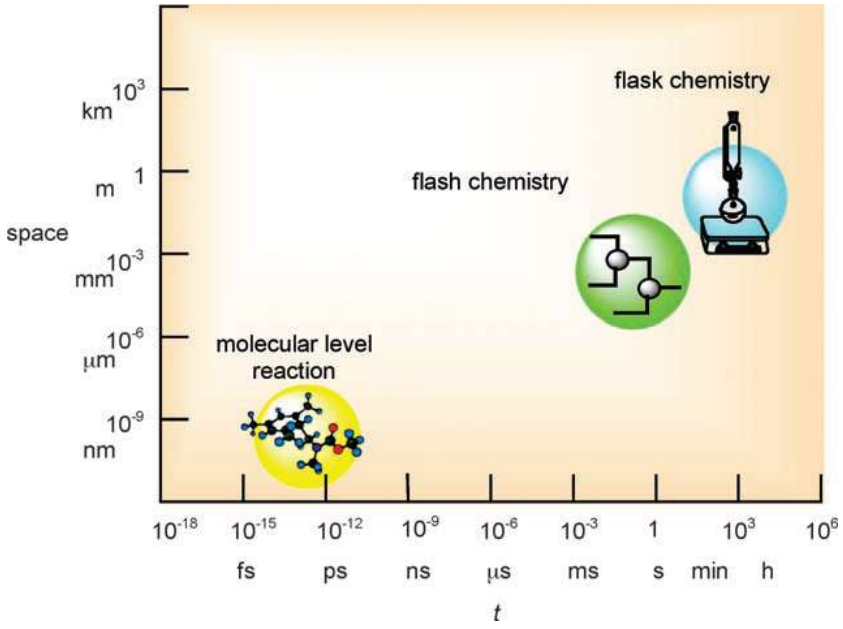

Figure 35: Time/Space relationship for chemical reactions. Taken from [244].

2.2.3 Advantages to Microfluidics

2.2.3.1 Improved mixing

Fluid flow in the micro-channels is dominated by viscous forces, as opposed to inertial forces, and generally results in the existence of laminar flow regimes with Reynolds number (Re) of less than 100.[245] Turbulent flow dominates in bulk systems, such as round-bottom flasks, where Reynolds number is greater than 1000. Mixing between adjacent laminae in micro-channels is diffusion dependent and can be problematic leading to inefficient mixing. Despite this, mixing of reagents can be extremely fast[246] provided the channel diameters (diffusion distances) are less than 100 μm. This leads to a significant improvement in reaction rates when compared to conventional laboratory practices.[247]

2.2.3.2 Improved surface area-to-volume ratio

The most important benefit gained upon moving from a bulk laboratory apparatus to a microfluidic reactor is the large increase in surface area-to-volume ratio. The typical surface area-to-volume ratio of conventional laboratory reactors does not exceed 1000 m^2m^{-3} whereas microreactor surface area-to volume ratios can be as high as 50000

m^2m^{-3}. The large surface area-to-volume ratio greatly enhances the mass transport via rapid diffusion timescales leading to better mixing and considerably improved heat transfer either toward or away from the reactor. Whilst the broad temperature profiles in batch reactors can lead to multiple reaction pathways, the narrow temperature distribution, characteristic of a microreactor, ideally restricts the reaction to the target product (Figure 36). This is enhanced by the fine temperature control achievable using a computer-operated microfluidic device.

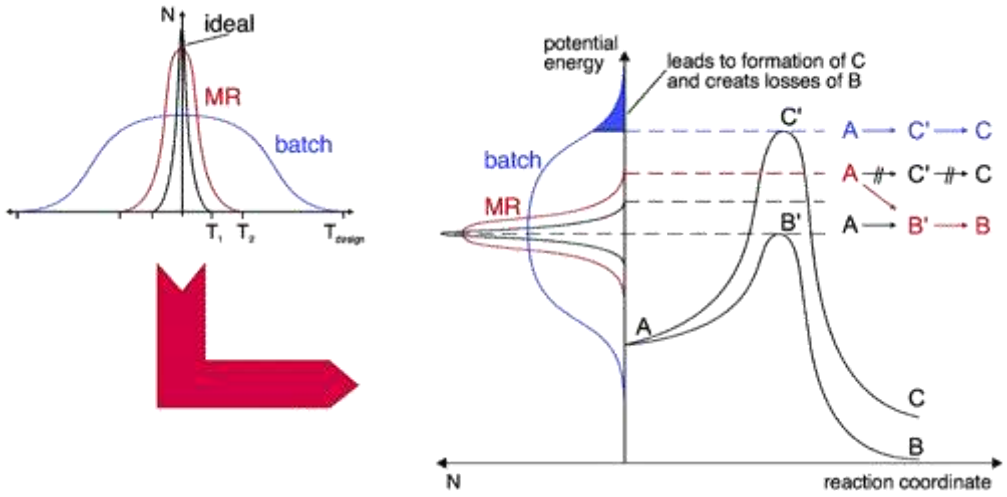

Figure 36: (left) Comparison between temperature distributions between an ideal hypothetical reaction (black) a batch reaction (blue) and a microfluidic reaction (red). (right) Schematic comparison of temperature distributions, to two possible by-product forming pathways. Taken from [248].

High heat exchange coefficients and rapid temperature changes[249] are also possible, depending upon the materials and heat exchanger used.[250]

2.2.3.3 Improved rates of reaction, yields and selectivities

Due to the improvement in mixing and heat transfer, reactions performed in microfluidic devices can be carried out significantly faster with increases in both yield and selectivity. Haswell and co-workers have shown that the aldol reaction between an aldehyde **229** and a silylenol ether **228** in the presence of tetrabutylammonium fluoride (TBAF) reaches completion after 24 h in a typical laboratory reactor, compared to just 20 min in a microreactor (Scheme 69).[251]

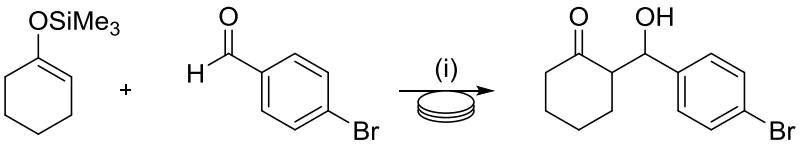

228 **229** **230**

(i) TBAF, 20 min

Scheme 69: Aldol reaction performed in a microreactor

Many rapid reactions, which show comparable reaction times between batch and microfluidic platforms, show significant improvements in yields upon transferring to the latter. Large improvements have been shown in Wittig reactions,[252, 253] oxidations,[254, 255] coupling reactions,[256, 257] and heterocycle formations.[258, 259]

2.2.3.4 Rapid optimisation with low volumes

Optimisation is essential at every step of a synthetic process and any reduction of material input and waste reduces the time taken and cost required of optimising reaction parameters. Due to the small volumes and short reaction times required, rapid optimisation of reaction conditions may be achieved using a microreactor. This is often facilitated by the immediate adjustment of conditions possible by controlling the microreactor environment with computer software which often accompany microfluidic systems (*e.g.* Advion NanoTek Microfluidic System).

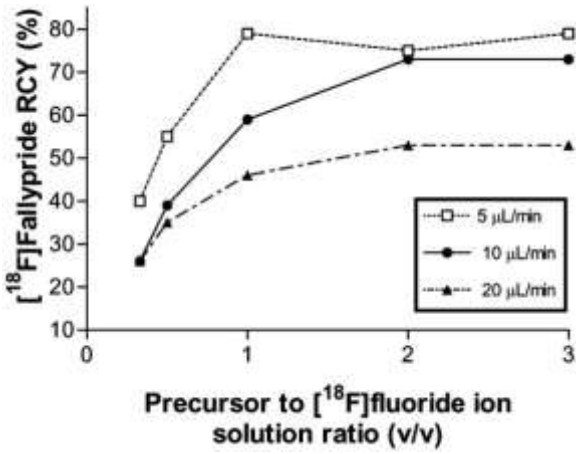

Image 1: Graph to show the rapid optimisation of reaction parameters possible using a microfluidic device. In this example, the precursor to [^{18}F]fluoride ion solution ratio (v/v) was optimised in the radiosynthesis of the imaging agent [^{18}F]fallypride, at different flow rates. Taken from [260].

2.2.3.5 Exothermic and runaway reactions

The unique heat transfer properties of micro-channel devices allow for reactions which were previously inaccessible on large scales, to be controlled and even manipulated. By rapidly cooling microreactors, large exotherms can be reduced creating a safer environment whilst improving selectivity. Aromatic nitrations are often dangerous as they can be very exothermic and generate explosive by-products. Ducry and Roberge used calorimetry to compare the autocatalytic nitration of phenol in a microreactor to similar reactions in batch.[261] When the reaction was performed in batch, two large exotherms were created, leading to an increase in temperature of 55 °C. However, upon reaching the equivalent stage, the same reaction increased by only 5 °C when being performed in a microreactor (Scheme 70). This rigid temperature control provided greater selectivity and higher yields whilst also reducing the formation of by-products.

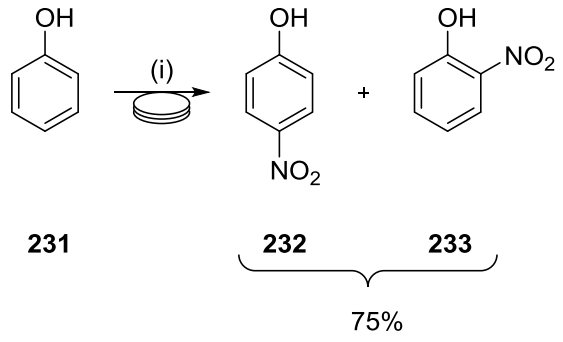

Scheme 70: Nitration of Phenol in a microreactor[261]

2.2.3.6 Improved efficiency and reduced waste

Reactions in microreactors typically provide higher yields and greater selectivity than batch reactions. Higher concentrations of reagents can be used due to the rapid heat transfer achieved in the micro-sized channels. This creates a higher atom economy,

thereby reducing the volume of waste material produced and reaction solvent required. Some microfluidic reactions may even be performed in neat conditions which are often inaccessible in batch reactors due to high exothermicity.

2.2.3.7 In-line integration of devices

Many microfluidic reactors allow for the in-line integration of other systems and devices. It is possible to monitor reactions *in situ* using UV/vis or IR analysis to provide real-time analysis on the transformation of a reaction. A common practice is to use an automated injector to load the reaction bolus onto a HPLC system for inline purification of products. By doing so, the speed with which reaction conditions can be optimised is further increased as outcomes or yields of microfluidic reactions can be immediately deduced. The loss of volatile products is also prevented.

2.2.3.8 No scale-up required

The unique mixing process and rapid heat transfer characteristic of microfluidic reactors does not allow for reactions to be scaled up. To increase production of a desired compound, several microreactors may be used in parallel (the “numbering up” principle). With this approach, the need to re-optimise reaction conditions for large scale production is negated as yields of reactions are consistent across the assembly of multiple microreactors. The savings in terms of time, resources, cost and waste is significant. An alternative strategy is to extend the product collection time or increase the length of the micro-sized channels used (the “scaling out” principle). This is better practice when the use of multiple microreactors employed in parallel is impractical or unnecessary, such as the scaling up from milligram quantities to grams.

2.2.3.9 Multi-step transformations

Many microfluidic systems allow for several microreactors to be connected in series thereby allowing multiple steps to be performed before isolation of the final products. After having demonstrated that peptide bonds could be formed in a microreactor, Haswell and co-workers extended their methodology to prepare longer chain peptides.[262] Using a bespoke microfluidic apparatus, the Dmab ester of Fmoc-β-alanine **234** was reacted with DBU to give the free amine which was then reacted with the pentafluorophenyl ester of Boc-β-alanine to form a protected dipeptide **236** (Scheme 71). Reaction conditions were optimised to improve yields from 25% to 96%, based on the amount of Dmab ester present at the end of the reaction.[262]

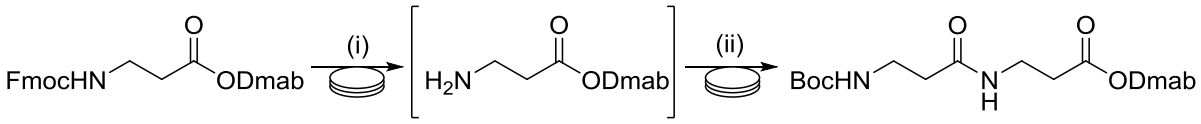

234 **235** **236**

(i) DBU (1 eq), DMF (ii) Pentafluorophenyl-*N*-Boc-β-alanine, DMF

Scheme 71: Multi-step synthesis of dipeptide in a microreactor[262]

2.2.3.10 Improved safety

As well enhanced control of potential exotherms, the low volumes of reagents required in microfluidic syntheses allows for far less potentially toxic material to be used. These systems are also often closed systems which can be controlled externally, outside the confines of a laboratory fumehood. This has major implications in radiochemistry whereby protective shielding (*e.g.* lead shielding) can be installed to separate the radiochemist from harmful radiation whilst allowing the microfluidic reaction to be controlled and monitored.

2.2.4 Microfluidics in PET Radiochemistry

Due to the inherent advantage of miniaturisation, microfluidic technology is becoming an invaluable tool in the development of PET radiochemical methods, allowing the relative quantities of precursors/reagents/solvents to be significantly reduced facilitating timely isolation of the final radiolabelled product.[245, 263-266] As discussed above, the rapid heat transfer and efficient mixing, coupled with the strict control of the reaction parameters, has the potential to enhance selectivity for the desired transformation over by-product generation, improve RCYs and thus increase the RCP. In addition, the high degree of reproducibility inherent to this approach is essential for the routine production of PET imaging agents. A critical advantage of microfluidic systems, in PET radiochemistry, when compared to conventional batch platforms, is that they enable multiple reactions to be conducted from a single batch of radioisotope allowing a degree of process optimisation not typically associated with short-lived radioisotopes. As mentioned above, the capacity to shield the radiation present throughout the microfluidic device from the radiochemist is an obvious advantage. The automation of microfluidic devices also promotes GMP standards for radiotracer production as the fine control of reaction conditions promotes reproducibility of the reaction yields and enhances the likelihood of outputs adhering to standards required for on-demand production of imaging agents.

The radiosynthesis of [^{18}F]FDG has dominated the proof-of-concept testing of various microfluidic devices, due to the broad application of this molecular imaging probe. Tseng and co-workers presented the most significant work in this field by building an integrated microfluidic device used to synthesise [^{18}F]FDG in high RCY (38%) and high

RCP (97.6%) with short synthesis times (14 min) when compared to commercial synthesisers (~50 min).[267]

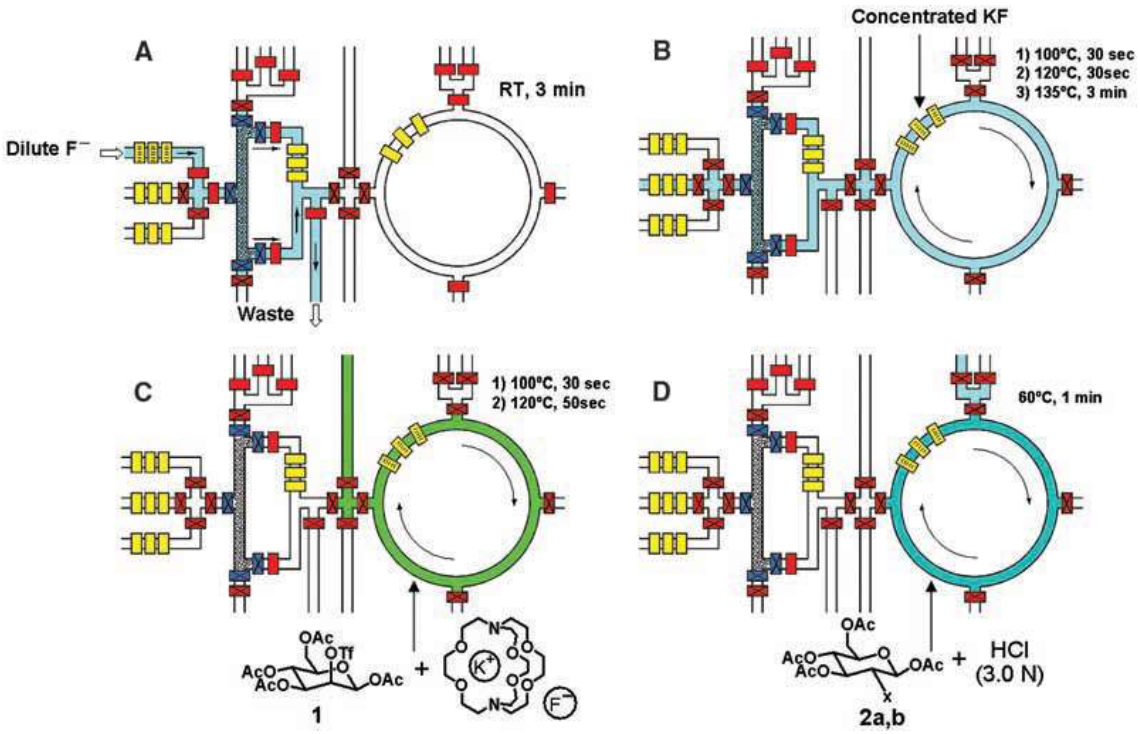

Figure 37: Schematic diagram to show the steps involved in the microfluidic synthesis of [^{18}F]FDG[267]

Five sequential steps ([^{18}F]fluoride concentration, water evaporation, radiofluorination, solvent exchange and hydrolytic deprotection) were performed in an integrated microfluidic chemical reaction circuit (Figure 37) designed to demonstrate the digital control of sequential chemical steps, in variable chemical environments and with variable physical conditions. The fluoride solution was first concentrated using a miniature anion-exchange column before a solution of K_2CO_3 was used to elute the [^{18}F]fluoride and create a solution of KF (Figure 37, A). Heat was applied to evaporate the water (Figure 37, B) before MeCN solution is introduced, wherein the [^{18}F]fluorination reaction takes place, using Kryptofix to heighten the reactivity of the [^{18}F]fluoride against the D-mannose triflate (Figure 37, C). A computer was used to control the temperature gradient within the reaction loop and therefore produce the

protected intermediate. After evaporation of the MeCN, an HCl solution is introduced into the reaction loop to hydrolyse the intermediate and give the final product (Figure 37, D).

This work was hugely significant to the field as the proof of concept result could be generalised to a range of radiolabelled substrates, thereby demonstrating the vast potential of microfluidics to the PET chemistry.

Since then, microfluidic reactors have become commercially available as individual or modular devices and used to create a vast array of potential imaging agents (Table 10).

Isotope	System	Product	RCY (%)	Processing time (residence time in reactor)	Reference
^{11}C	Custom	[^{11}C]methyl ester	64 (DC)	10 min (12 s)	Lu et al[268]
^{11}C	Custom	[^{11}C]amides	44-88 (DC)	15 min (2 s - gas reagents) (2 min - liquid reagents)	Miller et al[269]
^{11}C	Advion NanoTek	[^{11}C]DASB	45	34 min (1 min)	Ungersboeck *et al*[270]
^{18}F	Custom	[^{18}F]FDG	20	18 min (9 s)	Steel *et al*[271]
^{18}F	Scintomics	[^{18}F]FDG	88 (DC)	7 min	Wester[272]
^{18}F	Advion NanoTek	[^{18}F]Fallypride	88 (DC)	50 min (4 min)	Lu *et al*[260]
^{124}I	Custom	[^{124}I]Annexin-V protein	40	2 min	Gillies *et al*[273]
^{99m}Tc	Advion Nanotek	[^{99m}Tc]DTV-AHx-insulin	40	(15.7 min)	Simms *et al*[274]

Table 10: Selected examples of isotopic labelling reactions performed using various microfluidic devices

2.2.5 Advion NanoTek Microfluidic system

All microfluidic devices benefit from the features of miniaturisation and generate high RCYs, high RCPs and short residence times. The Advion NanoTek Microfluidic System (Advion Biosciences) is a commercially-available microfluidic system with the capacity to extend reaction conditions beyond those of conventional batch systems. The microreactor, central to the device, is a closed system capable of operating at

pressures of up to 400 psi (28 Bar) whilst tolerating temperatures up to 220 °C (Table 11).

Solvent	Boiling Point at 14.7 psi (Atmospheric Pressure)	Boiling Point at 400.0 psi (upper limit of NanoTek®)
MeCN	82	186
H_2O	100	217
DMF	153	312
DMSO	189	383

Table 11: Boiling Points of common solvents and boiling points within the NanoTek Microfluidic System (upper temperature limit – 220 °C)

The NanoTek system is also accompanied by a software package which operates the device and provides users with fine control of the reaction parameters (Image 2a). This makes the system highly reproducible, as the exact reaction parameters desired can be replicated with ease. The software also displays and records data regarding the system status (*e.g.* reactor temperature, Image 2b).

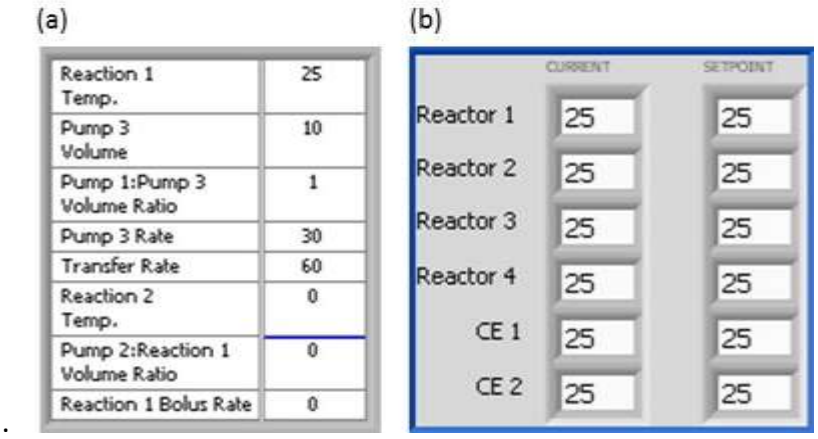

Image 2: Image taken from the NanoTek software showing (a) which reaction parameters can be manipulated following input from the user, and (b) the current and setpoint temperatures of the microreactors and the two CMs (Those parameters controlling 'Reaction 2' are ignored as only one-step reactions were performed throughout this project).

Due to these valuable features, the recent emergence in microfluidic technology for the preparation of PET imaging agents, has been dominated by the use of the NanoTek system (Figure 38), also thanks to the commercial availability of the device. The small system footprint, high through-put, and the ability to prepare both fluorine-18 and

carbon-11 radiolabelled materials, make this microfluidic system hugely attractive to the modern radiochemist.

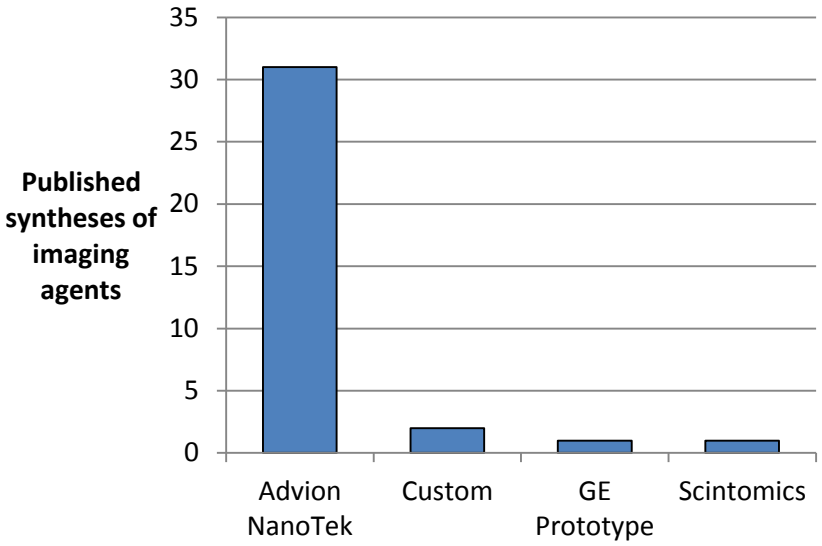

Figure 38: Graph to show number of publications reporting the syntheses of PET imaging agents performed using a microfluidic systems (1981-2013)[275]

It should be noted that the GE prototype and Scintomics devices were custom built at the facilities wherein the radiochemical syntheses took place. The GE system was fabricated from from glass by incorporating a single two-stage microfluidic device with localized heating capabilities.[271] The Scintomics device was assembled from various Scintomics modules.[272] To this author's knowledge, these devices are not commercially available. For the reasons described above, the NanoTek system was chosen to provide an efficient, versatile and convenient methodology for the rapid optimisation of microfluidic radiofluorination reactions, throughout this project.

2.2.6 Significant Radiochemical Syntheses performed using the Advion NanoTek Microfluidic System

Pike and colleagues reported the first synthesis of a PET imaging agent using the NanoTek system.[260] [^{18}F]Fallypride, which is widely used for imaging dopamine subtype-2 (D_2) receptors in living animal[276, 277] or human brain,[278] was synthesised in

one convenient step from the corresponding tosylate precursor (Scheme 72). Small doses of precursor and [^{18}F]fluoride ion were used to quickly optimise the labelling reaction, with respect to effects of precursor quantity, reaction temperature, flow rate (residence time) and [^{18}F]fluoride to precursor ratio. Excellent RCYs of up to 88% were achieved and found to be reproducible. The small amounts of material used allowed crude [^{18}F]fallypride to be purified rapidly using an in-line HPLC system, before formulation for intravenous injection. Scaling up the reaction was achieved by continuously infusing solutions of precursors.[260]

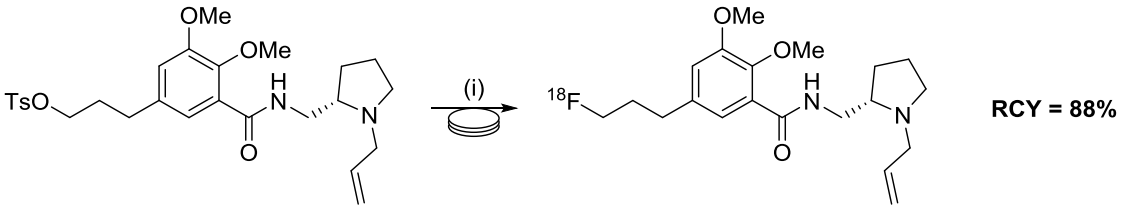

237 **238**

(i) [^{18}F]KF/K222, MeCN

Scheme 72: Synthesis of [^{18}F]fallypride **238** in a single-step using the NanoTek system.[260]

The NanoTek has also been used to optimise the radiosynthesis of a small library of related compounds. Pascali and colleagues adapted the NanoTek system to perform the synthesis and purification of [^{18}F]fluoromethyl, [^{18}F]fluoroethyl and [^{18}F]fluoropropyl choline **241a-c**.[279] The corresponding alkyl-ditosylate precursors **239a-c** were used to generate [^{18}F]fluoroalkyltosylates **240a-c** which would then react with neat DMEA to produce the desired products (Scheme 73). Purifications were performed using an in-line recyclable SPE cartridge set. Good RCYs (22-54%) were obtained in short processing times (15 min). Most significantly, the synthetic procedure allows for sequential production of **241a-c** using the same batch of isotope, which is strongly in accordance with the dose-on-demand (DOD) approach. Such

methodology allows for an efficient and direct comparison of **241a-c** for the diagnosis of prostate cancer.[279]

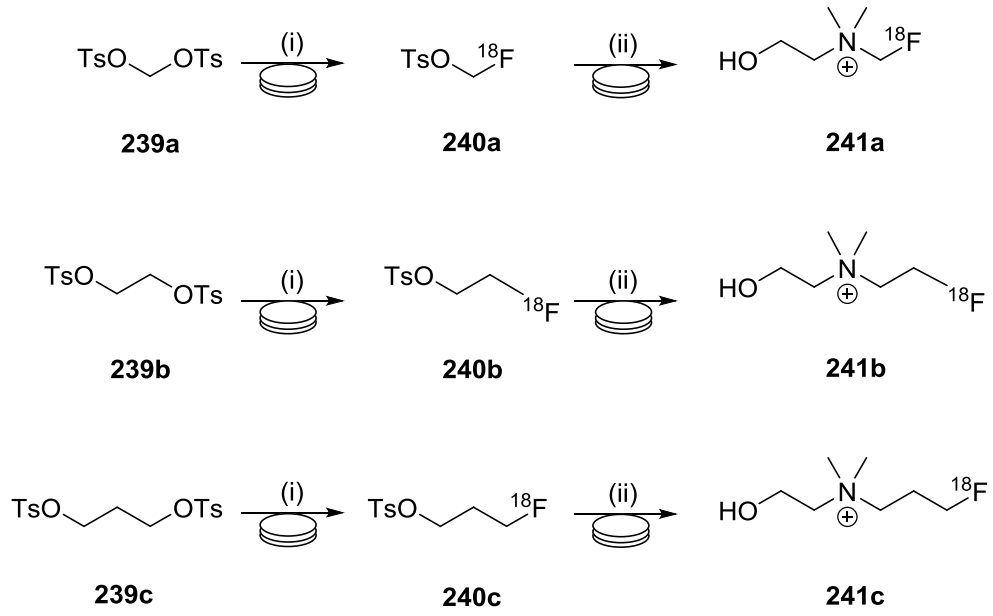

(i) [^{18}F]KF/K222, MeCN (ii) DMEA (neat.)

Scheme 73: Small library of [^{18}F]fluorocholine analogues produced using the NanoTek system. In this example, a two-step microfluidic process has been used to create the products. Taken from [279]

More recently, Ungersboech and colleagues have optimised the radiosynthesis of [^{18}F]Altanserin using the NanoTek system.[280] [^{18}F]Altanserin **243** has been found to have high binding affinities for 5-HT$_{2A}$ receptor sites and is, therefore, a specific radiotracer for the visualisation and quantification of this receptor subtype *in vivo*. The four parameters to be evaluated were precursor concentration, reaction temperature, flow rate and reagent volume. By applying optimised conditions, which required reaction temperatures of up to 220 °C, radiochemical incorporation yields (RCIYs) were raised to 54% for scaled-up syntheses of the one-step [^{18}F]fluorodenitration (Scheme 74).[280]

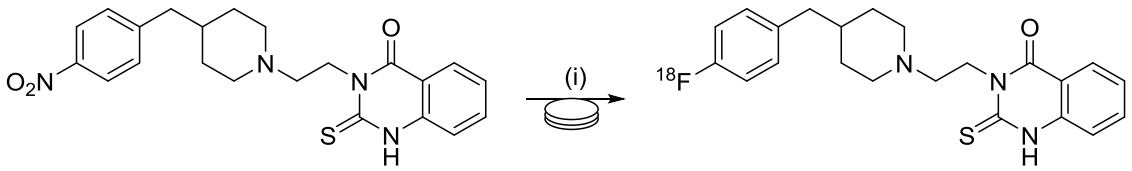

242 **243**

(i) [^{18}F]KF/K222, DMSO

Scheme 74: Radiosynthesis of [^{18}F]Altanserin **243** from corresponding nitro precursor, optimised using the NanoTek system.[280]

Interestingly, the authors found that applying higher reaction volumes resulted in increased radiochemical incorporation yield (RCIY) a so-called "bolus" effect. The authors propose that this is the result of heterogeneous distribution within the reaction volume caused by diffusion at the bolus interface (*i.e.* the reactor contents have not reached a steady state) – an effect which is less pronounced in larger volumes.

(RCIY is a recent term which has become frequently used to describe the extent to which the radioactive isotope has become incorporated into the precursor molecule thus creating the desired compound. The term differs from RCY, as it is calculated from the integration of peaks formed from a radio-chromatographic trace (*e.g.* radio-HPLC). When taking this approach to deduce the outcome of a radiochemical reaction, RCIY is a more appropriate descriptor. However, 'RCY' remains the conventional term and has been used to describe the outcome of radiosyntheses throughout this project, and the remainder of this report.)

2.2.7 System configuration

The NanoTek system consists of a base module (BM), and reactor module (RM) and concentrator module (CM) (Image 3) all are operated and controlled by the NanoTek 1.4 software.

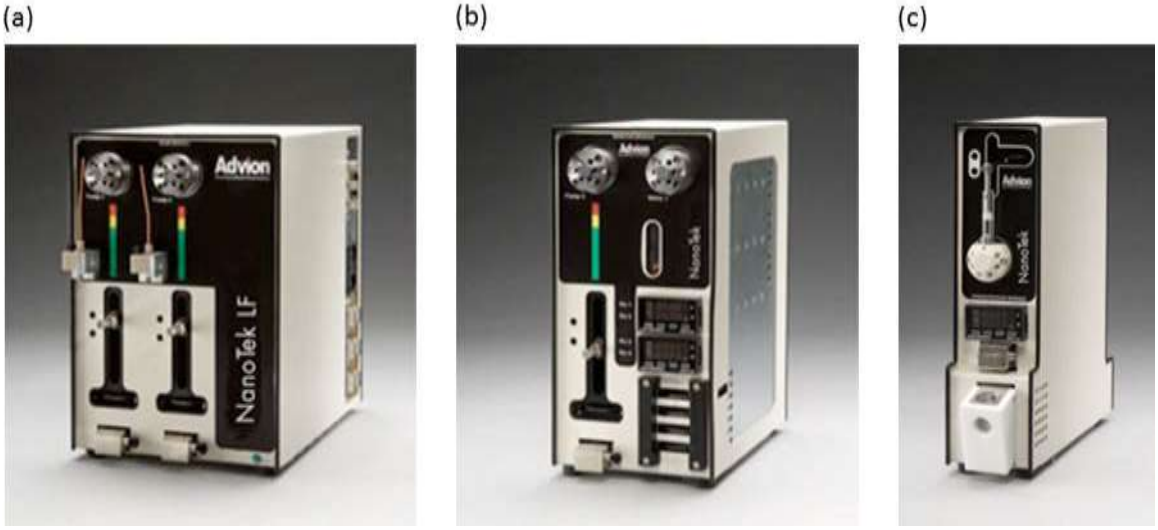

Image 3: Component modules of the Advion NanoTek Microfluidic System - (a) base module, BM (b) reactor module, RM (c) concentrator module, CM

The BM consists of two reagent cartridges (P1 and P2) used to dispense metered amounts of reactants to the microreactors for radiolabelling reactions. These cartridges comprise of a high-pressure syringe pump connected to an eight-way bridged valve supporting a looped-reservoir from which reagents are dispensed towards the microreactor, housed within the RM. The RM is the 'core' of the system and consists of the isotope reagent (P3) and microreactor cartridges (up to four) (Image 4).

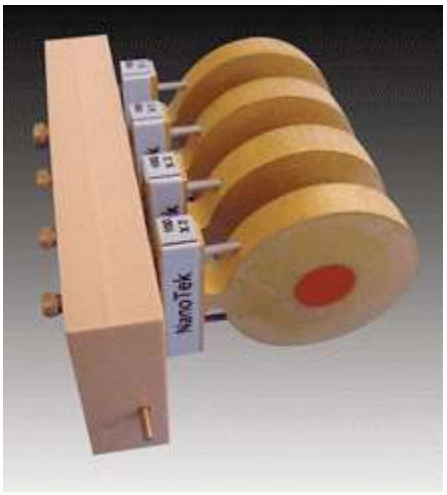

Image 4: Advion NanoTek reactor cartridge bearing four microreactors

In our setup, P3 receives a solution of reactive isotope ([^{18}F]fluoride) in a phase-transfer system (PTS) from the CM module where it is prepared from a volume of cyclotron-produced [^{18}F]fluoride in [^{18}O]H_2O. The CM module consists of a low-pressure, six-way valve reagent cartridge (CM1) and vessel chamber capable of rapid heating and evaporation of solvent. It is possible to subject the CM vessel to a combination of reduced pressure and positive flow of N_2 gas, thus allowing the [^{18}F]fluoride to be dried via several azeotropic distillations with MeCN, in accordance with the traditional anion-exchange resin trapping of [^{18}F]fluoride (Section 1.1.6). The apparatus was initially setup as shown (Figure 39).

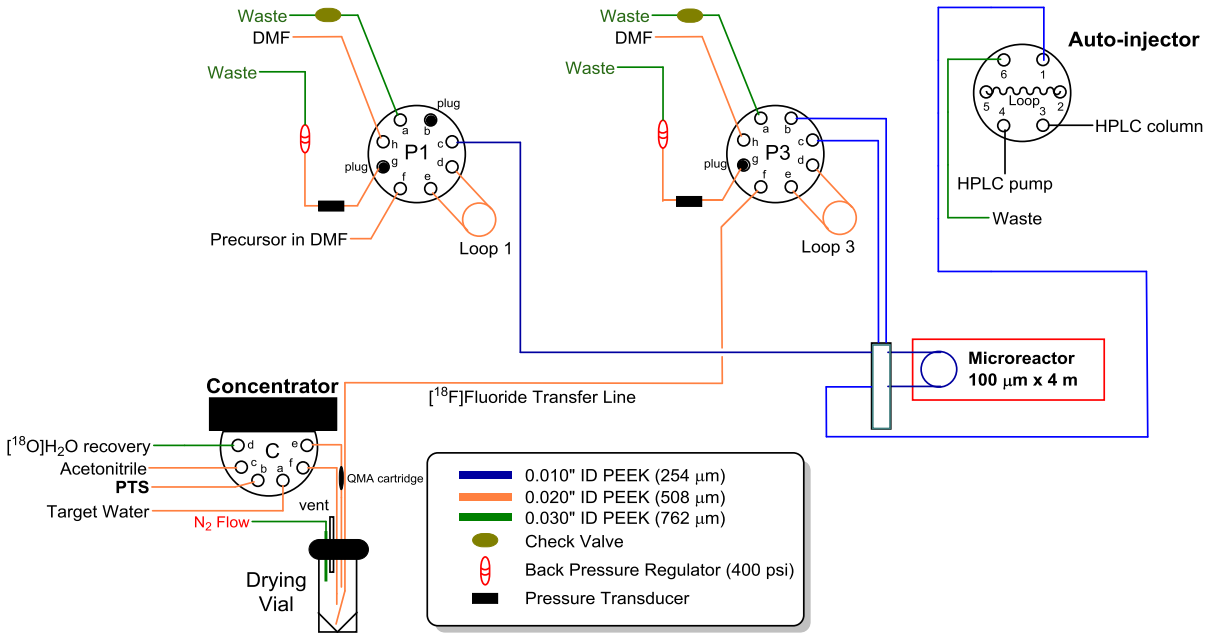

Figure 39: Initial NanoTek configuration

Throughout this project, the crude reaction mixture was swept into an electronic injection valve for direct injection onto the radio-HPLC system. The enclosed fluid paths of this tandem synthetic and analytical system ensured that the results obtained were representative of the crude reaction mixture as potential volatile products could

not be lost.[185] Operation of this valve and the initialisation of the HPLC analysis was controlled by the NanoTek software.

The accompanying software may be operated in several modes; in 'Discovery Mode' user-directed macros automate all procedures involved in the synthetic process, thereby allowing simple and rapid throughput of multiple reactions. These procedures can also be divided into their constituent parts and controlled separately within 'Manual Mode' which, therefore, allows for finer control of the system. In 'Sequence Mode' detailed macros can be written, manipulated and combined to enable extensive and complex processes to be performed with minimal user intervention. Throughout this project, user-control would fluctuate between the three modes, for optimal system management.

2.2.8 Automating the preparation of the reactive [^{18}F]fluoride in phase-transfer system

Before microfluidic reactions can be performed using the NanoTek system, the reactive [^{18}F]fluoride must be prepared from the solution of cyclotron-produced [^{18}F]fluoride in [^{18}O]H_2O. The specific approach towards achieving this using the NanoTek (Figure 40) is reflects the traditional approach described in a previous section (Section 1.1.6). Cyclotron-produced [^{18}F]fluoride (NCA) (5–100 mCi) in [^{18}O]H_2O (1–5 mL)[281] was adsorbed onto a pre-conditioned anion exchange resin (quaternary ammonium resin: Waters Sep-Pak® Light Accell Plus). The phase-transfer agent (PTA) which is dissolved in MeCN and H_2O (9:1) to create the phase-transfer system (PTS) is used to release the [^{18}F]fluoride and create a solution of radiofluorinating agent (RFA). This solution is then dried by two successive azeotropic evaporations using MeCN (450

μL) at 100 °C and under a positive flow of N_2. The RFA complex was then dissolved in DMF (450 μL) and loaded into the storage loop (P3) on the microfluidic system.

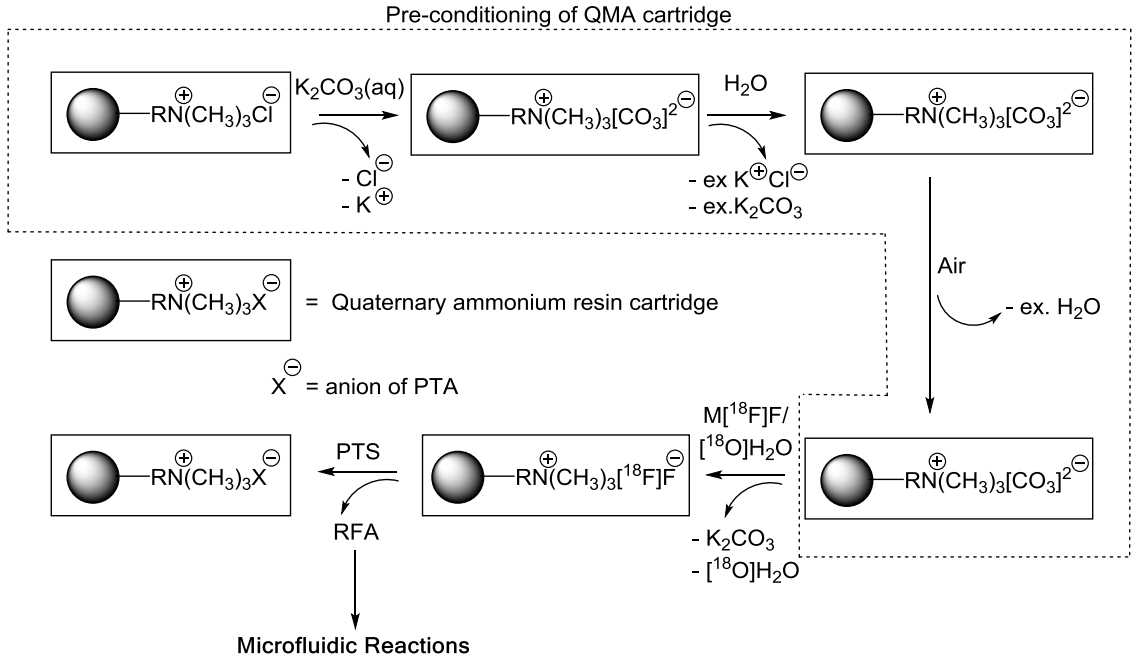

Figure 40: Process of preparing reactive [^{18}F]fluoride dissolved in PTS for microfluidic reactions using the NanoTek system.

The NanoTek system has been designed to automate this process by allowing users to program a set of commands bearing instructions to be carried out by the system modules. A sequence of operations, or "macro," can automate complex procedures and reduce the intervention made by users thereby elevating the reproducibility of routine processes. It was decided, therefore that the intial aim would be to develop a macro designed to automate the preparation of reactive [^{18}F]fluoride-PTS, using the sequence mode of the NanoTek software. Following extensive and methodical testing, a robust, reproducible, custom macro was written, instructing the CM to prepare a solution of RFA dissolved in organic solvent (Image 5, for translation see Table 12).

Command
Wait
┐L39020000800056 └┐L38020003000050E ┘
/6o1V1200A6000M3000o5V1200A0M2000R
/6o6V1200A6000M2000o3V1200A0R
┐L3902000100004F └┐L38020003000050E ┘
/7U2M5000U1M5000u2R
/6o2V1000P7200M2000go5V400D1350M15000G4o2V2000A0R
/6M90000R
/6o4V1000P6000M2000o5V75D4200M2000o6V75D1200M2000o2V2000A0R
/6M30000R
/6o4V1000P6000M2000o6V75D5400M2000o2V2000A0R
/6M30000R
/7u1R
/3o1V2000A0M2000o8V2000A15600M2000o6V800A0R
/3go4V1600A19200M2000V3200A0M2000G6o8V3200A3600M2000o4V3200A0R
┐L37020000250053 └┐L3602000300004E ┘
Wait

Image 5: Image taken from the NanoTek software showing the programming which forms the macro used to prepare the reactive [^{18}F]fluoride-PTS dissolved in organic solvent, from a solution of cyclotron-produced [^{18}F]fluoride in [^{18}O]H_2O.

This macro was used throughout the project to prepare reactive [^{18}F]fluoride. Several other macros were written to aid the microfluidic work and maintenance of the system:

1) Cleaning Macro

A list of instructions used to thoroughly sweep the contents of the system components to waste, using fresh solvent. This was executed at the start and end of each working day.

2) Preparation of the CM macro

Before the "drying macro" could be performed, the capillaries of the CM are swept thoroughly using clean solvent and the lines primed with the appropriate reagent. This was performed before every preparation of the reactive [^{18}F]fluoride-PTS, using the CM.

3) HPLC start macro

A robust method for automating the injection of the crude products into the HPLC system whilst initiating the start of the HPLC measurement was created. This was

designed to ensure that the retention times of the peaks were consistent and did not vary by manual injections. This was performed following every microfluidic reaction.

Instruction	Translation
Wait	Wait command used to prompt the user into cross-checking the system plumbing and that all reagents have been loaded onto the system.
┐L39020000800056┘┐L380200030000050E┘	Set concentrator temperature to 80 °C.
/6o1V1200A6000M3000o5V1200A0M2000R	Load target H_2O into concentrator, trapping the [^{18}F]fluoride onto the QMA cartridge.
/6o6V1200A6000M2000o3V1200A0R	Remove [^{18}O]H_2O from the concentrator vial and collect in separate vial.
┐L3902000100004F┘┐L380200030000050E┘	Set concentrator to 100 °C
/7U2M5000U1M5000u2R	Turn on the N_2 flow to the concentrator.
/6o2V1000P7200M200go5V400D1350M15000G4o2V2000A0R	Load PTS (450 μL) into the concentrator, releasing the [^{18}F]fluoride from the QMA cartridge, and collecting the [^{18}F]fluoride-PTS in the CM vial.
/6M90000R	Wait to allow the [^{18}F]fluoride-PTS to dry by evaporating the MeCN present to azeotropically remove H_2O.
/6o4v1000P6000M2000o5V75D4200M2000o6V75D1200M2000o2V2000A0R	Add 450 μL of MeCN, passing through the QMA cartridge to collect any residual [^{18}F]fluoride dissolved in PTS.
/6M30000R	Wait to allow the MeCN to evaporate and azeotropically remove H_2O from the CM vial.
/6o4V1000P6000M2000o6V75D5400M2000o2V2000A0R	Add 450 μL of MeCN, avoiding the QMA cartridge.
/6M30000R	Wait to allow the MeCN to evaporate and azeotropically remove H_2O from the CM vial.
/7u1R	Turn off the flow of N_2 to the concentrator vial.
/3o1v2000A0M2000o8V2000A15600M2000o6V800A0R	Add 325 μL of DMF to the concentrator vial thereby re-dissolving the [^{18}F]fluoride-PTS complex.
/3go4V1600A19200M2000V3200A0M2000G6o8V3200A3600M2000o4V3200A0R	Mix the DMF with the [^{18}F]fluoride-PTS complex thoroughly by repeatedly refilling and emptying the storage loop of P3 with the solution of [^{18}F]fluoride-PTS complex, using the syringe pump of P3. Add 75 μL of DMF.
┐L37020000250053┘┐L36020003000004E┘	Set the temperature of the concentrator to 25 °C.
Wait	Wait command used to prompt the user into acknowledging that the drying macro has finished and that the storage loop of P3 can be prepared for executing reactions in 'Discovery Mode'.

Table 12: Translation of drying macro instructions

2.2.9 Development of an independent control reaction

Before fluorine-18 studies using diaryliodonium salts could begin on the microfluidic system, independent control reactions, designed to ensure that the preparation and reactivity of [^{18}F]fluoride was suitable for microfluidic reactions, were devised. If the

control reactions were to work as expected, then anomalus results produced from an experiment could dismiss the initial preparation and subsequent reactivity of the [^{18}F]fluoride as a possible cause. Two reactions were investigated - (a) an ^{19}F/^{18}F isotopic exchange reaction, and (b) radiofluorodenitration reaction - with the intention of choosing one to be a model reaction. The ^{19}F/^{18}F isotopic exchange reaction[282] may provide rapid access to preliminary PET imaging studies as the fluorine-19 derivative is often available directly from drug discovery programmes.[6, 7] Conventional nucleophilic aromatic substitution is also a very common approach to the formation of electron-deficient [^{18}F]fluoroarenes. It is employed extensively where an electron-withdrawing group exists in the 4-position relative to the site for the introduction of fluorine-18, for example in the production of [^{18}F]altanserin,[283] [^{18}F]MPPF,[284] and [^{18}F]setoperone.[285] For these reasons, nitroacetophenone **246** and fluoroacetophenone **245** were chosen as the precursor compounds for the potential model reactions.

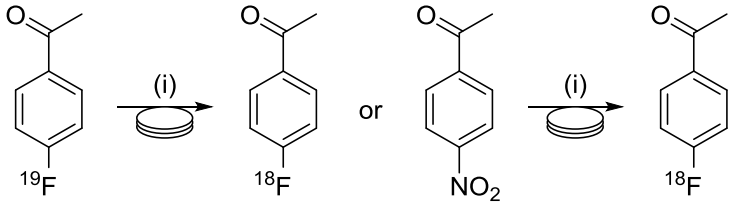

244 **245** **246** **245**

(i) [^{18}F]KF/K222, MeCN

Scheme 75: Potential model reactions to be optimised using the NanoTek microfluidic system

2.2.9.1 HPLC Method Development

Before microfluidic reactions could begin, HPLC method development was required to separate the **246** from the **245** product and, therefore, allow for the RCY of the reaction to be calculated. RCYs were deduced by integration of the peak corresponding to the desired compound with the total radioactivity detected. The isotopic exchange

reaction would produce two isotopomers of identical retention times and, therefore, not require further method development.

The ideal gradient was designed to fulfil two criteria: a) that the two compounds were fully resolved and b) that both peaks should be fully eluted with the shortest possible retention times. Following extensive work with the HPLC system, an optimal gradient for the separation of standard solutions of **246** and **244** was devised. Retention times were to be kept as low as possible to ensure that the activity of potential products from radiofluorination reactions would be as high as possible. An isocratic gradient at 24% MeCN in H_2O was found to be optimal (Image 6).

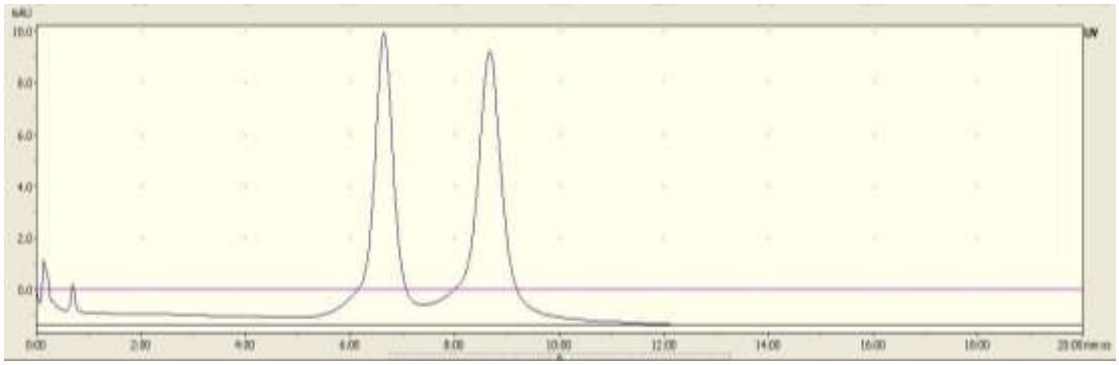

Image 6: HPLC UV-trace showing the separation of fluoroacetophenone (R_t = 6.5 min) and nitroacetophenone (R_t = 8.5 min)

2.2.9.2 Results of radiosyntheses using the traditional phase-transfer system

The NanoTek system would be used to rapidly optimise the reaction parameters with respect to reaction temperature, flow rate and ratio of [^{18}F]fluoride-PTS to precursor solutions. Kryptofix®222 and K_2CO_3 was chosen as the PTA as this mixture is well-established (Section 1.1.6). MeCN was used as the solvent as it is a polar aprotic organic solvent with a low viscosity. Discovery mode would be used to quickly vary reaction parameters between reactions (Image 7).

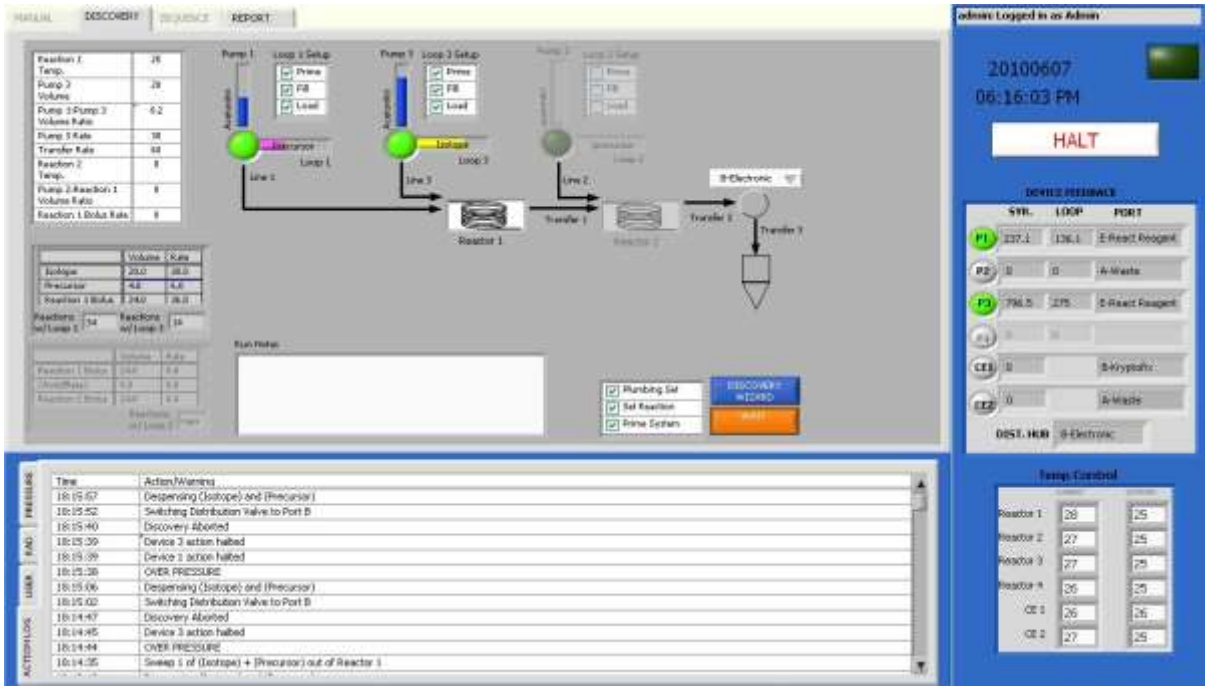

Image 7: Image taken from the NanoTek software whilst in 'Discovery Mode'. P1 and P3 have been prepared for the execution of reactions. The lines leading to these reagent cartridges have been primed, the storage loops have been filled, and the lines leading to the microreactors have been loaded.

Dry [^{18}F]fluoride-PTS (5–100 mCi, 450 μL DMF) and precursor solutions were loaded into their respective storage loops (loop 3 and loop 1 respectively). Capillaries that lead from P1 and P3 to the microreactor were primed with their respective reagents. Prior to recording data, several priming reaction runs were performed to confirm the integrity of the synthetic platform and the in-line analytical HPLC system. Set volumes (10–30 μL) of both solutions were dispensed into the pre-heated microreactor (130–190 °C) at pre-determined flow rates (10–30 μL/min). This is achieved by the syringes of P1 and P3, simultaneously dispensing precursor and [^{18}F]fluoride-PTS solutions from their respective loops, into the microreactor using a fixed volume of system solvent at a preset flow rate. The solutions initially mix at the entrance to the microreactor. User-operated computer software determines the reaction parameters — temperature, time and stoichiometry (P1:P3), which were to be optimised throughout this study. Following completion of the reaction, P3 sweeps the crude mixture to the electronic injector and radio-HPLC system, allowing the RCY of the process to be immediately

determined. At the start and end of each series of experiments the BM, RM, microreactor and associated transfer lines were cleaned using DMF and the CM system with MeCN.

2.2.9.3 Rapid optimisation of the radiofluorination of 4-nitroacetophenone

Initially, **246** was reacted with [^{18}F]KF/K222 to yield the **245** (Figure 42). Optimal conditions were found to be 20 μL/min (Figure 42a) 190 °C (Figure 42b) with a ratio of RFA to precursor of 1:0.5 (Figure 42c). It was found that increasing the temperature increased RCY, whilst increasing the ratio of precursor to PTS decreased RCYs. One delivery of [^{18}F]fluoride was used to create each graph which explains the broad range of RCYs from across the study. The variation may be a result of difference between production runs of [^{18}F]fluoride, with regard to SA, contamination, starting activity upon delivery and isotope dilution (see Section 1.2 for reasoning). The extent to which the [^{18}O]H_2O is removed from the concentrator vial during the preparation of the reactive [^{18}F]fluoride may also vary, slightly, thereby affecting the reactivity of the [^{18}F]fluoride. Despite this, the optimised conditions gave good RCYs (e.g. Figure 41).

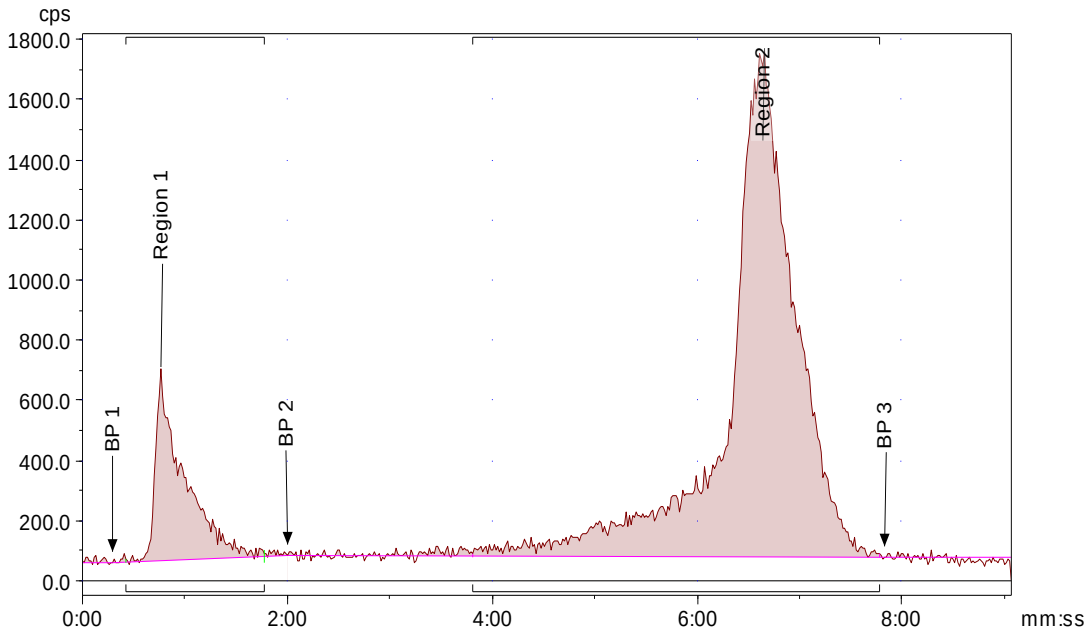

Figure 41: Radio-HPLC trace showing peaks corresponding to unreacted [^{18}F]KF/K222 and 4-[^{18}F]fluoroacetophenone.[21, 286]

Throughout this preliminary work, the micro-channels of the NanoTek microfluidic system, frequently became blocked, resulting in the system pressure increasing beyond the maximum upper limit and the loss of capacity to execute reactions. Several deliveries of [^{18}F]fluoride were required to produce the results as instances where blockages occurred, immediately halted work resulting in a loss of [^{18}F]fluoride and significant decline in output. Despite this, simultaneous work proceeded with the optimisation of the isotopic exchange reaction (Scheme 75).

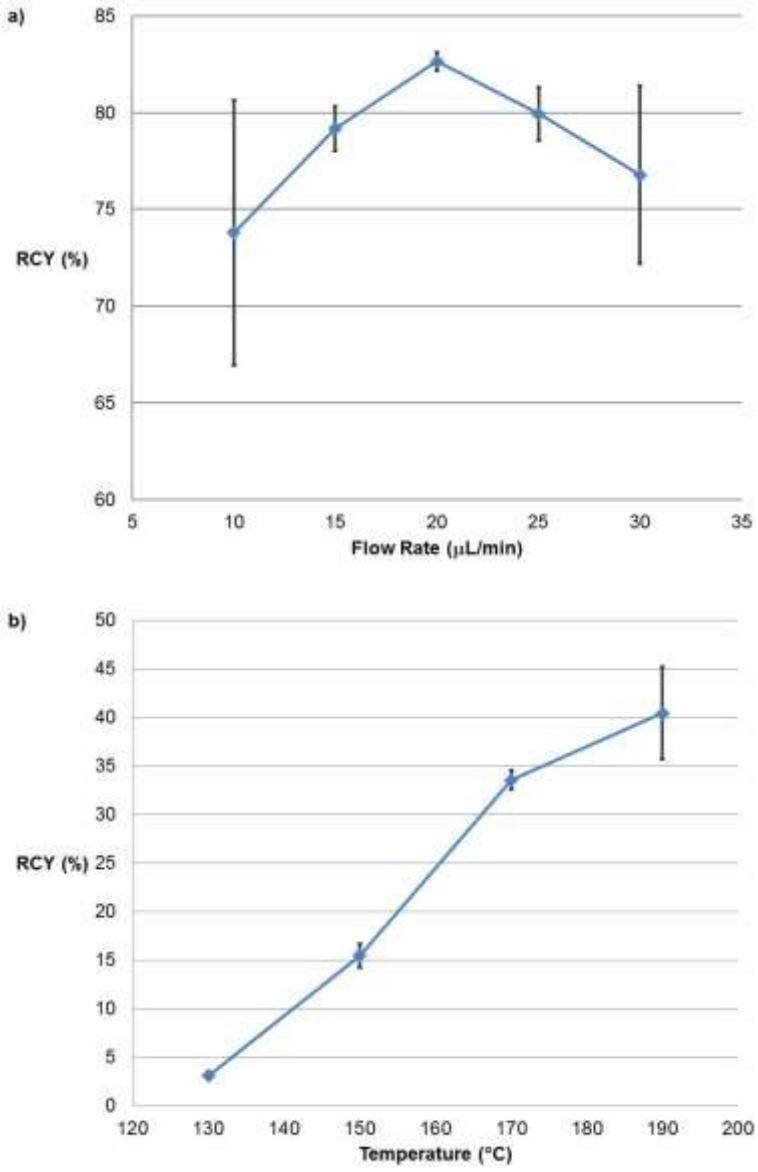

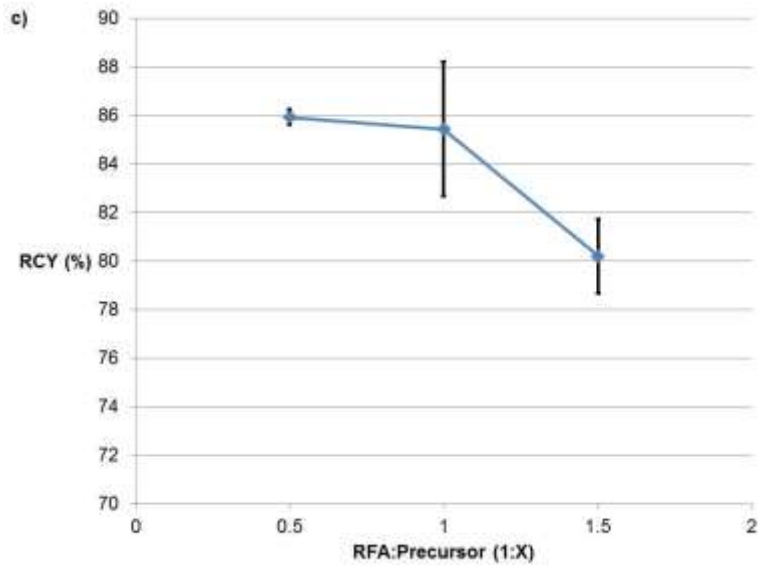

Figure 42: Graphs to show results of microfluidic reactions of **246** with [^{18}F]KF/K222 (n=3)

2.2.9.4 Rapid optimisation of the radiofluorination of 4-fluoroacetophenone

244 was reacted with [^{18}F]KF/K222 to yield the **245** (Figure 43). Optimal conditions were found to be 15 μL/min (Figure 43a) 190 °C (Figure 43b) with a ratio of PTA-[^{18}F]fluoride complex to precursor of 1:1.5 (Figure 43c). Despite obtaining some high RCYs, the results were poor. No trends could be identified across the various reaction parameters optimised and when varying the reaction temperate, RCYs were particularly poor. This is due to, once again, the frequent blockages of the microreactors.

As the precursors and reaction products are all highly soluble in organic solvent, it was proposed that reducing the concentration of the Kryptofix® 222/K_2CO_3 would prevent the micro-channels from being blocked. We propose that the large variation in RCYs observed across this study may be the result of the varying degrees of precipitation of the RFA. Total precipitation of reagents results in the blockage of the microreactors whilst zero precipitation leads to much improved RCYs demonstrated by the results.

It was found following various scoping studies that reducing the concentration continued to result in the blockage of the microreactors, although less frequently. Despite the improvement in output and efficiency, the potential for blocked reactors remained an issue and an alternative PTS was investigated.

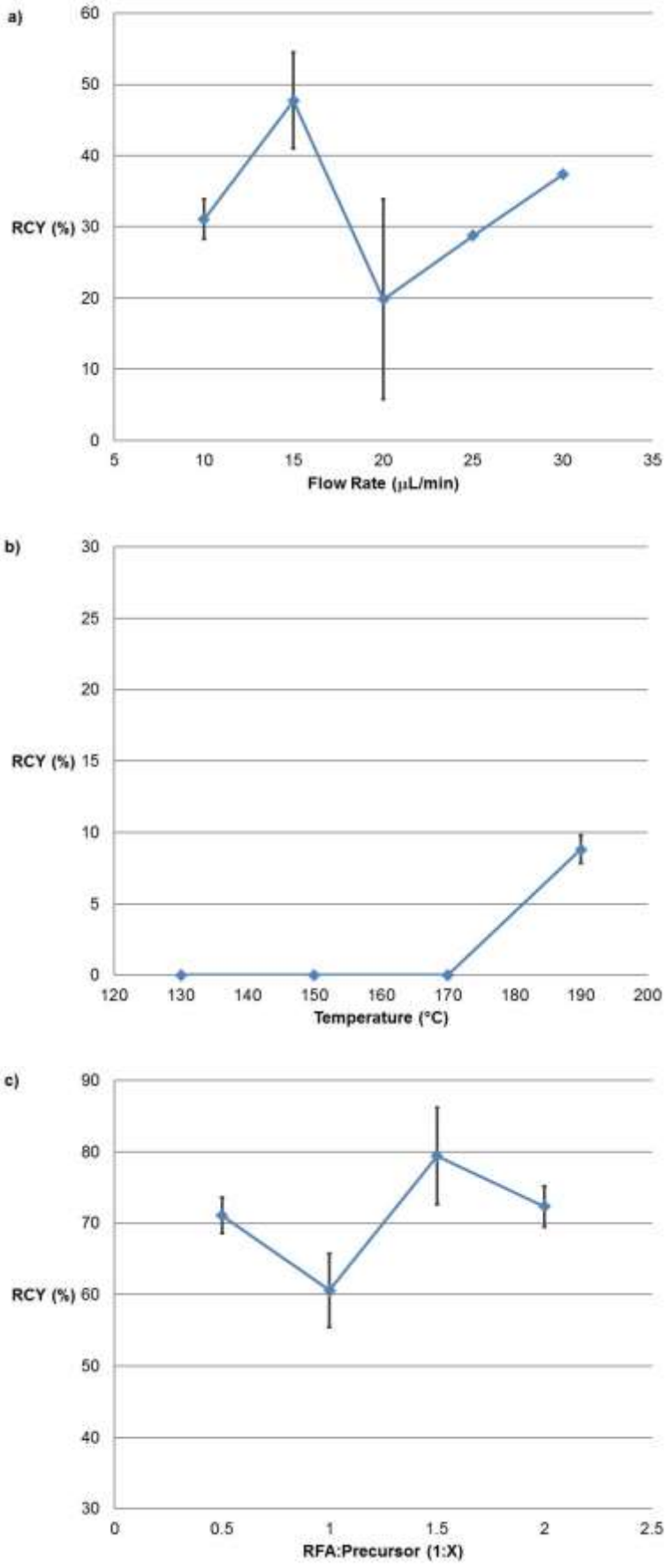

Figure 43: Graphs to show results of microfluidic reactions of **244** with [^{18}F]KF/K222 (n=3)

Tetraalkylammonium salts with their enhanced solubility in organic solvents have been widely used as an alternative to the Kryptofix® 222/K_2CO_3 system with $Bu_4N{\cdot}HCO_3$ **247** (Figure 44) being the most common. This is usually prepared, with very limited characterisation, by treating an aqueous solution of the $Bu_4N.OH$ with carbon dioxide.[287] Following elution of the [^{18}F]fluoride from the anion exchange resin (QMA) with the PTS, the next step is, conventionally, the generation of anhydrous [^{18}F]fluoride via azeotropic removal of the H_2O using multiple evaporations with MeCN. Given the propensity for tetraalkylammonium salts, and in particular the tetrabutylammonium salts, to form clathrates[288, 289] the generation of anhydrous [^{18}F]$Bu_4N{\cdot}F$ represents a significant challenge.

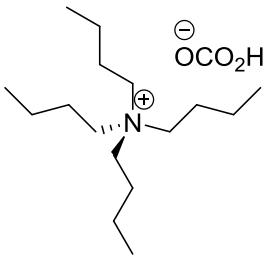

247

Figure 44: $Bu_4N{\cdot}HCO_3$ - alternative PTA

[^{18}F]Fluoroalkanes,[290] 16-[^{18}F]fluorohexadecanoic acid[291] and [^{18}F]FDG[292] have all been prepared successfully using the related [^{18}F]$Et_4N{\cdot}F$. This reagent had been prepared from $Et_4N{\cdot}OH$, either by direct treatment with [^{18}F]fluoride or, via [^{18}F]Me_3SiF to generate an anhydrous reagent. However, given the complexity of these production methods we proposed that access to [^{18}F]$Et_4N{\cdot}F$ may be more readily achieved by using tetraethylammonium bicarbonate **248** ($Et_4N{\cdot}HCO_3$) (Figure 45) as the PTA. Unlike the tetrabutyl- derivative $Et_4N{\cdot}HCO_3$ is readily available as a crystalline solid facilitating drying and characterisation yet retaining the required solubility in anhydrous organic

solvents. In addition, hydration of the tetraethylammonium cation is much reduced[293] due to the shorter alkyl chains making anhydrous [^{18}F]$Et_4N{\cdot}F$ a more realistic proposition. Given these favourable characteristics of $Et_4N{\cdot}HCO_3$ over $Bu_4N{\cdot}HCO_3$ we decided to test this material as a PTA in the model, microfluidic reactions.

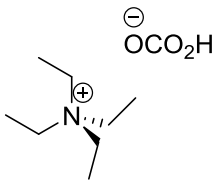

248

Figure 45: $Et_4N{\cdot}HCO_3$ - a potential, alternative PTA

2.2.9.5 Rapid optimisation radiosyntheses using $Et_4N.HCO_3$ as the phase-transfer agent

The Kryptofix®222/K_2CO_3 PTA was replaced by $Et_4N{\cdot}HCO_3$, of equal concentration, whilst the step-wise process by which the RFA is prepared, remained unchanged, thus forming $Et_4N{\cdot}[^{18}F]F$.

*2.2.9.6 Rapid optimisation of the radiofluorination of **246** using an alternative PTA*

As before **246** was reacted with [^{18}F]$Et_4N{\cdot}F$ to yield the **245** (Figure 46). Optimal conditions were found to be 15 μL/min (Figure 46a) 190 °C (Figure 46b) with a ratio of RFA to precursor of 1:1.5 (Figure 46c). Again, one delivery of [^{18}F]fluoride was used to create each graph. Generally, faster flow rates produced lower RCYs whilst higher temperatures increased RCYs. No distinct trend could be observed upon varying the ratio of the reagents. Most significantly, no instances of the micro-channels becoming blocked occurred when using $Et_4N{\cdot}HCO_3$ as the PTA. This drastically improved efficiency by increasing output, preventing the stoppages to work and, therefore, the forfeiture of [^{18}F]fluoride.

2.2.9.7 Rapid optimisation of the radiofluorination of 244 using an alternative PTA

Similar results were found upon repeating the optimisation of the isotopic exchange reaction of **246** (Figure 47). Again, higher RCYs were achieved with slower flow rates and higher temperatures. Interestingly, a clear trend could be observed upon varying the reagent ratio, with highest RCYs achieved with a higher ratio of precursor to PTS. Optimal conditions were found to be 10 μL/min (Figure 47a) 190 °C (Figure 47b) with a ratio of RFA to precursor of 1:2 (Figure 47c). These promising results support the hypothesis that the conventional PTS causes the frequent blockages to the micro-channels of the microfluidic system. Importantly, when using [^{18}F]$Et_4N{\cdot}F$ as the RFA, the RCYs were comparable to those achieved when using the conventional RFA.

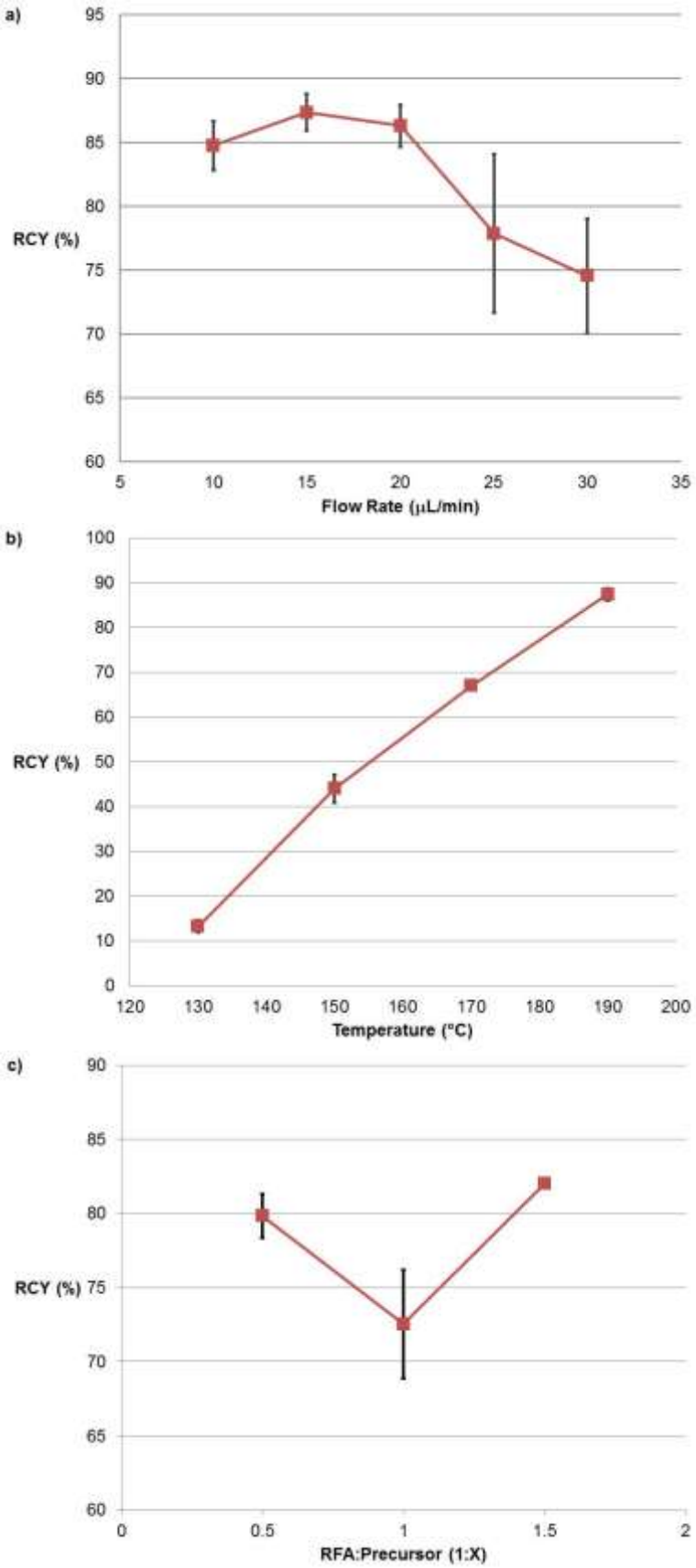

Figure 46: Graphs to show results of microfluidic reactions of **246** with [^{18}F]$Et_4N{\cdot}F$ (n=3).

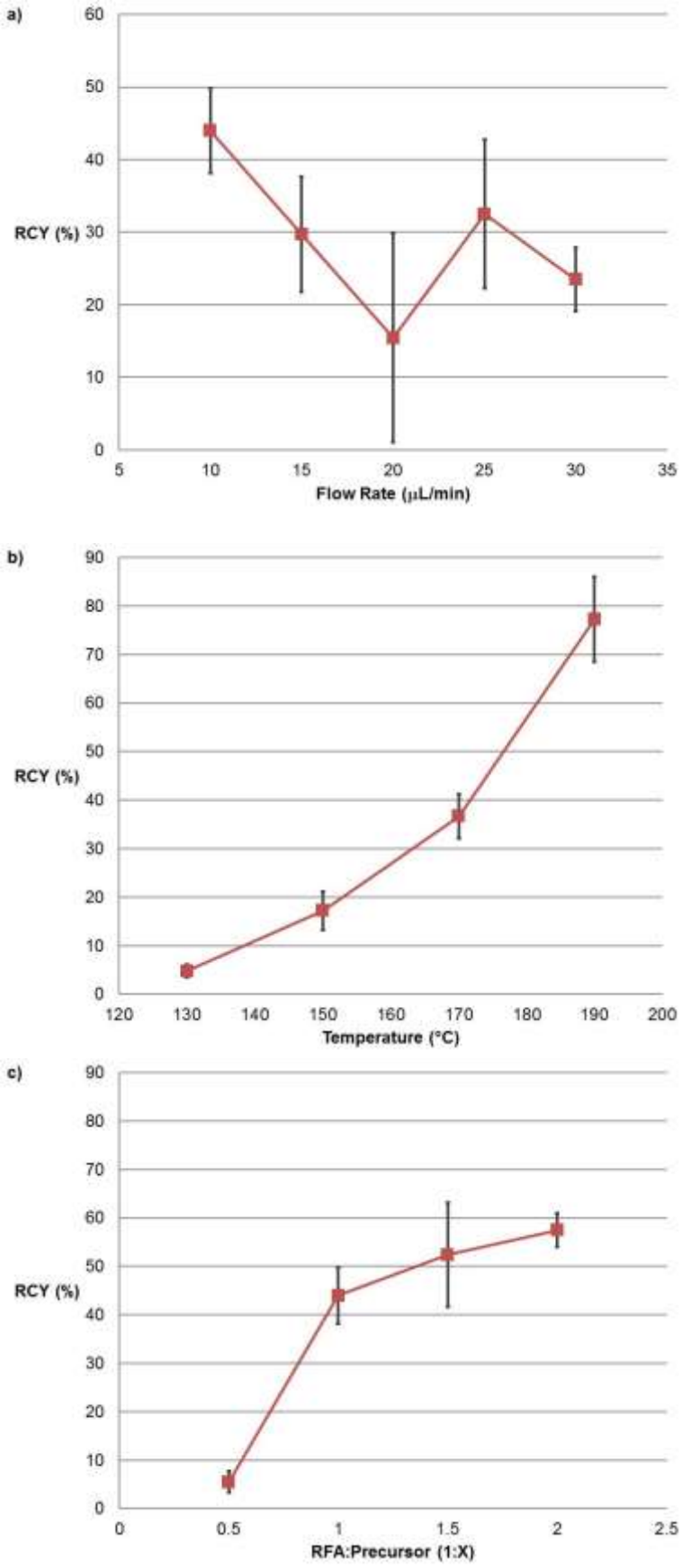

Figure 47: Graphs to show results of microfluidic reactions of **244** [^{18}F]$Et_4N{\cdot}F$ (n=3).

These results are highly promising but a more thorough investigation, involving the radiofluorination of diaryliodonium salts, is warranted before $Et_4N{\cdot}HCO_3$ can be presented as a viable alternative to the conventional PTA for the preparation of reactive [^{18}F]fluoride, within a microreactor.

2.2.10 Conclusion

Microfluidic technology has recently emerged as an invaluable tool in the development of PET radiochemistry allowing the quantities of reagents to be considerably reduced thus facilitating timely isolation of radiolabelled product. The Advion NanoTek Microfluidic System has dominated this recent emergence as it benefits from many distinct features which make it desirable to the radiochemist. This equipment has been used to optimise model reactions designed to evaluate the status of the system and validate investigations. It was noted that the use of conventional PTA (Kryptofix®222/K_2CO_3) causes blockages to the micro-channels wherein the radiochemical reactions take place. $Et_4N{\cdot}HCO_3$ appears to be a potential alternative which does not cause blockages but does generate compounds in RCYs comparable to those obtained when successfully using the conventional PTS. Further investigations involving the radiofluorinations of diaryliodonium salts are required before this compound can be presented as a viable alternative to the conventional PTA for the preparation of reactive [^{18}F]fluoride, within a microreactor.

2.3 Evaluation of tetraethylammonium bicarbonate as a phase-transfer agent in the formation of [^{18}F]fluoroarenes using a microreactor

Microfluidic technology is becoming a valuable tool for the synthetic chemist. Following the development of multiple custom microfluidic devices in the 1990s, numerous commercial microreactor systems have now become available. The emergence of this technology has coincided with increasing focus throughout the chemical industry, on sustainability and the principles of 'green' chemistry.[294] Flow chemical systems have, therefore, become desirable as they generate less waste, lessen the requirement for chromatography and reduce solvent usage, whilst improving yields and reducing reaction times. Many people believe that flow chemistry and in particular, microfluidic technology, is destined to become highly utilised throughout the chemistry industry. However, as this practice continues to develop, the problem of blocked micro-channels has become inherent (*e.g.* Kryptofix®222/K_2CO_3, Section 2.2). Many solutions have been created to overcome individual instances of blockages. For example, Ley and co-workers have used ultra-sonication to prevent reagents from precipitating in solution and, therefore, blocking the micro-channels.[295] The acoustic irradiation produces concentrated areas of elevated temperature, causing cavitation which generates pressure pulses that keep small solids flowing through the micro-channels and prevent blockages caused by less soluble material.

Such technology is not freely available and may not be able to, universally, prevent blockages to micro-channels. Individuals require unique solutions to address specific problems. Herein, we present a simple solution to one such instance of blocked microreactors.

2.3.1 Aims

Previous work within this project has suggested that the traditional PTA used in radiofluorination reactions (Kryptofix®222/K_2CO_3) has caused the blockage of micro-channels within the NanoTek system, thus preventing the microfluidic radiofluorination of arenes within the microreactor. $Et_4N{\cdot}HCO_3$ may be a viable alternative and warrants thorough evaluation. It was decided that the three most common approaches to generating [^{18}F]fluoroarenes - (a) radiofluorodenitration (S_NAr chemistry), (b) $^{19}F/^{18}F$ isotopic exchange (c) diaryliodonium salt chemistry, should be investigated to evaluate this reagent. It was also decided that the corresponding precursors chosen for this investigation should each produce ethyl 4-[^{18}F]fluorobenzoate, an initial target of the research project (Section 2.1.1), in one convenient step (Scheme 76).

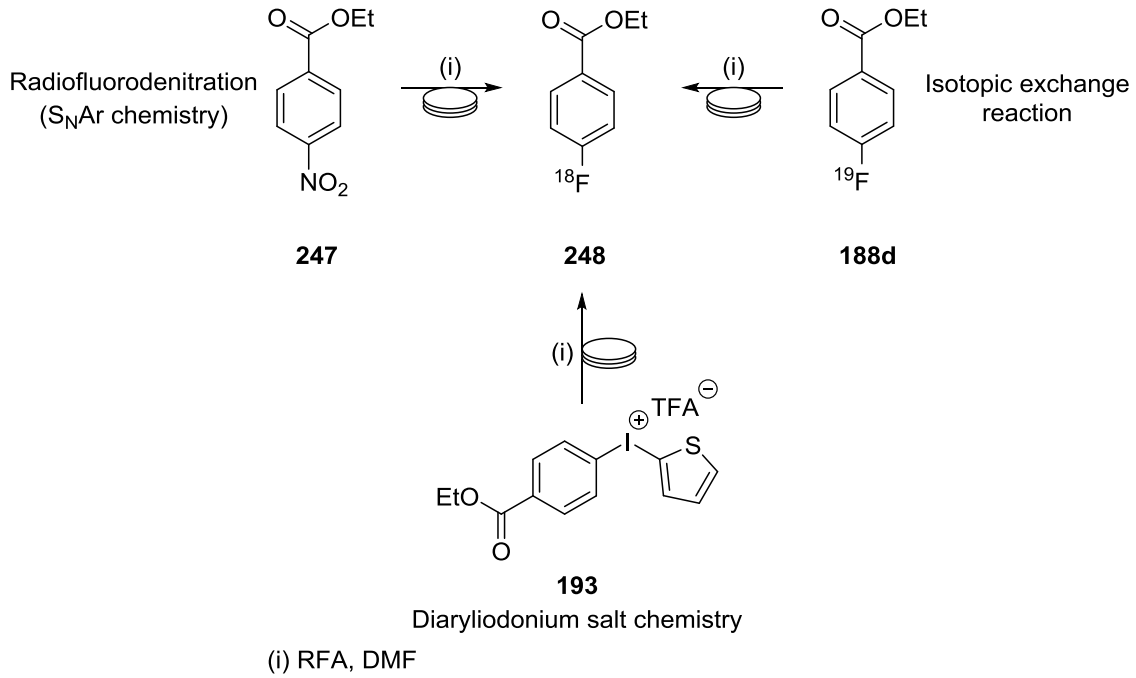

Scheme 76: Reactions to be evaluated using $Et_4N.HCO_3$ as a PTA.

DMF was chosen as the solvent for each reaction as it is a polar, aprotic organic solvent of low viscosity, successfully used in the radiofluorination of diaryliodonium salts[80, 200-

[202] and other substrates. The consistent use of solvent was an important factor, as varying solvents between reactions may influence the reactivity of the [^{18}F]fluoride.

2.3.2 Evaluating the elution capacity the PTA solution

Before radiofluorination reactions could begin, the elution capacity of each PTS was compared.

Method	Phase-transfer agent (PTA)	Phase-transfer system (PTS)		Radiofluorinating Agent (RFA)
Method A	Kryptofix® 222/K_2CO_3 (K222/K_2CO_3)	K_2CO_3 (1.18 mg; 8 μmol) and Kryptofix® 222 (6.75 mg; 18 μmol) in MeCN/H_2O (9:1 v/v 450 μL)	**PTS-1**	[^{18}F]KF/K222
Method B	$Et_4N{\cdot}HCO_3$	$Et_4N{\cdot}HCO_3$ (3.4 mg; 17 μmol) in MeCN/H_2O (9:1 v/v 450 μL)	**PTS-2**	[^{18}F]$Et_4N{\cdot}$F

Table 13: Definition of terms used throughout the evaluation of PTAs.

Following the loading of the [^{18}F]fluoride in [^{18}O]H_2O onto a QMA cartridge, the total radioactivity absorbed by the cartridge was deduced. This was achieved by determining the amount of activity which passed through the cartridge unabsorbed, the residual activity remaining inside the target water vial and the initial activity of the target water (Equation 1.1). The [^{18}F]fluoride was then eluted from the QMA cartridge, using either PTS-1 or PTS-2. The amount of activity remaining on the QMA was then deducted from the total activity absorbed, and the value expressed as a percentage (Equation 1.2).

Equation 1.1

Initial Activity (target water vial)	—	Activity not trapped by QMA cartridge	+	Activity remaining in target water vial	=	Activity trapped on QMA cartridge

Equation 1.2

$$\frac{\left(\text{Activity trapped on QMA cartridge} - \text{Activity remaining on QMA cartridge post PTS elution}\right)}{\text{Activity Trapped on QMA cartridge}} \times 100 = \textbf{PTS Elution Efficiency (\%)}$$

The amount of activity (5–100 mCi) and volume of $[^{18}O]H_2O$ (1–5 mL) differed between batches, however, these broad variations had no observed affect in elution efficiency with PTS-2 able to elute >99% (n=10) of the radioactivity from the QMA cartridge which is consistent with the performance of the Kryptofix®222/K_2CO_3 system (99%).

2.3.3 Radiofluorination reactions

The NanoTek was set up as described previously (Section 2.2.7). Before radiofluorination reactions could take place, the HPLC conditions required to resolve the radioactive peaks were established.

HPLC methods were carried out using an Agilent 1200 HPLC system equipped with a UV absorbance detector (l_{max} 254 nm) and a radioactivity detector (LabLogic Flow Count). The $[^{18}F]$fluoroarenes were not isolated and the radiochemical yield (RCY) reported relates to the amount of radioactivity of the product relative to the total radioactivity detected by radio-HPLC on analysis of the reaction mixture. The data acquisition software used was Laura (LabLogic).

2.3.3.1 Radioanalytical HPLC Methods

248 from 247

The radioactive product was separated on a PolymerX 5μm RP-1 100 column eluting at 1.1 mL/min with EtOH–water. Mobile phase composition started at 40% EtOH which increased linearly to 60% at EtOH over 2 min and then to 80% at 5 min which

continued at this composition for a further 7 min. Ethyl 4-[^{19}F]fluorobenzoate t_R = 6.2 min.

248 from 188d

The radioactive product was detected on a PolymerX 5μm RP-1 100 column eluting at 1.1 mL/min with EtOH–water. Mobile phase composition started at 60% EtOH which increased linearly to 80% at EtOH over 6 min. Ethyl 4-[^{19}F]fluorobenzoate t_R = 4.5 min.

248 from 193

The radioactive product was separated on a PolymerX 5μm RP-1 100 column (Phenomenex, USA) eluting at 1.1 mL/min with EtOH–water. Mobile phase composition started at 25% EtOH which increased linearly to 100% at EtOH over 7 min which continued at this composition for a further 2 min. Ethyl 4-[^{19}F]fluorobenzoate t_R = 7 min.

Each reaction was optimised with respect to flow rate (residence time), reaction temperature, and ratio of precursor to RFA.

2.3.4 Ethyl 4-[^{18}F]fluorobenzoate from ethyl 4-nitrobenzoate

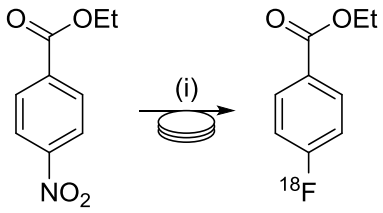

247 **248**

(i) Method A or Method B

Scheme 77: Formation of **248** by radiofluorodenitration

247 was [^{18}F]fluorinated via either method A or method B to produce **248** (Scheme 77). Optimal conditions were found to be 15 μL/min (Figure 48a) 190 °C (Figure 48b) with a ratio of RFA to precursor of 1:1.5 (Figure 48c) when using method A. When using

method B, optimal conditions were found to be 10 μL/min (Figure 48a) 190 °C (Figure 48b) with a ratio of RFA to precursor of 1:1 (Figure 48c). It was noticed that longer residence times gave improved RCYs but the effect was more pronounced when using method A (Figure 48a). Conducting the reaction at higher temperatures resulted in excellent incorporation of the fluorine-18 for both methods (Figure 48b). The difference in the absolute RCYs were attributed to inter-batch variation of the starting [^{18}F]fluoride due to the similarities observed during the evaluation of the other reaction parameters.[296] Overall, RCYs achieved when using method B were higher than those obtained using method A. Most importantly, no blockage to the micro-channels of the microreactors occurred when using method B. Blockages continued to occur when using method A resulting in the use of several production runs of [^{18}F]fluoride in order to obtain the results described here.

These promising results demonstrated that $Et_4N{\cdot}HCO_3$ system (method B) was a practical alternative to the Kryptofix®222/K_2CO_3 system (method A) for the fluorodenitration reaction.

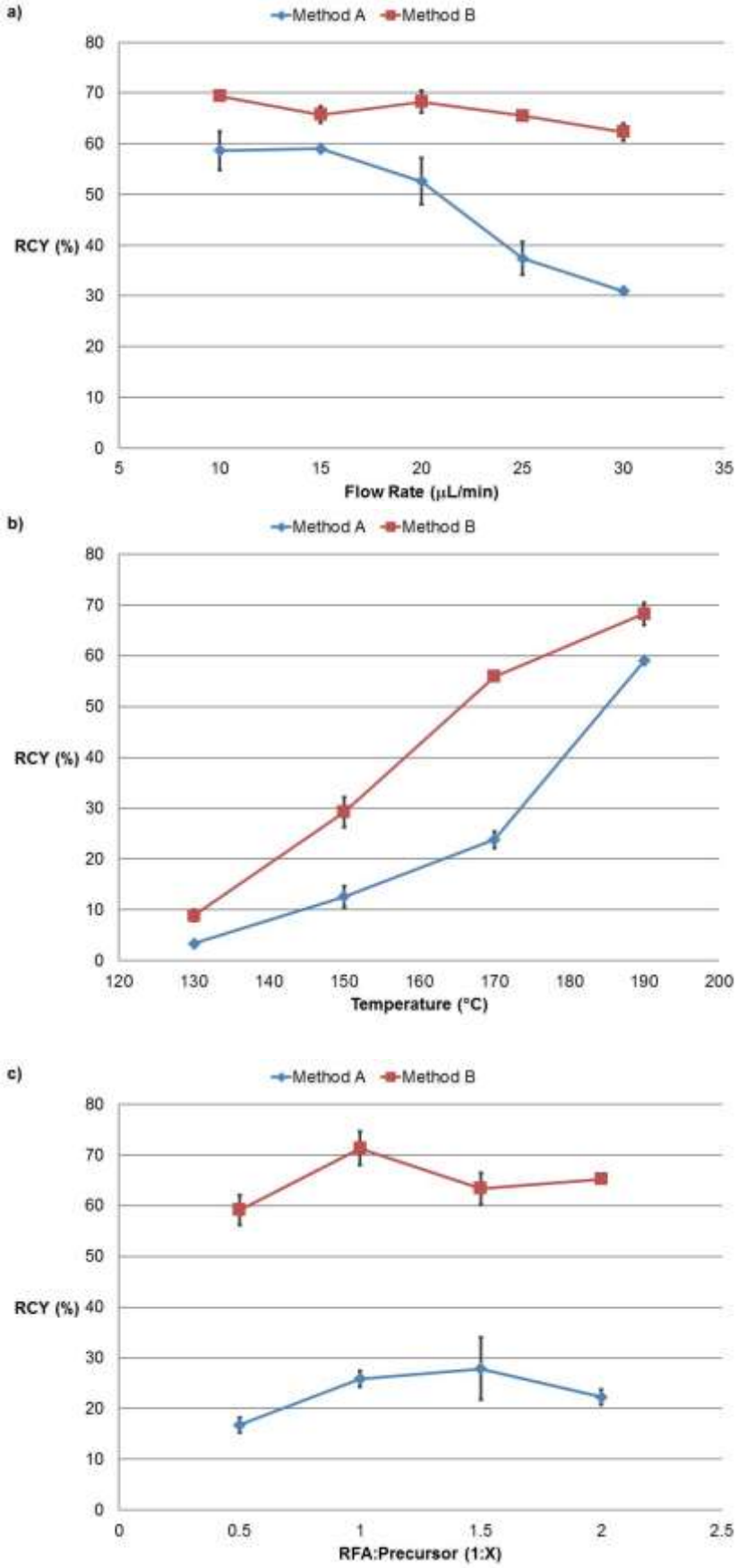

Figure 48: Graphs to show results of microfluidic radiofluorination of **247**

2.3.5 Ethyl 4-[^{18}F]fluorobenzoate from ethyl 4-[^{19}F]fluorobenzoate

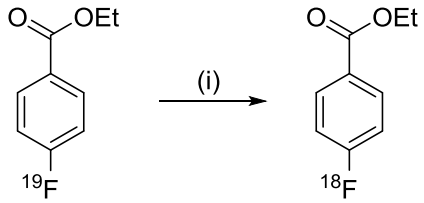

188d **248**

(i) Method A or Method B

Scheme 78: Formation of **248** by isotopic exchange

188d was [^{18}F]fluorinated via either method A or method B to produce **248** (Scheme 78). Optimal conditions were found to be 10 μL/min (Figure 49a) 190 °C (Figure 49b) with a ratio of RFA to precursor of 1:2 (Figure 49c) when using method A. When using method B, optimal conditions were found to be 20 μL/min (Figure 49a) 190 °C (Figure 49b) with a ratio of RFA to precursor of 1:1 (Figure 49c).

Again, the effect of flow-rate (Figure 49a) was found to be similar to that observed when using the ethyl 4-nitrobenzoate (Figure 48a) with the longer residence times producing higher RCYs. The effect was far less pronounced when using method B, with RCYs being approximately consistent across all flow rates investigated. Increasing the microreactor temperature had a positive effect when using either method with the best RCYs being obtained at 190 °C (Figure 49b). For method A, the effect of the RFA to precursor ratio was similar for both reaction types (Figure 48c and Figure 49c) with the preference for the 1:1 stoichiometry when using method B, strongly pronounced in both sets of results (Figure 48c and Figure 49c). Overall, the RCYs were comparable between both methods, however, no blockages to the micro-channels occurred when applying method B, whereas, blockages continued upon using method A.

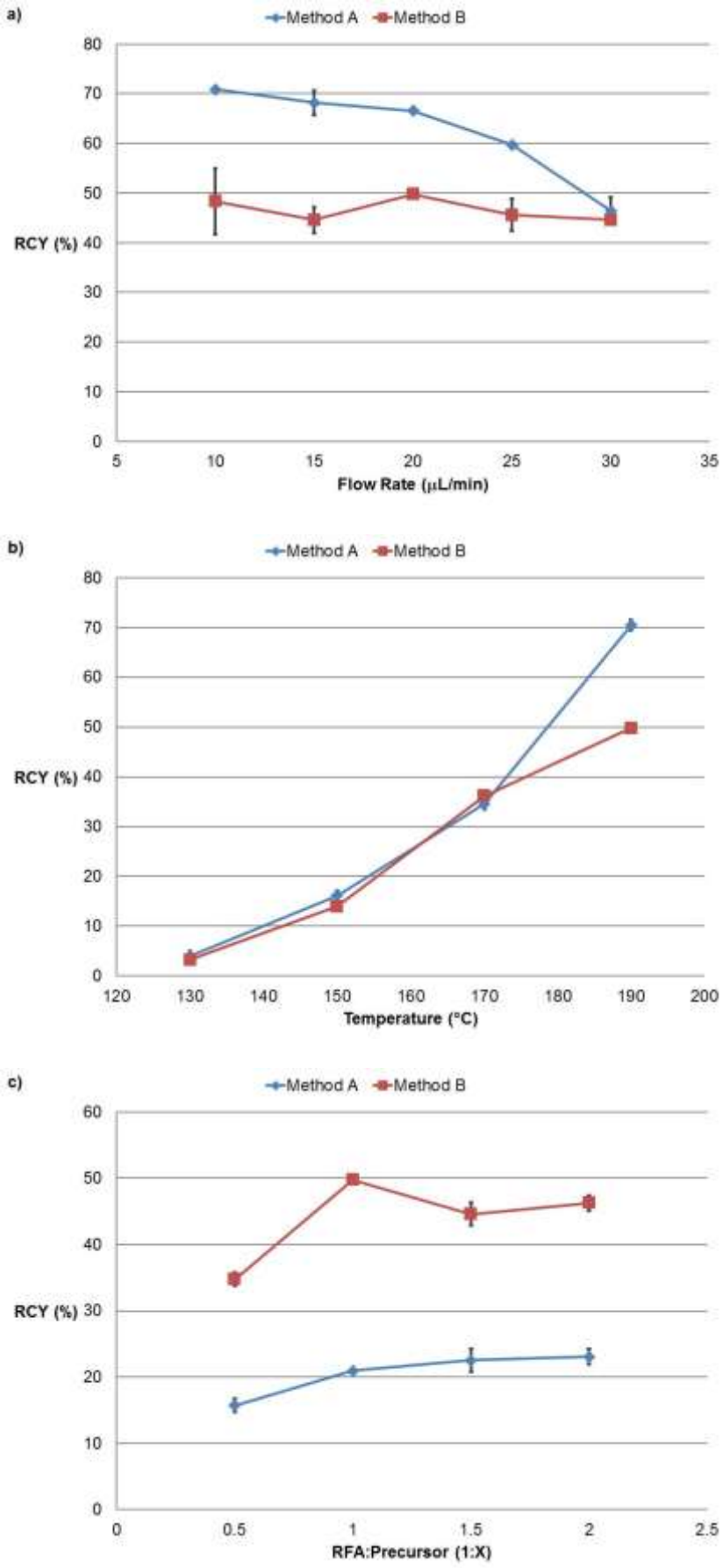

Figure 49: Graphs to show results of microfluidic radiofluorination of **188d**

2.3.6 Ethyl 4-[^{18}F]fluorobenzoate from trifluoroacetyl(4-ethoxycarbonyl, 2-thienyl)-λ^3-iodane

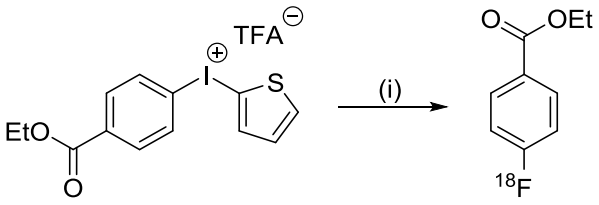

193 **248**

(i) Method A or Method B

Scheme 79: Formation of **248** using diaryliodonium salt chemistry

193 was [^{18}F]fluorinated via either method A or method B to produce **248** (Scheme 79). The 2-thienyl derivative was chosen as previous studies have shown the an electron-rich NTR induces selectivity for the incorporation of [^{18}F]fluoride onto the electron-deficient ring. Optimal conditions were found to be 30 μL/min (Figure 50a) 190 °C (Figure 50b) with a ratio of RFA to precursor of 1:2 (Figure 50c) when using method A. When using method B, optimal conditions were found to be 10 μL/min (Figure 50a) 190 °C (Figure 50b) with a ratio of RFA to precursor of 1:1 (Figure 50c).

Interestingly, for the diaryliodonium salt reaction, the effect of flow-rate (Figure 50a) was found to be opposite to that observed for the radiofluorodenitration and isotopic exchange reactions (Figure 49a and Figure 49a) with the longer residence times improving the RCYs obtained when using method B. However, increasing the microreactor temperature had a similar effect with the best RCYs being obtained at 190 °C (Figure 50b). For method A, increasing the RFA to precursor ratio produced a large small improvement in RCYs whilst there was a clear optimal ratio of 1:1 when using method B (Figure 50c). Once again, RCYs were comparable between methods of radiofluorination with excellent RCYs being achieved when using method B.

Importantly, no blockages to the micro-channels occurred when applying this method, whilst the blockages continued throughout the use of method A.

For the reasons described previously (Section 2.2) the RCYs obtained were found to vary between different batches of [^{18}F]fluoride.[296]

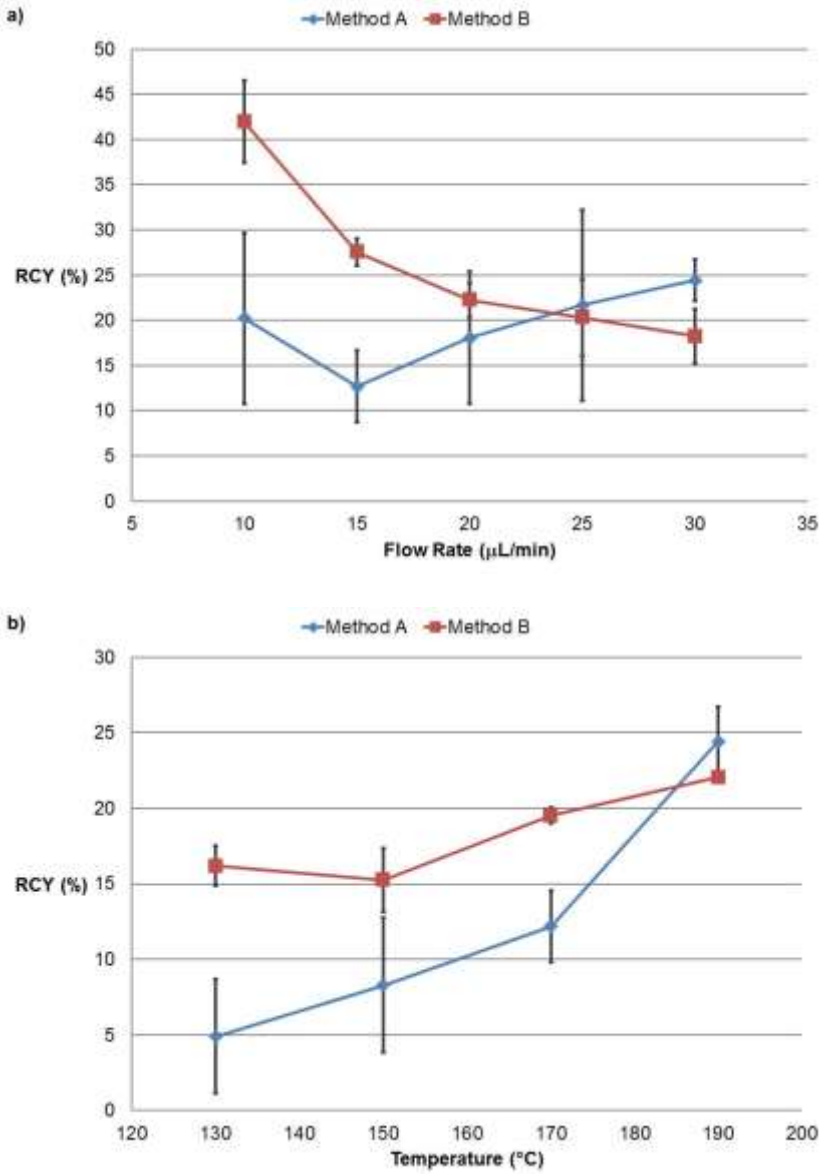

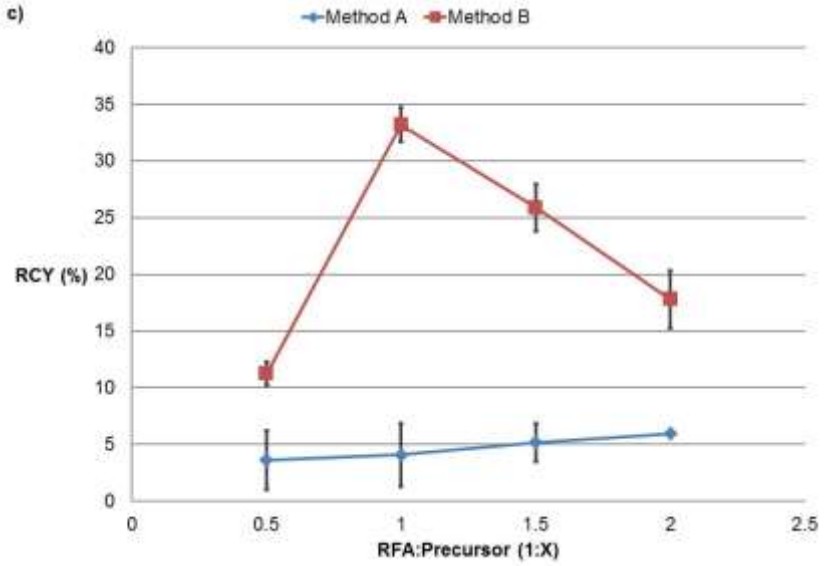

Figure 50: Graphs to show results of microfluidic radiofluorination of **193**

It is of note to observe that throughout this study, the reaction temperatures (up to 190 °C) exceeded the boiling point of the solvent (153 °C). This is possible due to the closed-system environment of the NanoTek microreactor which is able to tolerate high temperatures and pressures, and therefore, provide access to conditions not possible in batch methodology. This has resulted in the significant improvement of RCYs for these types of transformations.

2.3.7 Conclusion

We have demonstrated that $Et_4N{\cdot}HCO_3$ is a viable alternative to the traditional PTA, Kryptofix®222/K_2CO_3, for the production of [^{18}F]fluoroarenes using a key range of synthetic methods. Of particular benefit, in a microreactor, was the performance of $Et_4N{\cdot}HCO_3$ where the occurrence of blocked reactors experienced with the conventional phase-transfer system was eliminated thus dramatically increasing productivity. In addition, the Advion NanoTek Microfluidic System provided an efficient, versatile and convenient methodology for the rapid optimisation of radiofluorination reactions. Reaction temperatures were able to exceed the boiling

point of the solvent, thereby providing access to conditions not possible in batch methodology and, therefore, excellent RCYs.[186, 203, 239, 297-300]

2.4 Microfluidic radiofluorinations of diaryliodonium salts

Following the conclusion that of $Et_4N.HCO_3$ is a viable alternative to the traditional PTS for the production of [^{18}F]fluoroarenes using a microreactor, it was decided that this system should be used to investigate the microfluidic radiosynthesis of ethyl 4- and 3-[^{18}F]fluorobenzoate from various diaryliodonium salts.

2.4.1 Aims

This study had three aims:

- Synthesise the 3- and 4-regioisomers of ethyl [^{18}F]fluorobenzoate, which may serve as prosthetic groups for the indirect radiolabelling of macromolecules, and other species of biological interest.
- Demonstrate regioselective control in the radiofluorination of diaryliodonium salts, induced by the NTR.
- Investigate the effect of the presence of H_2O upon the radiofluorination of diaryliodonium salts.

In order to achieve these aims, the phenyl, 4-anisyl and 2-thienyl derivatives of the 4- and 3-ethoxycarbonylphenyl-λ^3-iodanes were chosen. The use of both electron-rich and electron-neutral NTRs would show the significance of electronic effects in the selectivity of the reaction. DMF was, once again, chosen to be the solvent for the reasons described previously (Section 1.4.2.7). Previous work from within the group has found that performing radiofluorinations of diaryliodonium salts in a solution 5% H_2O in DMF had a beneficial effect upon the RCYs.[301] It was decided that these conditions should be replicated and also compared to reactions performed in the absence of H_2O.

Throughout the investigation, the optimal reaction conditions achieved from the radiofluorination of **193** (Section 2.3.6) were applied (*i.e.* flow rate of 10 μL/min, temperature of 190 °C, RFA to precursor ratio of 1:1).

2.4.2 Radiofluorination reactions of diaryliodonium salts

Before the microfluidic reactions could begin, radio-HPLC conditions were to be optimised for the separation of all potential products of the radiofluorination reactions, including acid products which may form upon hydrolysis of the ester.

2.4.2.1 Radioanalytical HPLC Methods

For this study, a C18 column was used for radio-HPLC purification as it was found that a superior degree of resolution can be achieved when separating the various possible products. It was found that the same gradient conditions could be applied to the separation of products generated from radiofluorinating both **191-193** (Table 14) and **193-196** (Table 15). The radioactive product was detected on a ThermoFisher 5μm RP-C18 100 column eluting at 1.1 mL/min with MeCN–water. Mobile phase composition started at 18% MeCN for 4 min, increasing to 40% at 4 min 30 s, remaining at this composition for 11 min 30 s, before decresing back to 18 % over 30 s, where the composition remained constant for a further 1 min 30 s.

Compound	Relevant starting material	Retention Time (mm:ss)
Starting material	**191-193**	02:00
4-Fluorobenzoic acid		06:43
4-Iodobenzoic acid		09:11
Ethyl 4-fluorobenzoate		14:20
Ethyl 4-Iodobenzoate		08:33
Iodobenzene	**191**	09:09
Fluorobenzene	**191**	10:29
4-Iodoanisole	**192**	09:45
4-Fluoroanisole	**192**	10:32
2-Fluorothiophene	**193**	09:49
2-Iodothiophene	**193**	16:27

Table 14: Retention times (R_t) of possible products from all reactions of trifluoroacetyl(4-ethoxycarbonyl, aryl)-λ^3-iodanes

Compound	Relevant starting material	Retention Time (mm:ss)
Starting material		02:00
3-Fluorobenzoic acid		06:49
Ethyl 3-Iodobenzoate	**194-196**	07:29
3-Iodobenzoic acid		08:56
Ethyl 3-fluorobenzoate		15:02
Iodobenzene	**194**	09:09
Fluorobenzene	**194**	10:29
4-Iodoanisole	**195**	09:45
4-Fluoroanisole	**195**	10:32
2-Iodothiophene	**196**	16:27
2-Fluorothiophene	**196**	09:49

Table 15: Retention times (R_t) of possible products from all reactions of trifluoroacetyl(3-ethoxycarbonyl, aryl)-λ^3-iodanes

2.4.2.2 Radiofluorination of trifluoroacetyl(4-ethoxycarbonyl, aryl)-λ^3-iodanes, 191-193

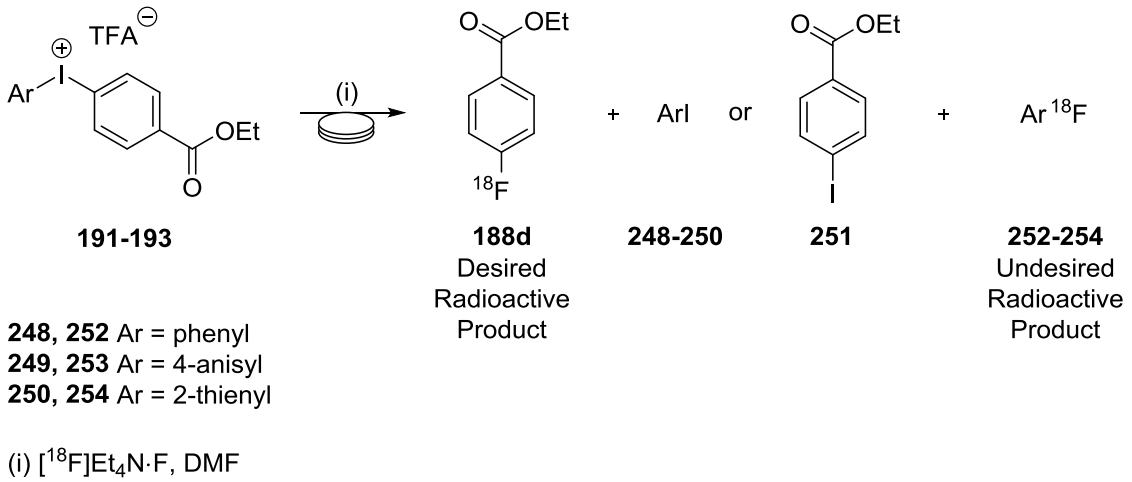

Scheme 80: Radiofluorination of **191-193** to produce the desired **188a** and undesired products **252-254**

Trifluoroacetyl(4-ethoxycarbonyl, aryl)-λ^3-iodanes were reacted with [^{18}F]Et$_4$N·F to yield **188d** (Scheme 80). Radio-HPLC was used to calculate the RCYs of both the desired and undesired products (Figure 51).

Overall, RCYs were very good. The highest RCYs were achieved using the 4-anisyl derivative and in the absence of water. Lowest RCYs of the desired product was obtained when using the 2-thienyl derivative and in the presence of water. Generally,

higher RCYs were achieved when reactions were performed without the addition of water. Interestingly, this is the opposite of the affect observed for the production of 4-FBA.[301]

The results clearly demonstrate selectivity in the radiofluorination of diaryliodonium salts with the ratio of desired [^{18}F]fluoroarene to undesired [^{18}F]fluoroarene, higher when using an electron-rich NTR. This selectivity was highest when radiofluorinating trifluoroacetyl(4-ethoxycarbonylphenyl, 2-thienyl)-λ^3-iodane, which bears a very electron-rich NTR. However, radiofluorination of this species produced the lowest RCYs. This may be due to the reduced thermal stability of the compound - a result of the strong positive inductive effect of the 2-thienyl ring. Trifluoroacetyl(4-ethoxycarbonylphenyl, 4-anisyl)-λ^3-iodane bears the 4-anisyl NTR which is of sufficient electron-density to promote the radiofluorination of the ester bearing ring, but insufficient to de-stabilise the starting material. This is reflected in the results which show that the 4-anisyl NTR generates the highest RCYs of ethyl 4[^{18}F]-fluorobenzoate. Interestingly, the radiofluorination of trifluoroacetyl(4-ethoxycarbonylphenyl, phenyl)-λ^3-iodane produced RCYs comparable to those resulting from the radiofluorination of the 4-anisyl derivative. However, the ratio of desired [^{18}F]fluoroarene to [^{18}F]fluoroarene produce was lowest when using the phenyl derivative, which is to be expected from the selectivity of the reaction, as the phenyl group is effectively electron-neutral.

Upon comparing the ratio of desired product to undesired product when reactions were conducted in the presence or absence of water, no distinct trend could be observed suggesting water has no effect upon the selectivity of this reaction.

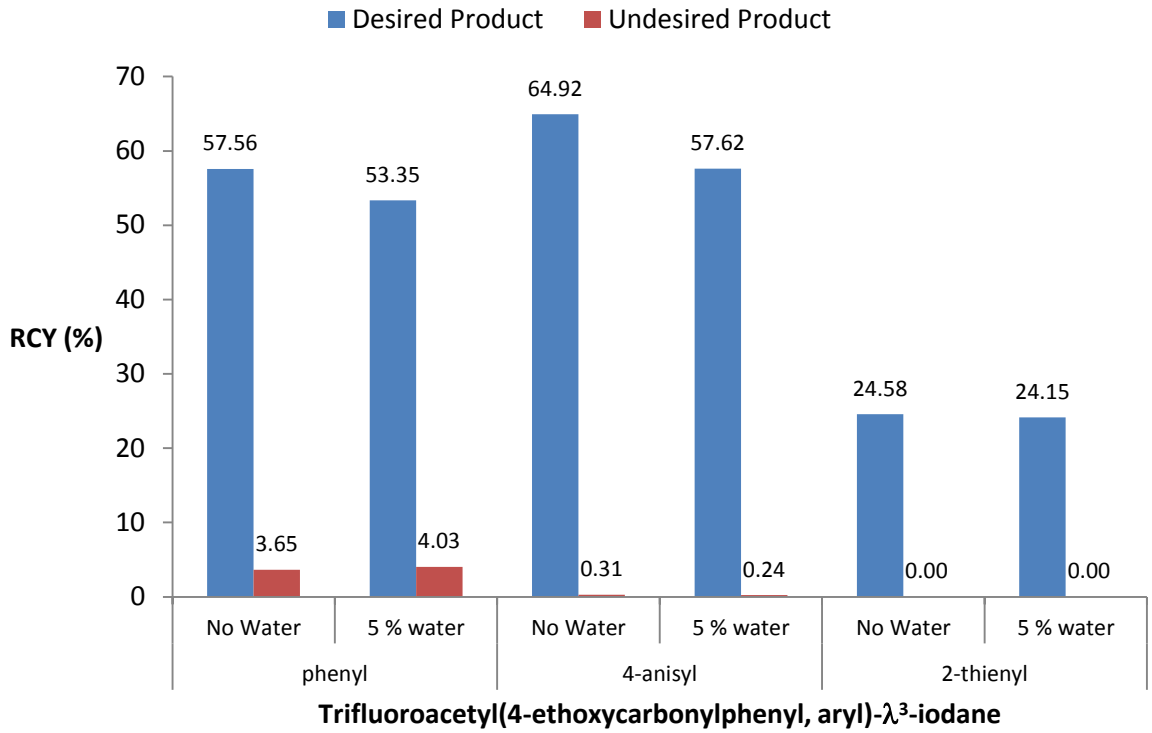

Figure 51: Radiofluorination of **191-193** (n=3)

Target of radiofluorination (Trifluoroacetyl(4-ethoxycarbonylphenyl, Ar)-λ^3-iodane		Ratio of RCYs (radioactive products)		
	Solvent	**Desired Product**	**to**	**Undesired Product**
191	DMF	1	:	0.063
	5 % H_2O in DMF	1	:	0.076
192	DMF	1	:	0.005
	5 % H_2O in DMF	1	:	0.004
193	DMF	1	:	0
	5 % H_2O in DMF	1	:	0

Table 16: Ratio of desired [^{18}F]fluoroarenes **188a** to undesired [^{18}F]fluoroarenes **252-254**

*2.4.2.3 Radiofluorination of trifluoroacetyl(3-ethoxycarbonyl, aryl)-λ^3-iodanes, **194-196***

Trifluoroacetyl(3-ethoxycarbonyl, aryl)-λ^3-iodanes were also reacted with [^{18}F]Et_4N.F to yield ethyl 3-[^{18}F]fluorobenzoate (Scheme 80). Radio-HPLC was used to determine the RCYs of both the desired and undesired radioactive products (Figure 52).

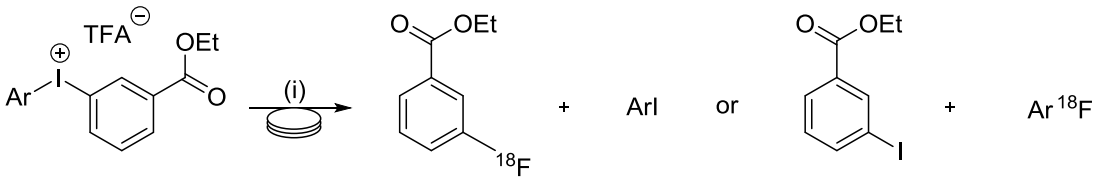

194-196

188b Desired Radioactive Product

248-250

255

252-254 Undesired Radioactive Product

248, 252 Ar = phenyl
249, 253 Ar = 4-anisyl
250, 254 Ar = 2-thienyl

(i) $[^{18}F]Et_4N{\cdot}F$, DMF

Scheme 81: Radiofluorination of **194-196** to produce the desired **188b** and undesired products **252–254**

Overall, RCYs were good with the highest RCYs of the desired product, once again, achieved when radiofluorinating trifluoroacetyl(3-ethoxycarbonyl, 4-anisyl)-λ^3-iodane in DMF. Lowest RCYs were obtained upon radiofluorinating trifluoroacetyl(3-ethoxycarbonyl, 2-thienyl)-λ^3-iodanes in the presence of water. RCYs for ethyl 3-[^{18}F]fluorobenzoate were lower than those resulting from the radiosynthesis of ethyl 4-[^{18}F]fluorobenzoate. This may be a result of the electron density at the ipso carbon of the ester bearing ring. As discussed earlier (Section 1.4.2.2) the attack of the nucleophile at the iodine is dependent upon the electron-density at the carbon atoms of the C-I-C bonds. The ester group *meta* to the C-I bond of the target ring induces a positive mesomeric effect upon the *ipso* carbon and therefore increases the electron-density at this site. This makes this carbon less electrophilic, and therefore, less susceptible to attack from the incoming [^{18}F]fluoride. This is also reflected in the decrease in the ratio of desired product to undesired product, a trend which is observed when comparing the radiofluorinations of the **191-193** to the radiofluorinations of the **194-196**.

It was noted, however, that the ratio was, again, lowest when radiofluorinating the phenyl derivative, and highest when radiofluorinating that bearing the 2-thienyl NTR.

This is also in strongly accordance with the proposed selectivity of the reaction and corresponds to the results for the radiofluorination of the trifluoroacetyl(4-ethoxycarbonyl, aryl)-λ^3-iodanes.

With the exception of one result, RCYs were lower when reactions were performed in the presence of water. However, the ratios of desired product to undesired product were higher when executed in pure DMF, suggesting that water has a negative effect on both the RCY and the selectivity of this reaction.

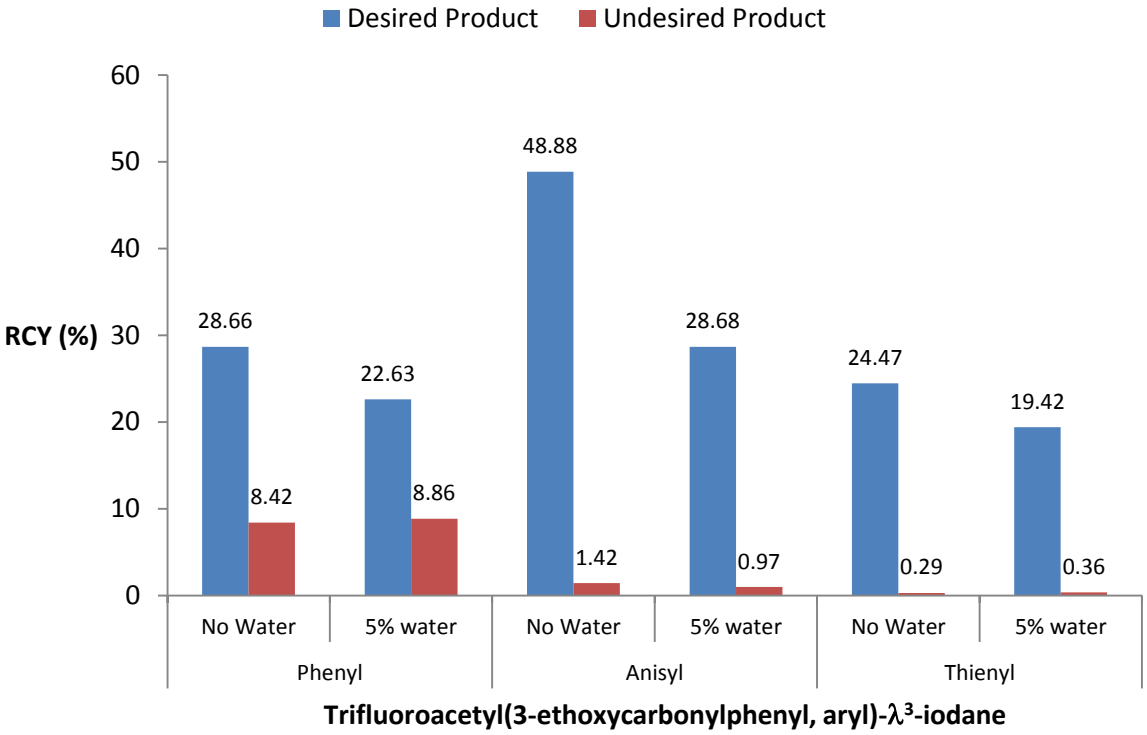

Figure 52: Graph to show results of the radiofluorination of **194-196** (n=3)

Target of radiofluorination (Trifluoroacetyl(3-ethoxycarbonylphenyl, Ar)-λ^3-iodane		Ratio of RCYs (radioactive products)		
	Solvent	**Desired Product**	**to**	**Undesired Product**
194	DMF	1	:	0.294
	5 % H_2O in DMF	1	:	0.392
195	DMF	1	:	0.029
	5 % H_2O in DMF	1	:	0.034
196	DMF	1	:	0.012
	5 % H_2O in DMF	1	:	0.019

Table 17: Ratio of desired [^{18}F]fluoroarenes **188b** to undesired [^{18}F]fluoroarenes **252**-**254**.

Previous work on the radiofluorination of diaryliodonium salts has focussed on the radiosynthesis of ethyl 3-[^{18}F]fluorobenzoate. The RCYs presented here are generally higher and of greater reproducibility than those reported earlier.[224]

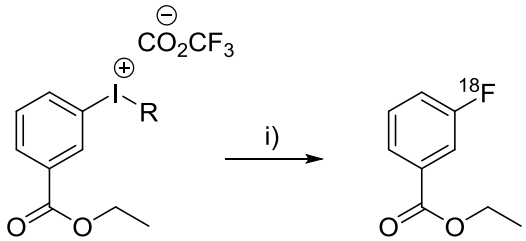

195 R = 4-anisole
195a R = 2-anisole
196 R = 2-thienyl

188b

i) [^{18}F]KF/K222, DMF, TEMPO, 5 min

Scheme 82: Previous syntheses of ethyl 3-[^{18}F]fluorobenzoate using a batch reactor[302]

Compound	R	n	RCY (%)
196	2-thienyl	6	21-80
195	4-anisyl	6	4-35
195a	2-anisyl	6	7-23

Table 18: RCYs of previous syntheses of ethyl 3-[^{18}F]fluorobenzoate using a batch reactor[302]

The previously reported results are, seemingly, of low reproducibility, whereas the reproducibility of the results reported here, using the microfluidic device was, generally, high. Higher yields were obtained here when using the 4-anisyl, whereas, lower RCYs were obtained when using the 2-thienyl derivative. As already stated, RCYs of radiofluorination reactions are difficult to compare and can be caused by various influences (Section 1.2) with the quality of the [^{18}F]fluoride having profound affects.

2.4.3 Conclusion

We have demonstrated that $Et_4N.HCO_3$ is a viable alternative to the traditional PTA, K222/K_2CO_3, for the radiosynthesis of [^{18}F]fluoroarenes, using a microreactor and via a key range of radiosynthetic strategies. Of particular benefit, in a microreactor, was the performance of $Et_4N{\cdot}HCO_3$ where the occurrence of blocked reactors experienced with the conventional PTS was eliminated thus dramatically increasing productivity. In addition, the Advion NanoTek Microfluidic System provided an efficient, versatile and convenient methodology for the rapid optimisation of radiofluorination reactions.

Various diaryliodonium salts have been reacted with Et_4N[^{18}F]F, to generate ethyl 4- and 3-[^{18}F]fluorobenzoate with the synthesis of the 4-position regioisomer, generally, producing higher RCYs. Excellent RCYs and selectivity were achieved for both isomers when using precursors bearing a 4-anisyl ring. The selectivity of the nucleophilic attack of [^{18}F]fluoride on a diaryliodonium salt has been clearly demonstrated using electron-neutral and electron-rich derivatives. It was also found that the presence of water has a negative effect upon the selectivity of reactions producing the 3-regioisomer.

With the evaluation of the PTS to generate [^{18}F]fluoroarenes in a microreactor conclusive, it was decided that in order to substantiate our proposal – that this system is a viable alternative to the conventional PTS for the preparation of [^{18}F]fluoride in a

radiochemistry laboratory – the new PTS must be evaluated on a commercially-available automated batch reactor, using the expensive fluoride and starting materials, generated from complex organic chemistry.

2.5 Automated Batch Radiochemistry

Integration of PET imaging into drug discovery programmes has generated high demands for the safe and reproducible preparation of PET radiopharmaceuticals. Fluorine-18 labelled radiotracers are of particular interest, due to the longer half-life of the isotope, increased availability from modern PET cyclotrons and high SA of the radiotracers. These advantages allow for large quantities of fluorine-18 labelled radiopharmaceuticals to be synthesised from a single production run for remote site application. Such syntheses require automated batch chemistry devices to protect chemists from harmful radiation, uphold high levels of reproducibility and reduce the time taken for synthesis, purification and formulation.

The construction of automated devices for the synthesis of radiotracers has been an important focus of radiochemistry research since the introduction of PET into drug discovery programmes. Several systems are now commercially available and have been used in the large-scale radiosynthesis of potential imaging agents. These devices are often customisable and have the capacity to adapt for reproducible production of different radiotracers. This is an important feature as the development of fluorine-18 labelled radiotracers can also involve various chemical transformations resulting in complex, multi-step labelling and purifying procedures. This becomes increasingly important when generating different radiotracers requiring diverse synthetic strategies.

2.5.1 Aims

Following the conclusion that $Et_4N{\cdot}HCO_3$ is a viable PTA for the generation of [^{18}F]fluoroarenes in a microreactor, it was decided that the same PTS should be evaluated for syntheses of [^{18}F]fluoroarenes on an automated batch chemistry

platform as this type of system is commonly found throughout radiochemistry laboratories. Diaryliodonium salts would be used to generate the initial targets of this project.

2.5.2 Automated Batch Chemistry Platforms

Automated batch chemistry platforms can be divided into two main categories. Firstly, "cassette-type" devices conduct the chemical synthesis within a disposable, readymade cassette mounted onto a stationary device. These cassettes, which contain reagents, vials and tubing, are connected to the mechanical syringes and valves of the computer-controlled unit. Cassettes can be removed and replaced after each batch thereby obviating a post-production cleaning procedure and promoting reproducibility of reactions corresponding to the cassette design. This also promotes the use of radiotracers made in this way for clinical studies. Examples of "cassette-type" devices are the TRACERlab Mx FDG synthesis module (GE Healthcare Technologies) and the PETtrace FDG II Microlab (GE Medical Systems).

Alternative to these devices are stationary systems wherein all connections of the tubes (plumbing) and valves are permanent. Reagents are loaded onto such systems which automate the mechanical operations controlled by the accompanying computer software. The system is rinsed with solvent, without the removal of vials or tubing - a process often referred to as a "clean in place" (CIP) procedure. The CIP requires extensive validation to ensure of no cross-contamination between batches. In practice, both these types of systems are used once for each delivery of [^{18}F]fluoride as levels of radiation remain at a harmful level after cleaning thus preventing the safe reloading of chemicals, and cartridges. Examples of such systems include the TRACERlab FxFDG module[303] (GE Medical Systems) CPCU, Chemistry Process Control Unit (CTI),

EBCO/Jaltech FDG synthesis module (EBCO) and Synchrom (raytest, Isotopenmeesgerate GmbH).

Image 8: TRACERlab FxFDG module (GE Medical Systems)[303]

Automated synthetic chemistry platforms for the radiosynthesis of PET radiotracers have been reviewed elsewhere[304, 305] and so will not be discussed in this report. Focus will lie with the specific automated batch reactor used for this project.

2.5.3 The Modular-Lab

The Modular Lab (Eckert & Ziegler) is a stationary, batch radiosynthetic device which uses modules to enable the automation of custom, radiopharmaceutical syntheses. A set of unit-operation modules, each designed to perform a different task, are connected by process tubing and communication cable. Automation of the modules is performed using the accompanying computer software. Due to its multi-functionality, the Modular-Lab can replace several single-purpose devices, such as HPLC system and batch-reactor, thereby significantly reducing cost, hot-cell space and total radiosynthesis times. The system can also be combined with disposable cassettes designed to prepare a variety of reactive radiolabelling agents.[286]

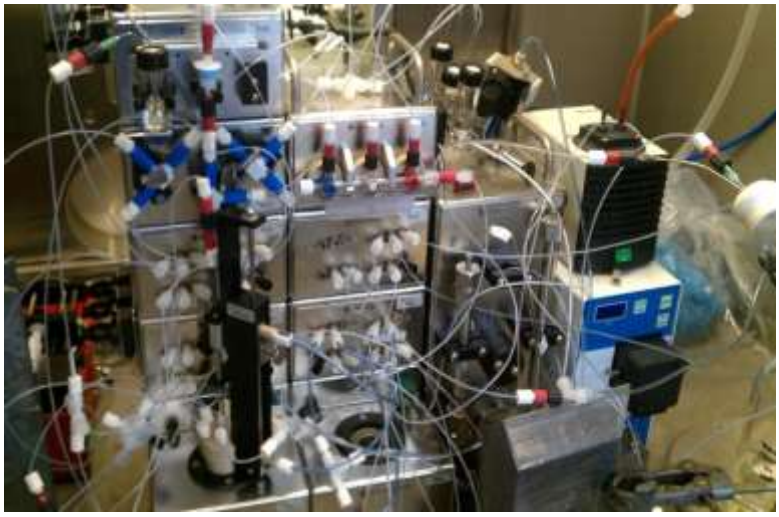

Image 9: Photo taken of the Eckert & Ziegler Modular-Lab housed within a "hot cell" of the Sir Bobby Robson Foundation PET Tracer Production Unit at Newcastle University

The accompanying computer software is used to coordinate actions between modules to create an automated, multi-step synthesis. Reaction parameters such as temperature, activity, UV detector readings, flow rates or valve positions can also be monitored in real-time.

2.5.3.1 Selected examples of radiochemical syntheses performed using the Modular-Lab

As the Eckert & Ziegler system is a recently developed device, there currently exists very few publications on the automated syntheses of radiotracers, within the literature. Herein this report, three examples have been presented.

Pascail and co-workers have used the Modular-Lab to automate the large-scale production of [^{18}F]fluoroethylcholine for PET imaging of prostate cancer.[296] The system was used to automate the two-step/one-pot synthesis by, firstly, radiolabelling ethyleneglycolditosylate to produce [^{18}F]fluoroethyltosylate. This was then coupled to DMEA before the final mixture was purified by means of SPE. The optimised procedure resulted in a RCY of 36% (NDC) (Scheme 83).[296]

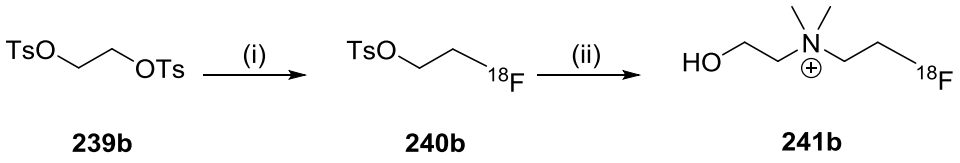

239b **240b** **241b**

(i) [^{18}F]KF/K222, MeCN, 90 °C (ii) DMEA (neat.) 100 °C

Scheme 83: Reaction scheme for the automated, large scale production of [^{18}F]fluoroethylcholine, performed using the Modular-Lab.[296]

The Modular-Lab has been specifically designed to allow for the use of a variety of isotopes in radiochemical syntheses with particular application in the preparation of gallium-68 radiolabelled materials.[306]

Steinback and co-workers used the Modular-Lab to automate a reliable procedure for the 3-step radiosynthesis and preparative HPLC-purification of [^{18}F]gefitinib **262** (Scheme 84).[307] [^{18}F]Gefitinib has been used in a wide number of applications ranging from oncology to *in vivo* studies of drug transporter proteins. The modular system was used to, routinely, produce the radiotracer in 17.2 ± 3.3% RCY (DC) (n = 22) with an exceptional RCP of >99%. This synthesis demonstrates the multi-functionality of the system, with the ability to incorporate a HPLC module, and execute the routine production of radiopharmaceuticals.[307]

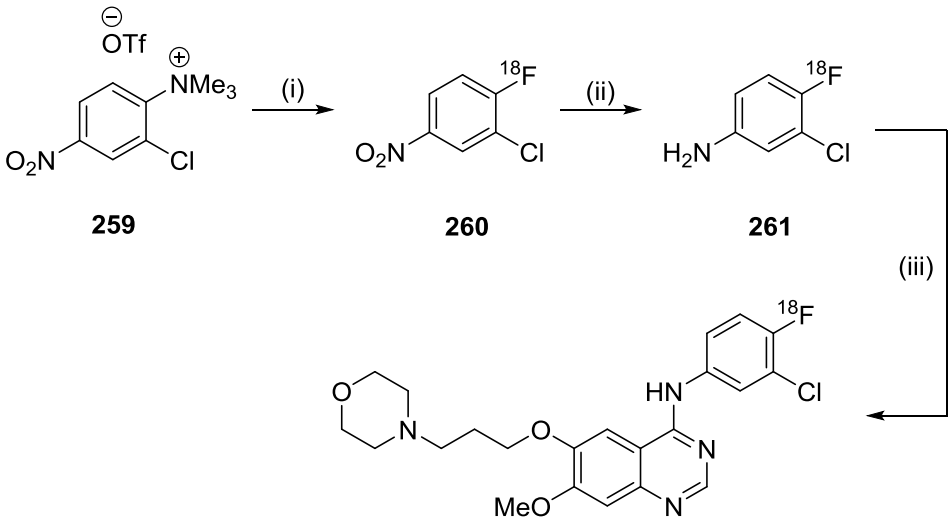

259 **260** **261** **262**

(i) [^{18}F]KF/K222, MeCN, 40 °C, 25 min (ii) $NaBH_4$, Pd/C, MeOH, RT, 7 min
(iii) Precursor, IPA, 120 °C, 15 min

Scheme 84: Radiosynthesis of [^{18}F]Gefitinib **262**[307]

The Modular-Lab has also been used for the radiosynthesis of tracers bearing inorganic radioisotopes and carbon-11. Passchier and colleagues have used the system to automate the GMP compatible radiosynthesis of the M_1 receptor agonist GSK1034702 with carbon-11 (Scheme 85).[308] A palladium-catalysed Stille reaction of the trimethylstannyl precursor **263** with [^{11}C]methyl iodide afforded [^{11}C]GSK1034702 **264** in an estimated RCY of 10 ± 3 % (NDC). The process allows for the reliable production of pharmaceutical grade material in excellent chemical yields.[308]

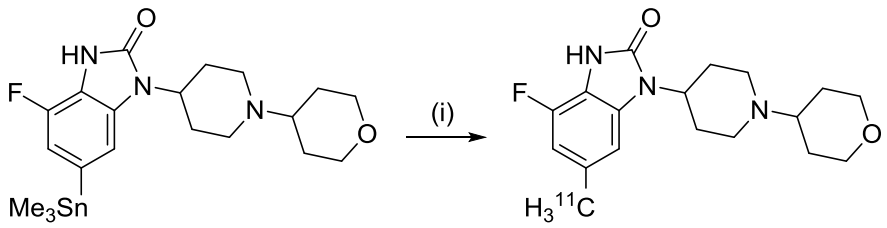

263 **264**

(i) [^{11}C]MeI, $Pd_2(dba)_3$, P(o-toyl)$_3$, CuCl, K_2CO_3, DMF, 130 °C, 5 min

Scheme 85: Synthesis of [^{11}C]GSK1034702[308]

2.5.3.2 System Configuration

The Modular-Lab system was purchased, factory-configured for [^{18}F]FEC production, however, after making minor adjustments to the plumbing, the system was ready to perform the preparation of the reactive RFA followed by a one-step radiofluorination reaction. The system consists of 1 x peltier reaction module (PRM) with transfer line fitted, 2 x single stopcock modules (SSM), 4 x solenoid valve modules (SVM), a vial holder module (VHM) to which was connected a pressure sensor and an activity detector in addition to the VHM's internal detector (Image 10). The transfer of liquids was operated by applying positive or negative pressure through FEP tubings inserted directly into the septa-sealed vials.

a) b c) d

Image 10: Images of the modules used on the Modular Lab system. (left) Peltier reaction module (PRM) (left middle) Single stopcock modules (SSM) (right middle) Solenoid valve modules (SVM) (right) Vial holder module (VHM)[286]

The computer software is used to create a programmed synthesis using a sequential flow-chart of control tasks (Figure 53) each created to automate a task and consisting of a series of commands or "macro blocks". The execution of the synthesis, represented by the flowchart, is overseen by a graphical interface (Figure 54) wherein user prompts can be programmed in order to manage the program. The interface is constantly being updated throughout the execution of a reaction, to represent the status of the system. Total syntheses can then be automated and monitored, using the custom program.

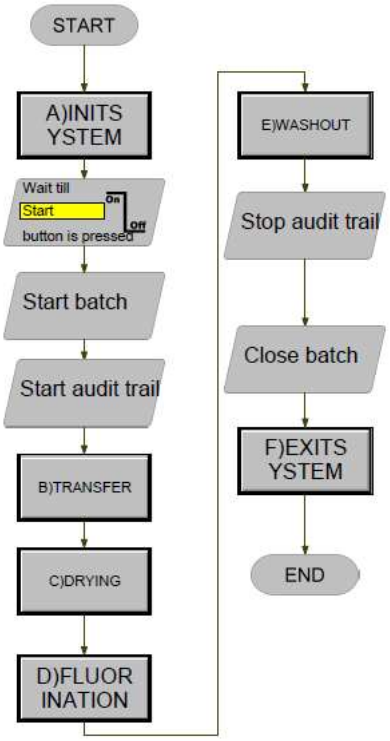

Figure 53: Flow-chart of control tasks for the custom program written for the radiofluorination of a diaryliodonium salt. Image taken from the Modular-Lab software.

Some macro-blocks perform simple and discrete actions (*e.g.* changing the position of a particular valve). Other macro-blocks are used to update the interface display representing the system status and the progress of a reaction. Combined sequentially, the macro-blocks automate a particular task (*e.g.* the preparation of the RFA) to form control tasks. Combining the control flasks, automates the radiosynthesis radiochemical synthesis (*e.g.* radiofluorodenitration of an arene). Each execution of program, or 'batch', is recorded by the software.

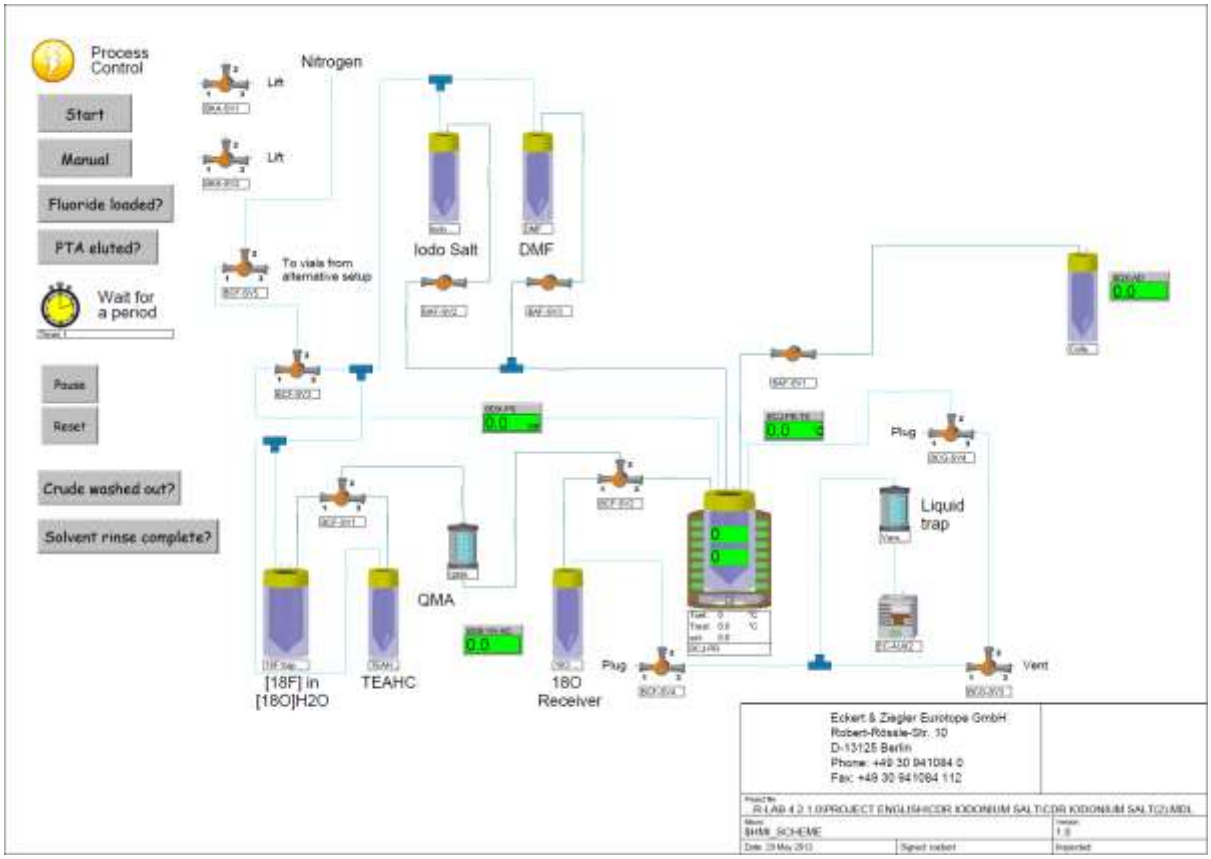

Figure 54: User-interface for the custom program written for the radiofluorination of a diaryliodonium salt. Image taken from the Modular-Lab software.

2.5.4 Radiofluorination of diaryliodonium salts using the Eckert & Ziegler Modular-Lab

Following extensive and methodical testing, a reproducible, custom program was written, instructing the modules to perform a simple reaction by combining solutions of diaryliodonium salt and RFA in the reactor vial and stirring for a specified time at a set temperature.

2.5.4.1 Flow-chart for the radiofluorination of a diaryliodonium salt.

'Start'

The program is started by the user. The computer communicates with all the modules present to ensure that the configuration is correct. Non-essential functions of the software, such as program editing, are no longer accessible.

'A)INITSYSTEM' (Figure 55)

The initial status of the system is displayed on the user interface. For example, macro blocks instruct the user interface to display the status of the vials. Generally, at this stage, the reagent vials are full whilst collection vials are empty. This information is displayed on the user interface. Actions are also taken to ensure that the system is prepared for the reaction. For example, valves are directed to the correct starting positions and the vacuum pump is turned on.

'Wait till Start button is pressed'

A user prompt is required to instruct the program to begin the reaction after satisfactory initialisation of the system. The user takes this moment to ensure that all systems are working correctly and that the images displayed on the user interface correspond to the physical arrangement of the system.

'Start batch'

This separates the synthesis stage of the process from the preparation of the system. The system has been prepared from the default status and shall now undergo the synthesis steps.

'Start audit trail'

The system begins recording an action-log of actions made throughout the programme. This is mainly of the purpose of creating an audit trail, a requirement of producing clinical-grade material.

'B)TRANSFER' (Figure 55)

The next step is to transfer the [^{18}F]fluoride onto the Modular-Lab system. Cyclotron-produced [^{18}F]fluoride in [^{18}O]H_2O is transferred from the delivery vial to the collection vial, thereby trapping the [^{18}F]fluoride on the QMA cartridge. The reactor is warmed to 60 °C, in preparation of the azeotropic evaporation of H_2O using MeCN for preparation

of the reactive RFA. A user prompt is required to ensure that all the [^{18}F]fluoride has been transferred. The PTA is then transferred to the reactor vial, via the QMA cartridge thereby releasing the trapped [^{18}F]fluoride and delivering the RFA to the reactor vial. The user is again prompted to ensure that the fluoride has been released from the QMA cartridge and delivered to the reactor vial. The reactor vial is then placed under a flow of N_2. The user interface is updated to reflect the system status.

'C)DRYING' (Figure 56)

The reactor vial is placed under vacuum and heated to 110 °C for 4 min to perform the azeotropic evaporation of H_2O and MeCN. The reactor was then cooled to 90 °C and placed under vacuum only for an extra 4 min to ensure the complete drying of the contents of the reactor vial. The reactor vial is then cooled to 30 °C and returned to atmospheric pressure. Preparation of the reactive RFA, located in the reactor vial, is complete.

'D)FLUORINATION' (Figure 56)

The solution of diaryliodonium salt is transferred to the reactor which is then heated to 130 °C. The reaction is then stirred at this temperature for 30 min.

'E)WASHOUT' (Figure 57)

The reactor is cooled to room temperature and contents are transferred to a collection vial. The user is prompted into ensuring that the reactor has been emptied, before proceeding. The reactor vial is then rinsed with DMF (1 mL) and the washings are transferred to the collection vial. The user is then prompted to ensure the reactor has been, once again, emptied. This concludes the reaction.

'Stop Audit Trail'

The system stops recording an action-log of actions made throughout the programme.

‘Close batch’

This separates the synthesis stage of the process from reverting to the default status. The system has been completed the synthesis steps and is now being prepared to return to the default status.

‘F)EXITSYSTEM’

The system is returned to a default status and the user interface is updated to reflect this.

‘END’

The system instructs the user that the process has ended.

Figure 55: (left) 'INITSYSTEM' control task. (right) 'TRANSFER' control task. Images taken from Modular-Lab software.

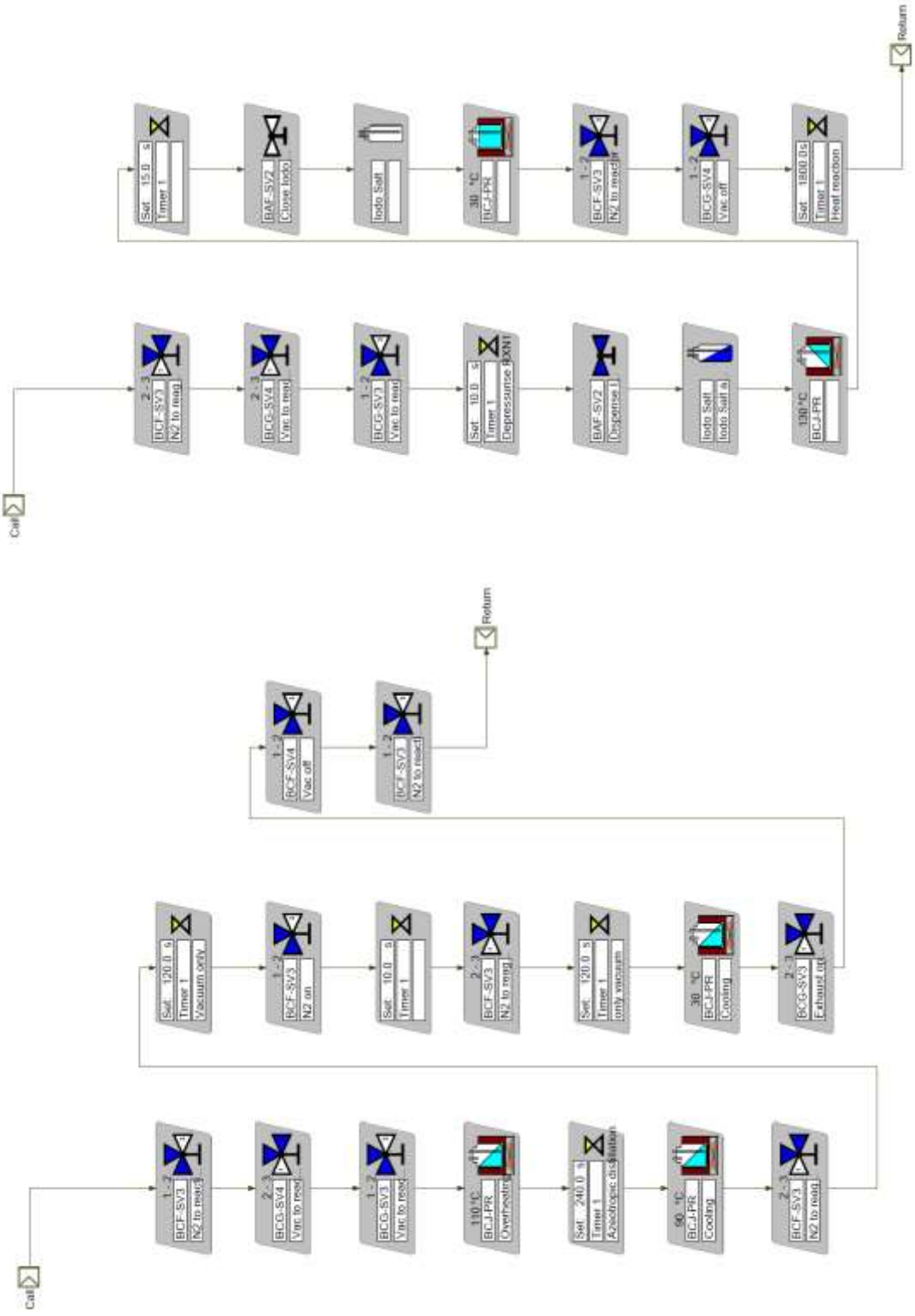

Figure 56: (left) 'DRYING' control task. (right) 'FLUORINATION' control task. Images taken from Modular-Lab software.

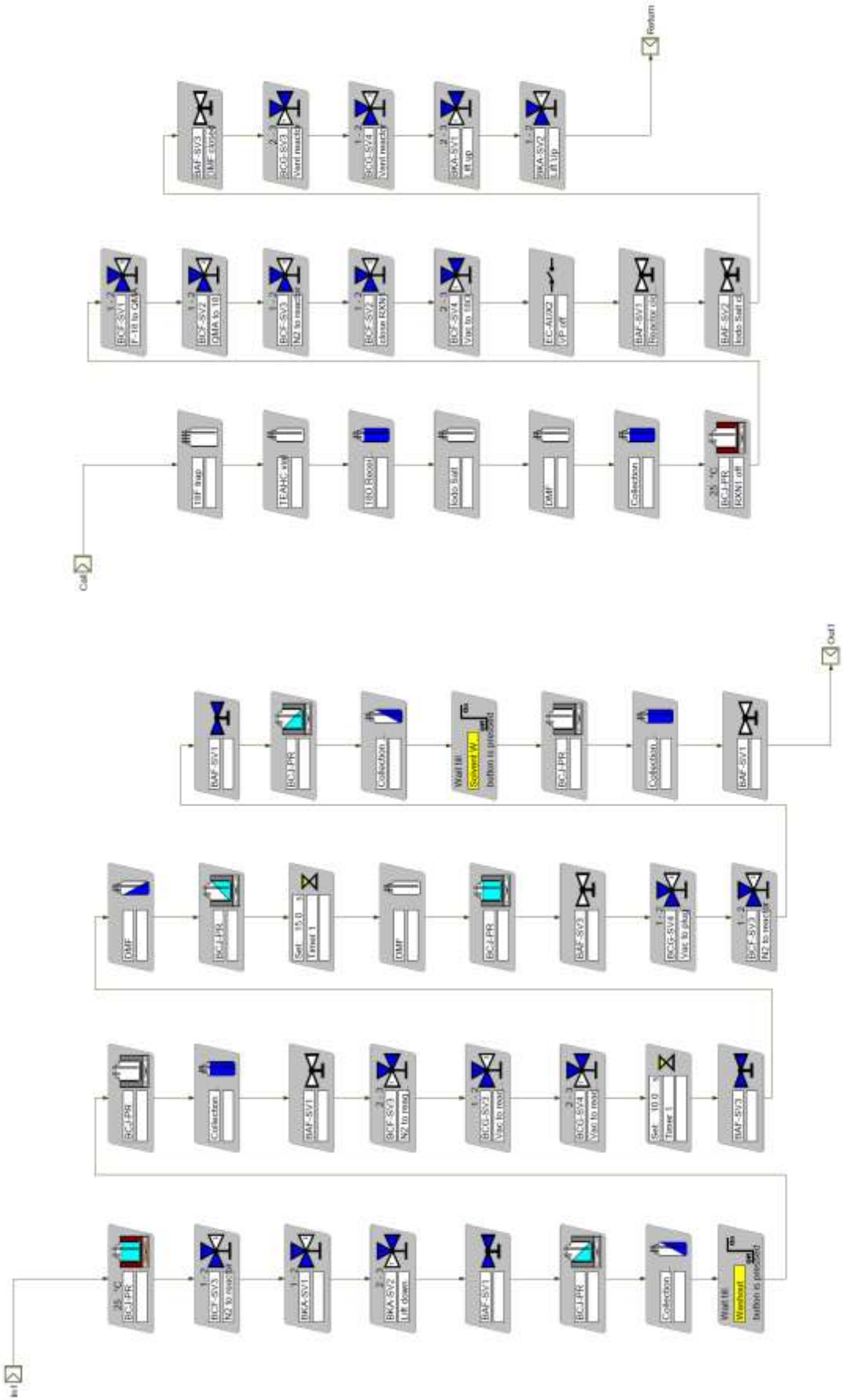

Figure 57: (left) 'WASHOUT' control task. (right) 'EXITSYSTEM' control task. Image taken from Modular-Lab software.

2.5.4.2 Radiofluorination reactions

A major drawback to the use of automated batch reactors for the synthesis of radiotracers is the limit of one radiosynthesis per production of isotope. The optimisation of reactions performed on such platforms is, therefore, very time-consuming and hence expensive. As a result, it was decided that reaction conditions for the initial scoping studies would be based on the data provided in the literature.[193] However, the reported reaction times are too long for radiochemical syntheses and it was decided, therefore, that reaction times would be reduced to 30 min. It was hypothesised that this duration would allow for reaction to occur without significant radioactive decay. DMF was chosen as the solvent as this had been used successfully in the microfluidic study and also by other research groups (Section 1.4.2.7). It was decided that trifluoroacetyl(4-ethoxycarbonylphenyl, 2-thienyl)-λ^3-iodane would be used to assess the ability of $Et_4N{\cdot}HCO_3$ as a PTA in the batch radiofluorination of a diaryliodonium salt. This salt was chosen as the microfluidic study showed that the 2-thienyl derivative produced the highest selectivity when generating ethyl 4-[^{18}F]fluorobenzoate, the initial target of this project.

*2.5.4.3 Radiofluorinations of trifluoroacetyl(4-ethoxycarbonylphenyl, 2-thienyl)-λ^3-iodane **193***

Radio-HPLC conditions for this process were used as described previously (Section 2.4.2.2). The PTS was prepared according to the conditions described for Method B of the microfluidic study. Using the custom program written, solutions of **193** were stirred with a vial charged with anhydrous [^{18}F]$Et_4N{\cdot}F$ at 130 °C for 30 min. A sample of

the crude reaction mixture was then manually injected into the radio-HPLC system for assessment of RCY.

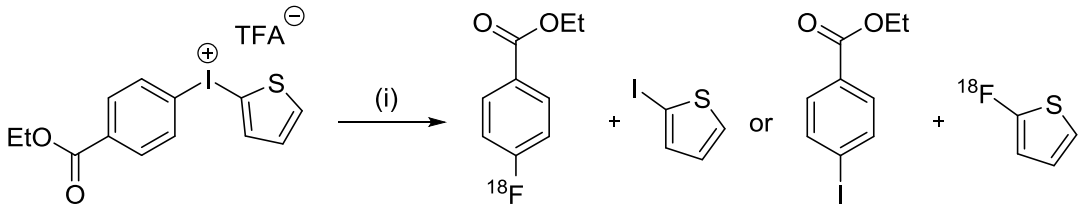

193 **188a** Desired Product **250** **251** **254** Undesired Product

(i) [^{18}F]Et_4N.F or [^{18}F]KF/K222, DMF, 130 °C, 30 min

Scheme 86: Automated batch radiofluorination of **191** to form the desired **248a** and undesired products

RCYs were low – the highest RCY achieved was 12% (Figure 58). However, the transformation is, generally, low yielding with chemical yields of around 20% reported for similar reactions performed over 90 min. Similar RCYs were achieved upon performing the same reaction using [^{18}F]KF/K222 as the RFA.

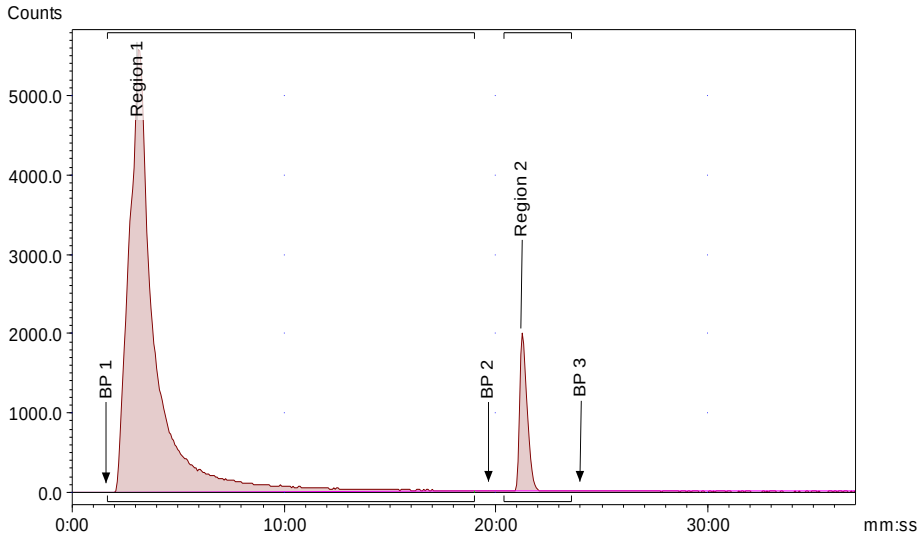

Figure 58: Radio-HPLC trace for the radiofluorination of **193** using the Modular Lab

Due to time-constraints of the project, and limited availability of radioisotope, this investigation was limited to the initial scoping studies. Despite this, the results clearly demonstrate the potential application of $Et_4N{\cdot}HCO_3$ as a PTA in the automated batch

radiofluorination of a diaryliodonium salt. However, significant further investigation is required.

2.5.5 Conclusion

The automation of radiochemical syntheses on a batch scale has become an important focus of practical radiochemistry since the introduction of PET. Systems capable of batch radiofluorinations allow for large quantities of fluorine-18 labelled radiopharmaceuticals to be synthesised from a single production of isotope, for remote site application. In this study, the Modular-Lab was used to generate ethyl 4-[^{18}F]fluorobenzoate from trifluoroacetyl(4-ethoxycarbonylphenyl, 2-thienyl)-λ^3-iodane using [^{18}F]$Et_4N{\cdot}F$ as the RFA. RCYs were low, however, the results have proved that [^{18}F]$Et_4N{\cdot}F$ may be used as an RFA in automated batch radiofluorinations. Further studies are required to form a more definite conclusion.

3 Experimental

Commercially available reagents were purchased from fine chemicals suppliers and used as received unless otherwise stated. Reactions requiring anhydrous conditions were performed using oven- or flame-dried glassware and conducted under a positive pressure of N_2. Anhydrous solvents were prepared as follows: DCM and MeCN were refluxed over CaH_2, toluene was refluxed over sodium and fluorobenzene was stored over 3Å molecular sieves. For radiofluorinations, MeCN (>99%) and DMF (>99%) were purchased from Fisher Chemicals (UK) and pre-dried on molecular sieves (24 h on 4 A˚ MS then stored on 3 A˚ MS) before being used. Thin-layer chromatography was performed using silica gel plates (Kieselgel $60F_{254}$; 0.2 mm) with aluminium backing and visualisation performed with UV light. Infrared spectra were recorded on a Varian Scimitar Series 800 FT-IR with internal calibration. ^{1}H, ^{13}C, ^{19}F and ^{119}Sn-NMR spectra were recorded on a Jeol ECS 400 MHz spectrometer, Jeol Lamda 500 MHz spectrometer or Bruker Avance Ultra 500MHz with residual tetramethylsilane solvent as the reference for ^{1}H and ^{13}C. ^{19}F spectra were referenced with $CFCl_3$ and ^{119}Sn spectra with Me_4Sn. Multiplicities are indicated by s (singlet), d (doublet) dd (doublet of doublets), t (triplet), q (quartet), quin (quintet), or combinations thereof. Coupling constants (J) are measure in Hertz (Hz). Elemental analysis was carried out at London Metropolitan University and results are reported as the average of two runs. Mass spectrometry was recorded at the EPSRC Mass Spectrometry Service, Swansea. It should be noted that hypervalent iodine compounds are known to exist as mixtures (incl. dimers/trimers) and these are evident in the MS data, only the data for the monomer is reported. Melting points were recorded on a Gallenkamp MF-370 melting point apparatus and are uncorrected. Automated flash chromatography was

performed using a Varian (now Agilent) IntelliFlash 971-FP discovery scale flash purification system.

CAUTION: Hypervalent iodine compounds are potentially explosive and should be handled taking appropriate precautions.[309, 310]

3.1 Ethyl 4-(tri-n-butylstannyl) benzoate, 201a

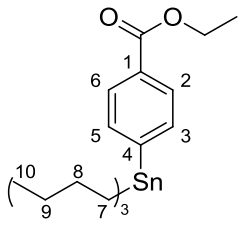

3.1.1 Method A[231]

Trifluoroacetic acid (50 µL, catalytic amount) was added to a reaction vessel containing zinc dust (355 mg, 5.43 mmol) and MeCN (0.5 mL). Cobalt bromide (79 mg, 0.36 mmol) was then added. After stirring for 5 min at RT, allyl chloride (88 µL, 1.08 mmol) was added. After 5 min of stirring, a solution of ethyl 4-iodobenzoate in MeCN (0.61 mL, 3.62 mmol, in 2.41 mL of MeCN, 1.5 M) was added followed immediately by tri-n-butyltin chloride (1.07 mL, 3.98 mmol). The solution was heated to 50 °C and allowed to stir for 1 h. After complete conversion of the iodo benzoate as determined by TLC, the reaction was quenched using sat. aq. ammonium chloride (30 mL) and the product extracted using diethyl ether (3 × 30 mL). The solvent was dried using $MgSO_4$, before being removed *in vacuo* to give the crude product. Purification using reverse-phase flash column chromatography (MeCN) gave the pure product as a colourless oil (1.08 g, 2.46 mmol, 85%). IR ν_{max}(neat) 2925, 1719, 1590, 1459, 1385, 1273; ^{1}H-NMR (500 MHz; $CDCl_3$) δ 7.97 (2H, d, H2/H6 J = 8.1 Hz), 7.55 (2H, d, H3/H5 J = 8.1 Hz), 4.37 (2H, q, O*C*H_2CH$_3$ J = 7.1 Hz), 1.54 (6H, quin, H8 J = 7.8 Hz), 1.38 (3H, t, OCH$_2$C*H*$_3$ J = 7.1 Hz), 1.33 (6H, h, H9 J = 7.3 Hz), 1.09 (6H, t, H7 J = 8.4 Hz), 0.88 (9H, t, H10 J = 7.3 Hz); ^{13}C-NMR (101 MHz; $CDCl_3$) δ 166.91 (CO), 149.28 (C4), 149.28 (^{119}Sn satellites, d, C4 J = 363.6 Hz), 149.28 (^{117}Sn satellites, d , C4 J = 347.44 Hz), 136.40 (C2/C6), 136.40 (Sn satellites, d, C2/C6 J = 30.3 Hz), 130.07 (C1), 128.47 (C3/C5), 128.47 (Sn satellites, d, C3/C5 J = 39.3 Hz), 60.75 (O*C*H$_2$CH$_3$), 29.15 (C9), 29.15 (Sn satellites, d, C9, J = 20.2),

27.42 (C8), 27.42 (Sn satellites, d, C8, J = 55.5 Hz), 14.39 (OCH_2CH_3), 13.72 (C10), 9.71 (C7), 9.71 (^{119}Sn satellites, d, C7 J = 343.4 Hz), 9.71 (^{117}Sn satellites, d, C7 J = 328.25 Hz); ^{119}Sn-NMR (149 MHz; $SnMe_3$) δ -38.49 (ArSn); *m/z* (E.I.) 301 (100), 393 (12), 463 ([^{120}Sn][M+Na]$^+$, 14, plus isotope pattern). Found [M+Na]$^+$, 463.1630. $C_{21}H_{36}O_2SnNa$ requires 463.1633. Anal. Calcd. for $C_{21}H_{36}O_2Sn$: C, 57.4; H, 8.2. Found: C, 57.5; H, 8.3.

3.2 Ethyl 3-(tri-n-butylstannyl) benzoate,[231] 201b

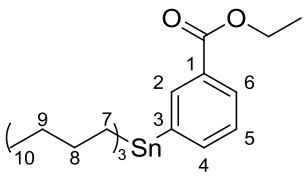

3.2.1 Method A[231]

Product prepared according to procedure outlined for **201a** (Section 3.1.1) using ethyl 3-iodobenzoate (1 g, 3.62 mmol). Purification using reverse-phase flash column chromatography (MeCN) gave the product as a colourless oil (0.99 g, 2.24 mmol, 62%).

R_f = 0.9 (Petrol: EtOAc, 9:1) IR ν_{max}/cm^{-1} (neat) 2957, 1719, 1255; ^{1}H-NMR (500 MHz, $CDCl_3$) δ 8.17 (1H, s, H2), 7.97 (1H, d, H6 J = 7.8 Hz), 7.65 (1H, d, H4 J = 7.1 Hz), 7.38 (1H, t, H5 J = 7.5 Hz), 4.38 (2H, q, OCH_2CH_3 J = 7.1 Hz), 1.56 (6H, p, H8 J = 7.7 Hz), 1.40 (3H, t, OCH_2CH_3 J = 7.1 Hz), 1.35 (6H, h, H9 J = 7.4 Hz), 1.1 (6H, t, H7 J = 8.1 Hz), 0.89 (9H, t, H10 J = 7 Hz); ^{13}C-NMR (101 MHz; $CDCl_3$) δ 167.24 (CO), 142.49 (C1), 140.97 (C4), 140.97 (Sn satellites, d, C4, J = 30.3), 137.36 (C2), 137.36 (Sn satellites, d, C2 J = 33.3 Hz), 129.76 (C3), 129.76 (Sn satellites, d, C3 J = 38.4 Hz), 129.17 (C6), 127.75 (C5), 127.75 (Sn satellites, d, C5 J = 38.4 Hz), 60.91 (OCH_2CH_3), 29.13 (C9), 29.13 (Sn satellites, d, C9 J = 20.2 Hz), 27.42 (C8), 27.42 (Sn satellites, d, C8 J = 56.6 Hz), 14.43 (OCH_2CH_3), 13.76 (C10), 9.71 (C7), 9.71 (^{119}Sn satellites, d, C7 J = 344.41 Hz), 9.71 (^{117}Sn satellites, d, C7 J = 328.25 Hz); ^{119}Sn-NMR (149 MHz, $CDCl_3$) δ -38.07 (ArSn); *m/z* (EI)

463 ([^{120}Sn][M+Na]$^+$, 100, plus isotope pattern), 347 (14), 235 (11), 178 (6). Found: [M+Na]$^+$ 463.1628. $C_{21}H_{36}O_2SnNa$ requires 463.1633. Anal. Calcd. for $C_{21}H_{36}O_2Sn$: C, 57.43; H, 8.26. Found: C, 57.59; H, 8.10.

3.3 Ethyl 2-(tri-n-butylstannyl) benzoate,[231] 201c

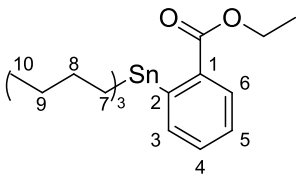

Product prepared according to procedure outlined for **201a** (Section 3.1.1) using ethyl 2-iodobenzoate (1 g, 3.62 mmol). Purification using reverse-phase flash chromatography (MeCN) gave the product as a colourless oil (0.92 g, 2.1 mmol, 58%).

R_f = 0.8 (Petrol: EtOAc, 9:1) IR ν_{max}/cm^{-1} (neat) 2918, 1703, 1267; ^{1}H-NMR (400 MHz, $CDCl_3$) δ 8.10 (1H, d, H6 J = 7.7 Hz), 7.65 (1H, d, H3 J = 7.3 Hz), 7.48 (1H, td, H4 J = 7.3, J = 1.3 Hz), 7.37 (1H, td, H5 J = 7.6, J = 1.3 Hz), 4.37 (2H, q, OC*H*$_2$CH$_3$ J = 7 Hz), 1.49 (6H, quin, H8 J = 7.6, J =7.6), 1.39 (3H, t, OCH$_2$C*H*$_3$ J = 7.1 Hz), 1.3 (6H, h, H9 J = 7.2 Hz), 1.05 (6H, t, H7 J = 8.2 Hz), 0.86 (9H, t, H10 J = 7.3 Hz); ^{13}C-NMR (101 MHz, $CDCl_3$) δ 168.69 (CO), 147.20 (C2), 147.20 (^{119}Sn satellites, d, C2 J = 384.81 Hz), 147.20 (^{117}Sn satellites, d, C2 J = 367.64 Hz), 137.08 (C3), 137.08 (Sn satellites, d, C3 J = 29.29 Hz), 135.83 (C1), 135.83 (Sn satellites, d, C1 J = 16.16 Hz), 131.73 (C4), 131.73 (Sn satellites, d, C4 J = 45.45 Hz), 129.7 (C6), 129.7 (Sn satellites, d, C6 J = 26.26 Hz), 127.96 (C5), 61.23 (O*C*H$_2$CH$_3$), 29.34 (C9), 29.34 (Sn satellites, d, C9 J = 18.18 Hz), 27.58 (C8), 27.58 (Sn satellites, d, C8 J = 60.59 Hz), 14.46 (OCH$_2$*C*H$_3$), 13.82 (C10), 11.21 (C7), 11.21 (^{119}Sn satellites, d, C7 J = 363.6 Hz) 11.21 (^{117}Sn satellites, d, C7 J = 347.44 Hz) ^{119}Sn-NMR (149 MHz, $CDCl_3$) δ -38.1 (ArSn); *m/z* (EI) 439 ([^{120}Sn][M-H]$^+$ 17, plus isotope pattern), 413

(79), 383 (100), 379 (43), 304 (69). Found $[M-H]^+$ 439.1649 $C_{21}H_{35}O_2Sn$ requires 439.1657. Anal. Calcd. for $C_{21}H_{35}O_2Sn$: C, 57.43; H, 8.26. Found: C, 57.33; H, 8.03.

3.4 Diacetoxyiodo-4-anisole,[237] 205

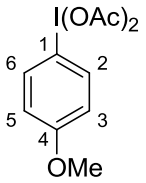

Sodium perborate tetrahydrate (101.56 g, 660 mmol) was added, in portions, to a solution of 2-iodoanisole (14.58 mL, 60 mmol) in acetic acid (540 mL) over 30 min. The mixture was then heated to 50 °C and stirred for 5 h before cooling to RT. Water (1 L) was added before the crude product was extracted with DCM (3 × 400 mL). The extracts were combined before being washed with water (1 L). The organic layer was concentrated *in vacuo* to give the crude product. Crystallisation gave the product as a white crystalline solid (7.26 g, 20.63 mmol, 33%); Mp 91–93 °C (from DCM–ether–petrol) (lit.[311] 92.4–96.0 °C); IR ν_{max}/cm^{-1} (neat) 2952, 1655, 1629, 1581, 1490, 1439, 1365, 1293, 1253, 1178; ^{1}H-NMR (400 MHz;$CDCl_3$) δ 7.99 (2H, d, H2/H6 *J* = 9.0 Hz), 6.95 (2H, d, H3/H5 *J* = 9.0 Hz), 3.85 (3H, s, OMe), 1.98 (6H, s, OAc).^{13}C-NMR (101 MHz;$CDCl_3$) δ 176.52, 162.25, 137.22, 116.74, 111.70, 55.69, 20.49; *m/z* (EI) 198 (13), 233 (48), 266 (4), 311 (6), 374 (100), 390 (5). Found $[M+Na]^+$, 374.9699. $C_{11}H_{13}IO_5$ requires 374.9700. Anal. Calcd. for $C_{11}H_{13}IO_5$: C, 37.52; H, 3.72. Found C, 37.48; H, 3.69.

For an X-ray crystal structure of the compound, see Appendix I (Table 1)

3.5 Diacetoxyiodo-2-thiophene,[237] 206

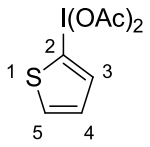

Product prepared according to procedure outlined for **205** (Section 3.4) using 2-iodothiophene (2.21 mL, 20 mmol). Crystallisation gave the product as a white crystalline solid (2.8 g, 8.53 mmol, 42%); mp 118–121 °C (decomp) (from DCM–ether) (lit.[312], 120–122 °C); IR ν_{max}/cm^{-1} (neat) 2360, 2342, 2185, 1634, 1365, 1267; ^{1}H-NMR (400 MHz; $CDCl_3$) δ 7.77 (1H, dd, H5 J = 3.8, J = 1.2 Hz), 7.63 (1H, dd, H4 J = 5.4, J = 1.3 Hz,), 7.12 (1H, dd, H3 J = 5.4, J = 3.8 Hz), 2.01 (6H, s, OAc); ^{13}C-NMR (101 MHz; $CDCl_3$) 177.09 (CO), 139.16 (C5), 134.96 (C3), 128.72 (C4), 106.32 (C2), 20.45 (CH_3); *m/z* (E.I.) 268 ([M-OAc]$^+$, 100), 226 (26), 209 (97). Found [M-OAc]$^+$ 268.9130. $C_6H_6IO_2S$ requires 268.9128. Anal. Calcd. for $C_8H_9IO_4S$: C, 29.3; H, 2.8. Found C, 29.2; H, 2.6.

For an X-ray crystal structure of the compound, see Appendix I (Table 2).

3.6 Trifluoroacetyl(4-ethoxycarbonylphenyl, phenyl)-λ^3-iodane, 191

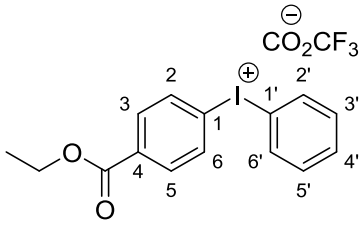

Trifluoroacetic acid was added (0.74 mL, 10 mmol), dropwise at –30 °C under N_2, to a solution of diacetoxyiodobenzene (1.61 g, 5 mmol) in DCM (50 mL, anhydrous). After 30 min of stirring at –30 °C, the solution was warmed to RT and stirred for 1 h. The solution was recooled to –30 °C and **201a** (1.74 mL, 5 mmol) was added. The solution was then allowed to warm to RT overnight whilst continuing to stir under N_2. The

solvent was dried using $MgSO_4$ before being removed *in vacuo*. The crude material was purified by recrystallisation in petrol to give the product (990 mg, 2.12 mmol, 56%). R_f = 0.25 (92:8 DCM:MeOH); M.p. = 153–155 °C (from DCM–ether–petrol); IR (neat) ν_{max}/cm^{-1} 3059, 1712, 1660, 1122; ^{1}H-NMR (400 MHz; d_6-DMSO) δ 8.33 (2H, d, H3/H5 J = 8.5 Hz), 8.23 (2H, d, H2'/H6' J = 7.4 Hz), 7.97 (2H, d, H2/H6 J = 8.6 Hz), 7.63 (1H, t, H4' J = 7.5 Hz), 7.49 (2H, t, H3'/H5' J = 7.7 Hz), 4.27 (2H, q, OC*H*$_2$CH$_3$ J = 7.1 Hz), 1.26 (3H, t, OCH$_2$C*H*$_3$ J = 7.1 Hz); ^{13}C-NMR (400 MHz; d_6-DMSO) δ 165.13, 136.01, 135.84, 133.25, 132.64, 132.33, 132.31, 122.08, 117.49, 61.97, 14.56. ^{19}F-NMR (376 MHz, d_6-DMSO) δ -73.43 (CO_2CF_3). *m/z* (E.I.) 353 ($[M]^+$ 100, plus isotope model) 181 (3) Found $[M]^+$, 353.0033. $C_{15}H_{14}IO_2$ requires 353.0031. Anal. Calcd. for $C_{17}H_{14}F_3IO_4$: C, 43.8; H, 3.0. Found C, 43.8; H, 3.0.

For an X-ray crystal structure of the compound, see Appendix II (Table 1).

3.7 Trifluoroacetyl(4-ethoxycarbonylphenyl, anis-4-yl)-λ^3-iodane, 192

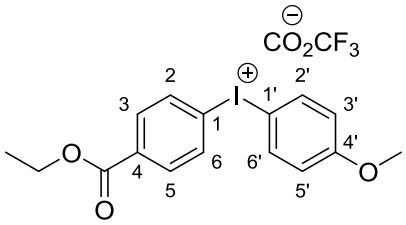

Product prepared according to procedure outlined for **191** (Section 3.6) using **205** (1.76 g, 5 mmol). White crystalline solid (1.71 g, 3.46 mmol, 73%). R_f = 0.25 (92:8 DCM:MeOH); M.p. = 127–130°C (from DCM–ether–petrol) IR ν_{max}/cm^{-1} (neat) 3061, 1703, 1650, 1129; ^{1}H-NMR (400 MHz; $CDCl_3$) δ 8.00 (2H, d, H3/H5 J = 8.2 Hz), 7.92 (2H, d, H'2/H'6 J = 7.3 Hz), 7.84 (2H, d, H2/H6 J = 7.9 Hz), 6.91 (2H, d, H'3/H'5 J = 8.6 Hz), 4.36 (2H, q, OC*H*$_2$CH$_3$ J = 7.0 Hz), 3.82 (3H, s, OCH$_3$), 1.36 (3H, t, OCH$_2$C*H*$_3$ J = 7.1 Hz); ^{13}C-NMR (400 MHz; $CDCl_3$) δ 165.03, 162.70, 137.30, 134.05, 133.40, 132.39, 121.45,

117.80, 104.84, 61.86, 55.74, 14.28. ^{19}F-NMR (376 MHz, $CDCl_3$) -73.45 (CO_2CF_3). *m/z* (E.I) 383 ($[M]^+$, 100, plus isotope pattern), 256 (5), 211 (3). Found $[Cation]^+$, 383.0133. $C_{16}H_{16}O_3I$ requires 383.0139. Anal. Calc. for $C_{18}H_{16}F_3IO_5$, 43.5; H, 3.2. Found: C, 43.5; H, 3.2.

For an X-ray crystal structure of the compound, see Appendix II (Table 7).

3.8 Trifluoroacetyl(4-ethoxycarbonylphenyl, thiophen-4-yl)-λ^3-iodane, 193

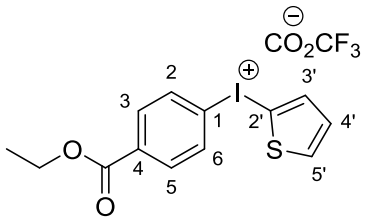

Product prepared according to procedure outlined for **191** (Section 3.6) using **206** (1.97 g, 6 mmol). White crystalline solid (1.93 g, 4.1 mmol 68%). R_f = 0.31 (DCM:MeOH, 93:7); M.p. = 136–138°C (decomp.) (from DCM–ether–petrol); IR ν_{max}/cm^{-1} (neat) 3087, 1704, 1651; ^{1}H-NMR (400 MHz, d_6-DMSO) δ 8.32 (2H, d, H2/H6 J = 9 Hz), 8.05 (1H, dd, H3' J = 4, J = 1 Hz), 7.97 (2H, d, H3/H5 J = 9 Hz), 7.94 (1H, dd, H4' J = 5, J = 1 Hz), 7.14 (1H, dd, H5' J = 5, J = 4 Hz), 4.28 (2H, q, OCH_2CH_3 J = 7 Hz), 1.26 (3H, t, OCH_2CH_3 J = 7 Hz) ^{13}C-NMR (101 MHz, d_6-DMSO) δ 165.10, 141.17, 138.03, 135.40, 133.24, 132.31, 130.19, 124.73, 101.90, 61.98, 14.56. ^{19}F-NMR (376 MHz, d_6-DMSO) δ -73.36 (CO_2CF_3). *m/z* (E.I.) 358 ($[Cation]^+$, 100, plus isotope pattern) 232 (7) 187 (6); Found 358.9588. $C_{13}H_{12}IO_2S$ requires 358.9597. Anal. Calcd. for $C_{15}H_{12}F_3IO_4S$: C, 38.2; H, 2.6. Found C, 38.2; H, 2.6.

For an X-ray crystal structure of the compound, see Appendix II (Table 12).

3.9 Trifluoroacetyl(3-ethoxycarbonylphenyl, phenyl)- λ^3-iodane, 194

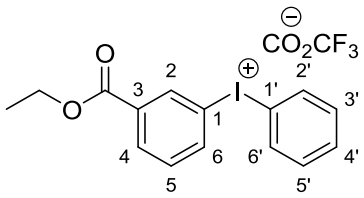

Product prepared according to procedure outlined for **191** (Section 3.6) using **201b** (2.18 g, 5 mmol) and diacetoxyiodobenzene (1.61 g, 5 mmol). White crystalline solid (1.3 g, 2.8 mmol, 56%).R_f = 0.31 (DCM:MeOH, 93:7); M.p. = 141–142°C (decomp.) (from DCM–ether–petrol); IR ν_{max}/cm^{-1} (neat) 3058, 1707, 1656, 1567, 1472, 1444, 1422, 1366, 1272, 1176; ^{1}H-NMR (400 MHz, d_6-DMSO) δ 8.73 (1H, t, H2 J = 1.7 Hz), 8.44 (1H, ddd, H6 J = 8.0, 1.8, 1.1 Hz) 8.26 (2H, dd, H2'/H6' J = 8.4, 1.1 Hz), 8.12 (1H, d, H2 J = 8.2 Hz), 7.66 – 7.59 (2H, m, H5 and H4'), 7.49 (2H, t, H3'/H5' J = 7.7 Hz), 4.30 (2H, q, OCH_2CH_3 J = 7.1 Hz), 1.28 (3H, t, OCH_2CH_3 J = 7.1 Hz); ^{13}C-NMR (101 MHz, d_6-DMSO) δ 165.10, 141.17, 138.03, 135.40, 133.24, 132.31, 130.19, 124.73, 101.90, 100.00, 61.98, 14.56. ^{19}F-NMR (376 MHz, d_6-DMSO) δ -73.42 (CO_2CF_3). *m/z* (E.I.); 353 ($[M]^+$, 100, plus isotope pattern), 818 (22), 1284 (8), 1750 (9). Found $[M]^+$, 353.0032. $C_{15}H_{14}IO_2$ requires 353.0033. Anal. Calcd. for $C_{17}H_{14}F_3IO_4$: C, 43.80; H, 3.03. Found C, 43.83; H, 2.97.

For an X-ray crystal structure of the compound, see Appendix II (Table 194).

3.10 Trifluoroacetyl(3-ethoxycarbonylphenyl, 4-anisyl)-λ^3-iodane, 195

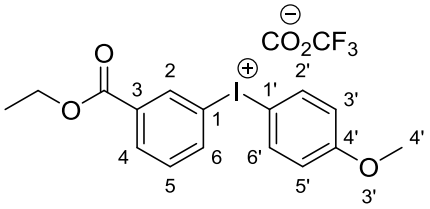

Product prepared according to procedure outlined for **191** (Section 3.6) using **201b** (2.16 g, 5 mmol) and **205** (1.76 g, 5 mmol). White crystalline solid (1.47 g, 2.96 mmol,

55%). R_f = 0.33 (DCM:MeOH, 92:8); M.p. = 106-108°C (decomp.) (from DCM–ether–petrol); IR ν_{max}/cm^{-1} (neat) 2972, 1706, 1652, 1582, 1488, 1461, 1396, 1366, 1253, 1170; ^{1}H-NMR (400 MHz, d_3-MeCN) δ 8.64 (1H, t, H2 J = 1.7 Hz), 8.27 – 8.22 (1H, m, H6), 8.15 (1H, dd, H'3 J = 7.8 Hz, J = 1.1 Hz), 7.86 (1H, dd, H'5 J = 3.8 Hz, J = 1.1 Hz), 7.74 (1H, dd, H4 J = 5.3 Hz, J = 1.1 Hz), 7.54 (1H, t, H'4 J = 8.0 Hz), 7.09 (1H, dd, H5 J = 5.3 Hz, J = 3.8 Hz), 4.31 (2H, q, J = 7.1 Hz, OC*H*$_2$CH$_3$), 1.32 (3H, t, OCH$_2$C*H*$_3$ J = 7.1 Hz); ^{13}C-NMR (400 MHz; d_6-DMSO) δ 164.54, 162.56, 139.57, 137.95, 135.56, 132.97, 132.54, 132.43, 118.00, 117.79, 106.24, 62.09, 56.23, 14.60. ^{19}F-NMR (376 MHz, d_6-DMSO) δ -73.32 (CO_2CF_3). *m/z* (E.I.) 232 (3), 358 (100), 879 (9), 1375 (2); Found $[M]^+$, 383.0130. $C_{16}H_{16}IO_3$ requires 383.0139. Anal. Calcd. for $C_{18}H_{16}F_3IO_5$: C, 43.57; H, 3.25. Found C, 43.62; H, 3.28.

For an X-ray crystal structure of the compound, see Appendix II (Table 22).

3.11 Trifluoroacetyl(3-ethoxycarbonylphenyl, 2-thienyl)- λ^3-iodane, 196

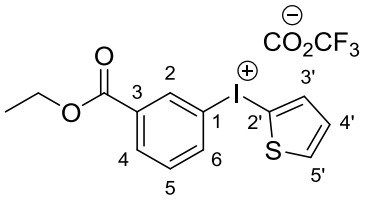

Product prepared according to procedure outlined for **191** (Section 3.6) using **201b** (2.98 g, 6.82 mmol) and **206** (2.24 g, 6.82 mmol). White crystalline solid (1.81 g, 3.82 mmol, 56%). R_f = 0.34 (DCM:MeOH, 92:8); M.p. = 102–103 °C (decomp.) (from DCM–ether–petrol); IR ν_{max}/cm^{-1} (neat) 3065, 1702, 1654; ^{1}H-NMR (400 MHz, d_3-MeCN) δ 8.64 (1H, dd, H2 J = 1.9, 1.6 Hz), 8.24 (1H, ddd, H6 J = 7.9, 1.8, 0.9 Hz,), 8.15 (1H dt, H4 J = 7.8, 1.1 Hz, 1H), 7.86 (1H, dd, H3' *J* = 3.8, 1.2 Hz), 7.74 (1H, dd, H5' J = 5.4, 1.2 Hz), 7.54 (1H, t, H5 J = 8.0 Hz), 7.09 (1H, dd, H4' J = 5.3, 3.8 Hz), 4.31 (2H, q, OC*H*$_2$CH$_3$ J = 7.1

Hz), 1.32 (3H, t, OCH_2CH_3 J = 7.1 Hz). ^{13}C-NMR (400 MHz; d_3-MeCN) 164.15, 140.63, 138.08, 137.06, 134.65, 133.56, 132.32, 131.75, 129.76, 120.14, 102.19, 61.83, 13.50. ^{19}F-NMR (376 MHz, d_6-DMSO) δ -74.87 (CO_2CF_3) *m/z* (E.I.) 358 ($[M]^+$, 100, plus isotope model) 232 (3) 830 (26) 1302 (4) 1774 (4); Found $[M]^+$, 358.9595. $C_{13}H_{12}IO_2S$ requires 358.9597. Anal. Calcd. for $C_{15}H_{12}F_3IO_4S$: C, 38.2; H, 2.6. Found C, 38.3; H, 2.5.

For an X-ray crystal structure of the compound, see Appendix II (Table 28).

3.12 Ethyl 4-fluorobenzoate, 188d

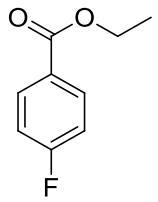

3.12.1 Method A[193]

A mixture of caesium fluoride (30.3 mg, 0.2 mmol) and **191** (90.8 mg, 0.2 mmol) in anhydrous *N, N*-dimethylformamide (3 mL) were added to a long glass tube flushed with N_2. The solution was heated to 130 °C for 1.5 h under N_2. When the mixture had cooled to room temperature, a sample was taken and diluted with $CDCl_3$ (0.4 mL) and analysed by ^{19}F NMR. For results see Section 2.1.5.

3.12.2 Method B

Product prepared according to procedure outlined for **188d** (Section 3.12.1) using **192** (96.8 mg, 0.2 mmol). For results see Section 2.1.5.

3.12.3 Method C

Product prepared according to procedure outlined for **188d** (Section 3.12.1) using **193** (92 mg, 0.2 mmol). For results see Section 2.1.5.

3.13 Ethyl 3-fluorobenzoate, 188e

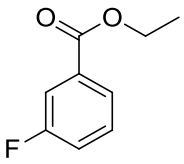

3.13.1 Method A[193]

Product prepared according to procedure outlined for **188d** (Section 3.12.1) using **194** (90.8 mg, 0.2 mmol). For results see Section 2.1.5.

3.13.2 Method B

Product prepared according to procedure outlined for **188d** (Section 3.12.1) using **195** (96.8 mg, 0.2 mmol). For results see Section 2.1.5.

3.13.3 Method C

Product prepared according to procedure outlined for **188d** (Section 3.12.1) using **196** (92 mg, 0.2 mmol). For results see Section 2.1.5.

3.14 4-[^{18}F]fluoroacetophenone, 245

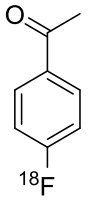

HPLC methods were carried out using an Agilent 1200 HPLC system equipped with a UV absorbance detector (l_{max} 254 nm) and a radioactivity detector (LabLogic Flow Count). The product were not isolated and the radiochemical yield (RCY) reported relates to the amount of radioactivity of the product relative to the total radioactivity detected by radio-HPLC on analysis of the reaction mixture. The radioactive product

was separated on a PolymerX 5 mm RP-1 100 column (Phenomenex, USA) eluting at 1.1 mL/min with MeCN-water. An isocratic gradient of 24% MeCN was used. t_R = 6.5 min.

3.14.1 Method A

NCA [^{18}F]fluoride (5–100 mCi) in [^{18}O]H_2O (1–5 mL) was adsorbed onto a pre-conditioned anion exchange resin (QMA: Waters Sep-Pak®Light Accell Plus) before being released using a solution of either K_2CO_3 (1.3 mg; 9.5 μmol) and Kryptofix®222 (7.2 mg; 19 μmol) in MeCN/H_2O (9:1 (v/v) 450 μL) (PTS-1); or $Et_4N.HCO_3$ (3.7 mg; 19 μmol) in MeCN/H_2O (9:1 (v/v) 450 μL) (PTS-2) and into a V-vial (2 mL, Wheaton). The solutions were dried by two successive azeotropic evaporations using MeCN (450 μL) at 100 °C and under a positive flow of N_2. The [^{18}F]KF/Kryptofix®222 or [^{18}F]Et_4NF generated was then dissolved in DMF (450 μL) and loaded into the storage loop (P3: 401 μL) on the microfluidic system.

Dry PTA-[^{18}F]fluoride (5–100 mCi, 450 μL DMF) and **246** (in DMF at 5–10 mg/mL) were loaded into their respective storage loops (loop 3 and loop 1 respectively). Capillaries that lead from P1 and P3 to the microreactor were primed with their respective reagents. Prior to recording data several priming reaction runs were performed to confirm the integrity of the synthetic platform and the in-line analytical HPLC system. Set volumes (10–30 μL) of both solutions were dispensed into the pre-heated microreactor (130–190 °C) at pre-determined flow rates (10–30 μL/min). This is achieved by the syringes of P1 and P3, simultaneously dispensing precursor and [^{18}F]fluoride solutions (either [^{18}F]KF/Kryptofix®222 or [^{18}F]Et_4NF) from their respective loops, into the microreactor using a fixed volume of system solvent (DMF) at a preset flow rate. The solutions initially mix at the entrance to the microreactor. User-operated computer software determines the reaction parameters — temperature,

time and stoichiometry (P1:P3). Following completion of the reaction, P3 sweeps the crude mixture to the electronic injector and radio-HPLC system allowing the RCY of the process to be determined. At the start and end of each series of experiments the base module, reactor module, microreactor and associated transfer lines were cleaned using DMF and the concentrator module, with MeCN.

For a table of results, see Appendix III (Tables 2 and 4)

3.14.2 Method B

Product prepared according to procedure outlined for **245** (Section 3.14.1) using **244** (10 mg/mL).

For a table of results, see Appendix III (Tables 1 and 3)

3.15 Ethyl 4-[^{18}F]fluorobenzoate, 188a

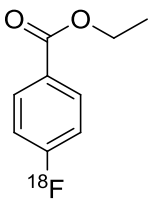

3.15.1 Method A

Product prepared according to procedure outlined for **244** (Section 3.14.1) using **247** (10 mg/mL).

HPLC methods were carried out using an Agilent 1200 HPLC system equipped with a UV absorbance detector (l_{max} 254 nm) and a radioactivity detector (LabLogic Flow Count). The [^{18}F]fluoroarenes were not isolated and the radiochemical yield (RCY) reported relates to the amount of radioactivity of the product relative to the total radioactivity detected by radio-HPLC on analysis of the reaction mixture. The radioactive product was separated on a PolymerX 5 mm RP-1 100 column

(Phenomenex, USA) eluting at 1.1 mL/min with EtOH‑water. Mobile phase composition started at 40% EtOH which increased linearly to 60% at EtOH over 2 min and then to 80% at 5 min which continued at this composition for a further 7 min. t_R = 6.2 min.

For a table of results, see Appendix III (Tables 5 and 6)

3.15.2 Method B

Product prepared according to procedure outlined for **244** (Section 3.14.1) using **188d** (10 mg/mL).

HPLC methods were carried out using an Agilent 1200 HPLC system equipped with a UV absorbance detector (l_{max} 254 nm) and a radioactivity detector (LabLogic Flow Count). The [^{18}F]fluoroarenes were not isolated and the radiochemical yield (RCY) reported relates to the amount of radioactivity of the product relative to the total radioactivity detected by radio-HPLC on analysis of the reaction mixture. The radioactive product was detected on a PolymerX 5 mm RP-1 100 column (Phenomenex, USA) eluting at 1.1 mL/min with EtOH-water.

Mobile phase composition started at 60% EtOH which increased linearly to 80% at EtOH over 6 min. t_R = 4.5 min.

For a table of results, see Appendix III (Tables 7 and 8).

3.15.3 Method C

Product prepared according to procedure outlined for **244** (Section 3.14.1) using **193** (10 mg/ml).

HPLC methods were carried out using an Agilent 1200 HPLC system equipped with a UV absorbance detector (l_{max} 254 nm) and a radioactivity detector (LabLogic Flow Count). The product was not isolated and the radiochemical yield (RCY) reported relates to the amount of radioactivity of the product relative to the total radioactivity detected by radio-HPLC on analysis of the reaction mixture. The radioactive product was separated on a PolymerX 5 mm RP-1 100 column (Phenomenex, USA) eluting at 1.1 mL/min with EtOH–water. Mobile phase composition started at 25% EtOH which increased linearly to 100% at EtOH over 7 min which continued at this composition for a further 2 min. t_R = 7 min.

For a table of results, see Appendix III (Tables 9 and 10).

3.15.4 Method D

Product prepared according to procedure outlined for **244** (Section 3.14.1) using **191** (10 mg/ml).

HPLC methods were carried out using an Agilent 1200 HPLC system equipped with a UV absorbance detector (l_{max} 254 nm) and a radioactivity detector (LabLogic Flow Count). The [^{18}F]fluoroarenes were not isolated and the radiochemical yield (RCY) reported relates to the amount of radioactivity of the product relative to the total radioactivity detected by radio-HPLC on analysis of the reaction mixture. The radioactive product was detected on a ThermoFisher 5μm RP-C18 100 column eluting at 1.1 mL/min with MeCN–water. Mobile phase composition started at 18% MeCN for 4 min, increasing to 40% at 4 min 30 s, remaining at this composition for 11 min 30 s, before decreasing back to 18 % over 30 s, where the composition remained constant for a further 1 min 30 s. t_R =

For a table of results, see Appendix III (Tables 11 and 12).

3.15.5 Method E

Product prepared according to procedure outlined for **244** (Section 3.14.1) using **192** (10 mg/ml).

HPLC methods were carried out using an Agilent 1200 HPLC system equipped with a UV absorbance detector (l_{max} 254 nm) and a radioactivity detector (LabLogic Flow Count). The [^{18}F]fluoroarenes were not isolated and the radiochemical yield (RCY) reported relates to the amount of radioactivity of the product relative to the total radioactivity detected by radio-HPLC on analysis of the reaction mixture. The radioactive product was detected on a ThermoFisher 5μm RP-C18 100 column eluting at 1.1 mL/min with MeCN–water. Mobile phase composition started at 18% MeCN for 4 min, increasing to 40% at 4 min 30 s, remaining at this composition for 11 min 30 s, before decreasing back to 18 % over 30 s, where the composition remained constant for a further 1 min 30 s. t_R = 14 min 20 s

For a table of results, see Appendix III (Tables 11 and 12).

3.15.6 Method F

The Eckert and Ziegler Modular Lab system performing the radiosyntheses consists of 1 × peltier reaction module (PRM) with transfer line fitted, 2 × single stopcock modules (SSM), 4 × solenoid valve modules (SVM), a vial holder module (VHM) to which was connected a pressure sensor and an activity detector in addition to the VHM's internal detector.

All the vials containing reagents as well as the reactor itself were standard glass Wheaton V-vial; the transfer of the liquids was operated by applying positive or negative pressure through FEP tubings directly inserted into vial septa.

Using the Eckert & Ziegler Modular Lab System no-carrier-added [^{18}F]fluoride (5–100 mCi) in [^{18}O]H_2O (1–5 mL) was adsorbed onto a pre-conditioned anion-exchange resin cartridge before being released using a solution of either Kryptofix®222/K_2CO_3 or $Et_4N.HCO_3$ (0.19 mmol) in MeCN/H_2O (9:1 (v/v) 1 mL) and into a v-vial. The solution was then heated to 110 °C under a positive flow of N_2 for 4 min then cooled to 90 °C for a further 4 min before being cooled to RT. **193** in DMF (0.021 M) was then added and the reaction stirred at 130 °C whilst under a positive flow of N_2 for 90 min. The reaction was then cooled to RT before being transferred to a collection vial. DMF (1 mL) was then added to the reaction vial and stirred for 1 min before being transferred to the collection vessel. Radio-HPLC was used to calculate the RCY.

HPLC methods were carried out using an Agilent 1200 HPLC system equipped with a UV absorbance detector (l_{max} 254 nm) and a radioactivity detector (LabLogic Flow Count). The [^{18}F]fluoroarenes were not isolated and the radiochemical yield (RCY) reported relates to the amount of radioactivity of the product relative to the total radioactivity detected by radio-HPLC on analysis of the reaction mixture. The radioactive product was detected on a ThermoFisher 5μm RP-C18 100 column eluting at 1.1 mL/min with MeCN–water. Mobile phase composition started at 18% MeCN for 4 min, increasing to 40% at 4 min 30 s, remaining at this composition for 11 min 30 s, before decreasing back to 18 % over 30 s, where the composition remained constant for a further 1 min 30 s. t_R = 14 min 20 s.

3.16 Ethyl 3-[^{18}F]fluorobenzoate, 188b

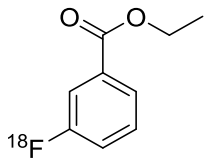

3.16.1 Method A

Product prepared according to procedure outlined for **244** (Section 3.14.1) using **194** (10 mg/mL).

HPLC methods were carried out using an Agilent 1200 HPLC system equipped with a UV absorbance detector (l_{max} 254 nm) and a radioactivity detector (LabLogic Flow Count). The [^{18}F]fluoroarenes were not isolated and the radiochemical yield (RCY) reported relates to the amount of radioactivity of the product relative to the total radioactivity detected by radio-HPLC on analysis of the reaction mixture. The radioactive product was detected on a ThermoFisher 5μm RP-C18 100 column eluting at 1.1 mL/min with MeCN–water. Mobile phase composition started at 18% MeCN for 4 min, increasing to 40% at 4 min 30 s, remaining at this composition for 11 min 30 s, before decreasing back to 18 % over 30 s, where the composition remained constant for a further 1 min 30 s. t_R = 14 min 20 s.

For a table of results, see Appendix III (Tables 11 and 12).

3.16.2 Method B

Product prepared according to procedure outlined for **244** (Section 3.14.1) using **195** (10 mg/mL).

HPLC methods were carried out using an Agilent 1200 HPLC system equipped with a UV absorbance detector (l_{max} 254 nm) and a radioactivity detector (LabLogic Flow

Count). The [^{18}F]fluoroarenes were not isolated and the radiochemical yield (RCY) reported relates to the amount of radioactivity of the product relative to the total radioactivity detected by radio-HPLC on analysis of the reaction mixture. The radioactive product was detected on a ThermoFisher 5μm RP-C18 100 column eluting at 1.1 mL/min with MeCN–water. Mobile phase composition started at 18% MeCN for 4 min, increasing to 40% at 4 min 30 s, remaining at this composition for 11 min 30 s, before decreasing back to 18 % over 30 s, where the composition remained constant for a further 1 min 30 s. t_R = 14 min 20 s.

For a table of results, see Appendix III (Tables 11 and 12).

3.16.3 Method C

Product prepared according to procedure outlined for **244** (Section 3.14.1) using **196** (10 mg/mL).

HPLC methods were carried out using an Agilent 1200 HPLC system equipped with a UV absorbance detector (l_{max} 254 nm) and a radioactivity detector (LabLogic Flow Count). The [^{18}F]fluoroarenes were not isolated and the radiochemical yield (RCY) reported relates to the amount of radioactivity of the product relative to the total radioactivity detected by radio-HPLC on analysis of the reaction mixture. The radioactive product was detected on a ThermoFisher 5μm RP-C18 100 column eluting at 1.1 mL/min with MeCN–water. Mobile phase composition started at 18% MeCN for 4 min, increasing to 40% at 4 min 30 s, remaining at this composition for 11 min 30 s, before decreasing back to 18 % over 30 s, where the composition remained constant for a further 1 min 30 s. t_R = 14 min 20 s.

For a table of results, see Appendix III (Tables 11 and 12).

4 References

1. B. Kuhnast, B. de Bruin, F. Hinnen, B. Tavitian and F. Dolle, *Bioconjugate Chem.*, 2004, **15**, 617-627.
2. H. N. Wagner, Jr., *J Nucl Med*, 1991, **32**, 561-564.
3. N. Oi, T. Iwaya, M. Itoh, K. Yamaguchi, Y. Tobimatsu and T. Fujimoto, *J Orthop Sci*, 2003, **8**, 55-61.
4. Z. Li and P. S. Conti, *Adv. Drug Deliv. Rev.*, 2010, **62**, 1031-1051.
5. J. Cal-Gonzalez, J. L. Herraiz, S. Espana, M. Desco, J. J. Vaquero and J. M. Udias, Nuclear Science Symposium Conference Record (NSS/MIC), 2009 IEEE, 2009.
6. D. O'Hagan, *J. Fluorine Chem.*, 2010, **131**, 1071-1081.
7. W. K. Hagmann, *J. Med. Chem.*, 2008, **51**, 4359-4369.
8. J. S. Fowler and T. Ido, in *Handbook of Radiopharmaceuticals*, John Wiley & Sons, Ltd, 2005, pp. 307-321.
9. F. M. D. Ismail, *J. Fluorine Chem.*, 2002, **118**, 27-33.
10. M. Guillaume, A. Luxen, B. Nebeling, M. Argentini, J. C. Clark and V. W. Pike, *Appl. Radiat. Isot.*, 1991, **42**, 749-762.
11. T. J. Ruth and A. P. Wolf, *Radiochim. Acta*, 1979, **26**, 21-24.
12. http://abt-mi.com/en/resources, 30/05/2015.
13. D. J. Schlyer, M. A. V. Bastos, D. Alexoff and A. P. Wolf, *Appl. Radiat. Isot.*, 1990, **41**, 531-533.
14. J. W. Brodack, M. R. Kilbourn, M. J. Welch and J. A. Katzenellenbogen, *Appl. Radiat. Isot.*, 1986, **37**, 217-222.
15. O. Solin, J. Bergman, M. Haaparanta and A. Reissell, *Appl. Radiat. Isot.*, 1988, **39**, 1065-1071.

16. M. S. Rosenthal, A. L. Bosch, R. J. Nickles and S. J. Gatley, *Int. J. Appl. Radiat. Is.*, 1985, **36**, 318-319.

17. S. J. Gatley, *Appl. Radiat. Isot.*, 1989, **40**, 541-544.

18. C. Lemaire, M. Guillaume, R. Cantineau and L. Christiaens, *J Nucl Med*, 1990, **31**, 1247-1251.

19. A. F. Shields, J. R. Grierson, B. M. Dohmen, H.-J. Machulla, J. C. Stayanoff, J. M. Lawhorn-Crews, J. E. Obradovich, O. Muzik and T. J. Mangner, *Nat. Med.*, 1998, **4**, 1334-1336.

20. R. E. Ehrenkaufer, J. F. Potocki and D. M. Jewett, *J. Nucl. Med.*, 1984, **25**, 333-337.

21. All RCYs obtained throughout this work are NDC.

22. H.Teare, E. G. Robins, E. Årstad, S. K. Luthra and V. Gouverneur, *Chem. Commun.*, 2007, 2330-2332.

23. B. Günther and S. Günther, *Ber. Chem.*, 1927, **60**, 1186-1190.

24. O. Wallach, *Justus Liebig's Annalen der Chemie*, 1886, **235**, 233-255.

25. T. Pages and B. R. Langlois, *J. Fluorine Chem.*, 2001, **107**, 321-327.

26. T. Pages, B. R. Langlois, D. L. Bars and P. Landais, *J. Fluorine Chem.*, 2001, **107**, 329-335.

27. M. Noel, V. Suryanarayanan and S. Chellammal, *J. Fluorine Chem.*, 1997, **83**, 31-40.

28. G. J. Kienzle, G. Reischl and H. J. Machulla, *J. Labell. Compd. Radiopharm.*, 2005, **48**, 259-273.

29. G. Reischl, G. J. Kienzle and H. J. Machulla, *J. Radioanal. Nucl. Chem.*, 2002, **254**, 409-411.

30. E. Lee, A. S. Kamlet, D. C. Powers, C. N. Neumann, G. B. Boursalian, T. Furuya, D. C. Choi, J. M. Hooker and T. Ritter, *Science*, 2011, **334**, 639-642.

31. T. Furuya, H. M. Kaiser and T. Ritter, *Angew. Chem. Int. Ed.*, 2008, **47**, 5993-5996.

32. Z. Gao, Y. H. Lim, M. Tredwell, L. Li, S. Verhoog, M. Hopkinson, W. Kaluza, T. L. Collier, J. Passchier, M. Huiban and V. Gouverneur, *Angew. Chem. Int. Ed.*, 2012, **51**, 6733-6737.

33. L. Martarello, C. Schaffrath, H. Deng, A. D. Gee, A. Lockhart and D. O'Hagan, *J. Labell. Compd. Radiopharm.*, 2003, **46**, 1181-1189.

34. M. Onega, J. Domarkas, H. Deng, L. F. Schweiger, T. A. D. Smith, A. E. Welch, C. Plisson, A. D. Gee and D. O'Hagan, *Chem. Commun.*, 2010, **46**, 139-141.

35. M. R. Kilbourn, M. J. Welch, C. S. Dence, T. J. Tewson, H. Saji and M. Maeda, *Int. J. Appl. Radiat. Is.*, 1984, **35**, 591-598.

36. N. Gou, M. S. Ansari, R. R. Price and R.M.Baldwin, *J. Labell. Compd. Radiopharm.*, 2007, **50**, S143.

37. T. G. Hamill, S. Krause, C. Ryan, C. Bonnefous, S. Govek, T. J. Seiders, N. D. P. Cosford, J. Roppe, T. Kamenecka, S. Patel, R. E. Gibson, S. Sanabria, K. Riffel, W. Eng, C. King, X. Yang, M. D. Green, S. S. O'malley, R. Hargreaves and H. D. Burns, *Synapse*, 2005, **56**, 205-216.

38. L. Mu, C. R. Fischer, J. P. Holland, J. Becaud, P. A. Schubiger, R. Schibli, S. M. Ametamey, K. Graham, T. Stellfeld, L. M. Dinkelborg and L. Lehmann, *Eur. J. Org. Chem.*, 2012, **2012**, 889-892.

39. D. Block, H. H. Coenen and G. Stöcklin, *J. Labell. Compd. Radiopharm.*, 1988, **25**, 201-216.

40. J. Zessin, O. Eskola, P. Brust, J. Bergman, J. Steinbach, P. Lehikoinen, O. Solin and B. Johannsen, *Nucl. Med. Biol.*, 2001, **28**, 857-863.

41. M. M. Goodman, C. D. Kilts, R. Keil, B. Shi, L. Martarello, D. Xing, J. Votaw, T. D. Ely, P. Lambert, M. J. Owens, V. M. Camp, E. Malveaux and J. M. Hoffman, *Nucl. Med. Biol.*, 2000, **27**, 1-12.

42. J. L. Musachio, J. Shah and V. W. Pike, *J. Labell. Compd. Radiopharm.*, 2005, **48**, 735-747.

43. Okarvi and S. Okarvi, *Eur J Nucl Med*, 2001, **28**, 929-938.

44. G. Tang, W. Zeng, M. Yu and G. Kabalka, *J. Labell. Compd. Radiopharm.*, 2008, **51**, 68-71.

45. M. Carroll, R. Yan, F. Aigbirhio, D. Soloviev and L. Brichard, *J. Nucl. Med.*, 2008, **49**, 298P.

46. B. de Bruin, B. Kuhnast, F. Hinnen, L. Yaouancq, M. Amessou, L. Johannes, A. Samson, R. Boisgard, B. Tavitian and F. Dollé, *Bioconjugate Chem.*, 2005, **16**, 406-420.

47. F. Wuest, M. Berndt, R. Bergmann, J. van den Hoff and J. Pietzsch, *Bioconjugate Chem.*, 2008, **19**, 1202-1210.

48. Y. Shai, K. L. Kirk, M. A. Channing, B. B. Dunn, M. A. Lesniak, R. C. Eastman, R. D. Finn, J. Roth and K. A. Jacobson, *Biochemistry*, 1989, **28**, 4801-4806.

49. Y. S. Chang, J. M. Jeong, Y.-S. Lee, H. W. Kim, G. B. Rai, S. J. Lee, D. S. Lee, J.-K. Chung and M. C. Lee, *Bioconjugate Chem.*, 2005, **16**, 1329-1333.

50. M. R. Kilbourn, C. S. Dence, M. J. Welch and C. J. Mathias, *J. Nucl. Med.*, 1987, **28**, 462-470.

51. P. Rosa-Neto, B. Wängler, L. Iovkova, G. Boening, A. Reader, K. Jurkschat and E. Schirrmacher, *ChemBioChem*, 2009, **10**, 1321-1324.

52. B. Langstrom and E. Hedberg, *Acta Chem. Scand.*, 1997, **51**, 1236-1240.

53. F. Wüst, M. Müller and R. Bergmann, *Radiochim. Acta*, 2004, **92**, 349-353.

54. V. W. Pike and F. I. Aigbirhio, *J. Chem. Soc., Chem. Commun.*, 1995, 2215-2216.

55. A. Shah, V. Pike and D. Widdowson, *J. Chem. Soc., Perkin Trans. 1*, 1998, 2043-2046.

56. R. Gail, C. Hocke and H. H. Coenen, *J. Labell. Compd. Radiopharm.*, 1997, **40**, 50-52.

57. Y. Yamada and M. Okawara, *Bull. Chem. Soc. Jpn.*, 1972, **45**, 1860-1863.

58. Y. Yamada, K. Kashima and M. Okawara, *Bull. Chem. Soc. Jpn.*, 1974, **47**, 3179-3180.

59. C. Willgerodt, *Journal für Praktische Chemie*, 1886, **33**, 154-160.

60. C. Willgerodt, *Die Organischen verbindungen mit mehrwertigem jod*, F. Enke, 1914. pp

61. D. F. Banks, *Chem. Rev.*, 1966, **66**, 243-266.

62. A. Varvoglis, *Synthesis*, 1984, **9**, 709-726.

63. R. M. Moriarty and O. Prakash, *Acc. Chem. Res.*, 1986, **19**, 244-250.

64. V. V. Zhdankin and P. J. Stang, *Chem. Rev.*, 2002, **102**, 2523-2584.

65. V. V. Zhdankin and P. J. Stang, *Chem. Rev.*, 2008, **108**, 5299-5358.

66. T. Wirth, M. Ochiai, A. Varvoglis, V. V. Zhdankin, G. F. Koser, H. Tohma and Y. Kita, *Hypervalent Iodine Chemistry*, Springer, London, 2003. pp

67. A. Varvoglis, *The Organic Chemistry of Polycoordinated Iodine*, John Wiley & Sons, 1992. pp

68. H.-Y. Niu, C. Xia, G.-R. Qu, Q. Zhang, Y. Jiang, R.-Z. Mao, D.-Y. Li and H.-M. Guo, *Org. Biomol. Chem.*, 2011, **9**, 5039-5042.

69. L. Wang and Z.-C. Chen, *Synth. Commun.*, 2000, **30**, 3607-3612.

70. L. Wang and Z.-C. Chen, *J. Chem. Res., Synop.*, 2000, 367-369.

71. L. Wang and Z.-C. Chen, *Synth. Commun.*, 2001, **31**, 1227-1232.

72. N. A. Bumagin, L. I. Sukhomlinova, T. P. Tolstaya and I. P. Beletskaya, *Zh. Org. Khim.*, 1996, **32**, 1724-1728.

73. X. Huang and A.-M. Sun, *Synth. Commun.*, 1998, **28**, 773-778.

74. Z.-x. Xiong and P. Zhong, *Neimenggu Shida Xuebao, Ziran Kexue (Hanwen)ban*, 2000, **29**, 44-47.

75. N. A. Bumagin and D. A. Tsarev, *Tetrahedron Lett.*, 1998, **39**, 8155-8158.

76. J.-H. Chun and V. W. Pike, *J. Org. Chem.*, 2012, **77**, 1931-1938.

77. F. Basuli, H. Wu and G. L. Griffiths, *J. Labell. Compd. Radiopharm.*, 2011, **54**, 224-228.

78. M. A. Carroll, J. Nairne and J. L. Woodcraft, *J. Labell. Compd. Radiopharm.*, 2007, **50**, 452-454.

79. B. S. Moon, H. S. Kil, J. H. Park, J. S. Kim, J. Park, D. Y. Chi, B. C. Lee and S. E. Kim, *Org. Biomol. Chem.*, 2011, **9**, 8346-8355.

80. J.-H. Chun, S. Lu, Y.-S. Lee and V. W. Pike, *J. Org. Chem.*, 2010, **75**, 3332-3338.

81. T. Ross, J. Ermert and H. H. Coenen, 16th International Symposium on Radiopharmaceutical Chemistry, University of Iowa, Iowa City, Iowa, 2005.

82. S. Quideau and T. Wirth, *Tetrahedron*, 2010, **66**, 5733.

83. R. M. Moriarty and R. K. Vaid, *Synthesis*, 1990, **6**, 431-447.

84. O. Prakash, N. Saini and P. K. Sharma, *Synlett*, 1994, **4**, 221-227.

85. P. J. Stang and V. V. Zhdankin, *Chem. Rev.*, 1996, **96**, 1123-1178.

86. Y. Kita, T. Takada and H. Tohma, *Pure Appl. Chem.*, 1996, **68**, 627-630.

87. T. Kitamura and Y. Fujiwara, *Org. Prep. Proced. Int.*, 1997, **29**, 409-458.

88. V. Anastasios, *Tetrahedron*, 1997, **53**, 1179-1255.

89. T. Wirth and U. H. Hirt, *Synthesis*, 1999, **08**, 1271-1287.

90. P. Dauban and R. H. Dodd, *Synlett*, 2003, 1571-1586.

91. H. Tohma and Y. Kita, *Adv. Synth. Catal.*, 2004, **346**, 111-124.

92. R. M. Moriarty, *J. Org. Chem.*, 2005, **70**, 2893-2903.

93. T. Wirth, *Angew. Chem. Int. Ed.*, 2005, **44**, 3656-3665.

94. R. D. Richardson and T. Wirth, *Angew. Chem. Int. Ed.*, 2006, **45**, 4402-4404.

95. N. R. Deprez and M. S. Sanford, *Inorg. Chem.*, 2007, **46**, 1924-1935.

96. E. A. Merritt and B. Olofsson, *Angew. Chem. Int. Ed.*, 2009, **48**, 9052-9070.

97. T. Dohi and Y. Kita, *Chem. Commun.*, 2009, 2073-2085.

98. M. S. Yusubov, A. V. Maskaev and V. V. Zhdankin, *Arkivoc*, 2011, 370-409.

99. P. J. Stang, *J. Org. Chem.*, 2003, **68**, 2997-3008.

100. J. I. Musher, *Angew. Chem. Int. Ed.*, 1969, **8**, 54-68.

101. G. F. Koser, in *The Chemistry of Functional Groups*, eds. S. Patai and Z. Rappoport, Wiley, Chichester, 1983, vol. Supplement D, pp. 774-806.

102. T. T. Nguyen and J. C. Martin, in *Comprehensive Heterocyclic Chemistry*, eds. A. R. Katritzky and C. W. Rees, Pergamon, Oxford, 1st edn., 1984, vol. 1, p. 563.

103. C. W. Perkins, J. C. Martin, A. J. Arduengo, W. Lau, A. Alegria and J. K. Kochi, *J. Am. Chem. Soc.*, 1980, **102**, 7753-7759.

104. U. Ladziata and V. V. Zhdankin, *Arkivoc*, 2006, **ix**, 26-58.

105. H.-J. Frohn, M. E. Hirschberg, R. Boese, D. Bläser and U. Flörke, *Z. Anorg. Allg. Chem.*, 2008, **634**, 2539-2550.

106. C. J. Carmalt, J. G. Crossley, J. G. Knight, P. Lightfoot, A. Martin, M. P. Muldowney, N. C. Norman and A. G. Orpen, *J. Chem. Soc., Chem. Commun.*, 1994, 2367-2368.

107. A. K. Mishra, M. M. Olmstead, J. J. Ellison and P. P. Power, *Inorg. Chem.*, 1995, **34**, 3210-3214.

108. H. W. Richter, B. R. Cherry, T. D. Zook and G. F. Koser, *J. Am. Chem. Soc.*, 1997, **119**, 9614-9623.

109. M. Ochiai, Y. Masaki and M. Shiro, *J. Org. Chem.*, 1991, **56**, 5511-5513.

110. T. Kawashima, K. Hoshiba and N. Kano, *J. Am. Chem. Soc.*, 2001, **123**, 1507-1508.

111. V. V. Zhdankin, A. E. Koposov, J. T. Smart, R. R. Tykwinski, R. McDonald and A. Morales-Izquierdo, *J. Am. Chem. Soc.*, 2001, **123**, 4095-4096.

112. M. Ochiai, ed. T. Wirth, Springer Berlin / Heidelberg, 2003, vol. 224, pp. 5-68.

113. M. Ochiai, M. Kida, K. Sato, T. Takino, S. Goto, N. Donkai and T. Okuyama, *Tetrahedron Lett.*, 1999, **40**, 1559-1562.

114. F. H. Allen, O. Kennard, D. G. Watson, L. Brammer, A. G. Orpen and R. Taylor, *J. Chem. Soc., Perkin Trans. 2*, 1987, S1-S19.

115. N. W. Alcock and R. M. Countryman, *J. Chem. Soc., Dalton Trans.*, 1977, 217-219.

116. G. A. Olah, K. K. Laali, Q. Wang and G. K. S. Prakash, *Onium Ions*, John Wiley and Sons, New York, 1998. pp

117. M. Ochiai, in *Chemistry of Hypervalent Compounds*, ed. K.-y. Akiba, Wiley, Hiroshima, Japan, 1st edn., 1999, vol. 30, pp. 359-384.

118. R. S. Berry, *The Journal of Chemical Physics*, 1960, **32**, 933-938.

119. S. Martin-Santamaria, M. A. Carroll, C. M. Carroll, C. D. Carter, V. W. Pike, H. S. Rzepa and D. A. Widdowson, *Chem. Commun.*, 2000, 649-650.

120. S. Oae and Y. Uchida, *Acc. Chem. Res.*, 1991, **24**, 202-208.

121. R. B. Sandin, M. Kulka and R. McCready, *J. Am. Chem. Soc.*, 1937, **59**, 2014-2015.

122. F. M. Beringer and M. Mausner, *J. Am. Chem. Soc.*, 1958, **80**, 4535-4536.

123. H. J. Lucas, E. R. Kennedy and C. A. Wilmot, *J. Am. Chem. Soc.*, 1936, **58**, 157-160.

124. C. Hartmann and V. Meyer, *Berichte der Deutschen Chemischen Gesellschaft* 1894, **27**, 426.

125. I. Masson and E. Race, *J. Chem. Soc.*, 1937, 1718-1723.

126. F. M. Beringer, A. Brierley, M. Drexler, E. M. Gindler and C. C. Lumpkin, *J. Am. Chem. Soc.*, 1953, **75**, 2708-2712.

127. F. M. Beringer, M. Drexler, E. M. Gindler and C. C. Lumpkin, *J. Am. Chem. Soc.*, 1953, **75**, 2705-2708.

128. F. M. Beringer and E. M. Gindler, *J. Am. Chem. Soc.*, 1955, **77**, 3203-3207.

129. F. M. Beringer, E. J. Geering, I. Kuntz and M. Mausner, *J. Phys. Chem.*, 1956, **60**, 141-150.

130. H. E. Bachofner, F. M. Beringer and L. Meites, *J. Am. Chem. Soc.*, 1958, **80**, 4274-4278.

131. H. E. Bachofner, F. M. Beringer and L. Meites, *J. Am. Chem. Soc.*, 1958, **80**, 4269-4274.

132. F. Beringer and M. Mausner, *J. Am. Chem. Soc.*, 1958, **80**, 6703-6703.

133. F. M. Beringer, H. E. Bachofner, R. A. Falk and M. Leff, *J. Am. Chem. Soc.*, 1958, **80**, 4279-4281.

134. F. M. Beringer and R. A. Falk, *J. Am. Chem. Soc.*, 1959, **81**, 2997-3000.

135. F. M. Beringer, R. A. Falk, M. Karniol, I. Lillien, G. Masullo, M. Mausner and E. Sommer, *J. Am. Chem. Soc.*, 1959, **81**, 342-351.

136. F. M. Beringer, E. M. Gindler, M. Rapoport and R. J. Taylor, *J. Am. Chem. Soc.*, 1959, **81**, 351-361.

137. F. M. Beringer, J. W. Dehn and M. Winicov, *J. Am. Chem. Soc.*, 1960, **82**, 2948-2952.

138. F. M. Beringer and I. Lillien, *J. Am. Chem. Soc.*, 1960, **82**, 5135-5140.

139. F. M. Beringer and I. Lillien, *J. Am. Chem. Soc.*, 1960, **82**, 725-731.

140. F. M. Beringer and I. Lillien, *J. Am. Chem. Soc.*, 1960, **82**, 5141-5142.

141. F. M. Beringer, S. A. Galton and S. J. Huang, *J. Am. Chem. Soc.*, 1962, **84**, 2819-2823.

142. G. F. Koser, R. H. Wettach and C. S. Smith, *J. Org. Chem.*, 1980, **45**, 1543-1544.

143. C. S. Carman and G. F. Koser, *J. Org. Chem.*, 1983, **48**, 2534-2539.

144. A. J. Margida and G. F. Koser, *J. Org. Chem.*, 1984, **49**, 3643-3646.

145. M. Ochiai, K. Sumi, Y. Takaoka, M. Kunishima, Y. Nagao, M. Shiro and E. Fujita, *Tetrahedron*, 1988, **44**, 4095-4112.

146. T. Kitamura, J.-i. Matsuyuki, K. Nagata, R. Furuki and H. Taniguchi, *Synthesis*, 1992, 945-946.

147. T. Kitamura, J. Matsuyuki and H. Taniguchi, *Synthesis*, 1994, 147.

148. A. Shah, V. W. Pike and D. A. Widdowson, *J. Chem. Soc., Perkin Trans. 1*, 1997, 2463-2466.

149. T. Kitamura, M. Yamane, K. Inoue, M. Todaka, N. Fukatsu, Z. Meng and Y. Fujiwara, *J. Am. Chem. Soc.*, 1999, **121**, 11674-11679.

150. V. V. Zhdankin, M. C. Scheuller and P. J. Stang, *Tetrahedron Lett.*, 1993, **34**, 6853-6856.

151. V. W. Pike, F. Butt, A. Shah and D. A. Widdowson, *J. Chem. Soc., Perkin Trans. 1*, 1999, 245-248.

152. S. Mart´ın-Santamar´ıa, M. A. Carroll, C. M. Carroll, C. D. Carter, V. W. Pike, H. S. Rzepa and D. A. Widdowson, *J. Chem. Soc., Chem. Commun.*, 2000, 637-722.

153. M. Ochiai, M. Toyonari, T. Sueda and Y. Kitagawa, *Tetrahedron Lett.*, 1996, **37**, 8421-8424.

154. M. Ochiai, M. Toyonari, T. Nagaoka, D.-W. Chen and M. Kida, *Tetrahedron Lett.*, 1997, **38**, 6709-6712.

155. M. A. Carroll, V. W. Pike and D. A. Widdowson, *Tetrahedron Lett.*, 2000, **41**, 5393-5396.

156. M. Yoshida, K. Osafune and S. Hara, *Synthesis*, 2007, 1542-1546.

157. P. J. Stang and V. V. Zhdankin, *J. Am. Chem. Soc.*, 1993, **115**, 9808-9809.

158. P. J. Stang and K. Chen, *J. Am. Chem. Soc.*, 1995, **117**, 1667-1668.

159. B. Olenyuk, J. A. Whiteford and P. J. Stang, *J. Am. Chem. Soc.*, 1996, **118**, 8221-8230.

160. F. Vögtle and E. Weber, *Host guest complex chemistry: macrocycles : synthesis, structures, applications*, Springer, 1985. pp

161. F. L. Carter, N. R. Laboratory and U. S. O. o. N. Research, *Molecular electronic devices*, M. Dekker, 1982. pp

162. J.-M. Lehn, *Angew. Chem. Int. Ed.*, 1990, **29**, 1304-1319.

163. P. L. Anelli, P. R. Ashton, R. Ballardini, V. Balzani, M. Delgado, M. T. Gandolfi, T. T. Goodnow, A. E. Kaifer and D. Philp, *J. Am. Chem. Soc.*, 1992, **114**, 193-218.

164. C. O. Dietrich-Buchecker and J. P. Sauvage, *Chem. Rev.*, 1987, **87**, 795-810.

165. M. Ochiai, Y. Kitagawa, N. Takayama, Y. Takaoka and M. Shiro, *J. Am. Chem. Soc.*, 1999, **121**, 9233-9234.

166. M. Ochiai, Y. Takaoka, Y. Masaki, Y. Nagao and M. Shiro, *J. Am. Chem. Soc.*, 1990, **112**, 5677-5678.

167. V. V. Zhdankin, A. Y. Koposov, L. Su, V. V. Boyarskikh, B. C. Netzel and V. G. Young, *Org. Lett.*, 2003, **5**, 1583-1586.

168. F. M. Beringer and R. A. Nathan, *J. Org. Chem.*, 1969, **34**, 685-689.

169. F. M. Beringer, P. Ganis, G. Avitabile and H. Jaffe, *J. Org. Chem.*, 1972, **37**, 879-886.

170. P. J. Stang, B. Olenyuk and K. Chen, *Synthesis*, 1995, 937-938.

171. V. K. Aggarwal and B. Olofsson, *Angew. Chem.*, 2005, **117**, 5652-5655.

172. M. Bielawski and B. Olofsson, *Chem. Commun.*, 2007, 2521–2523.

173. M. Bielawski and B. Olofsson, *Org. Synth.*, 2009, **86**, 308-314.

174. M. Zhu, N. Jalalian and B. Olofsson, *Synlett*, 2008, **4**, 592-596.

175. E. A. Merritt, J. Malmgren, F. J. Klinke and B. Olofsson, *Synlett*, 2009, 2277-2280.

176. T. K. Page and T. Wirth, *Synthesis*, 2006, **18**, 3153-3155.

177. T. Dohi, N. Yamaoka, I. Itani and Y. Kita, *Aust. J. Chem.*, 2011, **64**, 529-535.

178. T. Dohi, M. Ito, K. Morimoto, Y. Minamitsuji, N. Takenaga and Y. Kita, *Chem. Commun.*, 2007.

179. T. Dohi, N. Yamaoka and Y. Kita, *Tetrahedron*, 2010, **66**, 5775-5785.

180. M. V. Der Puy, *J. Fluorine Chem.*, 1982, **21**, 385-392.

181. V. V. Grushin, *Acc. Chem. Res.*, 1992, **25**, 529-536.

182. L. Cai, S. Lu and V. W. Pike, *Eur. J. Org. Chem.*, 2008, **17**, 2853-2873.

183. M. S. Yusubov, D. Y. Svitich, M. S. Larkina and V. V. Zhdankin, *Arkivoc*, 2013, **1**, 364-395.

184. T. L. Ross, J. Ermert, C. Hocke and H. H. Coenen, *J. Am. Chem. Soc.*, 2007, **129**, 8018-8025.

185. M. A. Carroll, C. Jones and S.-L. Tang, *J. Labell. Compd. Radiopharm.*, 2007, **50**, 450-451.

186. J. H. Chun, S. Telu, S. Lu and V. W. Pike, *Org. Biomol. Chem.*, 2013, **11**, 5094-5099.

187. B. Wang, J. W. Graskemper, L. Qin and S. G. DiMagno, *Angew. Chem. Int. Ed.*, 2010, **49**, 4079-4083.

188. H. Pinto de Magalhães, H. P. Lüthi and A. Togni, *Org. Lett.*, 2012, **14**, 3830-3833.

189. M. A. Carroll, S. Martín-Santamaría, V. W. Pike, H. S. Rzepa and D. A. Widdowson, *J. Chem. Soc., Perkin Trans. 2*, 1999, 2707-2713.

190. S. Martín-Santamaría, M. A. Carroll, V. W. Pike, H. S. Rzepa and D. A. Widdowson, *J. Chem. Soc., Perkin Trans. 2*, 2000, 2158-2161.

191. Y.-S. Lee, M. Hodošček, J.-H. Chun and V. W. Pike, *Chemistry – A European Journal*, 2010, **16**, 10418-10423.

192. N. W. Alcock and R. M. Countryman, *J. Chem. Soc., Dalton Trans.*, 1987, 193-196.

193. M. A. Carroll, J. Nairne, G. Smith and D. A. Widdowson, *J. Fluorine Chem.*, 2007, **128**, 127-132.

194. H. Irving and R. W. Reid, *Journal of the Chemical Society (Resumed)*, 1960, 2078-2081.

195. M. A. Carroll and R. A. Wood, *Tetrahedron*, 2007, **63**, 11349-11354.

196. F. M. Beringer and S. A. Galton, *J. Org. Chem.*, 1966, **31**, 1648-1651.

197. G. Fraenkel, *J. Chem. Phys.*, 1963, **39**, 1614-1615.

198. F. R. Wüst and T. Kniess, *J. Labell. Compd. Radiopharm.*, 2003, **46**, 699-713.

199. J.-H. Chun, S. Lu and V. W. Pike, *Eur. J. Org. Chem.*, 2011, **23**, 4439-4447.

200. J.-H. Chun and V. W. Pike, *Eur. J. Org. Chem.*, 2012, **24**, 4541-4547.

201. S. Telu, J.-H. Chun, F. G. Simeon, S. Lu and V. W. Pike, *Org. Biomol. Chem.*, 2011, **9**, 6629-6638.

202. J.-H. Chun and V. W. Pike, *Chem. Commun.*, 2012, **48**, 9921-9923.

203. J. H. Chun and V. W. Pike, *Org. Biomol. Chem.*, 2013, **11**, 6300-6306.

204. B. Wang, L. Qin, K. D. Neumann, S. Uppaluri, R. L. Cerny and S. G. DiMagno, *Org. Lett.*, 2010, **12**, 3352-3355.

205. R. Edwards, A. D. Westwell, S. Daniels and T. Wirth, *Eur. J. Org. Chem.*, 2015, **2015**, 625-630.

206. M.-R. Zhang, K. Kumata and K. Suzuki, *Tetrahedron Lett.*, 2007, **48**, 8632-8635.

207. B. C. Lee, C. S. Dence, H. Zhou, E. E. Parent, M. J. Welch and J. A. Katzenellenbogen, *Nucl. Med. Biol.*, 2009, **36**, 147-153.

208. B. C. Lee, J. S. Kim, B. S. Kim, J. Y. Son, S. K. Hong, H. S. Park, B. S. Moon, J. H. Jung, J. M. Jeong and S. E. Kim, *Biorg. Med. Chem.*, 2011, **19**, 2980-2990.

209. B. S. Moon, H. S. Kil, J. H. Park, J. S. Kim, J. Park, D. Y. Chi, B. C. Lee and S. E. Kim, *Org. Biomol. Chem.*, 2011, **9**, 8346-8355.

210. P. Ryvlin, S. Bouvard, D. Le Bars, G. De Lamérie, M. C. Grégoire, P. Kahane, J. C. Froment and F. Mauguière, *Brain*, 1998, **121**, 2067-2081.

211. A. L. Malizia, V. J. Cunningham, C. J. Bell, P. F. Liddle, T. Jones and D. J. Nutt, *Archives of General Psychiatry*, 1998, **55**, 715-720.

212. W.-D. Heiss, M. Grond, A. Thiel, M. Ghaemi, J. Sobesky, J. Rudolf, B. Bauer and K. Wienhard, *Stroke*, 1998, **29**, 454-461.

213. W.-D. Heiss, L. Kracht, M. Grond, J. Rudolf, B. Bauer, K. Wienhard and G. Pawlik, *Stroke*, 2000, **31**, 366-369.

214. V. A. Holthoff, R. A. Koeppe, K. A. Frey, J. B. Penney, D. S. Markel, D. E. Kuhl and A. B. Young, *Annals of Neurology*, 1993, **34**, 76-81.

215. M. Meyer, R. A. Koeppe, K. A. Frey, N. L. Foster and D. E. Kuhl, *Archives of Neurology*, 1995, **52**, 314-317.

216. I. Odano, C. Halldin, P. Karlsson, A. Varrone, A. J. Airaksinen, R. N. Krasikova and L. Farde, *NeuroImage*, 2009, **45**, 891-902.

217. G. Massaweh, E. Schirrmacher, C. la Fougere, M. Kovacevic, C. Wängler, D. Jolly, P. Gravel, A. J. Reader, A. Thiel and R. Schirrmacher, *Nucl. Med. Biol.*, 2009, **36**, 721-727.

218. S. V. Selivanova, T. Stellfeld, T. K. Heinrich, A. Müller, S. D. Krämer, P. A. Schubiger, R. Schibli, S. M. Ametamey, B. Vos, J. Meding, M. Bauser, J. Hütter and L. M. Dinkelborg, *J. Med. Chem.*, 2013, **56**, 4912-4920.

219. K. S. Jang, Y.-W. Jung, G. Gu, R. A. Koeppe, P. S. Sherman, C. A. Quesada and D. M. Raffel, *J. Med. Chem.*, 2013, **56**, 7312-7323.

220. F. R. Wust, A. Hohne and P. Metz, *Org. Biomol. Chem.*, 2005, **3**, 503-507.

221. F. R. Wüst and T. Kniess, *J. Labell. Compd. Radiopharm.*, 2004, **47**, 457-468.

222. F. Basuli, H. Wu, C. Li, Z.-D. Shi, A. Sulima and G. L. Griffiths, *J. Labell. Compd. Radiopharm.*, 2011, **54**, 633-636.

223. M. Carroll and R. Yan, *J. Labell. Compd. Radiopharm.*, 2008, **51**, 259-260.

224. R. Yan, L. Brichard, D. Soloviev, F. I. Aigbirhio and M. A. Carroll, *J. Labell. Compd. Radiopharm.*, 2009, **52**, 208-222.

225. T. Hayashi and M. Ishigedani, *Tetrahedron*, 2001, **57**, 2589-2595.

226. C. Eaborn and G. Seconi, *J. Chem. Soc., Perkin Trans. 2*, 1976, 925-930.

227. X. Zhu, B. E. Blough and F. I. Carroll, *Tetrahedron Lett.*, 2000, **41**, 9219-9222.

228. M. Kosugi, K. Shimizu, A. Ohtani and T. Migita, *Chem. Lett.*, 1981, 829.

229. P. Knochel, J. J. Almena Perea and P. Jones, *Tetrahedron*, 1998, **54**, 8275-8319.

230. P. Knochel and R. D. Singer, *Chem. Rev.*, 1993, **93**, 2117-2188.

231. I. Kazmierski, C. Gosmini, J.-M. Paris and J. Périchon, *Tetrahedron Lett.*, 2003, **44**, 6417-6420.

232. H. Fillon, C. Gosmini and J. Perichon, *J. Am. Chem. Soc.*, 2003, **125**, 3867-3870.

233. C. Gosmini and J. Perichon, *Tetrahedron Lett.*, 2005, **3**, 216-217.

234. J. R. Behling, J. S. Ng, K. A. Babiak, A. L. Campbell, E. Elsworth and B. H. Lipshutz, *Tetrahedron Lett.*, 1989, **30**, 27-30.

235. V. Farina, *J. Org. Chem.*, 1991, **56**, 4985-4987.

236. L. Kurti, P. l. Herczegh, J. l. Visy, M. Simonyi, S. Antus and A. Pelter, 1999, 379-380.

237. K. S. Daub, B. Habermann, T. Hahn, L. Teich and K. Eger, *Eur. J. Org. Chem.*, 2004, **4**, 894-898.

238. A. McKillop and W. R. Sanderson, *Tetrahedron*, 1995, **51**, 6145-6166.

239. R. Fortt and A. Gee, *Future Med. Chem.*, 2013, **5**, 241-244.

240. R. L. Hartman, J. P. McMullen and K. F. Jensen, *Angew. Chem. Int. Ed.*, 2011, **50**, 7502-7519.

241. A. J. deMello, *Nature*, 2006, **442**, 394-402.

242. P. Watts and S. J. Haswell, *Chem. Soc. Rev.*, 2005, **34**, 235-246.

243. K. Jähnisch, V. Hessel, H. Löwe and M. Baerns, *Angew. Chem. Int. Ed.*, 2004, **43**, 406-446.

244. J.-i. Yoshida, A. Nagaki and T. Yamada, *Chemistry – A European Journal*, 2008, **14**, 7450-7459.

245. P. W. Miller, *Journal of Chemical Technology & Biotechnology*, 2009, **84**, 309-315.

246. F. G. Bessoth, A. J. deMello and A. Manz, *Anal. Commun.*, 1999, **36**, 213-215.

247. B. P. Mason, K. E. Price, J. L. Steinbacher, A. R. Bogdan and D. T. McQuade, *Chem. Rev.*, 2007, **107**, 2300-2318.

248. T. Schwalbe, V. Autze, M. Hohmann and W. Stirner, *Organic Process Research & Development*, 2004, **8**, 440-454.

249. K. Sue, K. Murata, K. Kimura and K. Arai, *Green Chemistry*, 2003, **5**, 659-662.

250. H. Pennemann, V. Hessel and H. Löwe, *Chem. Eng. Sci.*, 2004, **59**, 4789-4794.

251. C. Wiles, P. Watts, S. J. Haswell and E. Pombo-Villar, *Lab on a Chip*, 2001, **1**, 100-101.

252. V. Skelton, G. M. Greenway, S. J. Haswell, P. Styring, D. O. Morgan, B. Warrington and S. Y. F. Wong, *Analyst*, 2001, **126**, 7-10.

253. V. Skelton, G. M. Greenway, S. J. Haswell, P. Styring, D. O. Morgan, B. H. Warrington and S. Y. F. Wong, *Analyst*, 2001, **126**, 11-13.

254. T. Kawaguchi, H. Miyata, K. Ataka, K. Mae and J.-i. Yoshida, *Angew. Chem. Int. Ed.*, 2005, **44**, 2413-2416.

255. S. Walter, S. Malmberg, B. Schmidt and M. A. Liauw, *Chem. Eng. Res. Des.*, 2005, **83**, 1019-1029.

256. G. M. Greenway, S. J. Haswell, D. O. Morgan, V. Skelton and P. Styring, *Sensors and Actuators B: Chemical*, 2000, **63**, 153-158.

257. P. D. I. Fletcher, S. J. Haswell, E. Pombo-Villar, B. H. Warrington, P. Watts, S. Y. F. Wong and X. Zhang, *Tetrahedron*, 2002, **58**, 4735-4757.

258. E. Garcia-Egido, V. Spikmans, S. Y. F. Wong and B. H. Warrington, *Lab on a Chip*, 2003, **3**, 73-76.

259. E. Garcia-Egido, S. Y. F. Wong and B. H. Warrington, *Lab on a Chip*, 2002, **2**, 31-33.

260. S. Lu, A. M. Giamis and V. W. Pike, *Current Radiopharmaceuticals*, 2009, **2**, 49-55.

261. L. Ducry and D. M. Roberge, *Angew. Chem. Int. Ed.*, 2005, **44**, 7972-7975.

262. P. Watts, C. Wiles, S. J. Haswell, E. Pombo-Villar and P. Styring, *Chem. Commun.*, 2001, 990-991.

263. H. J. Wester, M. Schottelius, P. A. Schubiger, L. Lehmann and M. Friebe, *PET Chemistry: The Driving Force in Molecular Imaging*, 2007. pp 271-287

264. G. Pascali, G. Mazzone, G. Saccomanni, C. Manera and P. A. Salvadori, *Nucl. Med. Biol.*, 2010, **37**, 547-555.

265. R. Bejot, A. M. Elizarov, E. Ball, J. Zhang, R. Miraghaie, H. C. Kolb and V. Gouverneur, *J. Labell. Compd. Radiopharm.*, 2011, **54**, 117-122.

266. H. Audrain, *Angew. Chem. Int. Ed.*, 2007, **46**, 1772-1775.

267. C.-C. Lee, G. Sui, A. Elizarov, C. J. Shu, Y.-S. Shin, A. N. Dooley, J. Huang, A. Daridon, P. Wyatt, D. Stout, H. C. Kolb, O. N. Witte, N. Satyamurthy, J. R. Heath, M. E. Phelps, S. R. Quake and H.-R. Tseng, *Science*, 2005, **310**, 1793-1796.

268. S.-Y. Lu, P. Watts, F. T. Chin, J. Hong, J. L. Musachio, E. Briard and V. W. Pike, *Lab on a Chip*, 2004, **4**, 523-525.

269. P. W. Miller, H. Audrain, D. Bender, A. J. deMello, A. D. Gee, N. J. Long and R. Vilar, *Chemistry – A European Journal*, 2011, **17**, 460-463.

270. J. Ungersboeck, C. Philippe, D. Haeusler, M. Mitterhauser, R. Lanzenberger, R. Dudczak and W. Wadsak, *Appl. Radiat. Isot.*, 2012, **70**, 2615-2620.

271. C. J. Steel, A. T. O'Brien, S. K. Luthra and F. Brady, *J. Labell. Compd. Radiopharm.*, 2007, **50**, 308-311.

272. H.-J. Wester, B. Schoultz, C. Hultsch and G. Henriksen, *Eur J Nucl Med*, 2009, **36**, 653-658.

273. J. M. Gillies, C. Prenant, G. N. Chimon, G. J. Smethurst, W. Perrie, I. Hamblett, B. Dekker and J. Zweit, *Appl. Radiat. Isot.*, 2006, **64**, 325-332.

274. R. W. Simms, P. W. Causey, D. M. Weaver, C. Sundararajan, K. A. Stephenson and J. F. Valliant, *J. Labell. Compd. Radiopharm.*, 2012, **55**, 18-22.

275. G. Pascali, P. Watts and P. A. Salvadori, *Nucl. Med. Biol.*, 2013, **40**, 776-787.

276. J. Mukherjee, Z.-Y. Yang, T. Brown, R. Lew, M. Wernick, X. Ouyang, N. Yasillo, C.-T. Chen, R. Mintzer and M. Cooper, *Nucl. Med. Biol.*, 1999, **26**, 519-527.

277. M. Honer, M. Brühlmeier, J. Missimer, A. P. Schubiger and S. M. Ametamey, *J. Nucl. Med.*, 2004, **45**, 464-470.

278. M. Slifstein, D.-R. Hwang, Y. Huang, N. Guo, Y. Sudo, R. Narendran, P. Talbot and M. Laruelle, *Psychopharm.*, 2004, **175**, 274-286.

279. G. Pascali, G. Nannavecchia, S. Pitzianti and P. A. Salvadori, *Nucl. Med. Biol.*, 2011, **38**, 637-644.

280. J. Ungersboeck, S. Richter, L. Collier, M. Mitterhauser, G. Karanikas, R. Lanzenberger, R. Dudczak and W. Wadsak, *Nucl. Med. Biol.*, 2012, **39**, 1087-1092.

281. http://www.erigal.co.uk, 03/07/2014.

282. E. Blom, F. Karimi and B. Långström, *J. Labell. Compd. Radiopharm.*, 2009, **52**, 504-511.

283. C. Lemaire, R. Cantineau, M. Guillaume, A. Plenevaux and L. Christiaens, *J. Nucl. Med.*, 1991, **32**, 2266-2272.

284. D. Le Bars, C. Lemaire, N. Ginovart, A. Plenevaux, J. Aerts, C. Brihaye, W. Hassoun, V. Leviel, P. Mekhsian, D. Weissmann, J. F. Pujol, A. Luxen and D. Comar, *Nucl. Med. Biol.*, 1998, **25**, 343-350.

285. J. Blin, S. Pappata, M. Kiyosawa, C. Crouzel and J. C. Baron, *Eur. J. Pharmacol.*, 1988, **147**, 73-82.

286. http://www.ezag.com/home/products/radiopharma/radiosynthesis-technology/modular-lab-standard.html, 03/07/2014.

287. P. A. Culbert, M. J. Adam, E. T. Hurtado, J. M. A. Huser, S. Jivan, J. Lu, T. J. Ruth and S. K. Zeisler, *Appl. Radiat. Isot.*, 1995, **46**, 887-891.

288. G. A. Jeffrey and R. K. McMullan, in *Prog. Inorg. Chem.*, John Wiley & Sons, Inc., 2007, pp. 43-108.

289. L. S. Aladko, Y. A. Dyadin, T. V. Rodionova and I. S. Terekhova, *J. Mol. Liq.*, 2003, **106**, 229-238.

290. S. J. Gatley, R. D. Hichwa, W. J. Shaughnessy and R. J. Nickles, *The International Journal of Applied Radiation and Isotopes*, 1981, **32**, 211-214.

291. A. L. Bosch, T. R. Degrado and S. J. Gatley, *International Journal of Radiation Applications and Instrumentation. Part A. Applied Radiation and Isotopes*, 1986, **37**, 305-308.

292. L. G. Hutchins, A. L. Bosch, M. S. Rosenthal, R. J. Nickles and S. J. Gatley, *The International Journal of Applied Radiation and Isotopes*, 1985, **36**, 375-378.

293. T. W. Mak, *Journal of Inclusion Phenomena*, 1985, **3**, 347-354.

294. J. M. Crow, (2012) 'Going with the flow', in *Chemistry World,* April 2012, 48-51

295. T. Noel, J. R. Naber, R. L. Hartman, J. P. McMullen, K. F. Jensen and S. L. Buchwald, *Chem. Sci.*, 2011, **2**, 287-290.

296. G. Pascali, L. D'Antonio, P. Bovone, P. Gerundini and T. August, *Nucl. Med. Biol.*, 2009, **36**, 569-574.

297. S. Begel, R. Puchta and R. Van Eldik, *Beilstein J. Org. Chem.*, 2013, **9**, 1252-1268.

298. E. Benedetto, M. Tredwell, C. Hollingworth, T. Khotavivattana, J. M. Brown and V. Gouverneur, *Chem. Sci.*, 2013, **4**, 89-96.

299. S. H. Liang, T. L. Collier, B. H. Rotstein, R. Lewis, M. Steck and N. Vasdev, *Chem. Commun.*, 2013, **49**, 8755-8757.

300. http://www.advion.com/reference-library/nanotek-select-references/, 13/07/2014.

301. M. A. Carroll and M. Charlton, *J. Labell. Compd. Radiopharm.*, 2013, **56**, 57-58.

302. M. Carroll, R. Yan, F. Aigbirhio, D. Soloviev and L. Brichard, *J. Nucl. Med.*, 2008, **49**, 303P.

303. http://www.abx.de/kits.html, 03/07/2014.

304. D. L. Alexoff, in *Handbook of Radiopharmaceuticals*, John Wiley & Sons, Ltd, 1st edn., 2005, pp. 283-305.

305. R. Krasikova, in *PET Chemistry*, eds. P. A. Schubiger, L. Lehmann and M. Friebe, Springer Berlin Heidelberg, 2007, vol. 64, pp. 289-316.

306. http://www.ezag.com/home/products/radiopharma/radiosynthesis-technology/pre-validated-syntheses/ga-68-synthesis.html, 03/07/2014.

307. T. Läppchen, M. L. H. Vlaming, E. Custers, J. Lub, C. F. Sio, J. DeGroot and O. C. Steinbach, *Appl. Radiat. Isot.*, 2012, **70**, 205-209.

308. M. Huiban, S. Pampols-Maso and J. Passchier, *Appl. Radiat. Isot.*, 2011, **69**, 1390-1394.

309. D. B. Dess and J. C. Martin, *J. Am. Chem. Soc.*, 1991, **113**, 7277-7287.

310. H. Tohma, S. Takizawa, T. Maegawa and Y. Kita, *Angew. Chem.*, 2000, **112**, 1362-1364.

311. J. E. Leffler and L. J. Story, *J. Am. Chem. Soc.*, 1967, **89**, 2333-2338.

312. H. Togo, T. Nabana and K. Yamaguchi, *J. Org. Chem.*, 2000, **65**, 8391-8394.

5 Appendix I – Crystallographic Data for compounds 205 and 206

Compound **205**

Table 1. Crystal data and structure refinement for **205**.

Identification code	mac120016	
Chemical formula (moiety)	$C_{11}H_{13}IO_5 \cdot 0.5CH_2Cl_2$	
Chemical formula (total)	$C_{11.50}H_{14}ClIO_5$	
Formula weight	394.58	
Temperature	150(2) K	
Radiation, wavelength	MoKα, 0.71073 Å	
Crystal system, space group	triclinic, $P\bar{1}$	
Unit cell parameters	a = 8.3053(5) Å	α = 70.375(5)°
	b = 8.9589(6) Å	β = 71.410(4)°
	c = 10.7489(5) Å	γ = 76.544(5)°
Cell volume	706.92(7) Å^3	
Z	2	
Calculated density	1.854 g/cm^3	
Absorption coefficient μ	2.465 mm^{-1}	
F(000)	386	
Crystal colour and size	colourless, 0.30 × 0.30 × 0.30 mm^3	
Reflections for cell refinement	3881 (θ range 2.9 to 28.6°)	
Data collection method	Oxford Diffraction Gemini A Ultra diffractometer	
	thick-slice ω scans	
θ range for data collection	2.9 to 28.6°	
Index ranges	h –11 to 9, k –8 to 11, l –11 to 12	
Completeness to θ = 25.0°	99.8 %	
Reflections collected	5095	
Independent reflections	2903 (R_{int} = 0.0231)	
Reflections with $F^2>2\sigma$	2694	
Absorption correction	semi-empirical from equivalents	
Min. and max. transmission	0.5251 and 0.5251	
Structure solution	direct methods	
Refinement method	Full-matrix least-squares on F^2	
Weighting parameters a, b	0.0414, 1.2585	
Data / restraints / parameters	2903 / 0 / 185	
Final R indices [$F^2>2\sigma$]	R1 = 0.0311, wR2 = 0.0804	
R indices (all data)	R1 = 0.0342, wR2 = 0.0836	
Goodness-of-fit on F^2	1.069	
Extinction coefficient	0.0108(12)	
Largest and mean shift/su	0.000 and 0.000	
Largest diff. peak and hole	1.09 and –0.95 e Å^{-3}	

Table 2. Atomic coordinates and equivalent isotropic displacement parameters ($Å^2$) for **205**. U_{eq} is defined as one third of the trace of the orthogonalized U^{ij} tensor.

	x	y	z	U_{eq}
I	0.25454(3)	0.52165(3)	0.41551(2)	0.02241(12)
O(5)	0.1486(4)	0.2075(4)	0.5229(3)	0.0313(7)
O(4)	0.2166(4)	0.3697(4)	0.3117(3)	0.0294(7)
O(2)	0.3111(4)	0.7143(4)	0.4639(3)	0.0308(7)
O(1)	0.4278(4)	0.9765(4)	−0.1726(3)	0.0342(7)
C(5)	0.2358(5)	0.9216(5)	0.0562(4)	0.0262(9)
O(3)	0.3430(7)	0.8027(6)	0.6375(6)	0.0795(15)
C(9)	0.2624(5)	0.5477(4)	0.6721(3)	0.0213(8)
C(1)	0.3080(5)	0.6752(5)	0.2180(4)	0.0243(8)
C(4)	0.3795(5)	0.8826(5)	−0.0422(4)	0.0263(9)
C(10)	0.1704(5)	0.2346(5)	0.4002(4)	0.0241(8)
C(11)	0.1489(6)	0.1174(5)	0.3362(4)	0.0296(9)
C(6)	0.1986(5)	0.8165(5)	0.1877(4)	0.0242(8)
C(8)	0.2998(6)	0.6736(6)	0.5954(5)	0.0318(10)
C(7)	0.3230(7)	1.1265(6)	−0.2123(5)	0.0410(12)
C(2)	0.4517(6)	0.6341(6)	0.1198(5)	0.0339(10)
C(3)	0.4855(6)	0.7372(6)	−0.0107(5)	0.0350(10)
C(12)	0.0602(15)	0.4763(13)	1.0226(13)	0.049(3)
Cl(1A)	0.0072(9)	0.6741(7)	0.9831(8)	0.0807(19)
Cl(1B)	−0.0741(6)	0.3728(8)	0.9975(8)	0.0737(19)

Table 3. Bond lengths [Å] and angles [°] for **205**.

I–O(4)	2.155(3)	I–O(2)	2.146(3)
I–C(1)	2.079(4)	O(5)–C(10)	1.219(5)
O(4)–C(10)	1.314(5)	O(2)–C(8)	1.313(5)
O(1)–C(4)	1.357(5)	O(1)–C(7)	1.432(6)
C(5)–H(5A)	0.950	C(5)–C(4)	1.384(6)
C(5)–C(6)	1.393(6)	O(3)–C(8)	1.523(6)
C(9)–H(9A)	0.980	C(9)–H(9B)	0.980
C(9)–H(9C)	0.980	C(9)–C(8)	1.193(6)
C(1)–C(6)	1.382(6)	C(1)–C(2)	1.388(6)
C(4)–C(3)	1.395(7)	C(10)–C(11)	1.503(6)
C(11)–H(11A)	0.980	C(11)–H(11B)	0.980
C(11)–H(11C)	0.980	C(6)–H(6A)	0.950
C(7)–H(7A)	0.980	C(7)–H(7B)	0.980
C(7)–H(7C)	0.980	C(2)–H(2A)	0.950
C(2)–C(3)	1.378(7)	C(3)–H(3A)	0.950
C(12)–H(12A)	0.990	C(12)–H(12B)	0.990
C(12)–Cl(1A)	1.663(12)	C(12)–Cl(1B)	1.738(11)

O(4)–I–O(2)	164.58(11)	O(4)–I–C(1)	81.98(13)
O(2)–I–C(1)	82.62(14)	I–O(4)–C(10)	110.2(2)
I–O(2)–C(8)	109.4(3)	C(4)–O(1)–C(7)	118.1(4)
H(5A)–C(5)–C(4)	120.1	H(5A)–C(5)–C(6)	120.1
C(4)–C(5)–C(6)	119.9(4)	H(9A)–C(9)–H(9B)	109.5
H(9A)–C(9)–H(9C)	109.5	H(9A)–C(9)–C(8)	109.5
H(9B)–C(9)–H(9C)	109.5	H(9B)–C(9)–C(8)	109.5
H(9C)–C(9)–C(8)	109.5	I–C(1)–C(6)	118.8(3)
I–C(1)–C(2)	119.6(3)	C(6)–C(1)–C(2)	121.6(4)
O(1)–C(4)–C(5)	124.6(4)	O(1)–C(4)–C(3)	115.3(4)
C(5)–C(4)–C(3)	120.1(4)	O(5)–C(10)–O(4)	122.5(4)
O(5)–C(10)–C(11)	123.5(4)	O(4)–C(10)–C(11)	114.0(3)
C(10)–C(11)–H(11A)	109.5	C(10)–C(11)–H(11B)	109.5
C(10)–C(11)–H(11C)	109.5	H(11A)–C(11)–H(11B)	109.5
H(11A)–C(11)–H(11C)	109.5	H(11B)–C(11)–H(11C)	109.5
C(5)–C(6)–C(1)	119.1(4)	C(5)–C(6)–H(6A)	120.5
C(1)–C(6)–H(6A)	120.5	O(2)–C(8)–O(3)	112.6(4)
O(2)–C(8)–C(9)	123.1(4)	O(3)–C(8)–C(9)	124.2(4)
O(1)–C(7)–H(7A)	109.5	O(1)–C(7)–H(7B)	109.5
O(1)–C(7)–H(7C)	109.5	H(7A)–C(7)–H(7B)	109.5
H(7A)–C(7)–H(7C)	109.5	H(7B)–C(7)–H(7C)	109.5
C(1)–C(2)–H(2A)	120.5	C(1)–C(2)–C(3)	118.9(4)
H(2A)–C(2)–C(3)	120.5	C(4)–C(3)–C(2)	120.3(4)
C(4)–C(3)–H(3A)	119.8	C(2)–C(3)–H(3A)	119.8
H(12A)–C(12)–H(12B)	107.5	H(12A)–C(12)–Cl(1A)	108.4
H(12A)–C(12)–Cl(1B)	108.4	H(12B)–C(12)–Cl(1A)	108.4
H(12B)–C(12)–Cl(1B)	108.4	Cl(1A)–C(12)–Cl(1B)	115.4(6)

Table 4. Anisotropic displacement parameters (Å^2) for **205**. The anisotropic displacement factor exponent takes the form: $-2\pi^2[h^2a^{*2}U^{11} + ...+ 2hka^*b^*U^{12}]$

	U^{11}	U^{22}	U^{33}	U^{23}	U^{13}	U^{12}
I	0.02495(18)	0.01731(17)	0.02162(16)	−0.00432(10)	−0.00180(10)	−0.00451(10)
O(5)	0.0432(19)	0.0243(16)	0.0219(15)	−0.0036(12)	−0.0029(13)	−0.0085(14)
O(4)	0.0399(18)	0.0230(16)	0.0241(14)	−0.0047(12)	−0.0037(13)	−0.0118(13)
O(2)	0.0407(18)	0.0221(16)	0.0293(16)	−0.0059(13)	−0.0069(13)	−0.0089(13)
O(1)	0.0372(18)	0.0411(19)	0.0208(14)	−0.0011(13)	−0.0052(12)	−0.0137(15)
C(5)	0.032(2)	0.022(2)	0.025(2)	−0.0047(17)	−0.0073(17)	−0.0079(17)
O(3)	0.105(4)	0.063(3)	0.085(4)	−0.027(3)	−0.037(3)	−0.015(3)
C(9)	0.043(2)	0.0107(18)	0.0087(16)	−0.0006(14)	0.0008(15)	−0.0149(17)
C(1)	0.032(2)	0.019(2)	0.0191(18)	−0.0021(15)	−0.0026(16)	−0.0093(17)
C(4)	0.032(2)	0.028(2)	0.0220(19)	−0.0036(17)	−0.0064(16)	−0.0158(18)
C(10)	0.019(2)	0.017(2)	0.030(2)	−0.0033(17)	−0.0032(16)	−0.0015(16)
C(11)	0.031(2)	0.026(2)	0.030(2)	−0.0071(18)	−0.0019(18)	−0.0105(18)
C(6)	0.029(2)	0.020(2)	0.0229(19)	−0.0073(16)	−0.0038(16)	−0.0059(17)
C(8)	0.027(2)	0.040(3)	0.032(2)	−0.019(2)	−0.0074(18)	0.0039(19)
C(7)	0.046(3)	0.043(3)	0.028(2)	0.007(2)	−0.013(2)	−0.014(2)
C(2)	0.035(3)	0.025(2)	0.031(2)	−0.0068(19)	0.0029(19)	−0.0028(19)
C(3)	0.035(3)	0.036(3)	0.026(2)	−0.0099(19)	0.0042(18)	−0.007(2)
C(12)	0.056(7)	0.030(6)	0.069(7)	0.001(5)	−0.036(6)	−0.013(5)
Cl(1A)	0.121(6)	0.038(2)	0.084(3)	−0.026(2)	−0.019(4)	−0.009(3)
Cl(1B)	0.051(3)	0.104(5)	0.097(4)	−0.072(4)	−0.001(2)	−0.030(3)

Table 5. Hydrogen coordinates and isotropic displacement parameters ($Å^2$) for **205**.

	x	y	z	U
H(5A)	0.1625	1.0197	0.0342	0.031
H(9A)	0.3280	0.4618	0.6312	0.032
H(9B)	0.1394	0.5467	0.6894	0.032
H(9C)	0.2893	0.5312	0.7586	0.032
H(11A)	0.0583	0.0541	0.3990	0.044
H(11B)	0.2570	0.0459	0.3174	0.044
H(11C)	0.1173	0.1757	0.2503	0.044
H(6A)	0.0995	0.8417	0.2556	0.029
H(7A)	0.3755	1.1840	−0.3069	0.061
H(7B)	0.3132	1.1908	−0.1516	0.061
H(7C)	0.2086	1.1072	−0.2053	0.061
H(2A)	0.5255	0.5364	0.1422	0.041
H(3A)	0.5816	0.7092	−0.0795	0.042
H(12A)	0.0620	0.4362	1.1200	0.059
H(12B)	0.1782	0.4513	0.9672	0.059

Table 6. Torsion angles [°] for **205**.

O(2)–I–O(4)–C(10)	178.0(4)	C(1)–I–O(4)–C(10)	−178.8(3)
O(4)–I–O(2)–C(8)	−174.9(4)	C(1)–I–O(2)–C(8)	−178.1(3)
O(4)–I–C(1)–C(6)	114.0(3)	O(4)–I–C(1)–C(2)	−66.0(3)
O(2)–I–C(1)–C(6)	−66.9(3)	O(2)–I–C(1)–C(2)	113.2(4)
C(7)–O(1)–C(4)–C(5)	−0.3(6)	C(7)–O(1)–C(4)–C(3)	179.1(4)
C(6)–C(5)–C(4)–O(1)	−179.5(4)	C(6)–C(5)–C(4)–C(3)	1.1(6)
I–O(4)–C(10)–O(5)	2.1(5)	I–O(4)–C(10)–C(11)	−177.3(3)
I–C(1)–C(6)–C(5)	178.7(3)	C(2)–C(1)–C(6)–C(5)	−1.4(6)
C(4)–C(5)–C(6)–C(1)	0.8(6)	I–O(2)–C(8)–O(3)	178.4(3)
I–O(2)–C(8)–C(9)	−0.4(6)	I–C(1)–C(2)–C(3)	−179.9(3)
C(6)–C(1)–C(2)–C(3)	0.1(7)	C(1)–C(2)–C(3)–C(4)	1.8(7)
O(1)–C(4)–C(3)–C(2)	178.2(4)	C(5)–C(4)–C(3)–C(2)	−2.4(7)

Compound **206**

Table 7. Crystal data and structure refinement for **206**.

Identification code	mac137	
Chemical formula (moiety)	$C_8H_9IO_4S$	
Chemical formula (total)	$C_8H_9IO_4S$	
Formula weight	328.11	
Temperature	150(2) K	
Radiation, wavelength	MoKα, 0.71073 Å	
Crystal system, space group	monoclinic, C12/c1	
Unit cell parameters	a = 16.5807(5) Å	α = 90°
	b = 17.4446(4) Å	β = 107.211(3)°
	c = 15.6122(4) Å	γ = 90°
Cell volume	4313.5(2) Å^3	
Z	16	
Calculated density	2.021 g/cm^3	
Absorption coefficient μ	3.149 mm^{-1}	
F(000)	2528	
Reflections for cell refinement	11000 (θ range 2.9 to 29.4°)	
Data collection method	Xcalibur, Atlas, Gemini ultra thick-slice ω scans	
θ range for data collection	2.9 to 25.0°	
Index ranges	h −19 to 19, k −20 to 20, l −18 to 18	
Completeness to θ = 25.0°	99.8 %	
Reflections collected	31978	
Independent reflections	3804 (R_{int} = 0.0387)	
Reflections with $F^2>2\sigma$	2611	
Absorption correction	semi-empirical from equivalents	
Min. and max. transmission	0.86238 and 1.00000	
Structure solution	direct methods	
Refinement method	Full-matrix least-squares on F^2	
Weighting parameters a, b	0.0284, 187.8210	
Data / restraints / parameters	3804 / 260 / 367	
Final R indices [$F^2>2\sigma$]	R1 = 0.0548, wR2 = 0.1478	
R indices (all data)	R1 = 0.0655, wR2 = 0.1709	
Goodness-of-fit on F^2	1.205	
Largest and mean shift/su	1.622 and 0.406	
Largest diff. peak and hole	1.18 and −1.31 e Å^{-3}	

Table 8. Atomic coordinates and equivalent isotropic displacement parameters ($Å^2$) for **206**. U_{eq} is defined as one third of the trace of the orthogonalized U^{ij} tensor.

	x	y	z	U_{eq}
I(1)	0.10151(5)	0.35104(5)	0.69720(5)	0.0169(3)
S(1)	–0.0598(3)	0.2702(2)	0.5547(3)	0.0362(9)
C(1)	0.0418(10)	0.2891(8)	0.5749(10)	0.028(2)
C(2)	0.0889(13)	0.2633(14)	0.5134(14)	0.024(2)
C(3)	0.0127(12)	0.2247(10)	0.4453(12)	0.032(2)
C(4)	–0.0612(11)	0.2277(10)	0.4648(12)	0.032(2)
I(1A)	0.14980(11)	0.39964(10)	0.80260(11)	0.0206(6)
S(1A)	0.0561(6)	0.2310(5)	0.4502(6)	0.0349(17)
C(1A)	–0.047(2)	0.2080(17)	0.425(2)	0.030(3)
C(2A)	–0.090(2)	0.2358(19)	0.486(2)	0.031(3)
C(3A)	–0.010(3)	0.2741(18)	0.555(2)	0.034(3)
C(4A)	0.073(3)	0.266(3)	0.521(3)	0.031(3)
C(5)	0.1961(6)	0.2427(6)	0.8249(6)	0.028(2)
C(6)	0.2314(7)	0.1688(6)	0.8671(7)	0.036(3)
C(7)	0.0573(6)	0.5077(6)	0.6738(6)	0.030(2)
C(8)	0.0207(7)	0.5812(6)	0.6324(7)	0.035(2)
O(1)	0.2159(5)	0.3047(4)	0.8664(5)	0.042(2)
O(2)	0.1451(4)	0.2405(4)	0.7455(5)	0.0313(16)
O(3)	0.0345(5)	0.4467(4)	0.6275(5)	0.039(2)
O(4)	0.1090(5)	0.5061(4)	0.7505(5)	0.0406(19)
I(2)	–0.14823(5)	0.10080(5)	0.19725(5)	0.0170(3)
S(2)	–0.3087(3)	0.0200(2)	0.0522(3)	0.0347(9)
C(9)	–0.2075(11)	0.0416(9)	0.0769(10)	0.027(3)
C(10)	–0.1598(13)	0.0159(15)	0.0160(16)	0.022(3)
C(11)	–0.2335(13)	–0.0244(10)	–0.0539(13)	0.032(3)
C(12)	–0.3067(12)	–0.0230(10)	–0.0354(14)	0.033(3)
I(2A)	–0.10102(11)	0.14981(10)	0.30204(11)	0.0205(6)
S(2A)	0.3100(7)	0.4796(6)	0.9454(7)	0.046(2)
C(9A)	0.207(2)	0.456(2)	0.923(2)	0.032(4)
C(10A)	0.162(2)	0.4877(19)	0.987(2)	0.027(4)
C(11A)	0.246(3)	0.523(2)	1.055(2)	0.035(4)
C(12A)	0.320(3)	0.516(4)	1.024(5)	0.038(4)
C(13)	–0.0592(6)	–0.0083(6)	0.3260(6)	0.027(2)
C(14)	–0.0250(7)	–0.0826(6)	0.3668(7)	0.035(2)
C(15)	–0.1868(6)	0.2595(5)	0.1730(6)	0.025(2)
C(16)	–0.2231(7)	0.3336(6)	0.1322(7)	0.033(2)
O(5)	–0.0415(5)	0.0525(4)	0.3687(5)	0.040(2)
O(6)	–0.1079(5)	–0.0102(4)	0.2448(5)	0.0353(18)
O(7)	–0.2089(5)	0.1988(4)	0.1250(5)	0.0330(17)
O(8)	–0.1379(5)	0.2565(4)	0.2506(5)	0.0369(18)

Table 9. Bond lengths [Å] and angles [°] for **206**.

I(1)–C(1)	2.161(15)	I(1)–O(2)	2.119(7)
I(1)–O(3)	2.118(7)	S(1)–C(1)	1.654(16)
S(1)–C(4)	1.58(2)	C(1)–C(2)	1.48(3)
C(2)–H(2A)	0.950	C(2)–C(3)	1.54(3)
C(3)–H(3A)	0.950	C(3)–C(4)	1.35(3)
C(4)–H(4A)	0.950	I(1A)–O(1)	2.071(7)
I(1A)–O(4)	2.059(8)	I(1A)–C(9A)	2.08(4)
S(1A)–C(1A)	1.68(3)	S(1A)–C(4A)	1.22(5)
C(1A)–C(2A)	1.44(5)	C(1A)–I(2A)	2.12(3)
C(2A)–H(2B)	0.950	C(2A)–C(3A)	1.58(5)
C(3A)–H(3B)	0.950	C(3A)–C(4A)	1.62(6)
C(4A)–H(4B)	0.950	C(5)–C(6)	1.487(14)
C(5)–O(1)	1.254(12)	C(5)–O(2)	1.279(11)
C(6)–H(6A)	0.980	C(6)–H(6B)	0.980
C(6)–H(6C)	0.980	C(7)–C(8)	1.482(14)
C(7)–O(3)	1.280(12)	C(7)–O(4)	1.250(12)
C(8)–H(8A)	0.980	C(8)–H(8B)	0.980
C(8)–H(8C)	0.980	I(2)–C(9)	2.115(15)
I(2)–O(6)	2.111(7)	I(2)–O(7)	2.130(7)
S(2)–C(9)	1.650(17)	S(2)–C(12)	1.57(2)
C(9)–C(10)	1.47(3)	C(10)–H(10A)	0.950
C(10)–C(11)	1.54(3)	C(11)–H(11A)	0.950
C(11)–C(12)	1.33(3)	C(12)–H(12A)	0.950
I(2A)–O(5)	2.081(7)	I(2A)–O(8)	2.048(7)
S(2A)–C(9A)	1.69(4)	S(2A)–C(12A)	1.35(7)
C(9A)–C(10A)	1.52(5)	C(10A)–H(10B)	0.950
C(10A)–C(11A)	1.60(5)	C(11A)–H(11B)	0.950
C(11A)–C(12A)	1.46(7)	C(12A)–H(12B)	0.950
C(13)–C(14)	1.481(14)	C(13)–O(5)	1.242(12)
C(13)–O(6)	1.286(12)	C(14)–H(14A)	0.980
C(14)–H(14B)	0.980	C(14)–H(14C)	0.980
C(15)–C(16)	1.487(14)	C(15)–O(7)	1.286(11)
C(15)–O(8)	1.244(11)	C(16)–H(16A)	0.980
C(16)–H(16B)	0.980	C(16)–H(16C)	0.980

C(1)–I(1)–O(2)	83.0(4)	C(1)–I(1)–O(3)	84.6(4)
O(2)–I(1)–O(3)	166.4(3)	C(1)–S(1)–C(4)	90.5(9)
I(1)–C(1)–S(1)	116.3(9)	I(1)–C(1)–C(2)	122.4(12)
S(1)–C(1)–C(2)	121.3(13)	C(1)–C(2)–H(2A)	132.4
C(1)–C(2)–C(3)	95.6(14)	H(2A)–C(2)–C(3)	131.9
C(2)–C(3)–H(3A)	122.3	C(2)–C(3)–C(4)	116.2(17)
H(3A)–C(3)–C(4)	121.4	S(1)–C(4)–C(3)	116.3(13)
S(1)–C(4)–H(4A)	121.7	C(3)–C(4)–H(4A)	122.0
O(1)–I(1A)–O(4)	167.4(3)	O(1)–I(1A)–C(9A)	85.0(9)
O(4)–I(1A)–C(9A)	86.3(9)	C(1A)–S(1A)–C(4A)	106(2)
S(1A)–C(1A)–C(2A)	115(3)	S(1A)–C(1A)–I(2A)	117(2)

C(2A)–C(1A)–I(2A)	127(2)	C(1A)–C(2A)–H(2B)	131.7
C(1A)–C(2A)–C(3A)	97(3)	H(2B)–C(2A)–C(3A)	131.6
C(2A)–C(3A)–H(3B)	124.3	C(2A)–C(3A)–C(4A)	111(3)
H(3B)–C(3A)–C(4A)	124.5	S(1A)–C(4A)–C(3A)	111(3)
S(1A)–C(4A)–H(4B)	125.3	C(3A)–C(4A)–H(4B)	123.8
C(6)–C(5)–O(1)	120.8(8)	C(6)–C(5)–O(2)	117.6(9)
O(1)–C(5)–O(2)	121.6(9)	C(5)–C(6)–H(6A)	109.5
C(5)–C(6)–H(6B)	109.5	C(5)–C(6)–H(6C)	109.4
H(6A)–C(6)–H(6B)	109.5	H(6A)–C(6)–H(6C)	109.5
H(6B)–C(6)–H(6C)	109.5	C(8)–C(7)–O(3)	117.3(8)
C(8)–C(7)–O(4)	120.9(10)	O(3)–C(7)–O(4)	121.8(9)
C(7)–C(8)–H(8A)	109.4	C(7)–C(8)–H(8B)	109.6
C(7)–C(8)–H(8C)	109.4	H(8A)–C(8)–H(8B)	109.5
H(8A)–C(8)–H(8C)	109.5	H(8B)–C(8)–H(8C)	109.5
I(1A)–O(1)–C(5)	114.9(6)	I(1)–O(2)–C(5)	112.0(6)
I(1)–O(3)–C(7)	110.0(6)	I(1A)–O(4)–C(7)	116.8(7)
C(9)–I(2)–O(6)	83.1(4)	C(9)–I(2)–O(7)	84.2(4)
O(6)–I(2)–O(7)	166.8(3)	C(9)–S(2)–C(12)	91.8(10)
I(2)–C(9)–S(2)	119.5(10)	I(2)–C(9)–C(10)	121.7(13)
S(2)–C(9)–C(10)	118.8(14)	C(9)–C(10)–H(10A)	131.3
C(9)–C(10)–C(11)	97.5(15)	H(10A)–C(10)–C(11)	131.1
C(10)–C(11)–H(11A)	122.2	C(10)–C(11)–C(12)	114.8(18)
H(11A)–C(11)–C(12)	123.0	S(2)–C(12)–C(11)	117.0(15)
S(2)–C(12)–H(12A)	121.7	C(11)–C(12)–H(12A)	121.2
C(1A)–I(2A)–O(5)	85.8(8)	C(1A)–I(2A)–O(8)	85.2(8)
O(5)–I(2A)–O(8)	168.5(3)	C(9A)–S(2A)–C(12A)	99(3)
I(1A)–C(9A)–S(2A)	118(2)	I(1A)–C(9A)–C(10A)	126(2)
S(2A)–C(9A)–C(10A)	116(3)	C(9A)–C(10A)–H(10B)	132.9
C(9A)–C(10A)–C(11A)	95(3)	H(10B)–C(10A)–C(11A)	132.4
C(10A)–C(11A)–H(11B)	122.3	C(10A)–C(11A)–C(12A)	114(4)
H(11B)–C(11A)–C(12A)	123.5	S(2A)–C(12A)–C(11A)	117(4)
S(2A)–C(12A)–H(12B)	121.4	C(11A)–C(12A)–H(12B)	122.0
C(14)–C(13)–O(5)	121.2(9)	C(14)–C(13)–O(6)	116.7(9)
O(5)–C(13)–O(6)	122.1(9)	C(13)–C(14)–H(14A)	109.4
C(13)–C(14)–H(14B)	109.5	C(13)–C(14)–H(14C)	109.5
H(14A)–C(14)–H(14B)	109.5	H(14A)–C(14)–H(14C)	109.5
H(14B)–C(14)–H(14C)	109.5	C(16)–C(15)–O(7)	117.2(8)
C(16)–C(15)–O(8)	121.2(9)	O(7)–C(15)–O(8)	121.7(9)
C(15)–C(16)–H(16A)	109.5	C(15)–C(16)–H(16B)	109.4
C(15)–C(16)–H(16C)	109.5	H(16A)–C(16)–H(16B)	109.5
H(16A)–C(16)–H(16C)	109.5	H(16B)–C(16)–H(16C)	109.5
I(2A)–O(5)–C(13)	115.3(6)	I(2)–O(6)–C(13)	111.4(6)
I(2)–O(7)–C(15)	110.1(6)	I(2A)–O(8)–C(15)	116.9(6)

Table 10. Anisotropic displacement parameters ($Å^2$) for **206**. The anisotropic displacement factor exponent takes the form: $-2\pi^2[h^2a^{*2}U^{11} + ...+ 2hka^*b^*U^{12}]$

	U^{11}	U^{22}	U^{33}	U^{23}	U^{13}	U^{12}
I(1)	0.0193(5)	0.0131(4)	0.0162(5)	−0.0003(3)	0.0019(3)	0.0018(3)
S(1)	0.034(2)	0.031(2)	0.036(2)	−0.0015(17)	−0.0004(18)	
−0.0021(18)						
C(1)	0.023(4)	0.017(4)	0.031(4)	0.004(4)	−0.012(4)	−0.011(4)
C(2)	0.025(4)	0.014(4)	0.022(5)	0.002(4)	−0.011(4)	−0.005(5)
C(3)	0.030(5)	0.023(4)	0.031(4)	−0.003(4)	−0.009(4)	−0.004(5)
C(4)	0.029(4)	0.023(4)	0.030(5)	−0.001(4)	−0.013(4)	−0.006(4)
I(1A)	0.0233(10)	0.0177(9)	0.0188(9)	−0.0001(7)	0.0033(7)	0.0011(7)
S(1A)	0.033(4)	0.028(3)	0.033(3)	−0.002(3)	−0.006(3)	−0.006(4)
C(1A)	0.028(5)	0.022(5)	0.030(5)	0.004(5)	−0.008(5)	−0.008(5)
C(2A)	0.030(5)	0.024(5)	0.027(5)	0.001(5)	−0.009(5)	−0.006(5)
C(3A)	0.030(5)	0.026(5)	0.033(5)	0.000(4)	−0.008(4)	−0.007(5)
C(4A)	0.030(5)	0.019(5)	0.030(5)	0.002(5)	−0.012(5)	−0.006(5)
C(5)	0.029(5)	0.029(5)	0.021(5)	−0.002(4)	0.001(4)	−0.003(4)
C(6)	0.042(6)	0.027(5)	0.034(5)	0.006(4)	0.004(5)	−0.004(5)
C(7)	0.034(5)	0.031(5)	0.020(5)	0.004(4)	0.001(4)	0.000(4)
C(8)	0.040(6)	0.028(5)	0.033(5)	0.006(4)	0.004(5)	0.004(4)
O(1)	0.045(5)	0.025(4)	0.043(4)	−0.005(3)	−0.006(4)	0.004(3)
O(2)	0.032(4)	0.025(4)	0.030(4)	0.005(3)	−0.002(3)	0.000(3)
O(3)	0.042(5)	0.021(4)	0.043(5)	−0.006(3)	−0.005(4)	0.005(3)
O(4)	0.046(5)	0.032(4)	0.033(4)	0.000(3)	−0.005(4)	−0.004(4)
I(2)	0.0200(5)	0.0128(4)	0.0154(4)	0.0000(3)	0.0012(3)	0.0018(3)
S(2)	0.032(2)	0.033(2)	0.033(2)	−0.0011(18)	0.0004(18)	
−0.0029(19)						
C(9)	0.026(5)	0.017(5)	0.027(5)	−0.001(4)	−0.010(5)	−0.011(5)
C(10)	0.024(5)	0.014(5)	0.016(6)	0.007(5)	−0.010(5)	−0.005(6)
C(11)	0.031(7)	0.027(6)	0.027(6)	−0.004(5)	−0.006(5)	−0.005(6)
C(12)	0.030(5)	0.026(6)	0.027(6)	0.001(5)	−0.018(5)	−0.010(5)
I(2A)	0.0228(10)	0.0172(9)	0.0185(10)	0.0000(7)	0.0014(7)	0.0013(7)
S(2A)	0.036(5)	0.046(5)	0.044(5)	−0.003(4)	−0.007(4)	−0.008(5)
C(9A)	0.031(7)	0.028(8)	0.026(7)	0.006(7)	−0.008(7)	−0.011(7)
C(10A)	0.030(7)	0.022(9)	0.014(8)	0.002(8)	−0.015(7)	−0.012(8)
C(11A)	0.029(9)	0.032(9)	0.029(8)	0.002(7)	−0.016(7)	−0.012(9)
C(12A)	0.030(8)	0.035(9)	0.033(8)	0.004(7)	−0.014(7)	−0.009(8)
C(13)	0.031(5)	0.027(5)	0.021(5)	0.005(4)	0.002(4)	−0.002(4)
C(14)	0.040(6)	0.027(5)	0.031(5)	0.005(4)	0.002(5)	0.002(4)
C(15)	0.028(5)	0.027(5)	0.018(5)	0.001(4)	0.004(4)	−0.007(4)
C(16)	0.040(6)	0.023(5)	0.033(5)	0.004(4)	0.007(5)	−0.003(4)
O(5)	0.045(5)	0.023(4)	0.040(4)	−0.006(3)	−0.006(4)	0.006(3)
O(6)	0.039(4)	0.031(4)	0.028(4)	0.003(3)	−0.003(3)	−0.004(3)
O(7)	0.039(4)	0.024(4)	0.030(4)	0.001(3)	0.000(3)	0.006(3)
O(8)	0.042(4)	0.032(4)	0.028(4)	0.005(3)	−0.004(3)	−0.002(3)

Table 11. Hydrogen coordinates and isotropic displacement parameters ($Å^2$) for **206**.

	x	y	z	U
H(2A)	0.1463	0.2687	0.5150	0.029
H(3A)	0.0176	0.2002	0.3928	0.038
H(4A)	−0.1113	0.2054	0.4266	0.039
H(2B)	−0.1472	0.2323	0.4858	0.037
H(3B)	−0.0107	0.2985	0.6094	0.040
H(4B)	0.1271	0.2861	0.5515	0.037
H(6A)	0.2419	0.1721	0.9321	0.054
H(6B)	0.2846	0.1581	0.8539	0.054
H(6C)	0.1911	0.1274	0.8429	0.054
H(8A)	0.0555	0.6238	0.6639	0.052
H(8B)	−0.0368	0.5865	0.6369	0.052
H(8C)	0.0191	0.5818	0.5692	0.052
H(10A)	−0.1022	0.0221	0.0188	0.026
H(11A)	−0.2270	−0.0483	−0.1061	0.038
H(12A)	−0.3557	−0.0469	−0.0735	0.040
H(10B)	0.1046	0.4869	0.9870	0.032
H(11B)	0.2468	0.5453	1.1106	0.042
H(12B)	0.3732	0.5368	1.0577	0.046
H(14A)	−0.0137	−0.0798	0.4320	0.052
H(14B)	0.0276	−0.0940	0.3528	0.052
H(14C)	−0.0663	−0.1233	0.3426	0.052
H(16A)	−0.1845	0.3754	0.1593	0.049
H(16B)	−0.2777	0.3420	0.1430	0.049
H(16C)	−0.2309	0.3322	0.0675	0.049

Table 12. Torsion angles [°] for **206**.

C(4)–S(1)–C(1)–I(1)	−179.4(9)	C(4)–S(1)–C(1)–C(2)	−0.7(15)
O(2)–I(1)–C(1)–S(1)	100.5(8)	O(2)–I(1)–C(1)–C(2)	−78.2(14)
O(3)–I(1)–C(1)–S(1)	−73.8(7)	O(3)–I(1)–C(1)–C(2)	107.5(14)
I(1)–C(1)–C(2)–C(3)	179.4(11)	S(1)–C(1)–C(2)–C(3)	0.7(19)
C(1)–C(2)–C(3)–C(4)	0(2)	C(2)–C(3)–C(4)–S(1)	0(2)
C(1)–S(1)–C(4)–C(3)	0.4(15)	C(4A)–S(1A)–C(1A)–C(2A)	2(4)
C(4A)–S(1A)–C(1A)–I(2A)	177(3)	S(1A)–C(1A)–C(2A)–C(3A)	−3(3)
I(2A)–C(1A)–C(2A)–C(3A)	−177(2)	C(1A)–C(2A)–C(3A)–C(4A)	2(4)
C(1A)–S(1A)–C(4A)–C(3A)	0(4)	C(2A)–C(3A)–C(4A)–S(1A)	−1(5)
C(6)–C(5)–O(1)–I(1A)	−173.2(8)	O(2)–C(5)–O(1)–I(1A)	6.8(14)
O(4)–I(1A)–O(1)–C(5)	−143.3(14)	C(9A)–I(1A)–O(1)–C(5)	170.5(13)
C(6)–C(5)–O(2)–I(1)	179.9(8)	O(1)–C(5)–O(2)–I(1)	−0.1(13)
C(1)–I(1)–O(2)–C(5)	175.1(9)	O(3)–I(1)–O(2)–C(5)	−159.9(12)
C(8)–C(7)–O(3)–I(1)	176.2(8)	O(4)–C(7)–O(3)–I(1)	−3.2(13)
C(1)–I(1)–O(3)–C(7)	−173.0(9)	O(2)–I(1)–O(3)–C(7)	162.1(11)
C(8)–C(7)–O(4)–I(1A)	176.7(8)	O(3)–C(7)–O(4)–I(1A)	−3.9(14)
O(1)–I(1A)–O(4)–C(7)	142.6(14)	C(9A)–I(1A)–O(4)–C(7)	−171.3(14)
C(12)–S(2)–C(9)–I(2)	−177.4(10)	C(12)–S(2)–C(9)–C(10)	−0.1(15)
O(6)–I(2)–C(9)–S(2)	98.4(9)	O(6)–I(2)–C(9)–C(10)	−78.8(15)
O(7)–I(2)–C(9)–S(2)	−78.1(8)	O(7)–I(2)–C(9)–C(10)	104.7(15)
I(2)–C(9)–C(10)–C(11)	177.9(12)	S(2)–C(9)–C(10)–C(11)	1(2)
C(9)–C(10)–C(11)–C(12)	−1(2)	C(10)–C(11)–C(12)–S(2)	1(3)
C(9)–S(2)–C(12)–C(11)	−0.7(17)	S(1A)–C(1A)–I(2A)–O(5)	77.7(16)
S(1A)–C(1A)–I(2A)–O(8)	−95.1(16)	C(2A)–C(1A)–I(2A)–O(5)	−108(3)
C(2A)–C(1A)–I(2A)–O(8)	80(3)	C(12A)–S(2A)–C(9A)–I(1A)	178(4)
C(12A)–S(2A)–C(9A)–C(10A)	5(4)	O(1)–I(1A)–C(9A)–S(2A)	75.1(17)
O(1)–I(1A)–C(9A)–C(10A)	−113(3)	O(4)–I(1A)–C(9A)–S(2A)	−95.8(18)
O(4)–I(1A)–C(9A)–C(10A)	76(3)	I(1A)–C(9A)–C(10A)–C(11A)	−178(2)
S(2A)–C(9A)–C(10A)–C(11A)	−6(3)	C(9A)–C(10A)–C(11A)–C(12A)	5(5)
C(9A)–S(2A)–C(12A)–C(11A)	−1(6)	C(10A)–C(11A)–C(12A)–S(2A)	−3(7)
C(14)–C(13)–O(5)–I(2A)	−176.8(8)	O(6)–C(13)–O(5)–I(2A)	3.0(14)
C(1A)–I(2A)–O(5)–C(13)	173.4(13)	O(8)–I(2A)–O(5)–C(13)	−148.0(15)
C(14)–C(13)–O(6)–I(2)	−178.8(7)	O(5)–C(13)–O(6)–I(2)	1.4(13)
C(9)–I(2)–O(6)–C(13)	177.0(9)	O(7)–I(2)–O(6)–C(13)	−167.5(11)
C(16)–C(15)–O(7)–I(2)	179.5(7)	O(8)–C(15)–O(7)–I(2)	−1.1(12)
C(9)–I(2)–O(7)–C(15)	−176.1(8)	O(6)–I(2)–O(7)–C(15)	168.5(12)
C(16)–C(15)–O(8)–I(2A)	174.8(8)	O(7)–C(15)–O(8)–I(2A)	−4.5(14)
C(1A)–I(2A)–O(8)–C(15)	−171.4(13)	O(5)–I(2A)–O(8)–C(15)	150.0(15)

Appendix II – Crystallographic Data for compounds 191-196

Compound **191**

Table 1. Crystal data and structure refinement for **191**.

Identification code	mac117	
Chemical formula (moiety)	$C_{15}H_{14}O_2I^+ \cdot C_2F_3O_2^-$	
Chemical formula (total)	$C_{17}H_{14}F_3IO_4$	
Formula weight	466.18	
Temperature	150(2) K	
Radiation, wavelength	MoKα, 0.71073 Å	
Crystal system, space group	triclinic, $P\bar{1}$	
Unit cell parameters	a = 5.2851(3) Å	α = 113.169(11)°
	b = 12.8616(16) Å	β = 96.508(7)°
	c = 13.7337(15) Å	γ = 98.752(7)°
Cell volume	832.71(15) Å^3	
Z	2	
Calculated density	1.859 g/cm^3	
Absorption coefficient μ	1.974 mm^{-1}	
F(000)	456	
Crystal colour and size	colourless, 0.30 $\times$ 0.30 $\times$ 0.25 mm^3	
Reflections for cell refinement	3467 (θ range 2.9 to 28.6°)	
Data collection method	Xcalibur, Atlas, Gemini ultra thick-slice ω scans	
θ range for data collection	2.9 to 28.6°	
Index ranges	h -7 to 6, k -16 to 16, l -14 to 16	
Completeness to θ = 25.0°	99.9 %	
Reflections collected	6967	
Independent reflections	3479 (R_{int} = 0.0466)	
Reflections with $F^2>2\sigma$	3159	
Absorption correction	semi-empirical from equivalents	
Min. and max. transmission	0.5889 and 0.6382	
Structure solution	direct methods	
Refinement method	Full-matrix least-squares on F^2	
Weighting parameters a, b	0.0304, 0.0204	
Data / restraints / parameters	3479 / 0 / 227	
Final R indices [$F^2>2\sigma$]	R1 = 0.0345, wR2 = 0.0736	
R indices (all data)	R1 = 0.0398, wR2 = 0.0788	
Goodness-of-fit on F^2	1.070	
Largest and mean shift/su	0.001 and 0.000	
Largest diff. peak and hole	1.30 and -1.30 e Å^{-3}	

Table 2. Atomic coordinates and equivalent isotropic displacement parameters (Å^2) for mac117. U_{eq} is defined as one third of the trace of the orthogonalized U^{ij} tensor.

	x	y	z	U_{eq}
I	0.88325(4)	0.203014(18)	0.601201(18)	0.01859(9)
O(1)	0.0918(5)	0.2082(2)	0.9805(2)	0.0271(6)
O(2)	0.3371(6)	0.3867(3)	1.0714(2)	0.0374(7)
O(3)	0.8097(5)	−0.2151(2)	0.5389(2)	0.0288(6)
O(4)	0.8170(6)	−0.0269(2)	0.5918(3)	0.0384(8)
F(1)	0.4019(5)	−0.1134(2)	0.6825(2)	0.0408(6)
F(2)	0.6616(5)	−0.2117(2)	0.7154(2)	0.0432(7)
F(3)	0.7696(5)	−0.0265(2)	0.7875(2)	0.0479(7)
C(1)	0.9567(7)	0.3779(3)	0.6269(3)	0.0171(7)
C(2)	1.1947(7)	0.4476(3)	0.6873(3)	0.0227(8)
C(3)	1.2444(7)	0.5625(3)	0.7038(3)	0.0245(8)
C(4)	1.0608(8)	0.6060(3)	0.6606(3)	0.0242(8)
C(5)	0.8230(7)	0.5336(3)	0.6012(3)	0.0219(8)
C(6)	0.7665(7)	0.4182(3)	0.5826(3)	0.0196(8)
C(7)	0.6755(7)	0.2348(3)	0.7298(3)	0.0193(8)
C(8)	0.4642(7)	0.1504(3)	0.7195(3)	0.0201(8)
C(9)	0.3341(7)	0.1684(3)	0.8051(3)	0.0222(8)
C(10)	0.4133(7)	0.2709(3)	0.8986(3)	0.0200(8)
C(11)	0.6239(8)	0.3542(3)	0.9065(3)	0.0267(9)
C(12)	0.7578(8)	0.3354(3)	0.8219(3)	0.0270(9)
C(13)	0.2806(8)	0.2963(3)	0.9928(3)	0.0244(8)
C(14)	−0.0466(8)	0.2306(4)	1.0706(3)	0.0284(9)
C(15)	−0.2458(9)	0.1243(4)	1.0462(4)	0.0380(11)
C(16)	0.7751(7)	−0.1196(3)	0.5992(3)	0.0201(8)
C(17)	0.6552(7)	−0.1185(3)	0.6970(3)	0.0210(8)

Table 3. Bond lengths [Å] and angles [°] for **191**.

I–C(1)	2.100(3)	I–C(7)	2.121(4)
O(1)–C(13)	1.333(5)	O(1)–C(14)	1.462(4)
O(2)–C(13)	1.200(5)	O(3)–C(16)	1.237(4)
O(4)–C(16)	1.225(4)	F(1)–C(17)	1.346(4)
F(2)–C(17)	1.323(4)	F(3)–C(17)	1.328(5)
C(1)–C(2)	1.382(5)	C(1)–C(6)	1.385(5)
C(2)–H(2A)	0.950	C(2)–C(3)	1.382(5)
C(3)–H(3A)	0.950	C(3)–C(4)	1.380(5)
C(4)–H(4A)	0.950	C(4)–C(5)	1.388(6)
C(5)–H(5A)	0.950	C(5)–C(6)	1.381(5)
C(6)–H(6A)	0.950	C(7)–C(8)	1.385(5)
C(7)–C(12)	1.372(5)	C(8)–H(8A)	0.950
C(8)–C(9)	1.388(5)	C(9)–H(9A)	0.950
C(9)–C(10)	1.392(5)	C(10)–C(11)	1.384(5)
C(10)–C(13)	1.489(5)	C(11)–H(11A)	0.950
C(11)–C(12)	1.388(5)	C(12)–H(12A)	0.950
C(14)–H(14A)	0.990	C(14)–H(14B)	0.990
C(14)–C(15)	1.486(6)	C(15)–H(15A)	0.980
C(15)–H(15B)	0.980	C(15)–H(15C)	0.980
C(16)–C(17)	1.546(5)		

C(1)–I–C(7)	92.40(13)	C(13)–O(1)–C(14)	114.5(3)
I–C(1)–C(2)	118.1(2)	I–C(1)–C(6)	118.9(3)
C(2)–C(1)–C(6)	122.9(3)	C(1)–C(2)–H(2A)	120.8
C(1)–C(2)–C(3)	118.3(3)	H(2A)–C(2)–C(3)	120.8
C(2)–C(3)–H(3A)	119.7	C(2)–C(3)–C(4)	120.6(4)
H(3A)–C(3)–C(4)	119.7	C(3)–C(4)–H(4A)	120.3
C(3)–C(4)–C(5)	119.4(3)	H(4A)–C(4)–C(5)	120.3
C(4)–C(5)–H(5A)	119.2	C(4)–C(5)–C(6)	121.7(3)
H(5A)–C(5)–C(6)	119.2	C(1)–C(6)–C(5)	117.1(4)
C(1)–C(6)–H(6A)	121.5	C(5)–C(6)–H(6A)	121.5
I–C(7)–C(8)	118.5(3)	I–C(7)–C(12)	119.7(3)
C(8)–C(7)–C(12)	121.7(3)	C(7)–C(8)–H(8A)	120.6
C(7)–C(8)–C(9)	118.9(4)	H(8A)–C(8)–C(9)	120.6
C(8)–C(9)–H(9A)	120.0	C(8)–C(9)–C(10)	120.0(3)
H(9A)–C(9)–C(10)	120.0	C(9)–C(10)–C(11)	119.9(3)
C(9)–C(10)–C(13)	122.8(3)	C(11)–C(10)–C(13)	117.3(4)
C(10)–C(11)–H(11A)	119.9	C(10)–C(11)–C(12)	120.2(4)
H(11A)–C(11)–C(12)	119.9	C(7)–C(12)–C(11)	119.3(4)
C(7)–C(12)–H(12A)	120.4	C(11)–C(12)–H(12A)	120.4
O(1)–C(13)–O(2)	123.6(4)	O(1)–C(13)–C(10)	112.9(3)
O(2)–C(13)–C(10)	123.6(4)	O(1)–C(14)–H(14A)	110.1
O(1)–C(14)–H(14B)	110.1	O(1)–C(14)–C(15)	108.2(3)
H(14A)–C(14)–H(14B)	108.4	H(14A)–C(14)–C(15)	110.1
H(14B)–C(14)–C(15)	110.1	C(14)–C(15)–H(15A)	109.5
C(14)–C(15)–H(15B)	109.5	C(14)–C(15)–H(15C)	109.5

H(15A)–C(15)–H(15B)	109.5	H(15A)–C(15)–H(15C)	109.5
H(15B)–C(15)–H(15C)	109.5	O(3)–C(16)–O(4)	129.8(4)
O(3)–C(16)–C(17)	114.7(3)	O(4)–C(16)–C(17)	115.5(3)
F(1)–C(17)–F(2)	105.7(3)	F(1)–C(17)–F(3)	105.6(3)
F(1)–C(17)–C(16)	111.0(3)	F(2)–C(17)–F(3)	107.7(3)
F(2)–C(17)–C(16)	114.0(3)	F(3)–C(17)–C(16)	112.3(3)

Table 4. Anisotropic displacement parameters (Å^2) for **191**. The anisotropic displacement factor exponent takes the form: $-2\pi^2[h^2a^{*2}U^{11} + ...+ 2hka^*b^*U^{12}]$

	U^{11}	U^{22}	U^{33}	U^{23}	U^{13}	U^{12}
I	0.02076(15)	0.01656(14)	0.02252(16)	0.01080(11)	0.00845(10)	0.00518(10)
O(1)	0.0277(15)	0.0298(15)	0.0235(15)	0.0100(12)	0.0120(12)	0.0037(13)
O(2)	0.051(2)	0.0299(16)	0.0278(17)	0.0076(14)	0.0177(15)	0.0022(15)
O(3)	0.0350(16)	0.0187(14)	0.0339(17)	0.0090(13)	0.0179(14)	0.0066(12)
O(4)	0.061(2)	0.0245(16)	0.0427(19)	0.0210(15)	0.0293(17)	0.0123(15)
F(1)	0.0282(13)	0.0539(17)	0.0566(18)	0.0343(15)	0.0231(13)	0.0132(12)
F(2)	0.0658(18)	0.0401(15)	0.0511(17)	0.0364(14)	0.0345(15)	0.0248(14)
F(3)	0.0584(18)	0.0436(16)	0.0232(14)	0.0017(12)	0.0124(13)	−0.0112(13)
C(1)	0.0195(18)	0.0155(17)	0.0206(19)	0.0092(15)	0.0113(15)	0.0058(15)
C(2)	0.0195(19)	0.027(2)	0.026(2)	0.0135(17)	0.0076(17)	0.0067(16)
C(3)	0.023(2)	0.023(2)	0.024(2)	0.0067(16)	0.0090(17)	−0.0001(17)
C(4)	0.031(2)	0.0182(19)	0.027(2)	0.0101(17)	0.0151(18)	0.0073(17)
C(5)	0.026(2)	0.022(2)	0.023(2)	0.0128(17)	0.0078(17)	0.0084(17)
C(6)	0.0190(19)	0.0216(19)	0.020(2)	0.0094(16)	0.0075(16)	0.0063(16)
C(7)	0.0215(19)	0.0213(19)	0.020(2)	0.0114(16)	0.0079(16)	0.0086(16)
C(8)	0.0202(19)	0.0187(18)	0.022(2)	0.0086(16)	0.0047(16)	0.0055(15)
C(9)	0.0203(19)	0.0218(19)	0.025(2)	0.0114(16)	0.0054(16)	0.0012(16)
C(10)	0.0207(19)	0.024(2)	0.020(2)	0.0136(16)	0.0035(16)	0.0068(16)
C(11)	0.034(2)	0.021(2)	0.024(2)	0.0095(17)	0.0080(18)	0.0025(17)
C(12)	0.030(2)	0.023(2)	0.029(2)	0.0129(18)	0.0075(18)	0.0011(17)
C(13)	0.028(2)	0.024(2)	0.027(2)	0.0132(18)	0.0087(18)	0.0101(17)
C(14)	0.030(2)	0.039(2)	0.021(2)	0.0138(18)	0.0143(18)	

	0.0081(19)					
C(15)	0.039(3)	0.046(3)	0.037(3)	0.023(2)	0.021(2)	0.008(2)
C(16)	0.0172(18)	0.0165(18)	0.027(2)	0.0103(16)	0.0050(16)	
	0.0011(15)					
C(17)	0.023(2)	0.0181(19)	0.021(2)	0.0084(16)	0.0057(16)	
	0.0031(16)					

Table 5. Hydrogen coordinates and isotropic displacement parameters ($Å^2$) for **191**.

	x	y	z	U
H(2A)	1.3209	0.4172	0.7167	0.027
H(3A)	1.4065	0.6120	0.7453	0.029
H(4A)	1.0968	0.6848	0.6714	0.029
H(5A)	0.6958	0.5642	0.5727	0.026
H(6A)	0.6042	0.3686	0.5413	0.024
H(8A)	0.4093	0.0814	0.6549	0.024
H(9A)	0.1910	0.1108	0.7999	0.027
H(11A)	0.6768	0.4244	0.9700	0.032
H(12A)	0.9049	0.3916	0.8278	0.032
H(14A)	−0.1318	0.2964	1.0801	0.034
H(14B)	0.0775	0.2504	1.1381	0.034
H(15A)	−0.3411	0.1377	1.1057	0.057
H(15B)	−0.1596	0.0598	1.0373	0.057
H(15C)	−0.3681	0.1056	0.9794	0.057

Table 6. Torsion angles [°] for **191**.

C(7)–I–C(1)–C(2)	97.2(3)	C(7)–I–C(1)–C(6)	−83.0(3)
I–C(1)–C(2)–C(3)	179.6(3)	C(6)–C(1)–C(2)–C(3)	−0.2(5)
C(1)–C(2)–C(3)–C(4)	−0.2(5)	C(2)–C(3)–C(4)–C(5)	0.8(6)
C(3)–C(4)–C(5)–C(6)	−1.1(6)	C(4)–C(5)–C(6)–C(1)	0.7(5)
I–C(1)–C(6)–C(5)	−179.9(2)	C(2)–C(1)–C(6)–C(5)	−0.1(5)
C(1)–I–C(7)–C(8)	145.0(3)	C(1)–I–C(7)–C(12)	−37.3(3)
I–C(7)–C(8)–C(9)	177.3(2)	C(12)–C(7)–C(8)–C(9)	−0.3(5)
C(7)–C(8)–C(9)–C(10)	1.2(5)	C(8)–C(9)–C(10)–C(11)	−0.8(5)
C(8)–C(9)–C(10)–C(13)	179.3(3)	C(9)–C(10)–C(11)–C(12)	−0.6(5)
C(13)–C(10)–C(11)–C(12)	179.4(3)	I–C(7)–C(12)–C(11)	−178.6(3)
C(8)–C(7)–C(12)–C(11)	−1.0(5)	C(10)–C(11)–C(12)–C(7)	1.5(5)
C(14)–O(1)–C(13)–O(2)	0.9(5)	C(14)–O(1)–C(13)–C(10)	−178.9(3)
C(9)–C(10)–C(13)–O(1)	4.2(5)	C(9)–C(10)–C(13)–O(2)	−175.7(4)
C(11)–C(10)–C(13)–O(1)	−175.8(3)	C(11)–C(10)–C(13)–O(2)	4.3(5)
C(13)–O(1)–C(14)–C(15)	−178.9(3)	O(3)–C(16)–C(17)–F(1)	−104.7(4)
O(3)–C(16)–C(17)–F(2)	14.4(5)	O(3)–C(16)–C(17)–F(3)	137.3(3)
O(4)–C(16)–C(17)–F(1)	74.0(4)	O(4)–C(16)–C(17)–F(2)	−166.9(3)
O(4)–C(16)–C(17)–F(3)	−44.1(5)		

Table 7. Crystal data and structure refinement for **192**.

Identification code	mac12	
Chemical formula (moiety)	$C_{16}H_{16}O_3I^+ \cdot C_2O_2F_3^- \cdot C_2H_4O_2$	
Chemical formula (total)	$C_{20}H_{20}F_3IO_7$	
Formula weight	556.26	
Temperature	150(2) K	
Radiation, wavelength	MoKα, 0.71073 Å	
Crystal system, space group	triclinic, $P\bar{1}$	
Unit cell parameters	a = 8.1419(3) Å	α = 94.411(3)°
	b = 10.6745(4) Å	β = 107.271(4)°
	c = 13.2025(6) Å	γ = 91.471(3)°
Cell volume	1091.04(8) Å^3	
Z	2	
Calculated density	1.693 g/cm^3	
Absorption coefficient μ	1.531 mm^{-1}	
F(000)	552	
Crystal colour and size	colourless, 0.40 × 0.30 × 0.30 mm^3	
Reflections for cell refinement	5049 (θ range 3.2 to 28.5°)	
Data collection method	Xcalibur, Atlas, Gemini ultra thick-slice ω scans	
θ range for data collection	3.2 to 28.6°	
Index ranges	h –9 to 10, k –13 to 14, l –17 to 14	
Completeness to θ = 25.0°	99.8 %	
Reflections collected	8569	
Independent reflections	4499 (R_{int} = 0.0279)	
Reflections with $F^2>2\sigma$	4025	
Absorption correction	semi-empirical from equivalents	
Min. and max. transmission	0.5794 and 0.6565	
Structure solution	direct methods	
Refinement method	Full-matrix least-squares on F^2	
Weighting parameters a, b	0.0264, 0.7938	
Data / restraints / parameters	4499 / 1 / 311	
Final R indices [$F^2>2\sigma$]	R1 = 0.0323, wR2 = 0.0694	
R indices (all data)	R1 = 0.0393, wR2 = 0.0738	
Goodness-of-fit on F^2	1.095	
Extinction coefficient	0.0000(3)	
Largest and mean shift/su	1.561 and 0.005	
Largest diff. peak and hole	0.77 and –0.50 e Å^{-3}	

Table 8. Atomic coordinates and equivalent isotropic displacement parameters ($Å^2$) for **192**. U_{eq} is defined as one third of the trace of the orthogonalized U^{ij} tensor.

	x	y	z	U_{eq}
I(1)	1.62883(3)	0.050390(19)	0.364561(17)	0.02348(9)
O(1)	2.0142(3)	−0.1744(2)	−0.01436(19)	0.0286(5)
O(2)	2.2593(3)	−0.1083(2)	0.1129(2)	0.0358(6)
O(3)	1.4415(3)	0.5220(2)	0.1162(2)	0.0347(6)
O(4)	1.2275(4)	0.1836(2)	0.5649(2)	0.0490(8)
O(5)	1.3874(4)	0.1377(2)	0.4602(2)	0.0410(7)
F(1)	1.1434(4)	0.3069(3)	0.3464(2)	0.0825(10)
F(2)	1.3855(3)	0.3900(2)	0.4337(3)	0.0748(10)
F(3)	1.1734(4)	0.4077(2)	0.4939(2)	0.0721(9)
C(1)	1.7864(4)	−0.0069(3)	0.2702(3)	0.0208(7)
C(2)	1.7077(4)	−0.0539(3)	0.1663(3)	0.0224(7)
C(3)	1.8107(4)	−0.0903(3)	0.1038(3)	0.0228(7)
C(4)	1.9899(4)	−0.0795(3)	0.1459(3)	0.0207(7)
C(5)	2.0649(4)	−0.0300(3)	0.2505(3)	0.0241(7)
C(6)	1.9635(4)	0.0061(3)	0.3147(3)	0.0237(7)
C(7)	2.1048(4)	−0.1210(3)	0.0812(3)	0.0244(7)
C(8)	2.1077(5)	−0.2350(3)	−0.0819(3)	0.0326(8)
C(9)	2.1029(5)	−0.3729(4)	−0.0737(4)	0.0443(10)
C(10)	1.5671(4)	0.2138(3)	0.2849(3)	0.0215(7)
C(11)	1.6751(4)	0.3205(3)	0.3190(3)	0.0265(7)
C(12)	1.6372(4)	0.4265(3)	0.2639(3)	0.0265(7)
C(13)	1.4912(4)	0.4247(3)	0.1764(3)	0.0235(7)
C(14)	1.3846(4)	0.3160(3)	0.1437(3)	0.0276(8)
C(15)	1.4209(4)	0.2100(3)	0.1979(3)	0.0263(7)
C(16)	1.5513(5)	0.6338(3)	0.1402(4)	0.0401(10)
C(17)	1.2496(5)	0.3295(3)	0.4432(3)	0.0310(8)
C(18)	1.2950(4)	0.2054(3)	0.4954(3)	0.0254(7)
O(7)	1.0830(7)	0.7367(6)	0.4212(5)	0.0408(16)
O(6)	0.9611(6)	0.6427(5)	0.2620(5)	0.0539(18)
C(20)	1.2643(9)	0.6660(8)	0.3267(6)	0.049(2)
O(6A)	0.9213(19)	0.6897(16)	0.3157(15)	0.045(6)
C(20A)	1.194(10)	0.645(4)	0.267(6)	0.27(5)
O(7A)	1.133(6)	0.756(3)	0.444(3)	0.140(18)
C(19)	1.0904(5)	0.6821(4)	0.3373(4)	0.0456(11)

Table 9. Bond lengths [Å] and angles [°] for **192**.

I(1)–C(1)	2.108(3)	I(1)–C(10)	2.100(3)
O(1)–C(7)	1.333(4)	O(1)–C(8)	1.461(4)
O(2)–C(7)	1.203(4)	O(3)–C(13)	1.353(4)
O(3)–C(16)	1.430(4)	O(4)–C(18)	1.235(4)
O(5)–C(18)	1.220(4)	F(1)–C(17)	1.312(4)
F(2)–C(17)	1.310(4)	F(3)–C(17)	1.311(4)
C(1)–C(2)	1.378(5)	C(1)–C(6)	1.385(4)
C(2)–H(2A)	0.950	C(2)–C(3)	1.384(5)
C(3)–H(3A)	0.950	C(3)–C(4)	1.397(4)
C(4)–C(5)	1.389(5)	C(4)–C(7)	1.496(5)
C(5)–H(5A)	0.950	C(5)–C(6)	1.389(5)
C(6)–H(6A)	0.950	C(8)–H(8A)	0.990
C(8)–H(8B)	0.990	C(8)–C(9)	1.484(5)
C(9)–H(9A)	0.980	C(9)–H(9B)	0.980
C(9)–H(9C)	0.980	C(10)–C(11)	1.382(5)
C(10)–C(15)	1.385(5)	C(11)–H(11A)	0.950
C(11)–C(12)	1.384(4)	C(12)–H(12A)	0.950
C(12)–C(13)	1.388(5)	C(13)–C(14)	1.391(5)
C(14)–H(14A)	0.950	C(14)–C(15)	1.376(5)
C(15)–H(15A)	0.950	C(16)–H(16A)	0.980
C(16)–H(16B)	0.980	C(16)–H(16C)	0.980
C(17)–C(18)	1.543(5)	O(7)–C(19)	1.230(8)
O(6)–C(19)	1.251(6)	C(20)–H(20A)	0.980
C(20)–H(20B)	0.980	C(20)–H(20C)	0.980
C(20)–C(19)	1.477(8)	O(6A)–C(19)	1.326(17)
C(20A)–H(20D)	0.980	C(20A)–H(20E)	0.980
C(20A)–H(20F)	0.980	C(20A)–C(19)	1.469(19)
O(7A)–C(19)	1.50(3)		

C(1)–I(1)–C(10)	91.74(12)	C(7)–O(1)–C(8)	118.2(3)
C(13)–O(3)–C(16)	118.1(3)	I(1)–C(1)–C(2)	118.2(2)
I(1)–C(1)–C(6)	118.7(2)	C(2)–C(1)–C(6)	123.1(3)
C(1)–C(2)–H(2A)	120.8	C(1)–C(2)–C(3)	118.4(3)
H(2A)–C(2)–C(3)	120.8	C(2)–C(3)–H(3A)	119.9
C(2)–C(3)–C(4)	120.3(3)	H(3A)–C(3)–C(4)	119.9
C(3)–C(4)–C(5)	119.8(3)	C(3)–C(4)–C(7)	121.6(3)
C(5)–C(4)–C(7)	118.6(3)	C(4)–C(5)–H(5A)	119.7
C(4)–C(5)–C(6)	120.7(3)	H(5A)–C(5)–C(6)	119.7
C(1)–C(6)–C(5)	117.7(3)	C(1)–C(6)–H(6A)	121.1
C(5)–C(6)–H(6A)	121.1	O(1)–C(7)–O(2)	124.9(3)
O(1)–C(7)–C(4)	111.5(3)	O(2)–C(7)–C(4)	123.6(3)
O(1)–C(8)–H(8A)	109.8	O(1)–C(8)–H(8B)	109.8
O(1)–C(8)–C(9)	109.5(3)	H(8A)–C(8)–H(8B)	108.2
H(8A)–C(8)–C(9)	109.8	H(8B)–C(8)–C(9)	109.8
C(8)–C(9)–H(9A)	109.5	C(8)–C(9)–H(9B)	109.5
C(8)–C(9)–H(9C)	109.5	H(9A)–C(9)–H(9B)	109.5

H(9A)–C(9)–H(9C)	109.5	H(9B)–C(9)–H(9C)	109.5
I(1)–C(10)–C(11)	119.3(2)	I(1)–C(10)–C(15)	118.7(2)
C(11)–C(10)–C(15)	121.9(3)	C(10)–C(11)–H(11A)	120.5
C(10)–C(11)–C(12)	119.1(3)	H(11A)–C(11)–C(12)	120.5
C(11)–C(12)–H(12A)	120.1	C(11)–C(12)–C(13)	119.9(3)
H(12A)–C(12)–C(13)	120.1	O(3)–C(13)–C(12)	125.2(3)
O(3)–C(13)–C(14)	114.9(3)	C(12)–C(13)–C(14)	119.9(3)
C(13)–C(14)–H(14A)	119.6	C(13)–C(14)–C(15)	120.8(3)
H(14A)–C(14)–C(15)	119.6	C(10)–C(15)–C(14)	118.4(3)
C(10)–C(15)–H(15A)	120.8	C(14)–C(15)–H(15A)	120.8
O(3)–C(16)–H(16A)	109.5	O(3)–C(16)–H(16B)	109.5
O(3)–C(16)–H(16C)	109.5	H(16A)–C(16)–H(16B)	109.5
H(16A)–C(16)–H(16C)	109.5	H(16B)–C(16)–H(16C)	109.5
F(1)–C(17)–F(2)	106.3(3)	F(1)–C(17)–F(3)	106.0(3)
F(1)–C(17)–C(18)	110.4(3)	F(2)–C(17)–F(3)	107.4(3)
F(2)–C(17)–C(18)	112.1(3)	F(3)–C(17)–C(18)	114.1(3)
O(4)–C(18)–O(5)	127.4(3)	O(4)–C(18)–C(17)	116.1(3)
O(5)–C(18)–C(17)	116.4(3)	H(20A)–C(20)–H(20B)	109.5
H(20A)–C(20)–H(20C)	109.5	H(20A)–C(20)–C(19)	109.5
H(20B)–C(20)–H(20C)	109.5	H(20B)–C(20)–C(19)	109.5
H(20C)–C(20)–C(19)	109.5	H(20D)–C(20A)–H(20E)	109.5
H(20D)–C(20A)–H(20F)	109.5	H(20D)–C(20A)–C(19)	109.5
H(20E)–C(20A)–H(20F)	109.5	H(20E)–C(20A)–C(19)	109.5
H(20F)–C(20A)–C(19)	109.5	O(7)–C(19)–O(6)	124.0(5)
O(7)–C(19)–C(20)	116.5(5)	O(7)–C(19)–O(6A)	79.8(10)
O(7)–C(19)–C(20A)	149(3)	O(7)–C(19)–O(7A)	15.5(18)
O(6)–C(19)–C(20)	119.5(6)	O(6)–C(19)–O(6A)	44.4(8)
O(6)–C(19)–C(20A)	87(3)	O(6)–C(19)–O(7A)	139.2(17)
C(20)–C(19)–O(6A)	162.9(11)	C(20)–C(19)–C(20A)	33(4)
C(20)–C(19)–O(7A)	101.1(18)	O(6A)–C(19)–C(20A)	130(4)
O(6A)–C(19)–O(7A)	94.8(18)	C(20A)–C(19)–O(7A)	133(3)

Table 10. Anisotropic displacement parameters (Å^2) for **192**. The anisotropic displacement factor exponent takes the form: $-2\pi^2[h^2a^{*2}U^{11} + ...+ 2hka^*b^*U^{12}]$

	U^{11}	U^{22}	U^{33}	U^{23}	U^{13}	U^{12}
I(1)	0.02970(13)	0.02115(13)	0.02352(13)	0.00311(9)	0.01367(10)	0.00133(8)
O(1)	0.0294(12)	0.0331(13)	0.0257(14)	−0.0038(11)	0.0136(11)	0.0018(10)
O(2)	0.0224(12)	0.0465(16)	0.0387(16)	−0.0038(12)	0.0117(12)	−0.0012(11)
O(3)	0.0325(13)	0.0262(13)	0.0417(16)	0.0126(12)	0.0032(12)	0.0001(10)
O(4)	0.077(2)	0.0382(16)	0.056(2)	0.0207(14)	0.0510(18)	0.0219(15)
O(5)	0.0555(17)	0.0331(14)	0.0497(18)	0.0110(13)	0.0363(15)	0.0157(12)
F(1)	0.115(2)	0.0559(17)	0.0470(18)	0.0121(14)	−0.0241(18)	0.0092(16)
F(2)	0.0636(17)	0.0449(15)	0.133(3)	0.0413(17)	0.0473(19)	0.0005(13)
F(3)	0.128(3)	0.0395(14)	0.081(2)	0.0216(14)	0.073(2)	0.0394(16)
C(1)	0.0270(16)	0.0182(16)	0.0217(17)	0.0039(13)	0.0138(14)	−0.0013(13)
C(2)	0.0192(15)	0.0243(17)	0.0234(18)	0.0011(14)	0.0062(14)	0.0009(13)
C(3)	0.0245(16)	0.0222(16)	0.0200(17)	−0.0026(13)	0.0052(14)	−0.0012(13)
C(4)	0.0242(16)	0.0167(15)	0.0246(18)	0.0052(13)	0.0118(14)	−0.0006(12)
C(5)	0.0221(16)	0.0246(17)	0.0251(18)	0.0034(14)	0.0065(14)	−0.0033(13)
C(6)	0.0278(17)	0.0217(17)	0.0206(17)	0.0019(14)	0.0063(14)	−0.0055(13)
C(7)	0.0258(17)	0.0221(17)	0.0285(19)	0.0053(14)	0.0119(15)	0.0024(13)
C(8)	0.0362(19)	0.037(2)	0.030(2)	−0.0002(16)	0.0184(17)	0.0052(16)
C(9)	0.046(2)	0.036(2)	0.059(3)	0.004(2)	0.028(2)	0.0123(18)
C(10)	0.0275(16)	0.0194(16)	0.0211(17)	0.0026(13)	0.0124(14)	0.0021(13)
C(11)	0.0249(16)	0.0267(18)	0.0260(19)	0.0026(15)	0.0049(15)	−0.0008(14)
C(12)	0.0268(17)	0.0216(17)	0.031(2)	0.0014(15)	0.0097(15)	−0.0043(13)
C(13)	0.0214(15)	0.0231(17)	0.0278(19)	0.0046(14)	0.0094(14)	0.0028(13)
C(14)	0.0231(16)	0.0291(18)	0.0280(19)	0.0022(15)	0.0039(15)	

−0.0005(14)						
C(15)	0.0274(17)	0.0235(17)	0.0283(19)	−0.0009(15)	0.0102(15)	
−0.0054(14)						
C(16)	0.038(2)	0.0245(19)	0.057(3)	0.0147(19)	0.011(2)	
−0.0006(16)						
C(17)	0.039(2)	0.0290(19)	0.029(2)	0.0027(16)	0.0155(17)	
	0.0017(16)					
C(18)	0.0301(17)	0.0214(17)	0.0252(19)	0.0026(14)	0.0090(16)	
−0.0020(14)						
O(7)	0.045(3)	0.046(4)	0.037(4)	0.009(3)	0.020(2)	0.013(2)
O(6)	0.040(2)	0.056(3)	0.054(4)	−0.010(3)	0.002(2)	−0.008(2)
C(20)	0.055(4)	0.043(5)	0.058(4)	0.017(3)	0.028(3)	0.015(3)
O(6A)	0.049(9)	0.041(9)	0.048(11)	−0.002(8)	0.021(7)	−0.020(6)
C(20A)	0.37(9)	0.05(2)	0.58(13)	−0.05(5)	0.44(11)	−0.01(4)
O(7A)	0.31(5)	0.032(11)	0.037(13)	−0.008(9)	−0.01(2)	−0.041(18)
C(19)	0.042(2)	0.037(2)	0.057(3)	0.023(2)	0.010(2)	0.0015(19)

Table 11. Hydrogen coordinates and isotropic displacement parameters ($Å^2$) for **192**.

	x	y	z	U
H(2A)	1.5857	−0.0612	0.1384	0.027
H(3A)	1.7593	−0.1228	0.0319	0.027
H(5A)	2.1868	−0.0207	0.2784	0.029
H(6A)	2.0140	0.0385	0.3867	0.028
H(8A)	2.2287	−0.2012	−0.0591	0.039
H(8B)	2.0544	−0.2172	−0.1568	0.039
H(9A)	2.1645	−0.4136	−0.1197	0.067
H(9B)	1.9830	−0.4059	−0.0963	0.067
H(9C)	2.1581	−0.3901	0.0002	0.067
H(11A)	1.7740	0.3212	0.3795	0.032
H(12A)	1.7110	0.5003	0.2859	0.032
H(14A)	1.2855	0.3149	0.0834	0.033
H(15A)	1.3475	0.1361	0.1761	0.032
H(16A)	1.4989	0.6967	0.0917	0.060
H(16B)	1.6635	0.6141	0.1314	0.060
H(16C)	1.5669	0.6673	0.2138	0.060
H(20A)	1.2548	0.6217	0.2572	0.073
H(20B)	1.3306	0.6169	0.3833	0.073
H(20C)	1.3230	0.7487	0.3325	0.073
H(20D)	1.3165	0.6628	0.3054	0.411
H(20E)	1.1622	0.6937	0.2044	0.411
H(20F)	1.1730	0.5554	0.2441	0.411

Compound **193**

Table 12. Crystal data and structure refinement for **193**.

Identification code	mac116	
Chemical formula (moiety)	$C_{15}H_{12}F_3IO_4S$	
Chemical formula (total)	$C_{15}H_{12}F_3IO_4S$	
Formula weight	472.21	
Temperature	150(2) K	
Radiation, wavelength	MoKα, 0.71073 Å	
Crystal system, space group	triclinic, $P\bar{1}$	
Unit cell parameters	a = 8.0310(4) Å	α = 113.271(6)°
	b = 9.7726(6) Å	β = 93.574(5)°
	c = 11.7901(7) Å	γ = 100.238(5)°
Cell volume	827.48(8) Å^3	
Z	2	
Calculated density	1.895 g/cm^3	
Absorption coefficient μ	2.109 mm^{-1}	
F(000)	460	
Reflections for cell refinement	2826 (θ range 3.0 to 28.5°)	
Data collection method	Xcalibur, Atlas, Gemini ultra thick-slice ω scans	
θ range for data collection	3.0 to 28.5°	
Index ranges	h –10 to 8, k –12 to 10, l –14 to 15	
Completeness to θ = 25.0°	99.8 %	
Reflections collected	6081	
Independent reflections	3430 (R_{int} = 0.0431)	
Reflections with $F^2>2\sigma$	3153	
Absorption correction	semi-empirical from equivalents	
Min. and max. transmission	0.72417 and 1.00000	
Structure solution	direct methods	
Refinement method	Full-matrix least-squares on F^2	
Weighting parameters a, b	0.0324, 0.9665	
Data / restraints / parameters	3430 / 0 / 218	
Final R indices [$F^2>2\sigma$]	R1 = 0.0326, wR2 = 0.0749	
R indices (all data)	R1 = 0.0376, wR2 = 0.0815	
Goodness-of-fit on F^2	1.084	
Largest and mean shift/su	0.001 and 0.000	
Largest diff. peak and hole	0.97 and –0.97 e Å^{-3}	

Table 13. Atomic coordinates and equivalent isotropic displacement parameters ($Å^2$) for **193**. U_{eq} is defined as one third of the trace of the orthogonalized U^{ij} tensor.

	x	y	z	U_{eq}
I	0.73610(2)	0.80544(2)	0.38224(2)	0.01508(9)
S	0.81437(14)	0.55660(13)	0.11302(11)	0.0303(2)
O(1)	−0.0214(3)	0.2790(3)	0.3125(3)	0.0229(6)
O(2)	−0.1252(3)	0.4901(3)	0.3669(3)	0.0254(6)
O(3)	0.6873(3)	0.8989(3)	0.6188(3)	0.0226(6)
O(4)	0.9490(3)	1.0401(3)	0.6466(3)	0.0261(6)
F(1)	0.7599(4)	1.1603(4)	0.8703(3)	0.0566(9)
F(2)	0.9842(3)	1.0770(4)	0.8853(3)	0.0429(7)
F(3)	0.7411(4)	0.9326(3)	0.8546(3)	0.0480(8)
C(1)	−0.2850(6)	0.1564(6)	0.1661(5)	0.0367(11)
C(2)	−0.1949(5)	0.1897(5)	0.2922(4)	0.0233(9)
C(3)	−0.0067(4)	0.4275(4)	0.3473(4)	0.0177(8)
C(4)	0.1723(4)	0.5124(4)	0.3598(4)	0.0158(7)
C(5)	0.3123(4)	0.4440(4)	0.3522(4)	0.0181(8)
C(6)	0.4748(5)	0.5275(4)	0.3615(4)	0.0185(8)
C(7)	0.4932(4)	0.6785(4)	0.3771(3)	0.0146(7)
C(8)	0.3570(5)	0.7481(4)	0.3857(4)	0.0203(8)
C(9)	0.1961(5)	0.6640(4)	0.3768(4)	0.0197(8)
C(10)	0.7191(5)	0.7031(4)	0.1891(4)	0.0202(8)
C(11)	0.6331(5)	0.7477(5)	0.1084(4)	0.0227(8)
C(12)	0.6508(6)	0.6574(5)	−0.0164(4)	0.0329(10)
C(13)	0.7436(5)	0.5518(5)	−0.0279(4)	0.0321(10)
C(14)	0.8244(4)	0.9871(4)	0.6821(4)	0.0160(7)
C(15)	0.8284(5)	1.0392(5)	0.8240(4)	0.0220(8)

Table 14. Bond lengths [Å] and angles [°] for **193**.

I–C(7)	2.101(3)	I–C(10)	2.078(4)
S–C(10)	1.703(4)	S–C(13)	1.702(5)
O(1)–C(2)	1.457(4)	O(1)–C(3)	1.323(4)
O(2)–C(3)	1.206(4)	O(3)–C(14)	1.251(4)
O(4)–C(14)	1.218(4)	F(1)–C(15)	1.327(5)
F(2)–C(15)	1.318(5)	F(3)–C(15)	1.332(5)
C(1)–H(1A)	0.980	C(1)–H(1B)	0.980
C(1)–H(1C)	0.980	C(1)–C(2)	1.496(6)
C(2)–H(2A)	0.990	C(2)–H(2B)	0.990
C(3)–C(4)	1.494(5)	C(4)–C(5)	1.396(5)
C(4)–C(9)	1.390(5)	C(5)–H(5)	0.950
C(5)–C(6)	1.383(5)	C(6)–H(6)	0.950
C(6)–C(7)	1.392(5)	C(7)–C(8)	1.376(5)
C(8)–H(8)	0.950	C(8)–C(9)	1.376(5)
C(9)–H(9)	0.950	C(10)–C(11)	1.388(5)
C(11)–H(11)	0.950	C(11)–C(12)	1.416(6)
C(12)–H(12)	0.950	C(12)–C(13)	1.347(7)
C(13)–H(13)	0.950	C(14)–C(15)	1.541(5)

C(7)–I–C(10)	91.97(14)	C(10)–S–C(13)	91.5(2)
C(2)–O(1)–C(3)	115.7(3)	H(1A)–C(1)–H(1B)	109.5
H(1A)–C(1)–H(1C)	109.5	H(1A)–C(1)–C(2)	109.5
H(1B)–C(1)–H(1C)	109.5	H(1B)–C(1)–C(2)	109.5
H(1C)–C(1)–C(2)	109.5	O(1)–C(2)–C(1)	110.8(3)
O(1)–C(2)–H(2A)	109.5	O(1)–C(2)–H(2B)	109.5
C(1)–C(2)–H(2A)	109.5	C(1)–C(2)–H(2B)	109.5
H(2A)–C(2)–H(2B)	108.1	O(1)–C(3)–O(2)	124.0(3)
O(1)–C(3)–C(4)	113.5(3)	O(2)–C(3)–C(4)	122.4(3)
C(3)–C(4)–C(5)	122.4(3)	C(3)–C(4)–C(9)	117.4(3)
C(5)–C(4)–C(9)	120.1(3)	C(4)–C(5)–H(5)	120.1
C(4)–C(5)–C(6)	119.9(3)	H(5)–C(5)–C(6)	120.1
C(5)–C(6)–H(6)	120.8	C(5)–C(6)–C(7)	118.3(3)
H(6)–C(6)–C(7)	120.8	I–C(7)–C(6)	119.4(2)
I–C(7)–C(8)	117.9(3)	C(6)–C(7)–C(8)	122.6(3)
C(7)–C(8)–H(8)	120.8	C(7)–C(8)–C(9)	118.4(3)
H(8)–C(8)–C(9)	120.8	C(4)–C(9)–C(8)	120.6(3)
C(4)–C(9)–H(9)	119.7	C(8)–C(9)–H(9)	119.7
I–C(10)–S	123.1(2)	I–C(10)–C(11)	124.3(3)
S–C(10)–C(11)	112.7(3)	C(10)–C(11)–H(11)	125.1
C(10)–C(11)–C(12)	109.7(4)	H(11)–C(11)–C(12)	125.1
C(11)–C(12)–H(12)	122.9	C(11)–C(12)–C(13)	114.2(4)
H(12)–C(12)–C(13)	122.9	S–C(13)–C(12)	111.8(3)
S–C(13)–H(13)	124.1	C(12)–C(13)–H(13)	124.1
O(3)–C(14)–O(4)	128.8(4)	O(3)–C(14)–C(15)	113.9(3)
O(4)–C(14)–C(15)	117.2(3)	F(1)–C(15)–F(2)	107.3(4)
F(1)–C(15)–F(3)	106.9(3)	F(1)–C(15)–C(14)	110.1(3)

F(2)–C(15)–F(3)	105.7(3)	F(2)–C(15)–C(14)	113.2(3)
F(3)–C(15)–C(14)	113.2(3)		

Table 15. Anisotropic displacement parameters (Å^2) for **193**. The anisotropic displacement factor exponent takes the form: $-2\pi^2[h^2a^{*2}U^{11} + ...+ 2hka^*b^*U^{12}]$

	U^{11}	U^{22}	U^{33}	U^{23}	U^{13}	U^{12}
I	0.01236(14)	0.01063(14)	0.02036(15)	0.00567(11)	0.00207(9)	−0.00022(9)
S	0.0331(6)	0.0274(6)	0.0271(6)	0.0062(5)	0.0075(4)	0.0097(5)
O(1)	0.0136(13)	0.0148(14)	0.0391(18)	0.0118(13)	0.0027(11)	−0.0013(10)
O(2)	0.0147(13)	0.0178(15)	0.0408(19)	0.0092(14)	0.0060(12)	0.0024(11)
O(3)	0.0160(13)	0.0224(15)	0.0245(16)	0.0080(13)	0.0004(11)	−0.0032(11)
O(4)	0.0209(14)	0.0252(16)	0.0305(17)	0.0134(14)	0.0055(11)	−0.0043(11)
F(1)	0.085(2)	0.054(2)	0.0331(18)	0.0062(15)	0.0167(16)	0.0450(18)
F(2)	0.0293(14)	0.063(2)	0.0269(15)	0.0148(14)	−0.0044(11)	−0.0024(13)
F(3)	0.0568(18)	0.0474(19)	0.0294(16)	0.0179(14)	0.0073(13)	−0.0194(14)
C(1)	0.028(2)	0.031(3)	0.041(3)	0.011(2)	−0.009(2)	−0.0048(19)
C(2)	0.0165(18)	0.016(2)	0.036(2)	0.0117(18)	0.0012(16)	−0.0026(15)
C(3)	0.0148(18)	0.016(2)	0.022(2)	0.0093(17)	0.0016(14)	−0.0001(14)
C(4)	0.0152(17)	0.0122(19)	0.0187(19)	0.0059(16)	0.0011(13)	0.0013(14)
C(5)	0.0177(18)	0.0113(19)	0.024(2)	0.0075(16)	0.0005(14)	0.0011(14)
C(6)	0.0164(18)	0.0133(19)	0.025(2)	0.0070(17)	0.0034(14)	0.0030(14)
C(7)	0.0095(16)	0.0157(19)	0.0152(18)	0.0048(15)	0.0011(13)	−0.0018(13)
C(8)	0.0232(19)	0.0095(19)	0.028(2)	0.0066(17)	0.0036(15)	0.0044(15)
C(9)	0.0166(18)	0.019(2)	0.025(2)	0.0093(17)	0.0052(15)	0.0059(15)
C(10)	0.0169(18)	0.014(2)	0.023(2)	0.0044(17)	0.0052(15)	−0.0032(14)
C(11)	0.024(2)	0.019(2)	0.024(2)	0.0087(18)	0.0028(15)	0.0013(16)
C(12)	0.034(2)	0.036(3)	0.025(2)	0.015(2)	−0.0009(18)	−0.006(2)
C(13)	0.030(2)	0.031(3)	0.022(2)	0.001(2)	0.0076(17)	

−0.0033(19)					
C(14)	0.0174(18)	0.0075(18)	0.023(2)	0.0068(16)	0.0023(14)
	0.0020(14)				
C(15)	0.0177(19)	0.020(2)	0.024(2)	0.0054(17)	0.0038(15)
	0.0012(15)				

Table 15. Hydrogen coordinates and isotropic displacement parameters ($Å^2$) for **193**.

	x	y	z	U
H(1A)	−0.4030	0.1006	0.1559	0.055
H(1B)	−0.2255	0.0942	0.1015	0.055
H(1C)	−0.2854	0.2525	0.1584	0.055
H(2A)	−0.2590	0.2469	0.3573	0.028
H(2B)	−0.1910	0.0925	0.2990	0.028
H(5)	0.2959	0.3404	0.3406	0.022
H(6)	0.5714	0.4829	0.3574	0.022
H(8)	0.3737	0.8519	0.3976	0.024
H(9)	0.1004	0.7100	0.3823	0.024
H(11)	0.5716	0.8268	0.1330	0.027
H(12)	0.6014	0.6701	−0.0859	0.039
H(13)	0.7669	0.4829	−0.1054	0.039

Table 16. Torsion angles [°] for **193**.

C(3)–O(1)–C(2)–C(1)	80.9(4)	C(2)–O(1)–C(3)–O(2)	3.1(5)
C(2)–O(1)–C(3)–C(4)	−176.7(3)	O(1)–C(3)–C(4)–C(5)	−8.3(5)
O(1)–C(3)–C(4)–C(9)	170.2(3)	O(2)–C(3)–C(4)–C(5)	171.9(4)
O(2)–C(3)–C(4)–C(9)	−9.6(6)	C(3)–C(4)–C(5)–C(6)	178.4(4)
C(9)–C(4)–C(5)–C(6)	0.0(6)	C(4)–C(5)–C(6)–C(7)	−0.7(6)
C(5)–C(6)–C(7)–I	−176.8(3)	C(5)–C(6)–C(7)–C(8)	1.2(6)
C(10)–I–C(7)–C(6)	79.1(3)	C(10)–I–C(7)–C(8)	−99.0(3)
I–C(7)–C(8)–C(9)	177.1(3)	C(6)–C(7)–C(8)–C(9)	−0.9(6)
C(7)–C(8)–C(9)–C(4)	0.2(6)	C(3)–C(4)–C(9)–C(8)	−178.3(4)
C(5)–C(4)–C(9)–C(8)	0.3(6)	C(13)–S–C(10)–I	−178.3(2)
C(13)–S–C(10)–C(11)	0.4(3)	C(7)–I–C(10)–S	−99.7(2)
C(7)–I–C(10)–C(11)	81.7(3)	I–C(10)–C(11)–C(12)	178.3(3)
S–C(10)–C(11)–C(12)	−0.4(4)	C(10)–C(11)–C(12)–C(13)	0.2(5)
C(11)–C(12)–C(13)–S	0.1(5)	C(10)–S–C(13)–C(12)	−0.3(3)
O(3)–C(14)–C(15)–F(1)	−85.8(4)	O(3)–C(14)–C(15)–F(2)	154.1(3)
O(3)–C(14)–C(15)–F(3)	33.8(5)	O(4)–C(14)–C(15)–F(1)	91.5(4)
O(4)–C(14)–C(15)–F(2)	−28.6(5)	O(4)–C(14)–C(15)–F(3)	−149.0(3)

Compound **194**

Table 17. Crystal data and structure refinement for **194**.

Identification code	mac124	
Chemical formula (moiety)	$C_{15}H_{14}O_2I^+ \cdot C_2O_2F_3^-$	
Chemical formula (total)	$C_{17}H_{14}F_3IO_4$	
Formula weight	466.18	
Temperature	150(2) K	
Radiation, wavelength	MoKα, 0.71073 Å	
Crystal system, space group	monoclinic, $P12_1/n1$	
Unit cell parameters	a = 12.5807(8) Å	α = 90°
	b = 13.1447(9) Å	β = 94.017(5)°
	c = 20.9719(12) Å	γ = 90°
Cell volume	3459.6(4) Å^3	
Z	8	
Calculated density	1.790 g/cm^3	
Absorption coefficient μ	1.901 mm^{-1}	
F(000)	1824	
Reflections for cell refinement	7630 (θ range 2.9 to 28.6°)	
Data collection method	Xcalibur, Atlas, Gemini ultra thick-slice ω scans	
θ range for data collection	2.9 to 28.6°	
Index ranges	h –12 to 15, k –14 to 17, l –27 to 25	
Completeness to θ = 25.0°	99.8 %	
Reflections collected	20543	
Independent reflections	7542 (R_{int} = 0.0267)	
Reflections with $F^2>2\sigma$	6420	
Absorption correction	semi-empirical from equivalents	
Min. and max. transmission	0.61754 and 1.00000	
Structure solution	direct methods	
Refinement method	Full-matrix least-squares on F^2	
Weighting parameters a, b	0.0274, 5.9644	
Data / restraints / parameters	7542 / 0 / 454	
Final R indices [$F^2>2\sigma$]	R1 = 0.0315, wR2 = 0.0687	
R indices (all data)	R1 = 0.0423, wR2 = 0.0761	
Goodness-of-fit on F^2	1.084	
Extinction coefficient	0.00007(5)	
Largest and mean shift/su	0.003 and 0.000	
Largest diff. peak and hole	1.01 and –1.31 e Å^{-3}	

Table 18. Atomic coordinates and equivalent isotropic displacement parameters ($Å^2$) for **194**. U_{eq} is defined as one third of the trace of the orthogonalized U^{ij} tensor.

	x	y	z	U_{eq}
I(1)	0.488259(17)	0.822233(18)	0.523213(10)	0.02655(7)
I(2)	0.449177(16)	0.855849(16)	0.742365(9)	0.01983(7)
O(1)	0.7817(2)	0.45106(19)	0.41336(11)	0.0319(6)
O(2)	0.6211(2)	0.4292(2)	0.45157(13)	0.0387(6)
O(3)	–0.03025(18)	0.99071(17)	0.82795(10)	0.0230(5)
O(4)	0.08344(19)	1.08579(18)	0.77586(11)	0.0281(5)
O(5)	0.2973(3)	0.9085(3)	0.53160(15)	0.0767(13)
O(6)	0.3347(2)	0.9417(3)	0.63416(13)	0.0534(8)
O(7)	0.66103(19)	0.8773(2)	0.73395(10)	0.0296(6)
O(8)	0.6267(2)	0.8321(2)	0.63232(12)	0.0418(7)
F(1)	0.1005(3)	0.9006(3)	0.6052(2)	0.1198(17)
F(2)	0.1536(3)	1.0467(3)	0.63083(15)	0.0925(13)
F(3)	0.1186(2)	1.0103(2)	0.53511(12)	0.0588(7)
F(4)	0.8050(2)	0.9440(2)	0.61181(12)	0.0623(8)
F(5)	0.8509(2)	0.8028(3)	0.65070(18)	0.0828(10)
F(6)	0.8539(2)	0.9351(4)	0.70921(13)	0.0991(14)
C(1)	0.8851(4)	0.3323(3)	0.3601(2)	0.0474(11)
C(2)	0.7792(3)	0.3483(3)	0.38760(18)	0.0373(9)
C(3)	0.6959(3)	0.4824(3)	0.44255(15)	0.0260(7)
C(4)	0.7057(3)	0.5914(3)	0.46166(14)	0.0229(7)
C(5)	0.6160(3)	0.6407(3)	0.48116(14)	0.0227(7)
C(6)	0.6242(3)	0.7427(3)	0.49677(15)	0.0240(7)
C(7)	0.7191(3)	0.7956(3)	0.49549(16)	0.0282(8)
C(8)	0.8079(3)	0.7451(3)	0.47704(18)	0.0354(9)
C(9)	0.8015(3)	0.6434(3)	0.45953(17)	0.0301(8)
C(10)	0.4179(3)	0.8174(3)	0.42940(15)	0.0221(7)
C(11)	0.4409(3)	0.8945(3)	0.38777(17)	0.0320(8)
C(12)	0.3955(3)	0.8899(3)	0.32583(18)	0.0351(9)
C(13)	0.3287(3)	0.8105(3)	0.30680(17)	0.0305(8)
C(14)	0.3077(3)	0.7340(3)	0.34935(16)	0.0289(8)
C(15)	0.3529(3)	0.7368(3)	0.41150(15)	0.0245(7)
C(16)	–0.1992(3)	1.0483(3)	0.85958(19)	0.0353(9)
C(17)	–0.0952(3)	1.0812(3)	0.83528(17)	0.0289(8)
C(18)	0.0576(3)	1.0048(2)	0.79795(13)	0.0192(6)
C(19)	0.1255(2)	0.9123(2)	0.79522(14)	0.0192(6)
C(20)	0.2267(2)	0.9230(3)	0.77307(14)	0.0208(7)
C(21)	0.2919(3)	0.8393(2)	0.77197(14)	0.0197(7)
C(22)	0.2600(3)	0.7443(3)	0.79204(15)	0.0231(7)
C(23)	0.1588(3)	0.7343(3)	0.81369(16)	0.0260(7)
C(24)	0.0922(3)	0.8176(2)	0.81568(15)	0.0216(7)
C(25)	0.5173(2)	0.8144(3)	0.83308(14)	0.0205(7)
C(26)	0.5303(3)	0.7123(3)	0.84746(16)	0.0268(7)
C(27)	0.5725(3)	0.6858(3)	0.90816(18)	0.0358(9)

C(28)	0.6000(3)	0.7596(4)	0.95222(17)	0.0402(10)
C(29)	0.5876(3)	0.8612(4)	0.93703(17)	0.0395(10)
C(30)	0.5460(3)	0.8901(3)	0.87653(16)	0.0290(8)
C(31)	0.2772(3)	0.9372(3)	0.58487(16)	0.0264(7)
C(32)	0.1620(3)	0.9738(3)	0.58926(17)	0.0300(8)
C(33)	0.6838(3)	0.8634(2)	0.67806(15)	0.0227(7)
C(34)	0.7993(3)	0.8872(3)	0.66339(17)	0.0354(9)

Table 19. Bond lengths [Å] and angles [°] for **194**.

I(1)–C(6)	2.112(3)	I(1)–C(10)	2.101(3)
I(2)–C(21)	2.125(3)	I(2)–C(25)	2.103(3)
O(1)–C(2)	1.454(4)	O(1)–C(3)	1.343(4)
O(2)–C(3)	1.198(4)	O(3)–C(17)	1.457(4)
O(3)–C(18)	1.322(4)	O(4)–C(18)	1.215(4)
O(5)–C(31)	1.222(4)	O(6)–C(31)	1.221(4)
O(7)–C(33)	1.240(4)	O(8)–C(33)	1.229(4)
F(1)–C(32)	1.294(5)	F(2)–C(32)	1.304(4)
F(3)–C(32)	1.316(4)	F(4)–C(34)	1.321(4)
F(5)–C(34)	1.321(5)	F(6)–C(34)	1.304(4)
C(1)–H(1A)	0.980	C(1)–H(1B)	0.980
C(1)–H(1C)	0.980	C(1)–C(2)	1.504(6)
C(2)–H(2A)	0.990	C(2)–H(2B)	0.990
C(3)–C(4)	1.490(5)	C(4)–C(5)	1.388(5)
C(4)–C(9)	1.389(5)	C(5)–H(5A)	0.950
C(5)–C(6)	1.382(5)	C(6)–C(7)	1.383(5)
C(7)–H(7A)	0.950	C(7)–C(8)	1.378(5)
C(8)–H(8A)	0.950	C(8)–C(9)	1.387(5)
C(9)–H(9A)	0.950	C(10)–C(11)	1.381(5)
C(10)–C(15)	1.374(5)	C(11)–H(11A)	0.950
C(11)–C(12)	1.383(5)	C(12)–H(12A)	0.950
C(12)–C(13)	1.381(5)	C(13)–H(13A)	0.950
C(13)–C(14)	1.382(5)	C(14)–H(14A)	0.950
C(14)–C(15)	1.386(5)	C(15)–H(15A)	0.950
C(16)–H(16A)	0.980	C(16)–H(16B)	0.980
C(16)–H(16C)	0.980	C(16)–C(17)	1.500(5)
C(17)–H(17A)	0.990	C(17)–H(17B)	0.990
C(18)–C(19)	1.490(4)	C(19)–C(20)	1.392(4)
C(19)–C(24)	1.391(4)	C(20)–H(20A)	0.950
C(20)–C(21)	1.374(5)	C(21)–C(22)	1.387(5)
C(22)–H(22A)	0.950	C(22)–C(23)	1.388(5)
C(23)–H(23A)	0.950	C(23)–C(24)	1.380(5)
C(24)–H(24A)	0.950	C(25)–C(26)	1.382(5)
C(25)–C(30)	1.380(5)	C(26)–H(26A)	0.950
C(26)–C(27)	1.389(5)	C(27)–H(27A)	0.950
C(27)–C(28)	1.367(6)	C(28)–H(28A)	0.950
C(28)–C(29)	1.379(6)	C(29)–H(29A)	0.950
C(29)–C(30)	1.391(5)	C(30)–H(30A)	0.950
C(31)–C(32)	1.536(5)	C(33)–C(34)	1.538(5)

C(6)–I(1)–C(10)	92.02(12)	C(21)–I(2)–C(25)	92.17(12)
C(2)–O(1)–C(3)	117.2(3)	C(17)–O(3)–C(18)	115.5(3)
H(1A)–C(1)–H(1B)	109.5	H(1A)–C(1)–H(1C)	109.5
H(1A)–C(1)–C(2)	109.5	H(1B)–C(1)–H(1C)	109.5
H(1B)–C(1)–C(2)	109.5	H(1C)–C(1)–C(2)	109.5
O(1)–C(2)–C(1)	106.0(3)	O(1)–C(2)–H(2A)	110.5

O(1)–C(2)–H(2B)	110.5	C(1)–C(2)–H(2A)	110.5
C(1)–C(2)–H(2B)	110.5	H(2A)–C(2)–H(2B)	108.7
O(1)–C(3)–O(2)	123.9(3)	O(1)–C(3)–C(4)	111.3(3)
O(2)–C(3)–C(4)	124.8(3)	C(3)–C(4)–C(5)	118.4(3)
C(3)–C(4)–C(9)	121.4(3)	C(5)–C(4)–C(9)	120.3(3)
C(4)–C(5)–H(5A)	120.8	C(4)–C(5)–C(6)	118.3(3)
H(5A)–C(5)–C(6)	120.8	I(1)–C(6)–C(5)	119.6(2)
I(1)–C(6)–C(7)	118.2(3)	C(5)–C(6)–C(7)	122.2(3)
C(6)–C(7)–H(7A)	120.6	C(6)–C(7)–C(8)	118.8(3)
H(7A)–C(7)–C(8)	120.6	C(7)–C(8)–H(8A)	119.8
C(7)–C(8)–C(9)	120.3(4)	H(8A)–C(8)–C(9)	119.8
C(4)–C(9)–C(8)	120.1(3)	C(4)–C(9)–H(9A)	120.0
C(8)–C(9)–H(9A)	120.0	I(1)–C(10)–C(11)	118.5(3)
I(1)–C(10)–C(15)	118.8(2)	C(11)–C(10)–C(15)	122.7(3)
C(10)–C(11)–H(11A)	121.0	C(10)–C(11)–C(12)	118.1(3)
H(11A)–C(11)–C(12)	121.0	C(11)–C(12)–H(12A)	119.8
C(11)–C(12)–C(13)	120.5(3)	H(12A)–C(12)–C(13)	119.8
C(12)–C(13)–H(13A)	119.9	C(12)–C(13)–C(14)	120.2(3)
H(13A)–C(13)–C(14)	119.9	C(13)–C(14)–H(14A)	119.9
C(13)–C(14)–C(15)	120.2(3)	H(14A)–C(14)–C(15)	119.9
C(10)–C(15)–C(14)	118.3(3)	C(10)–C(15)–H(15A)	120.8
C(14)–C(15)–H(15A)	120.8	H(16A)–C(16)–H(16B)	109.5
H(16A)–C(16)–H(16C)	109.5	H(16A)–C(16)–C(17)	109.5
H(16B)–C(16)–H(16C)	109.5	H(16B)–C(16)–C(17)	109.5
H(16C)–C(16)–C(17)	109.5	O(3)–C(17)–C(16)	108.1(3)
O(3)–C(17)–H(17A)	110.1	O(3)–C(17)–H(17B)	110.1
C(16)–C(17)–H(17A)	110.1	C(16)–C(17)–H(17B)	110.1
H(17A)–C(17)–H(17B)	108.4	O(3)–C(18)–O(4)	124.0(3)
O(3)–C(18)–C(19)	113.9(3)	O(4)–C(18)–C(19)	122.1(3)
C(18)–C(19)–C(20)	118.1(3)	C(18)–C(19)–C(24)	122.2(3)
C(20)–C(19)–C(24)	119.7(3)	C(19)–C(20)–H(20A)	120.5
C(19)–C(20)–C(21)	119.0(3)	H(20A)–C(20)–C(21)	120.5
I(2)–C(21)–C(20)	119.5(2)	I(2)–C(21)–C(22)	118.4(2)
C(20)–C(21)–C(22)	122.0(3)	C(21)–C(22)–H(22A)	120.8
C(21)–C(22)–C(23)	118.4(3)	H(22A)–C(22)–C(23)	120.8
C(22)–C(23)–H(23A)	119.7	C(22)–C(23)–C(24)	120.5(3)
H(23A)–C(23)–C(24)	119.7	C(19)–C(24)–C(23)	120.2(3)
C(19)–C(24)–H(24A)	119.9	C(23)–C(24)–H(24A)	119.9
I(2)–C(25)–C(26)	118.9(2)	I(2)–C(25)–C(30)	118.8(3)
C(26)–C(25)–C(30)	122.3(3)	C(25)–C(26)–H(26A)	120.8
C(25)–C(26)–C(27)	118.4(3)	H(26A)–C(26)–C(27)	120.8
C(26)–C(27)–H(27A)	119.9	C(26)–C(27)–C(28)	120.2(4)
H(27A)–C(27)–C(28)	119.9	C(27)–C(28)–H(28A)	119.6
C(27)–C(28)–C(29)	120.8(3)	H(28A)–C(28)–C(29)	119.6
C(28)–C(29)–H(29A)	119.9	C(28)–C(29)–C(30)	120.3(4)
H(29A)–C(29)–C(30)	119.9	C(25)–C(30)–C(29)	118.0(4)
C(25)–C(30)–H(30A)	121.0	C(29)–C(30)–H(30A)	121.0
O(5)–C(31)–O(6)	129.8(4)	O(5)–C(31)–C(32)	114.1(3)

O(6)–C(31)–C(32)	116.1(3)	F(1)–C(32)–F(2)	107.2(4)
F(1)–C(32)–F(3)	105.9(4)	F(1)–C(32)–C(31)	111.5(3)
F(2)–C(32)–F(3)	105.1(3)	F(2)–C(32)–C(31)	113.1(3)
F(3)–C(32)–C(31)	113.5(3)	O(7)–C(33)–O(8)	128.8(3)
O(7)–C(33)–C(34)	116.3(3)	O(8)–C(33)–C(34)	114.9(3)
F(4)–C(34)–F(5)	104.7(3)	F(4)–C(34)–F(6)	105.9(4)
F(4)–C(34)–C(33)	112.6(3)	F(5)–C(34)–F(6)	108.3(4)
F(5)–C(34)–C(33)	110.7(3)	F(6)–C(34)–C(33)	114.0(3)

Table 20. Anisotropic displacement parameters ($Å^2$) for **194**. The anisotropic displacement factor exponent takes the form: $-2\pi^2[h^2a^{*2}U^{11} + ...+ 2hka^*b^*U^{12}]$

	U^{11}	U^{22}	U^{33}	U^{23}	U^{13}	U^{12}
I(1)	0.02202(13)	0.03214(13)	0.02554(12)	−0.01003(9)	0.00210(8)	0.00253(9)
I(2)	0.01593(11)	0.02448(12)	0.01913(11)	0.00202(8)	0.00151(8)	−0.00061(8)
O(1)	0.0363(15)	0.0279(13)	0.0318(13)	−0.0018(10)	0.0049(11)	0.0095(11)
O(2)	0.0334(16)	0.0313(14)	0.0519(17)	−0.0007(12)	0.0057(12)	−0.0025(13)
O(3)	0.0201(12)	0.0205(12)	0.0293(12)	−0.0016(9)	0.0066(9)	0.0017(10)
O(4)	0.0250(13)	0.0212(12)	0.0386(13)	0.0061(10)	0.0051(10)	−0.0014(10)
O(5)	0.053(2)	0.133(4)	0.0428(18)	−0.035(2)	−0.0041(15)	0.052(2)
O(6)	0.0368(17)	0.092(3)	0.0304(15)	0.0068(15)	−0.0052(12)	0.0154(17)
O(7)	0.0221(13)	0.0477(16)	0.0192(11)	0.0041(10)	0.0017(9)	−0.0024(11)
O(8)	0.0323(15)	0.0617(19)	0.0309(14)	−0.0114(13)	−0.0001(11)	−0.0132(14)
F(1)	0.0439(19)	0.079(2)	0.242(5)	0.079(3)	0.049(2)	0.0046(18)
F(2)	0.083(2)	0.116(3)	0.075(2)	−0.060(2)	−0.0221(17)	0.063(2)
F(3)	0.0403(15)	0.087(2)	0.0478(14)	0.0036(14)	−0.0087(11)	0.0270(14)
F(4)	0.0618(18)	0.080(2)	0.0459(14)	0.0127(13)	0.0115(12)	−0.0387(16)
F(5)	0.0449(18)	0.085(2)	0.123(3)	0.014(2)	0.0405(18)	0.0208(17)
F(6)	0.0417(17)	0.211(4)	0.0454(16)	−0.044(2)	0.0100(13)	−0.066(2)
C(1)	0.060(3)	0.037(2)	0.046(2)	−0.0039(19)	0.011(2)	0.021(2)
C(2)	0.048(3)	0.0277(19)	0.035(2)	−0.0001(16)	−0.0047(18)	0.0125(18)
C(3)	0.029(2)	0.0290(19)	0.0193(15)	0.0023(13)	−0.0006(13)	0.0070(16)
C(4)	0.0223(17)	0.0275(18)	0.0189(15)	0.0011(13)	0.0007(12)	0.0046(14)
C(5)	0.0196(17)	0.0285(17)	0.0197(15)	0.0011(13)	0.0001(12)	−0.0018(14)
C(6)	0.0185(17)	0.0327(19)	0.0207(15)	−0.0030(13)	0.0012(12)	0.0023(14)
C(7)	0.0243(19)	0.0307(19)	0.0302(18)	−0.0044(15)	0.0060(14)	−0.0024(15)

C(8)	0.027(2)	0.037(2)	0.043(2)	−0.0027(17)	0.0078(16) −0.0053(17)
C(9)	0.0244(19)	0.035(2)	0.0313(18)	0.0003(15)	0.0064(14) 0.0062(16)
C(10)	0.0174(16)	0.0266(17)	0.0223(16)	−0.0047(13)	0.0019(12) 0.0049(14)
C(11)	0.037(2)	0.0219(17)	0.037(2)	−0.0054(15)	0.0048(16) −0.0019(16)
C(12)	0.045(2)	0.0246(18)	0.036(2)	0.0056(16)	0.0043(17) 0.0093(17)
C(13)	0.027(2)	0.034(2)	0.0302(18)	−0.0026(15)	0.0010(15) 0.0113(16)
C(14)	0.0174(17)	0.035(2)	0.0336(18)	−0.0054(15)	−0.0007(14) −0.0009(15)
C(15)	0.0173(17)	0.0292(18)	0.0276(17)	0.0002(14)	0.0049(13) 0.0002(14)
C(16)	0.030(2)	0.034(2)	0.043(2)	−0.0047(17)	0.0100(16) 0.0052(17)
C(17)	0.0270(19)	0.0239(18)	0.0369(19)	−0.0030(15)	0.0099(15) 0.0052(15)
C(18)	0.0211(17)	0.0211(16)	0.0150(14)	−0.0020(12)	−0.0012(12) −0.0006(13)
C(19)	0.0176(16)	0.0217(16)	0.0181(14)	−0.0013(12)	−0.0008(12) −0.0029(13)
C(20)	0.0179(16)	0.0239(17)	0.0205(15)	0.0007(13)	0.0007(12) −0.0024(13)
C(21)	0.0163(16)	0.0256(17)	0.0174(14)	−0.0015(12)	0.0014(12) −0.0012(13)
C(22)	0.0200(17)	0.0222(17)	0.0275(16)	−0.0042(13)	0.0038(13) −0.0009(14)
C(23)	0.0278(19)	0.0194(17)	0.0313(18)	0.0003(14)	0.0062(14) −0.0040(14)
C(24)	0.0188(17)	0.0227(16)	0.0236(16)	−0.0015(13)	0.0038(13) −0.0028(13)
C(25)	0.0130(15)	0.0329(18)	0.0159(14)	0.0016(13)	0.0026(11) −0.0005(14)
C(26)	0.0197(18)	0.0316(19)	0.0289(17)	0.0049(15)	−0.0002(13) −0.0042(15)
C(27)	0.0231(19)	0.050(2)	0.035(2)	0.0165(18)	0.0026(15) −0.0018(18)
C(28)	0.027(2)	0.070(3)	0.0233(18)	0.0092(18)	0.0001(15) −0.003(2)
C(29)	0.024(2)	0.069(3)	0.0251(18)	−0.0166(19)	−0.0012(15) −0.0051(19)
C(30)	0.0234(18)	0.037(2)	0.0270(17)	−0.0083(15)	0.0040(14) −0.0025(16)
C(31)	0.0275(19)	0.0242(17)	0.0273(17)	0.0013(14)	0.0011(14)

	0.0023(15)				
C(32)	0.030(2)	0.0282(19)	0.0322(19)	−0.0029(15)	0.0045(15)
	0.0044(16)				
C(33)	0.0240(18)	0.0213(16)	0.0227(16)	0.0042(13)	−0.0003(13)
	0.0010(14)				
C(34)	0.027(2)	0.052(2)	0.0276(18)	−0.0007(17)	0.0072(15)
−0.0060(19)					

Table 21. Hydrogen coordinates and isotropic displacement parameters ($Å^2$) for **194**.

	x	y	z	U
H(1A)	0.8873	0.2642	0.3412	0.071
H(1B)	0.9423	0.3388	0.3941	0.071
H(1C)	0.8949	0.3835	0.3270	0.071
H(2A)	0.7204	0.3410	0.3540	0.045
H(2B)	0.7687	0.2981	0.4218	0.045
H(5A)	0.5506	0.6053	0.4837	0.027
H(7A)	0.7230	0.8654	0.5071	0.034
H(8A)	0.8739	0.7802	0.4763	0.042
H(9A)	0.8626	0.6093	0.4461	0.036
H(11A)	0.4866	0.9491	0.4013	0.038
H(12A)	0.4104	0.9418	0.2962	0.042
H(13A)	0.2971	0.8085	0.2643	0.037
H(14A)	0.2621	0.6793	0.3359	0.035
H(15A)	0.3393	0.6844	0.4410	0.029
H(16A)	–0.2420	1.1084	0.8682	0.053
H(16B)	–0.1856	1.0092	0.8991	0.053
H(16C)	–0.2380	1.0058	0.8274	0.053
H(17A)	–0.1079	1.1162	0.7937	0.035
H(17B)	–0.0583	1.1289	0.8659	0.035
H(20A)	0.2503	0.9873	0.7589	0.025
H(22A)	0.3063	0.6873	0.7910	0.028
H(23A)	0.1351	0.6697	0.8273	0.031
H(24A)	0.0234	0.8102	0.8311	0.026
H(26A)	0.5108	0.6615	0.8166	0.032
H(27A)	0.5824	0.6161	0.9191	0.043
H(28A)	0.6280	0.7407	0.9938	0.048
H(29A)	0.6075	0.9116	0.9680	0.047
H(30A)	0.5377	0.9598	0.8654	0.035

Table 21. Torsion angles [°] for **194**.

C(3)–O(1)–C(2)–C(1)	−178.1(3)	C(2)–O(1)–C(3)–O(2)	4.4(5)
C(2)–O(1)–C(3)–C(4)	−175.3(3)	O(1)–C(3)–C(4)–C(5)	167.9(3)
O(1)–C(3)–C(4)–C(9)	−11.4(4)	O(2)–C(3)–C(4)–C(5)	−11.8(5)
O(2)–C(3)–C(4)–C(9)	169.0(3)	C(3)–C(4)–C(5)–C(6)	−177.8(3)
C(9)–C(4)–C(5)–C(6)	1.5(5)	C(4)–C(5)–C(6)–I(1)	177.6(2)
C(4)–C(5)–C(6)–C(7)	−2.1(5)	C(10)–I(1)–C(6)–C(5)	−70.6(3)
C(10)–I(1)–C(6)–C(7)	109.1(3)	I(1)–C(6)–C(7)–C(8)	−178.7(3)
C(5)–C(6)–C(7)–C(8)	1.0(5)	C(6)–C(7)–C(8)–C(9)	0.6(5)
C(7)–C(8)–C(9)–C(4)	−1.2(6)	C(3)–C(4)–C(9)–C(8)	179.4(3)
C(5)–C(4)–C(9)–C(8)	0.1(5)	C(6)–I(1)–C(10)–C(11)	−88.1(3)
C(6)–I(1)–C(10)–C(15)	90.5(3)	I(1)–C(10)–C(11)–C(12)	179.0(3)
C(15)–C(10)–C(11)–C(12)	0.5(5)	C(10)–C(11)–C(12)–C(13)	0.4(5)
C(11)–C(12)–C(13)–C(14)	−0.9(6)	C(12)–C(13)–C(14)–C(15)	0.5(5)
I(1)–C(10)–C(15)–C(14)	−179.4(2)	C(11)–C(10)–C(15)–C(14)	−0.9(5)
C(13)–C(14)–C(15)–C(10)	0.4(5)	C(18)–O(3)–C(17)–C(16)	170.3(3)
C(17)–O(3)–C(18)–O(4)	−1.9(4)	C(17)–O(3)–C(18)–C(19)	176.1(3)
O(3)–C(18)–C(19)–C(20)	−170.7(3)	O(3)–C(18)–C(19)–C(24)	7.4(4)
O(4)–C(18)–C(19)–C(20)	7.3(4)	O(4)–C(18)–C(19)–C(24)	−174.6(3)
C(18)–C(19)–C(20)–C(21)	178.1(3)	C(24)–C(19)–C(20)–C(21)	−0.1(4)
C(19)–C(20)–C(21)–I(2)	−177.2(2)	C(19)–C(20)–C(21)–C(22)	0.2(5)
C(25)–I(2)–C(21)–C(20)	115.9(3)	C(25)–I(2)–C(21)–C(22)	−61.6(3)
I(2)–C(21)–C(22)–C(23)	177.5(2)	C(20)–C(21)–C(22)–C(23)	0.1(5)
C(21)–C(22)–C(23)–C(24)	−0.6(5)	C(22)–C(23)–C(24)–C(19)	0.8(5)
C(18)–C(19)–C(24)–C(23)	−178.5(3)	C(20)–C(19)–C(24)–C(23)	−0.4(5)
C(21)–I(2)–C(25)–C(26)	84.6(3)	C(21)–I(2)–C(25)–C(30)	−94.5(3)
I(2)–C(25)–C(26)–C(27)	−178.2(3)	C(30)–C(25)–C(26)–C(27)	0.9(5)
C(25)–C(26)–C(27)–C(28)	0.2(5)	C(26)–C(27)–C(28)–C(29)	−0.8(6)
C(27)–C(28)–C(29)–C(30)	0.5(6)	I(2)–C(25)–C(30)–C(29)	177.9(3)
C(26)–C(25)–C(30)–C(29)	−1.2(5)	C(28)–C(29)–C(30)–C(25)	0.5(5)
O(5)–C(31)–C(32)–F(1)	91.5(5)	O(5)–C(31)–C(32)–F(2)	−147.6(4)
O(5)–C(31)–C(32)–F(3)	−28.0(5)	O(6)–C(31)–C(32)–F(1)	−89.0(5)
O(6)–C(31)–C(32)–F(2)	31.8(5)	O(6)–C(31)–C(32)–F(3)	151.4(4)
O(7)–C(33)–C(34)–F(4)	−131.7(3)	O(7)–C(33)–C(34)–F(5)	111.5(4)
O(7)–C(33)–C(34)–F(6)	−10.9(5)	O(8)–C(33)–C(34)–F(4)	49.0(5)
O(8)–C(33)–C(34)–F(5)	−67.9(4)	O(8)–C(33)–C(34)–F(6)	169.7(4)

Table 22. Crystal data and structure refinement for **195**.

Identification code	mac134	
Chemical formula (moiety)	$C_{18}H_{16}F_3IO_5$	
Chemical formula (total)	$C_{18}H_{16}F_3IO_5$	
Formula weight	496.21	
Temperature	150(2) K	
Radiation, wavelength	MoKα, 0.71073 Å	
Crystal system, space group	triclinic, $P\bar{1}$	
Unit cell parameters	a = 13.1851(3) Å	α = 104.315(2)°
	b = 13.4508(3) Å	β = 103.687(2)°
	c = 22.7604(5) Å	γ = 94.474(2)°
Cell volume	3760.00(15) Å^3	
Z	8	
Calculated density	1.753 g/cm^3	
Absorption coefficient μ	1.758 mm^{-1}	
F(000)	1952	
Crystal colour and size	colourless, 0.30 × 0.20 × 0.20 mm^3	
Reflections for cell refinement	21891 (θ range 2.9 to 28.6°)	
Data collection method	Xcalibur, Atlas, Gemini ultra thick-slice ω scans	
θ range for data collection	2.9 to 28.6°	
Index ranges	h −15 to 17, k −15 to 17, l −30 to 27	
Completeness to θ = 25.0°	99.8 %	
Reflections collected	47991	
Independent reflections	16184 (R_{int} = 0.0354)	
Reflections with $F^2>2\sigma$	13220	
Absorption correction	semi-empirical from equivalents	
Min. and max. transmission	0.6205 and 0.7200	
Structure solution	direct methods	
Refinement method	Full-matrix least-squares on F^2	
Weighting parameters a, b	0.0201, 3.1903	
Data / restraints / parameters	16184 / 0 / 981	
Final R indices [$F^2>2\sigma$]	R1 = 0.0319, wR2 = 0.0602	
R indices (all data)	R1 = 0.0458, wR2 = 0.0667	
Goodness-of-fit on F^2	1.053	
Largest and mean shift/su	0.003 and 0.000	
Largest diff. peak and hole	1.08 and −0.76 e Å^{-3}	

Table 23. Atomic coordinates and equivalent isotropic displacement parameters ($Å^2$) for **195**. U_{eq} is defined as one third of the trace of the orthogonalized U^{ij} tensor.

	x	y	z	U_{eq}
I(1)	0.303045(16)	0.945440(15)	0.979191(8)	0.02082(5)
I(2)	0.223270(17)	0.569427(15)	0.897321(9)	0.02216(5)
I(3)	0.663237(16)	0.917159(15)	0.483554(9)	0.02203(5)
I(4)	0.679795(16)	0.578073(15)	0.506471(8)	0.02053(5)
O(1)	–0.08452(18)	1.21026(19)	0.90447(11)	0.0341(6)
O(2)	–0.08884(18)	1.08776(19)	0.95503(11)	0.0328(6)
O(3)	0.4865(2)	1.31764(19)	1.21454(11)	0.0371(6)
O(4)	0.10829(17)	0.27636(17)	1.07440(10)	0.0251(5)
O(5)	0.01511(19)	0.39370(19)	1.04178(11)	0.0346(6)
O(6)	–0.0591(2)	0.18331(18)	0.70333(10)	0.0381(6)
O(7)	0.3817(2)	0.7005(2)	1.00377(11)	0.0406(6)
O(8)	0.4366(2)	0.86452(18)	1.06209(10)	0.0325(6)
O(9)	0.2273(2)	0.8027(2)	0.86249(11)	0.0445(7)
O(10)	0.1451(2)	0.64862(19)	0.80232(10)	0.0435(7)
O(11)	1.01243(18)	1.34274(17)	0.60468(10)	0.0281(5)
O(12)	1.04473(19)	1.18263(19)	0.56385(11)	0.0343(6)
O(13)	0.6547(2)	0.99725(18)	0.22616(10)	0.0329(6)
O(14)	0.94608(18)	0.19796(17)	0.41335(10)	0.0278(5)
O(15)	1.01266(18)	0.36577(18)	0.45818(10)	0.0305(5)
O(16)	0.80409(19)	0.54078(19)	0.78021(9)	0.0309(5)
O(17)	0.6712(2)	0.94137(18)	0.60657(10)	0.0358(6)
O(18)	0.6441(3)	0.7692(2)	0.57461(11)	0.0523(8)
O(19)	0.5749(2)	0.71828(19)	0.41539(11)	0.0441(7)
O(20)	0.6157(2)	0.56175(19)	0.37671(10)	0.0343(6)
F(1)	0.45612(18)	0.63123(16)	1.10232(10)	0.0430(5)
F(2)	0.58011(16)	0.75816(18)	1.12790(10)	0.0459(6)
F(3)	0.44099(18)	0.77833(17)	1.16016(9)	0.0430(5)
F(4)	0.0477(2)	0.73758(19)	0.71752(10)	0.0578(7)
F(5)	0.21032(19)	0.78107(18)	0.72448(10)	0.0493(6)
F(6)	0.12616(18)	0.88669(16)	0.77441(10)	0.0455(6)
F(7)	0.7677(3)	0.8078(2)	0.70056(11)	0.0856(11)
F(8)	0.6040(3)	0.7895(2)	0.68915(11)	0.0856(10)
F(9)	0.6920(2)	0.93842(17)	0.72375(9)	0.0548(7)
F(10)	0.6438(2)	0.7076(2)	0.29608(10)	0.0620(7)
F(11)	0.4851(2)	0.72261(19)	0.29904(10)	0.0652(8)
F(12)	0.52481(18)	0.57538(15)	0.26079(8)	0.0421(5)
C(1)	–0.1993(3)	1.3347(3)	0.89668(17)	0.0357(9)
C(2)	–0.1791(3)	1.2429(3)	0.92134(18)	0.0357(9)
C(3)	–0.0459(3)	1.1339(2)	0.92634(14)	0.0249(7)
C(4)	0.0563(2)	1.1154(2)	0.91228(13)	0.0204(6)
C(5)	0.0961(3)	1.1632(3)	0.87347(14)	0.0251(7)
C(6)	0.1932(3)	1.1452(3)	0.86293(15)	0.0284(8)
C(7)	0.2516(3)	1.0817(3)	0.89205(14)	0.0260(7)

C(8)	0.2104(2)	1.0352(2)	0.93097(13)	0.0203(6)
C(9)	0.1135(2)	1.0508(2)	0.94170(13)	0.0214(7)
C(10)	0.3637(2)	1.0736(2)	1.05763(13)	0.0201(7)
C(11)	0.4503(3)	1.1381(2)	1.05811(14)	0.0237(7)
C(12)	0.4940(3)	1.2217(3)	1.11021(15)	0.0267(7)
C(13)	0.4481(3)	1.2398(3)	1.16037(14)	0.0267(7)
C(14)	0.3586(3)	1.1765(3)	1.15742(14)	0.0281(7)
C(15)	0.3160(3)	1.0914(3)	1.10634(14)	0.0264(7)
C(16)	0.5900(3)	1.3673(3)	1.2271(2)	0.0509(11)
C(17)	0.0705(3)	0.1801(3)	1.14327(17)	0.0379(9)
C(18)	0.0286(3)	0.2515(3)	1.10540(16)	0.0295(8)
C(19)	0.0917(3)	0.3494(2)	1.04481(14)	0.0228(7)
C(20)	0.1805(2)	0.3743(2)	1.01774(13)	0.0200(6)
C(21)	0.2745(3)	0.3348(2)	1.03022(14)	0.0247(7)
C(22)	0.3561(3)	0.3654(3)	1.00735(15)	0.0299(8)
C(23)	0.3441(3)	0.4344(3)	0.97055(14)	0.0262(7)
C(24)	0.2494(3)	0.4715(2)	0.95801(13)	0.0203(7)
C(25)	0.1666(3)	0.4430(2)	0.98069(13)	0.0219(7)
C(26)	0.1255(3)	0.4459(2)	0.82660(13)	0.0218(7)
C(27)	0.1697(3)	0.3728(2)	0.78997(14)	0.0260(7)
C(28)	0.1050(3)	0.2874(3)	0.74816(14)	0.0297(8)
C(29)	−0.0023(3)	0.2733(2)	0.74316(13)	0.0275(8)
C(30)	−0.0460(3)	0.3497(3)	0.77849(15)	0.0308(8)
C(31)	0.0187(3)	0.4363(3)	0.82042(14)	0.0279(7)
C(32)	−0.1639(3)	0.1590(3)	0.70656(17)	0.0468(10)
C(33)	0.4249(2)	0.7693(3)	1.05209(14)	0.0229(7)
C(34)	0.4756(3)	0.7341(3)	1.11122(15)	0.0277(7)
C(35)	0.1739(3)	0.7423(3)	0.81389(14)	0.0252(7)
C(36)	0.1384(3)	0.7871(3)	0.75724(15)	0.0288(8)
C(37)	1.1376(3)	1.4939(3)	0.65438(16)	0.0359(8)
C(38)	1.1230(3)	1.3841(3)	0.61641(15)	0.0299(8)
C(39)	0.9838(3)	1.2418(3)	0.57737(14)	0.0249(7)
C(40)	0.8691(2)	1.2102(2)	0.56603(13)	0.0213(7)
C(41)	0.8019(3)	1.2800(3)	0.58293(14)	0.0263(7)
C(42)	0.6964(3)	1.2465(3)	0.57249(16)	0.0308(8)
C(43)	0.6552(3)	1.1431(3)	0.54450(15)	0.0275(7)
C(44)	0.7236(2)	1.0748(2)	0.52774(13)	0.0201(6)
C(45)	0.8286(2)	1.1065(2)	0.53759(13)	0.0211(7)
C(46)	0.6577(3)	0.9387(2)	0.39466(13)	0.0213(7)
C(47)	0.5659(3)	0.9633(2)	0.36172(14)	0.0246(7)
C(48)	0.5616(3)	0.9828(2)	0.30425(14)	0.0249(7)
C(49)	0.6502(3)	0.9773(2)	0.28117(13)	0.0239(7)
C(50)	0.7414(3)	0.9517(2)	0.31466(14)	0.0246(7)
C(51)	0.7463(3)	0.9312(2)	0.37211(14)	0.0237(7)
C(52)	0.5726(3)	1.0473(3)	0.19793(16)	0.0423(10)
C(53)	1.0392(3)	0.0625(3)	0.37585(19)	0.0416(9)
C(54)	1.0512(3)	0.1740(3)	0.41179(16)	0.0323(8)
C(55)	0.9386(3)	0.2970(3)	0.43792(13)	0.0221(7)

C(56)	0.8279(2)	0.3129(2)	0.43775(13)	0.0198(6)
C(57)	0.7446(3)	0.2330(2)	0.41087(14)	0.0240(7)
C(58)	0.6430(3)	0.2508(3)	0.41150(15)	0.0297(8)
C(59)	0.6240(3)	0.3495(3)	0.43885(15)	0.0272(7)
C(60)	0.7079(2)	0.4282(2)	0.46451(13)	0.0195(6)
C(61)	0.8105(2)	0.4126(2)	0.46501(13)	0.0199(6)
C(62)	0.7220(3)	0.5602(2)	0.59811(13)	0.0212(7)
C(63)	0.6422(3)	0.5393(3)	0.62476(14)	0.0254(7)
C(64)	0.6670(3)	0.5322(3)	0.68614(14)	0.0276(8)
C(65)	0.7716(3)	0.5453(2)	0.71927(14)	0.0235(7)
C(66)	0.8522(3)	0.5650(3)	0.69192(14)	0.0263(7)
C(67)	0.8265(3)	0.5734(2)	0.63096(14)	0.0234(7)
C(68)	0.7236(3)	0.5180(3)	0.80893(15)	0.0356(9)
C(69)	0.6654(3)	0.8539(3)	0.61425(14)	0.0258(7)
C(70)	0.6853(3)	0.8488(3)	0.68257(15)	0.0335(8)
C(71)	0.5862(3)	0.6456(3)	0.37350(14)	0.0257(7)
C(72)	0.5590(3)	0.6630(3)	0.30707(15)	0.0311(8)

Table 24. Bond lengths [Å] and angles [°] for **195**.

I(1)–C(8)	2.099(3)	I(1)–C(10)	2.094(3)
I(2)–C(24)	2.123(3)	I(2)–C(26)	2.092(3)
I(3)–C(44)	2.108(3)	I(3)–C(46)	2.099(3)
I(4)–C(60)	2.108(3)	I(4)–C(62)	2.106(3)
O(1)–C(2)	1.457(4)	O(1)–C(3)	1.332(4)
O(2)–C(3)	1.206(4)	O(3)–C(13)	1.362(4)
O(3)–C(16)	1.404(5)	O(4)–C(18)	1.459(4)
O(4)–C(19)	1.325(4)	O(5)–C(19)	1.209(4)
O(6)–C(29)	1.357(4)	O(6)–C(32)	1.418(5)
O(7)–C(33)	1.228(4)	O(8)–C(33)	1.235(4)
O(9)–C(35)	1.216(4)	O(10)–C(35)	1.231(4)
O(11)–C(38)	1.457(4)	O(11)–C(39)	1.328(4)
O(12)–C(39)	1.212(4)	O(13)–C(49)	1.358(4)
O(13)–C(52)	1.427(4)	O(14)–C(54)	1.454(4)
O(14)–C(55)	1.333(4)	O(15)–C(55)	1.207(4)
O(16)–C(65)	1.370(3)	O(16)–C(68)	1.423(4)
O(17)–C(69)	1.231(4)	O(18)–C(69)	1.229(4)
O(19)–C(71)	1.231(4)	O(20)–C(71)	1.234(4)
F(1)–C(34)	1.342(4)	F(2)–C(34)	1.330(4)
F(3)–C(34)	1.326(4)	F(4)–C(36)	1.326(4)
F(5)–C(36)	1.334(4)	F(6)–C(36)	1.334(4)
F(7)–C(70)	1.283(4)	F(8)–C(70)	1.345(4)
F(9)–C(70)	1.313(4)	F(10)–C(72)	1.332(4)
F(11)–C(72)	1.318(4)	F(12)–C(72)	1.334(4)
C(1)–H(1A)	0.980	C(1)–H(1B)	0.980
C(1)–H(1C)	0.980	C(1)–C(2)	1.494(5)
C(2)–H(2A)	0.990	C(2)–H(2B)	0.990
C(3)–C(4)	1.482(4)	C(4)–C(5)	1.385(4)
C(4)–C(9)	1.387(4)	C(5)–H(5A)	0.950
C(5)–C(6)	1.385(4)	C(6)–H(6A)	0.950
C(6)–C(7)	1.379(4)	C(7)–H(7A)	0.950
C(7)–C(8)	1.386(4)	C(8)–C(9)	1.378(4)
C(9)–H(9A)	0.950	C(10)–C(11)	1.376(5)
C(10)–C(15)	1.380(4)	C(11)–H(11A)	0.950
C(11)–C(12)	1.385(5)	C(12)–H(12A)	0.950
C(12)–C(13)	1.393(4)	C(13)–C(14)	1.379(5)
C(14)–H(14A)	0.950	C(14)–C(15)	1.382(5)
C(15)–H(15A)	0.950	C(16)–H(16A)	0.980
C(16)–H(16B)	0.980	C(16)–H(16C)	0.980
C(17)–H(17A)	0.980	C(17)–H(17B)	0.980
C(17)–H(17C)	0.980	C(17)–C(18)	1.495(4)
C(18)–H(18A)	0.990	C(18)–H(18B)	0.990
C(19)–C(20)	1.497(4)	C(20)–C(21)	1.383(4)
C(20)–C(25)	1.392(4)	C(21)–H(21A)	0.950
C(21)–C(22)	1.378(5)	C(22)–H(22A)	0.950
C(22)–C(23)	1.391(4)	C(23)–H(23A)	0.950

C(23)–C(24)	1.374(4)	C(24)–C(25)	1.380(4)
C(25)–H(25A)	0.950	C(26)–C(27)	1.384(4)
C(26)–C(31)	1.374(5)	C(27)–H(27A)	0.950
C(27)–C(28)	1.369(5)	C(28)–H(28A)	0.950
C(28)–C(29)	1.387(5)	C(29)–C(30)	1.392(5)
C(30)–H(30A)	0.950	C(30)–C(31)	1.381(5)
C(31)–H(31A)	0.950	C(32)–H(32A)	0.980
C(32)–H(32B)	0.980	C(32)–H(32C)	0.980
C(33)–C(34)	1.556(4)	C(35)–C(36)	1.545(4)
C(37)–H(37A)	0.980	C(37)–H(37B)	0.980
C(37)–H(37C)	0.980	C(37)–C(38)	1.486(5)
C(38)–H(38A)	0.990	C(38)–H(38B)	0.990
C(39)–C(40)	1.482(4)	C(40)–C(41)	1.388(4)
C(40)–C(45)	1.388(4)	C(41)–H(41A)	0.950
C(41)–C(42)	1.374(5)	C(42)–H(42A)	0.950
C(42)–C(43)	1.384(5)	C(43)–H(43A)	0.950
C(43)–C(44)	1.387(4)	C(44)–C(45)	1.365(4)
C(45)–H(45A)	0.950	C(46)–C(47)	1.375(4)
C(46)–C(51)	1.384(4)	C(47)–H(47A)	0.950
C(47)–C(48)	1.385(4)	C(48)–H(48A)	0.950
C(48)–C(49)	1.389(5)	C(49)–C(50)	1.380(4)
C(50)–H(50A)	0.950	C(50)–C(51)	1.390(4)
C(51)–H(51A)	0.950	C(52)–H(52A)	0.980
C(52)–H(52B)	0.980	C(52)–H(52C)	0.980
C(53)–H(53A)	0.980	C(53)–H(53B)	0.980
C(53)–H(53C)	0.980	C(53)–C(54)	1.497(5)
C(54)–H(54A)	0.990	C(54)–H(54B)	0.990
C(55)–C(56)	1.491(4)	C(56)–C(57)	1.381(5)
C(56)–C(61)	1.393(4)	C(57)–H(57A)	0.950
C(57)–C(58)	1.382(5)	C(58)–H(58A)	0.950
C(58)–C(59)	1.388(5)	C(59)–H(59A)	0.950
C(59)–C(60)	1.376(5)	C(60)–C(61)	1.383(4)
C(61)–H(61A)	0.950	C(62)–C(63)	1.377(4)
C(62)–C(67)	1.378(4)	C(63)–H(63A)	0.950
C(63)–C(64)	1.387(4)	C(64)–H(64A)	0.950
C(64)–C(65)	1.380(5)	C(65)–C(66)	1.392(4)
C(66)–H(66A)	0.950	C(66)–C(67)	1.383(4)
C(67)–H(67A)	0.950	C(68)–H(68A)	0.980
C(68)–H(68B)	0.980	C(68)–H(68C)	0.980
C(69)–C(70)	1.534(4)	C(71)–C(72)	1.550(4)

C(8)–I(1)–C(10)	91.41(11)	C(24)–I(2)–C(26)	89.62(11)
C(44)–I(3)–C(46)	91.25(11)	C(60)–I(4)–C(62)	93.63(11)
C(2)–O(1)–C(3)	116.6(2)	C(13)–O(3)–C(16)	117.9(3)
C(18)–O(4)–C(19)	116.4(2)	C(29)–O(6)–C(32)	117.2(3)
C(38)–O(11)–C(39)	117.3(3)	C(49)–O(13)–C(52)	117.0(3)
C(54)–O(14)–C(55)	116.4(3)	C(65)–O(16)–C(68)	116.6(3)
H(1A)–C(1)–H(1B)	109.5	H(1A)–C(1)–H(1C)	109.5

H(1A)–C(1)–C(2)	109.5	H(1B)–C(1)–H(1C)	109.5
H(1B)–C(1)–C(2)	109.5	H(1C)–C(1)–C(2)	109.5
O(1)–C(2)–C(1)	105.8(3)	O(1)–C(2)–H(2A)	110.6
O(1)–C(2)–H(2B)	110.6	C(1)–C(2)–H(2A)	110.6
C(1)–C(2)–H(2B)	110.6	H(2A)–C(2)–H(2B)	108.7
O(1)–C(3)–O(2)	123.4(3)	O(1)–C(3)–C(4)	111.7(3)
O(2)–C(3)–C(4)	124.9(3)	C(3)–C(4)–C(5)	122.1(3)
C(3)–C(4)–C(9)	117.2(3)	C(5)–C(4)–C(9)	120.7(3)
C(4)–C(5)–H(5A)	120.1	C(4)–C(5)–C(6)	119.9(3)
H(5A)–C(5)–C(6)	120.1	C(5)–C(6)–H(6A)	119.8
C(5)–C(6)–C(7)	120.4(3)	H(6A)–C(6)–C(7)	119.8
C(6)–C(7)–H(7A)	120.7	C(6)–C(7)–C(8)	118.7(3)
H(7A)–C(7)–C(8)	120.7	I(1)–C(8)–C(7)	118.6(2)
I(1)–C(8)–C(9)	119.1(2)	C(7)–C(8)–C(9)	122.2(3)
C(4)–C(9)–C(8)	118.2(3)	C(4)–C(9)–H(9A)	120.9
C(8)–C(9)–H(9A)	120.9	I(1)–C(10)–C(11)	117.9(2)
I(1)–C(10)–C(15)	119.8(2)	C(11)–C(10)–C(15)	122.3(3)
C(10)–C(11)–H(11A)	120.4	C(10)–C(11)–C(12)	119.2(3)
H(11A)–C(11)–C(12)	120.4	C(11)–C(12)–H(12A)	120.3
C(11)–C(12)–C(13)	119.4(3)	H(12A)–C(12)–C(13)	120.3
O(3)–C(13)–C(12)	124.2(3)	O(3)–C(13)–C(14)	115.6(3)
C(12)–C(13)–C(14)	120.2(3)	C(13)–C(14)–H(14A)	119.6
C(13)–C(14)–C(15)	120.8(3)	H(14A)–C(14)–C(15)	119.6
C(10)–C(15)–C(14)	118.1(3)	C(10)–C(15)–H(15A)	120.9
C(14)–C(15)–H(15A)	120.9	O(3)–C(16)–H(16A)	109.5
O(3)–C(16)–H(16B)	109.5	O(3)–C(16)–H(16C)	109.5
H(16A)–C(16)–H(16B)	109.5	H(16A)–C(16)–H(16C)	109.5
H(16B)–C(16)–H(16C)	109.5	H(17A)–C(17)–H(17B)	109.5
H(17A)–C(17)–H(17C)	109.5	H(17A)–C(17)–C(18)	109.5
H(17B)–C(17)–H(17C)	109.5	H(17B)–C(17)–C(18)	109.5
H(17C)–C(17)–C(18)	109.5	O(4)–C(18)–C(17)	107.2(3)
O(4)–C(18)–H(18A)	110.3	O(4)–C(18)–H(18B)	110.3
C(17)–C(18)–H(18A)	110.3	C(17)–C(18)–H(18B)	110.3
H(18A)–C(18)–H(18B)	108.5	O(4)–C(19)–O(5)	123.8(3)
O(4)–C(19)–C(20)	112.7(3)	O(5)–C(19)–C(20)	123.5(3)
C(19)–C(20)–C(21)	122.5(3)	C(19)–C(20)–C(25)	117.2(3)
C(21)–C(20)–C(25)	120.2(3)	C(20)–C(21)–H(21A)	120.0
C(20)–C(21)–C(22)	120.1(3)	H(21A)–C(21)–C(22)	120.0
C(21)–C(22)–H(22A)	119.7	C(21)–C(22)–C(23)	120.6(3)
H(22A)–C(22)–C(23)	119.7	C(22)–C(23)–H(23A)	120.8
C(22)–C(23)–C(24)	118.3(3)	H(23A)–C(23)–C(24)	120.8
I(2)–C(24)–C(23)	119.9(2)	I(2)–C(24)–C(25)	117.5(2)
C(23)–C(24)–C(25)	122.5(3)	C(20)–C(25)–C(24)	118.3(3)
C(20)–C(25)–H(25A)	120.8	C(24)–C(25)–H(25A)	120.8
I(2)–C(26)–C(27)	119.8(2)	I(2)–C(26)–C(31)	118.5(2)
C(27)–C(26)–C(31)	121.6(3)	C(26)–C(27)–H(27A)	120.7
C(26)–C(27)–C(28)	118.7(3)	H(27A)–C(27)–C(28)	120.7
C(27)–C(28)–H(28A)	119.6	C(27)–C(28)–C(29)	120.9(3)

H(28A)–C(28)–C(29)	119.6	O(6)–C(29)–C(28)	116.8(3)
O(6)–C(29)–C(30)	123.6(3)	C(28)–C(29)–C(30)	119.6(3)
C(29)–C(30)–H(30A)	120.2	C(29)–C(30)–C(31)	119.6(3)
H(30A)–C(30)–C(31)	120.2	C(26)–C(31)–C(30)	119.4(3)
C(26)–C(31)–H(31A)	120.3	C(30)–C(31)–H(31A)	120.3
O(6)–C(32)–H(32A)	109.5	O(6)–C(32)–H(32B)	109.5
O(6)–C(32)–H(32C)	109.5	H(32A)–C(32)–H(32B)	109.5
H(32A)–C(32)–H(32C)	109.5	H(32B)–C(32)–H(32C)	109.5
O(7)–C(33)–O(8)	130.4(3)	O(7)–C(33)–C(34)	116.8(3)
O(8)–C(33)–C(34)	112.7(3)	F(1)–C(34)–F(2)	105.9(3)
F(1)–C(34)–F(3)	106.7(3)	F(1)–C(34)–C(33)	113.2(3)
F(2)–C(34)–F(3)	107.6(3)	F(2)–C(34)–C(33)	111.3(3)
F(3)–C(34)–C(33)	111.8(3)	O(9)–C(35)–O(10)	129.3(3)
O(9)–C(35)–C(36)	116.5(3)	O(10)–C(35)–C(36)	114.1(3)
F(4)–C(36)–F(5)	106.9(3)	F(4)–C(36)–F(6)	106.3(3)
F(4)–C(36)–C(35)	113.4(3)	F(5)–C(36)–F(6)	106.8(3)
F(5)–C(36)–C(35)	110.3(3)	F(6)–C(36)–C(35)	112.8(3)
H(37A)–C(37)–H(37B)	109.5	H(37A)–C(37)–H(37C)	109.5
H(37A)–C(37)–C(38)	109.5	H(37B)–C(37)–H(37C)	109.5
H(37B)–C(37)–C(38)	109.5	H(37C)–C(37)–C(38)	109.5
O(11)–C(38)–C(37)	106.9(3)	O(11)–C(38)–H(38A)	110.3
O(11)–C(38)–H(38B)	110.3	C(37)–C(38)–H(38A)	110.3
C(37)–C(38)–H(38B)	110.3	H(38A)–C(38)–H(38B)	108.6
O(11)–C(39)–O(12)	123.8(3)	O(11)–C(39)–C(40)	112.0(3)
O(12)–C(39)–C(40)	124.2(3)	C(39)–C(40)–C(41)	122.6(3)
C(39)–C(40)–C(45)	117.9(3)	C(41)–C(40)–C(45)	119.5(3)
C(40)–C(41)–H(41A)	119.8	C(40)–C(41)–C(42)	120.4(3)
H(41A)–C(41)–C(42)	119.8	C(41)–C(42)–H(42A)	119.6
C(41)–C(42)–C(43)	120.7(3)	H(42A)–C(42)–C(43)	119.6
C(42)–C(43)–H(43A)	121.0	C(42)–C(43)–C(44)	118.0(3)
H(43A)–C(43)–C(44)	121.0	I(3)–C(44)–C(43)	119.0(2)
I(3)–C(44)–C(45)	118.7(2)	C(43)–C(44)–C(45)	122.3(3)
C(40)–C(45)–C(44)	119.2(3)	C(40)–C(45)–H(45A)	120.4
C(44)–C(45)–H(45A)	120.4	I(3)–C(46)–C(47)	118.0(2)
I(3)–C(46)–C(51)	119.5(2)	C(47)–C(46)–C(51)	122.4(3)
C(46)–C(47)–H(47A)	120.4	C(46)–C(47)–C(48)	119.3(3)
H(47A)–C(47)–C(48)	120.4	C(47)–C(48)–H(48A)	120.3
C(47)–C(48)–C(49)	119.3(3)	H(48A)–C(48)–C(49)	120.3
O(13)–C(49)–C(48)	123.8(3)	O(13)–C(49)–C(50)	115.6(3)
C(48)–C(49)–C(50)	120.6(3)	C(49)–C(50)–H(50A)	119.7
C(49)–C(50)–C(51)	120.6(3)	H(50A)–C(50)–C(51)	119.7
C(46)–C(51)–C(50)	117.8(3)	C(46)–C(51)–H(51A)	121.1
C(50)–C(51)–H(51A)	121.1	O(13)–C(52)–H(52A)	109.5
O(13)–C(52)–H(52B)	109.5	O(13)–C(52)–H(52C)	109.5
H(52A)–C(52)–H(52B)	109.5	H(52A)–C(52)–H(52C)	109.5
H(52B)–C(52)–H(52C)	109.5	H(53A)–C(53)–H(53B)	109.5
H(53A)–C(53)–H(53C)	109.5	H(53A)–C(53)–C(54)	109.5
H(53B)–C(53)–H(53C)	109.5	H(53B)–C(53)–C(54)	109.5

H(53C)–C(53)–C(54)	109.5	O(14)–C(54)–C(53)	107.1(3)
O(14)–C(54)–H(54A)	110.3	O(14)–C(54)–H(54B)	110.3
C(53)–C(54)–H(54A)	110.3	C(53)–C(54)–H(54B)	110.3
H(54A)–C(54)–H(54B)	108.5	O(14)–C(55)–O(15)	124.0(3)
O(14)–C(55)–C(56)	112.1(3)	O(15)–C(55)–C(56)	123.9(3)
C(55)–C(56)–C(57)	121.9(3)	C(55)–C(56)–C(61)	117.5(3)
C(57)–C(56)–C(61)	120.6(3)	C(56)–C(57)–H(57A)	119.9
C(56)–C(57)–C(58)	120.3(3)	H(57A)–C(57)–C(58)	119.9
C(57)–C(58)–H(58A)	119.9	C(57)–C(58)–C(59)	120.1(3)
H(58A)–C(58)–C(59)	119.9	C(58)–C(59)–H(59A)	120.7
C(58)–C(59)–C(60)	118.6(3)	H(59A)–C(59)–C(60)	120.7
I(4)–C(60)–C(59)	118.8(2)	I(4)–C(60)–C(61)	118.5(2)
C(59)–C(60)–C(61)	122.6(3)	C(56)–C(61)–C(60)	117.8(3)
C(56)–C(61)–H(61A)	121.1	C(60)–C(61)–H(61A)	121.1
I(4)–C(62)–C(63)	118.0(2)	I(4)–C(62)–C(67)	120.6(2)
C(63)–C(62)–C(67)	121.4(3)	C(62)–C(63)–H(63A)	120.2
C(62)–C(63)–C(64)	119.6(3)	H(63A)–C(63)–C(64)	120.2
C(63)–C(64)–H(64A)	120.4	C(63)–C(64)–C(65)	119.3(3)
H(64A)–C(64)–C(65)	120.4	O(16)–C(65)–C(64)	123.7(3)
O(16)–C(65)–C(66)	115.3(3)	C(64)–C(65)–C(66)	121.0(3)
C(65)–C(66)–H(66A)	120.4	C(65)–C(66)–C(67)	119.2(3)
H(66A)–C(66)–C(67)	120.4	C(62)–C(67)–C(66)	119.5(3)
C(62)–C(67)–H(67A)	120.2	C(66)–C(67)–H(67A)	120.2
O(16)–C(68)–H(68A)	109.5	O(16)–C(68)–H(68B)	109.5
O(16)–C(68)–H(68C)	109.5	H(68A)–C(68)–H(68B)	109.5
H(68A)–C(68)–H(68C)	109.5	H(68B)–C(68)–H(68C)	109.5
O(17)–C(69)–O(18)	129.0(3)	O(17)–C(69)–C(70)	116.0(3)
O(18)–C(69)–C(70)	114.9(3)	F(7)–C(70)–F(8)	105.9(3)
F(7)–C(70)–F(9)	108.2(3)	F(7)–C(70)–C(69)	113.0(3)
F(8)–C(70)–F(9)	104.3(3)	F(8)–C(70)–C(69)	110.2(3)
F(9)–C(70)–C(69)	114.5(3)	O(19)–C(71)–O(20)	129.7(3)
O(19)–C(71)–C(72)	114.5(3)	O(20)–C(71)–C(72)	115.8(3)
F(10)–C(72)–F(11)	107.2(3)	F(10)–C(72)–F(12)	106.0(3)
F(10)–C(72)–C(71)	110.8(3)	F(11)–C(72)–F(12)	105.9(3)
F(11)–C(72)–C(71)	113.1(3)	F(12)–C(72)–C(71)	113.5(3)

Table 25. Anisotropic displacement parameters ($Å^2$) for **195**. The anisotropic displacement factor exponent takes the form: $-2\pi^2[h^2a^{*2}U^{11} + ...+ 2hka^*b^*U^{12}]$

	U^{11}	U^{22}	U^{33}	U^{23}	U^{13}	U^{12}
I(1)	0.02199(11)	0.02206(11)	0.02159(9)	0.00952(8)	0.00689(8)	0.00702(8)
I(2)	0.02844(12)	0.01948(11)	0.02015(9)	0.00785(8)	0.00743(9)	0.00192(9)
I(3)	0.02601(12)	0.01880(11)	0.02103(10)	0.00753(8)	0.00461(8)	0.00007(8)
I(4)	0.02634(12)	0.01635(11)	0.02099(9)	0.00636(8)	0.00856(8)	0.00418(8)
O(1)	0.0273(14)	0.0406(15)	0.0536(15)	0.0307(12)	0.0236(12)	0.0195(12)
O(2)	0.0289(14)	0.0377(15)	0.0460(14)	0.0259(12)	0.0201(12)	0.0106(11)
O(3)	0.0337(15)	0.0343(15)	0.0343(13)	−0.0011(11)	0.0034(11)	0.0038(12)
O(4)	0.0276(13)	0.0246(13)	0.0314(12)	0.0150(10)	0.0145(10)	0.0073(10)
O(5)	0.0270(14)	0.0429(16)	0.0480(14)	0.0281(12)	0.0171(12)	0.0150(12)
O(6)	0.0551(18)	0.0254(14)	0.0255(12)	−0.0013(10)	0.0063(12)	−0.0025(12)
O(7)	0.0446(17)	0.0363(15)	0.0297(12)	0.0012(11)	0.0005(12)	−0.0055(13)
O(8)	0.0447(16)	0.0243(14)	0.0288(12)	0.0107(10)	0.0057(11)	0.0084(11)
O(9)	0.0592(19)	0.0304(15)	0.0292(13)	0.0042(11)	−0.0089(13)	−0.0022(13)
O(10)	0.076(2)	0.0247(15)	0.0278(12)	0.0121(11)	0.0065(13)	0.0009(14)
O(11)	0.0226(13)	0.0245(13)	0.0330(12)	0.0054(10)	0.0052(10)	−0.0066(10)
O(12)	0.0261(14)	0.0309(14)	0.0451(14)	0.0080(11)	0.0105(11)	0.0035(11)
O(13)	0.0471(16)	0.0346(14)	0.0231(11)	0.0150(10)	0.0115(11)	0.0122(12)
O(14)	0.0251(13)	0.0229(13)	0.0355(12)	0.0057(10)	0.0090(10)	0.0079(10)
O(15)	0.0242(13)	0.0299(14)	0.0369(12)	0.0057(11)	0.0113(11)	0.0020(11)
O(16)	0.0325(14)	0.0407(15)	0.0201(11)	0.0116(10)	0.0037(10)	0.0077(11)
O(17)	0.0593(18)	0.0211(13)	0.0251(11)	0.0080(10)	0.0085(12)	−0.0025(12)
O(18)	0.106(3)	0.0248(15)	0.0294(13)	0.0069(11)	0.0226(15)	

	0.0197(16)					
O(19)	0.077(2)	0.0240(14)	0.0287(12)	0.0035(11)	0.0148(13)	
	0.0032(14)					
O(20)	0.0449(16)	0.0313(15)	0.0301(12)	0.0117(10)	0.0104(11)	
	0.0132(12)					
F(1)	0.0472(14)	0.0287(12)	0.0579(13)	0.0226(10)	0.0119(11)	
	0.0058(10)					
F(2)	0.0225(12)	0.0561(15)	0.0602(13)	0.0319(12)	−0.0021(10)	
	0.0015(10)					
F(3)	0.0573(15)	0.0518(14)	0.0265(10)	0.0166(10)	0.0156(10)	
	0.0129(12)					
F(4)	0.0516(16)	0.0547(16)	0.0532(13)	0.0304(12)	−0.0207(12)	
−0.0184(13)						
F(5)	0.0629(16)	0.0620(16)	0.0408(12)	0.0298(11)	0.0289(12)	
	0.0153(13)					
F(6)	0.0573(16)	0.0315(13)	0.0517(13)	0.0211(10)	0.0100(11)	
	0.0123(11)					
F(7)	0.111(3)	0.109(2)	0.0389(13)	0.0220(14)	0.0017(15)	0.075(2)
F(8)	0.112(3)	0.096(2)	0.0433(14)	0.0255(14)	0.0208(15)	
−0.0407(19)						
F(9)	0.096(2)	0.0410(14)	0.0263(10)	0.0032(10)	0.0189(12)	
	0.0160(13)					
F(10)	0.0749(19)	0.0677(17)	0.0398(12)	0.0196(12)	0.0162(12)	
−0.0301(14)						
F(11)	0.094(2)	0.0514(16)	0.0456(13)	0.0154(11)	−0.0011(13)	
	0.0357(15)					
F(12)	0.0644(16)	0.0287(12)	0.0238(9)	0.0024(8)	0.0025(10)	
−0.0043(11)						
C(1)	0.032(2)	0.032(2)	0.051(2)	0.0150(17)	0.0180(18)	
	0.0123(17)					
C(2)	0.027(2)	0.041(2)	0.054(2)	0.0269(18)	0.0205(18)	
	0.0165(17)					
C(3)	0.0273(19)	0.0211(18)	0.0300(16)	0.0109(14)	0.0093(15)	
	0.0061(14)					
C(4)	0.0197(17)	0.0215(17)	0.0198(14)	0.0058(12)	0.0043(13)	
	0.0038(13)					
C(5)	0.0235(18)	0.0291(19)	0.0261(16)	0.0144(14)	0.0050(14)	
	0.0071(14)					
C(6)	0.031(2)	0.036(2)	0.0285(16)	0.0195(15)	0.0154(15)	
	0.0076(16)					
C(7)	0.0222(18)	0.038(2)	0.0240(15)	0.0136(14)	0.0108(14)	
	0.0091(15)					
C(8)	0.0214(17)	0.0201(17)	0.0201(14)	0.0075(12)	0.0041(13)	
	0.0055(13)					
C(9)	0.0225(18)	0.0225(17)	0.0203(14)	0.0081(12)	0.0054(13)	
	0.0024(13)					
C(10)	0.0224(17)	0.0211(17)	0.0197(14)	0.0097(12)	0.0054(13)	
	0.0080(13)					

C(11)	0.0258(18)	0.0271(19)	0.0266(16)	0.0143(14)	0.0127(14)	0.0128(15)
C(12)	0.0190(18)	0.0273(19)	0.0369(18)	0.0151(15)	0.0064(15)	0.0050(14)
C(13)	0.0255(19)	0.0267(19)	0.0282(16)	0.0101(14)	0.0025(15)	0.0108(15)
C(14)	0.0281(19)	0.034(2)	0.0237(16)	0.0069(14)	0.0107(15)	0.0051(16)
C(15)	0.0232(18)	0.033(2)	0.0273(16)	0.0137(15)	0.0102(14)	0.0028(15)
C(16)	0.033(2)	0.042(3)	0.062(3)	−0.007(2)	0.004(2)	0.004(2)
C(17)	0.040(2)	0.038(2)	0.048(2)	0.0263(18)	0.0209(19)	0.0081(18)
C(18)	0.028(2)	0.036(2)	0.0344(18)	0.0173(15)	0.0179(16)	0.0053(16)
C(19)	0.0228(18)	0.0244(18)	0.0220(15)	0.0076(13)	0.0058(14)	0.0043(14)
C(20)	0.0244(18)	0.0187(17)	0.0162(13)	0.0032(12)	0.0059(13)	0.0023(13)
C(21)	0.0304(19)	0.0224(18)	0.0264(16)	0.0128(13)	0.0094(15)	0.0085(14)
C(22)	0.028(2)	0.033(2)	0.0364(18)	0.0158(15)	0.0128(16)	0.0129(16)
C(23)	0.0251(19)	0.030(2)	0.0268(16)	0.0117(14)	0.0090(14)	0.0049(15)
C(24)	0.0283(19)	0.0147(16)	0.0183(14)	0.0064(12)	0.0049(13)	0.0020(13)
C(25)	0.0247(18)	0.0216(17)	0.0200(14)	0.0066(12)	0.0057(13)	0.0039(14)
C(26)	0.0315(19)	0.0179(17)	0.0151(13)	0.0058(12)	0.0036(13)	0.0013(14)
C(27)	0.033(2)	0.0254(19)	0.0239(15)	0.0100(14)	0.0118(15)	0.0081(15)
C(28)	0.048(2)	0.0240(19)	0.0212(15)	0.0070(14)	0.0149(16)	0.0119(17)
C(29)	0.046(2)	0.0193(18)	0.0161(14)	0.0077(13)	0.0035(15)	0.0049(16)
C(30)	0.034(2)	0.028(2)	0.0292(17)	0.0080(15)	0.0053(16)	0.0034(16)
C(31)	0.034(2)	0.0212(18)	0.0273(16)	0.0048(14)	0.0063(15)	0.0067(15)
C(32)	0.059(3)	0.035(2)	0.036(2)	0.0006(17)	0.008(2)	−0.014(2)
C(33)	0.0177(17)	0.030(2)	0.0250(16)	0.0098(14)	0.0094(14)	0.0076(14)
C(34)	0.0239(19)	0.027(2)	0.0339(18)	0.0128(15)	0.0072(15)	0.0028(15)
C(35)	0.031(2)	0.026(2)	0.0243(16)	0.0110(14)	0.0122(15)	0.0089(15)

C(36)	0.033(2)	0.0244(19)	0.0299(17)	0.0120(14)	0.0055(16)	0.0001(15)
C(37)	0.035(2)	0.034(2)	0.0337(18)	0.0096(16)	0.0049(17)	−0.0074(17)
C(38)	0.0212(18)	0.034(2)	0.0291(17)	0.0065(15)	0.0017(15)	−0.0061(15)
C(39)	0.0263(19)	0.0267(19)	0.0215(15)	0.0113(14)	0.0027(14)	−0.0007(15)
C(40)	0.0225(18)	0.0210(17)	0.0222(15)	0.0115(13)	0.0039(13)	0.0010(13)
C(41)	0.033(2)	0.0176(17)	0.0284(16)	0.0071(13)	0.0081(15)	0.0012(15)
C(42)	0.028(2)	0.025(2)	0.0402(19)	0.0080(15)	0.0112(16)	0.0083(15)
C(43)	0.0225(18)	0.0267(19)	0.0341(17)	0.0102(15)	0.0076(15)	0.0022(15)
C(44)	0.0232(17)	0.0172(16)	0.0192(14)	0.0083(12)	0.0024(13)	−0.0013(13)
C(45)	0.0241(18)	0.0217(17)	0.0194(14)	0.0093(12)	0.0049(13)	0.0046(14)
C(46)	0.0269(18)	0.0157(16)	0.0214(14)	0.0072(12)	0.0048(14)	0.0026(13)
C(47)	0.0241(18)	0.0207(18)	0.0275(16)	0.0046(13)	0.0070(14)	0.0000(14)
C(48)	0.0246(19)	0.0236(18)	0.0243(15)	0.0076(13)	0.0003(14)	0.0060(14)
C(49)	0.034(2)	0.0151(17)	0.0207(15)	0.0044(12)	0.0036(14)	0.0035(14)
C(50)	0.0259(19)	0.0208(18)	0.0279(16)	0.0059(13)	0.0097(14)	0.0034(14)
C(51)	0.0227(18)	0.0211(18)	0.0249(15)	0.0061(13)	0.0015(14)	0.0035(14)
C(52)	0.067(3)	0.039(2)	0.0262(17)	0.0178(16)	0.0072(18)	0.022(2)
C(53)	0.034(2)	0.033(2)	0.060(2)	0.0106(19)	0.016(2)	0.0166(18)
C(54)	0.026(2)	0.035(2)	0.0401(19)	0.0110(16)	0.0131(16)	0.0137(16)
C(55)	0.0268(19)	0.0233(18)	0.0180(14)	0.0085(13)	0.0060(14)	0.0045(15)
C(56)	0.0243(18)	0.0198(17)	0.0186(14)	0.0087(12)	0.0071(13)	0.0072(13)
C(57)	0.0287(19)	0.0156(17)	0.0250(15)	0.0027(13)	0.0050(14)	0.0043(14)
C(58)	0.0260(19)	0.0192(18)	0.0389(18)	0.0030(14)	0.0052(16)	0.0008(15)
C(59)	0.0232(19)	0.0227(19)	0.0350(17)	0.0067(14)	0.0075(15)	0.0036(14)
C(60)	0.0250(18)	0.0153(16)	0.0178(14)	0.0041(12)	0.0049(13)	0.0041(13)

C(61)	0.0246(18)	0.0192(17)	0.0168(14)	0.0065(12)	0.0056(13)
	0.0024(13)				
C(62)	0.0308(19)	0.0173(17)	0.0168(14)	0.0061(12)	0.0072(14)
	0.0037(14)				
C(63)	0.0230(18)	0.0294(19)	0.0249(15)	0.0115(14)	0.0034(14)
	0.0070(15)				
C(64)	0.028(2)	0.033(2)	0.0295(17)	0.0149(15)	0.0140(15)
	0.0095(15)				
C(65)	0.031(2)	0.0190(17)	0.0220(15)	0.0078(13)	0.0067(14)
	0.0085(14)				
C(66)	0.0209(18)	0.0273(19)	0.0286(16)	0.0081(14)	0.0021(14)
	0.0029(14)				
C(67)	0.0214(18)	0.0193(17)	0.0271(16)	0.0040(13)	0.0051(14)
	0.0008(13)				
C(68)	0.044(2)	0.042(2)	0.0232(16)	0.0130(15)	0.0072(16)
	0.0081(18)				
C(69)	0.030(2)	0.027(2)	0.0243(16)	0.0093(14)	0.0109(15)
	0.0059(15)				
C(70)	0.047(2)	0.029(2)	0.0271(17)	0.0110(15)	0.0111(17)
	0.0075(18)				
C(71)	0.0265(19)	0.0237(19)	0.0237(16)	0.0051(14)	0.0048(14)
−0.0048(15)					
C(72)	0.040(2)	0.0211(19)	0.0275(17)	0.0051(14)	0.0041(16)
−0.0031(16)					

Table 26. Hydrogen coordinates and isotropic displacement parameters ($Å^2$) for **195**.

	x	y	z	U
H(1A)	−0.2563	1.3662	0.9117	0.054
H(1B)	−0.2199	1.3125	0.8506	0.054
H(1C)	−0.1351	1.3856	0.9115	0.054
H(2A)	−0.1677	1.2621	0.9675	0.043
H(2B)	−0.2396	1.1865	0.9020	0.043
H(5A)	0.0569	1.2083	0.8541	0.030
H(6A)	0.2196	1.1767	0.8355	0.034
H(7A)	0.3188	1.0702	0.8856	0.031
H(9A)	0.0866	1.0181	0.9685	0.026
H(11A)	0.4798	1.1255	1.0232	0.028
H(12A)	0.5547	1.2663	1.1117	0.032
H(14A)	0.3257	1.1916	1.1909	0.034
H(15A)	0.2557	1.0464	1.1048	0.032
H(16A)	0.6126	1.4111	1.2706	0.076
H(16B)	0.5925	1.4104	1.1983	0.076
H(16C)	0.6373	1.3151	1.2211	0.076
H(17A)	0.0169	0.1579	1.1625	0.057
H(17B)	0.1340	0.2164	1.1763	0.057
H(17C)	0.0881	0.1193	1.1158	0.057
H(18A)	−0.0383	0.2173	1.0737	0.035
H(18B)	0.0149	0.3154	1.1331	0.035
H(21A)	0.2829	0.2865	1.0546	0.030
H(22A)	0.4210	0.3391	1.0168	0.036
H(23A)	0.4000	0.4554	0.9545	0.031
H(25A)	0.1019	0.4697	0.9713	0.026
H(27A)	0.2433	0.3816	0.7938	0.031
H(28A)	0.1341	0.2371	0.7222	0.036
H(30A)	−0.1200	0.3423	0.7738	0.037
H(31A)	−0.0103	0.4889	0.8448	0.033
H(32A)	−0.1955	0.0913	0.6769	0.070
H(32B)	−0.2055	0.2123	0.6957	0.070
H(32C)	−0.1632	0.1565	0.7493	0.070
H(37A)	1.2101	1.5261	0.6608	0.054
H(37B)	1.1243	1.4963	0.6952	0.054
H(37C)	1.0882	1.5315	0.6322	0.054
H(38A)	1.1412	1.3802	0.5762	0.036
H(38B)	1.1690	1.3439	0.6396	0.036
H(41A)	0.8290	1.3513	0.6018	0.032
H(42A)	0.6513	1.2948	0.5846	0.037
H(43A)	0.5822	1.1196	0.5370	0.033
H(45A)	0.8735	1.0580	0.5251	0.025
H(47A)	0.5060	0.9669	0.3782	0.030
H(48A)	0.4988	0.9997	0.2809	0.030

H(50A)	0.8013	0.9481	0.2983	0.029
H(51A)	0.8084	0.9125	0.3951	0.028
H(52A)	0.5933	1.0737	0.1654	0.064
H(52B)	0.5604	1.1051	0.2301	0.064
H(52C)	0.5077	0.9975	0.1789	0.064
H(53A)	1.1091	0.0418	0.3767	0.062
H(53B)	0.9993	0.0531	0.3322	0.062
H(53C)	1.0013	0.0194	0.3951	0.062
H(54A)	1.0964	0.1857	0.4551	0.039
H(54B)	1.0842	0.2189	0.3908	0.039
H(57A)	0.7572	0.1655	0.3919	0.029
H(58A)	0.5861	0.1955	0.3932	0.036
H(59A)	0.5545	0.3623	0.4398	0.033
H(61A)	0.8673	0.4681	0.4834	0.024
H(63A)	0.5706	0.5298	0.6013	0.030
H(64A)	0.6126	0.5185	0.7052	0.033
H(66A)	0.9240	0.5726	0.7148	0.032
H(67A)	0.8806	0.5882	0.6119	0.028
H(68A)	0.7559	0.5149	0.8518	0.053
H(68B)	0.6813	0.4510	0.7844	0.053
H(68C)	0.6782	0.5723	0.8104	0.053

Table 27. Torsion angles [°] for **195**.

C(3)–O(1)–C(2)–C(1)	174.6(3)	C(2)–O(1)–C(3)–O(2)	5.0(5)
C(2)–O(1)–C(3)–C(4)	−173.6(3)	O(1)–C(3)–C(4)–C(5)	−8.3(4)
O(1)–C(3)–C(4)–C(9)	169.1(3)	O(2)–C(3)–C(4)–C(5)	173.0(3)
O(2)–C(3)–C(4)–C(9)	−9.5(5)	C(3)–C(4)–C(5)–C(6)	178.5(3)
C(9)–C(4)–C(5)–C(6)	1.1(5)	C(4)–C(5)–C(6)–C(7)	−1.5(5)
C(5)–C(6)–C(7)–C(8)	1.2(5)	C(6)–C(7)–C(8)–I(1)	−176.6(2)
C(6)–C(7)–C(8)–C(9)	−0.4(5)	C(10)–I(1)–C(8)–C(7)	92.4(3)
C(10)–I(1)–C(8)–C(9)	−84.0(3)	I(1)–C(8)–C(9)–C(4)	176.2(2)
C(7)–C(8)–C(9)–C(4)	0.0(5)	C(3)–C(4)–C(9)–C(8)	−177.9(3)
C(5)–C(4)–C(9)–C(8)	−0.3(5)	C(8)–I(1)–C(10)–C(11)	−85.9(2)
C(8)–I(1)–C(10)–C(15)	93.5(2)	I(1)–C(10)–C(11)–C(12)	−178.1(2)
C(15)–C(10)–C(11)–C(12)	2.5(5)	C(10)–C(11)–C(12)–C(13)	−1.3(4)
C(16)–O(3)–C(13)–C(12)	−15.3(5)	C(16)–O(3)–C(13)–C(14)	164.1(3)
C(11)–C(12)–C(13)–O(3)	177.9(3)	C(11)–C(12)–C(13)–C(14)	−1.6(5)
O(3)–C(13)–C(14)–C(15)	−176.2(3)	C(12)–C(13)–C(14)–C(15)	3.3(5)
I(1)–C(10)–C(15)–C(14)	179.8(2)	C(11)–C(10)–C(15)–C(14)	−0.9(5)
C(13)–C(14)–C(15)–C(10)	−2.0(5)	C(19)–O(4)–C(18)–C(17)	−171.7(3)
C(18)–O(4)–C(19)–O(5)	−1.1(5)	C(18)–O(4)–C(19)–C(20)	176.6(3)
O(4)–C(19)–C(20)–C(21)	−8.2(4)	O(4)–C(19)–C(20)–C(25)	174.2(3)
O(5)–C(19)–C(20)–C(21)	169.4(3)	O(5)–C(19)–C(20)–C(25)	−8.2(5)
C(19)–C(20)–C(21)–C(22)	−175.9(3)	C(25)–C(20)–C(21)–C(22)	1.7(5)
C(20)–C(21)–C(22)–C(23)	−1.3(5)	C(21)–C(22)–C(23)–C(24)	0.4(5)
C(22)–C(23)–C(24)–I(2)	−176.1(2)	C(22)–C(23)–C(24)–C(25)	0.2(5)
C(26)–I(2)–C(24)–C(23)	105.3(3)	C(26)–I(2)–C(24)–C(25)	−71.2(2)
I(2)–C(24)–C(25)–C(20)	176.5(2)	C(23)–C(24)–C(25)–C(20)	0.1(5)
C(19)–C(20)–C(25)–C(24)	176.6(3)	C(21)–C(20)–C(25)–C(24)	−1.1(5)
C(24)–I(2)–C(26)–C(27)	−81.8(2)	C(24)–I(2)–C(26)–C(31)	94.3(2)
I(2)–C(26)–C(27)–C(28)	173.8(2)	C(31)–C(26)–C(27)–C(28)	−2.2(4)
C(26)–C(27)–C(28)–C(29)	−1.0(4)	C(32)–O(6)–C(29)–C(28)	168.3(3)
C(32)–O(6)–C(29)–C(30)	−11.3(4)	C(27)–C(28)–C(29)–O(6)	−176.0(3)
C(27)–C(28)–C(29)–C(30)	3.7(4)	O(6)–C(29)–C(30)–C(31)	176.5(3)
C(28)–C(29)–C(30)–C(31)	−3.2(5)	I(2)–C(26)–C(31)–C(30)	−173.3(2)
C(27)–C(26)–C(31)–C(30)	2.7(5)	C(29)–C(30)–C(31)–C(26)	0.0(5)
O(7)–C(33)–C(34)–F(1)	−5.9(4)	O(7)–C(33)–C(34)–F(2)	113.3(3)
O(7)–C(33)–C(34)–F(3)	−126.5(3)	O(8)–C(33)–C(34)–F(1)	175.0(3)
O(8)–C(33)–C(34)–F(2)	−65.9(4)	O(8)–C(33)–C(34)–F(3)	54.4(4)
O(9)–C(35)–C(36)–F(4)	−151.0(3)	O(9)–C(35)–C(36)–F(5)	89.1(4)
O(9)–C(35)–C(36)–F(6)	−30.2(4)	O(10)–C(35)–C(36)–F(4)	30.5(4)
O(10)–C(35)–C(36)–F(5)	−89.4(4)	O(10)–C(35)–C(36)–F(6)	151.4(3)
C(39)–O(11)–C(38)–C(37)	−172.6(2)	C(38)–O(11)–C(39)–O(12)	2.6(4)
C(38)–O(11)–C(39)–C(40)	−178.0(2)	O(11)–C(39)–C(40)–C(41)	−0.4(4)
O(11)–C(39)–C(40)–C(45)	179.9(2)	O(12)–C(39)–C(40)–C(41)	179.1(3)
O(12)–C(39)–C(40)–C(45)	−0.6(4)	C(39)–C(40)–C(41)–C(42)	−178.7(3)
C(45)–C(40)–C(41)–C(42)	0.9(4)	C(40)–C(41)–C(42)–C(43)	−0.6(5)

C(41)–C(42)–C(43)–C(44)	0.3(5)	C(42)–C(43)–C(44)–I(3)	−178.9(2)
C(42)–C(43)–C(44)–C(45)	−0.4(4)	C(46)–I(3)–C(44)–C(43)	98.5(2)
C(46)–I(3)–C(44)–C(45)	−80.1(2)	I(3)–C(44)–C(45)–C(40)	179.31(19)
C(43)–C(44)–C(45)–C(40)	0.8(4)	C(39)–C(40)–C(45)–C(44)	178.7(2)
C(41)–C(40)–C(45)–C(44)	−1.1(4)	C(44)–I(3)–C(46)–C(47)	−91.5(3)
C(44)–I(3)–C(46)–C(51)	86.5(3)	I(3)–C(46)–C(47)–C(48)	177.0(2)
C(51)–C(46)–C(47)–C(48)	−1.0(5)	C(46)–C(47)–C(48)–C(49)	−0.1(5)
C(52)–O(13)–C(49)–C(48)	13.7(5)	C(52)–O(13)–C(49)–C(50)	−165.5(3)
C(47)–C(48)–C(49)–O(13)	−178.5(3)	C(47)–C(48)–C(49)–C(50)	0.7(5)
O(13)–C(49)–C(50)–C(51)	179.0(3)	C(48)–C(49)–C(50)–C(51)	−0.1(5)
I(3)–C(46)–C(51)–C(50)	−176.5(2)	C(47)–C(46)–C(51)–C(50)	1.5(5)
C(49)–C(50)–C(51)–C(46)	−0.9(5)	C(55)–O(14)–C(54)–C(53)	−173.4(3)
C(54)–O(14)–C(55)–O(15)	0.2(4)	C(54)–O(14)–C(55)–C(56)	−179.5(2)
O(14)–C(55)–C(56)–C(57)	−4.0(4)	O(14)–C(55)–C(56)–C(61)	177.0(2)
O(15)–C(55)–C(56)–C(57)	176.3(3)	O(15)–C(55)–C(56)–C(61)	−2.7(4)
C(55)–C(56)–C(57)–C(58)	−179.9(3)	C(61)–C(56)–C(57)–C(58)	−0.9(4)
C(56)–C(57)–C(58)–C(59)	0.4(5)	C(57)–C(58)–C(59)–C(60)	0.5(5)
C(58)–C(59)–C(60)–I(4)	−179.7(2)	C(58)–C(59)–C(60)–C(61)	−1.1(5)
C(62)–I(4)–C(60)–C(59)	97.5(2)	C(62)–I(4)–C(60)–C(61)	−81.2(2)
I(4)–C(60)–C(61)–C(56)	179.27(19)	C(59)–C(60)–C(61)–C(56)	0.6(4)
C(55)–C(56)–C(61)–C(60)	179.4(2)	C(57)–C(56)–C(61)–C(60)	0.4(4)
C(60)–I(4)–C(62)–C(63)	−101.9(3)	C(60)–I(4)–C(62)–C(67)	80.7(3)
I(4)–C(62)–C(63)–C(64)	−176.8(2)	C(67)–C(62)–C(63)–C(64)	0.6(5)
C(62)–C(63)–C(64)–C(65)	−0.6(5)	C(68)–O(16)–C(65)–C(64)	2.1(4)
C(68)–O(16)–C(65)–C(66)	−178.4(3)	C(63)–C(64)–C(65)–O(16)	179.3(3)
C(63)–C(64)–C(65)–C(66)	−0.3(5)	O(16)–C(65)–C(66)–C(67)	−178.4(3)
C(64)–C(65)–C(66)–C(67)	1.2(5)	I(4)–C(62)–C(67)–C(66)	177.7(2)
C(63)–C(62)–C(67)–C(66)	0.4(5)	C(65)–C(66)–C(67)–C(62)	−1.2(5)
O(17)–C(69)–C(70)–F(7)	−115.9(4)	O(17)–C(69)–C(70)–F(8)	125.9(4)
O(17)–C(69)–C(70)–F(9)	8.8(5)	O(18)–C(69)–C(70)–F(7)	65.3(5)
O(18)–C(69)–C(70)–F(8)	−53.0(4)	O(18)–C(69)–C(70)–F(9)	−170.1(3)
O(19)–C(71)–C(72)–F(10)	89.9(4)	O(19)–C(71)–C(72)–F(11)	−30.5(4)
O(19)–C(71)–C(72)–F(12)	−151.1(3)	O(20)–C(71)–C(72)–F(10)	−90.2(4)
O(20)–C(71)–C(72)–F(11)	149.5(3)	O(20)–C(71)–C(72)–F(12)	28.9(5)

Compound **196**

Table 1. Crystal data and structure refinement for **196**.

Identification code	mac140002
Chemical formula (moiety)	$C_{30}H_{24}F_6I_2O_8S_2 \cdot C_2H_3N$
Chemical formula (total)	$C_{32}H_{27}F_6I_2NO_8S_2$
Formula weight	985.46
Temperature	100(2) K
Radiation, wavelength	synchrotron, 0.6889 Å
Crystal system, space group	triclinic, $P\bar{1}$
Unit cell parameters	a = 12.228(2) Å α = 86.152(2)°
	b = 12.497(2) Å β = 74.917(2)°
	c = 13.466(3) Å γ = 64.079(2)°
Cell volume	1784.4(6) $Å^3$
Z	2
Calculated density	1.834 g/cm^3
Absorption coefficient μ	1.749 mm^{-1}
F(000)	964
Crystal colour and size	colourless, 0.300 × 0.010 × 0.010 mm^3
Reflections for cell refinement	9712 (θ range 2.4 to 29.3°)
Data collection method	Rigaku Saturn 724+ on kappa diffractometer wide-frame ω scans
θ range for data collection	1.5 to 27.3°
Index ranges	h −16 to 16, k −16 to 15, l −17 to 17
Completeness to θ = 24.4°	97.1 %
Reflections collected	18147
Independent reflections	8329 (R_{int} = 0.0432)
Reflections with $F^2>2\sigma$	6644
Absorption correction	multi-scan
Min. and max. transmission	0.60 and 0.98
Structure solution	direct methods
Refinement method	Full-matrix least-squares on F^2
Weighting parameters a, b	0.0943, 6.7894
Data / restraints / parameters	8329 / 255 / 516
Final R indices [$F^2>2\sigma$]	R1 = 0.0621, wR2 = 0.1706
R indices (all data)	R1 = 0.0743, wR2 = 0.1797
Goodness-of-fit on F^2	1.042
Largest and mean shift/su	0.002 and 0.000
Largest diff. peak and hole	3.02 and −1.95 e $Å^{-3}$

Table 2. Atomic coordinates and equivalent isotropic displacement parameters ($Å^2$) for **196**.
U_{eq} is defined as one third of the trace of the orthogonalized U^{ij} tensor.

	x	y	z	U_{eq}
I(1)	0.04069(3)	0.47596(3)	0.31908(3)	0.03258(13)
C(1)	−0.1407(6)	0.4875(5)	0.3620(4)	0.0368(12)
C(2)	−0.192(2)	0.453(3)	0.3001(17)	0.042(4)
C(3)	−0.320(2)	0.479(4)	0.348(2)	0.048(5)
C(4)	−0.357(2)	0.531(3)	0.445(2)	0.046(4)
S(1)	−0.2402(6)	0.5523(7)	0.4772(4)	0.0444(14)
C(2')	−0.2284(18)	0.544(2)	0.4475(14)	0.048(4)
C(3')	−0.3455(19)	0.542(3)	0.451(2)	0.054(4)
C(4')	−0.3339(17)	0.479(3)	0.3657(15)	0.044(4)
S(1')	−0.1882(5)	0.4296(5)	0.2803(4)	0.0447(12)
C(5)	−0.0172(5)	0.6342(5)	0.2388(4)	0.0315(11)
C(6)	−0.0375(6)	0.6316(5)	0.1427(5)	0.0330(12)
C(7)	−0.0830(6)	0.7392(5)	0.0952(4)	0.0328(12)
C(8)	−0.1070(6)	0.8442(5)	0.1439(5)	0.0367(13)
C(9)	−0.0831(7)	0.8435(6)	0.2393(5)	0.0409(14)
C(10)	−0.0374(6)	0.7369(5)	0.2887(5)	0.0364(13)
C(11)	−0.1019(6)	0.7362(5)	−0.0089(5)	0.0343(12)
C(12)	−0.1862(7)	0.8560(6)	−0.1403(5)	0.0430(14)
C(13)	−0.2449(9)	0.9848(8)	−0.1579(6)	0.063(2)
O(1)	−0.0676(5)	0.6476(4)	−0.0612(4)	0.0444(11)
O(2)	−0.1613(4)	0.8464(4)	−0.0395(3)	0.0372(9)
I(2)	0.47421(4)	0.21715(4)	0.25123(4)	0.04827(16)
C(14)	0.6511(6)	0.1923(6)	0.1647(6)	0.0516(18)
C(15)	0.6904(6)	0.1821(6)	0.0602(6)	0.0466(16)
C(16)	0.8196(8)	0.1576(7)	0.0261(9)	0.074(3)
C(17)	0.8720(8)	0.1493(7)	0.1054(9)	0.079(3)
S(2)	0.7661(3)	0.1744(2)	0.2217(3)	0.0818(8)
C(18)	0.5315(7)	0.0301(5)	0.2537(6)	0.0455(16)
C(19)	0.5433(6)	−0.0301(6)	0.1677(6)	0.0418(14)
C(20)	0.5850(6)	−0.1541(6)	0.1709(6)	0.0418(15)
C(21)	0.6117(7)	−0.2111(6)	0.2584(6)	0.0484(17)
C(22)	0.5996(10)	−0.1471(7)	0.3442(7)	0.069(3)
C(23)	0.5567(9)	−0.0234(7)	0.3419(6)	0.064(2)
C(24)	0.5974(6)	−0.2199(5)	0.0771(6)	0.0415(15)
C(25)	0.6746(7)	−0.4088(6)	−0.0056(6)	0.0485(16)
C(26)	0.7286(7)	−0.5368(6)	0.0254(6)	0.0492(16)
O(3)	0.5578(5)	−0.1722(4)	0.0041(4)	0.0521(12)
O(4)	0.6578(5)	−0.3368(4)	0.0829(4)	0.0441(11)
O(5)	0.2601(5)	0.4987(5)	0.2534(5)	0.0553(14)
O(6)	0.4591(6)	0.4395(5)	0.2554(7)	0.077(2)
C(27)	0.3539(6)	0.5132(6)	0.2510(6)	0.0409(14)

C(28)	0.3389(7)	0.6431(7)	0.2367(8)	0.057(2)
F(1)	0.3985(7)	0.6510(7)	0.1360(6)	0.108(2)
F(2)	0.2284(5)	0.7222(5)	0.2479(7)	0.100(2)
F(3)	0.3999(5)	0.6688(5)	0.2930(6)	0.0853(18)
O(7)	0.2559(7)	0.2168(7)	0.3471(8)	0.112(3)
O(8)	0.0663(6)	0.2861(6)	0.4467(5)	0.0672(17)
C(29)	0.1728(7)	0.2077(6)	0.4154(5)	0.0453(15)
C(30)	0.2027(11)	0.0918(10)	0.4595(7)	0.084(3)
F(4)	0.1103(7)	0.0768(5)	0.5262(5)	0.0900(19)
F(5)	0.2745(7)	−0.0039(5)	0.3962(5)	0.093(2)
F(6)	0.2844(8)	0.0796(9)	0.5212(6)	0.124(3)
N	1.013(3)	0.085(2)	0.345(3)	0.259(19)
C(31)	0.9191(15)	0.1472(16)	0.4012(14)	0.078(4)
C(32)	0.8255(12)	0.2156(13)	0.4997(12)	0.106(4)
N'	0.626(2)	0.209(2)	0.4525(17)	0.075(6)
C(31')	0.712(2)	0.213(2)	0.470(2)	0.074(6)

Table 3. Bond lengths [Å] and angles [°] for **196**.

I(1)–C(1)	2.083(6)	I(1)–C(5)	2.114(6)
I(1)–O(5)	2.731(5)	I(1)–O(8)	2.787(5)
C(1)–C(2)	1.355(16)	C(1)–S(1)	1.693(7)
C(1)–C(2')	1.335(15)	C(1)–S(1')	1.697(7)
C(2)–H(2)	0.950	C(2)–C(3)	1.423(19)
C(3)–H(3)	0.950	C(3)–C(4)	1.368(15)
C(4)–H(4)	0.950	C(4)–S(1)	1.721(16)
C(2')–H(2')	0.950	C(2')–C(3')	1.436(18)
C(3')–H(3')	0.950	C(3')–C(4')	1.372(15)
C(4')–H(4')	0.950	C(4')–S(1')	1.716(14)
C(5)–C(6)	1.385(8)	C(5)–C(10)	1.383(8)
C(6)–H(6)	0.950	C(6)–C(7)	1.393(8)
C(7)–C(8)	1.385(8)	C(7)–C(11)	1.484(8)
C(8)–H(8)	0.950	C(8)–C(9)	1.387(9)
C(9)–H(9)	0.950	C(9)–C(10)	1.397(9)
C(10)–H(10)	0.950	C(11)–O(1)	1.201(7)
C(11)–O(2)	1.342(7)	C(12)–H(12A)	0.990
C(12)–H(12B)	0.990	C(12)–C(13)	1.479(11)
C(12)–O(2)	1.453(8)	C(13)–H(13A)	0.980
C(13)–H(13B)	0.980	C(13)–H(13C)	0.980
I(2)–C(14)	2.070(7)	I(2)–C(18)	2.128(6)
I(2)–O(6)	2.707(6)	I(2)–O(7)	2.647(7)
C(14)–C(15)	1.358(10)	C(14)–S(2)	1.697(7)
C(15)–H(15)	0.950	C(15)–C(16)	1.420(10)
C(16)–H(16)	0.950	C(16)–C(17)	1.359(13)
C(17)–H(17)	0.950	C(17)–S(2)	1.698(10)
C(18)–C(19)	1.364(10)	C(18)–C(23)	1.363(11)
C(19)–H(19)	0.950	C(19)–C(20)	1.406(9)
C(20)–C(21)	1.373(10)	C(20)–C(24)	1.491(10)
C(21)–H(21)	0.950	C(21)–C(22)	1.388(12)
C(22)–H(22)	0.950	C(22)–C(23)	1.399(11)
C(23)–H(23)	0.950	C(24)–O(3)	1.214(9)
C(24)–O(4)	1.326(8)	C(25)–H(25A)	0.990
C(25)–H(25B)	0.990	C(25)–C(26)	1.517(9)
C(25)–O(4)	1.458(9)	C(26)–H(26A)	0.980
C(26)–H(26B)	0.980	C(26)–H(26C)	0.980
O(5)–C(27)	1.229(8)	O(6)–C(27)	1.226(9)
C(27)–C(28)	1.556(10)	C(28)–F(1)	1.382(11)
C(28)–F(2)	1.254(9)	C(28)–F(3)	1.330(9)
O(7)–C(29)	1.222(10)	O(8)–C(29)	1.220(9)
C(29)–C(30)	1.456(12)	C(30)–F(4)	1.325(13)
C(30)–F(5)	1.325(12)	C(30)–F(6)	1.412(14)
N–C(31)	1.16(2)	C(31)–C(32)	1.52(2)
C(32)–C(31')	1.55(2)	N'–C(31')	1.16(2)

C(1)–I(1)–C(5)	91.9(2)	C(1)–I(1)–O(5)	170.5(2)

C(1)–I(1)–O(8)	77.5(2)	C(5)–I(1)–O(5)	78.83(19)
C(5)–I(1)–O(8)	168.5(2)	O(5)–I(1)–O(8)	111.57(18)
I(1)–C(1)–C(2)	124.4(9)	I(1)–C(1)–S(1)	121.0(3)
I(1)–C(1)–C(2')	125.2(9)	I(1)–C(1)–S(1')	119.2(3)
C(2)–C(1)–S(1)	114.5(9)	C(2')–C(1)–S(1')	115.5(9)
C(1)–C(2)–H(2)	124.4	C(1)–C(2)–C(3)	111.2(15)
H(2)–C(2)–C(3)	124.4	C(2)–C(3)–H(3)	124.3
C(2)–C(3)–C(4)	111.5(18)	H(3)–C(3)–C(4)	124.3
C(3)–C(4)–H(4)	123.6	C(3)–C(4)–S(1)	112.9(16)
H(4)–C(4)–S(1)	123.6	C(1)–S(1)–C(4)	90.0(8)
C(1)–C(2')–H(2')	124.4	C(1)–C(2')–C(3')	111.1(14)
H(2')–C(2')–C(3')	124.4	C(2')–C(3')–H(3')	124.8
C(2')–C(3')–C(4')	110.4(16)	H(3')–C(3')–C(4')	124.8
C(3')–C(4')–H(4')	123.2	C(3')–C(4')–S(1')	113.7(13)
H(4')–C(4')–S(1')	123.2	C(1)–S(1')–C(4')	89.2(7)
I(1)–C(5)–C(6)	119.6(4)	I(1)–C(5)–C(10)	116.8(4)
C(6)–C(5)–C(10)	123.6(6)	C(5)–C(6)–H(6)	121.2
C(5)–C(6)–C(7)	117.7(5)	H(6)–C(6)–C(7)	121.2
C(6)–C(7)–C(8)	120.3(6)	C(6)–C(7)–C(11)	117.8(5)
C(8)–C(7)–C(11)	121.9(6)	C(7)–C(8)–H(8)	119.7
C(7)–C(8)–C(9)	120.6(6)	H(8)–C(8)–C(9)	119.7
C(8)–C(9)–H(9)	119.8	C(8)–C(9)–C(10)	120.4(6)
H(9)–C(9)–C(10)	119.8	C(5)–C(10)–C(9)	117.5(6)
C(5)–C(10)–H(10)	121.3	C(9)–C(10)–H(10)	121.3
C(7)–C(11)–O(1)	125.5(6)	C(7)–C(11)–O(2)	111.4(5)
O(1)–C(11)–O(2)	123.1(6)	H(12A)–C(12)–H(12B)	108.6
H(12A)–C(12)–C(13)	110.5	H(12A)–C(12)–O(2)	110.5
H(12B)–C(12)–C(13)	110.5	H(12B)–C(12)–O(2)	110.5
C(13)–C(12)–O(2)	106.4(6)	C(12)–C(13)–H(13A)	109.5
C(12)–C(13)–H(13B)	109.5	C(12)–C(13)–H(13C)	109.5
H(13A)–C(13)–H(13B)	109.5	H(13A)–C(13)–H(13C)	109.5
H(13B)–C(13)–H(13C)	109.5	C(11)–O(2)–C(12)	117.0(5)
C(14)–I(2)–C(18)	91.5(3)	C(14)–I(2)–O(6)	77.7(2)
C(14)–I(2)–O(7)	170.9(3)	C(18)–I(2)–O(6)	165.6(2)
C(18)–I(2)–O(7)	80.6(3)	O(6)–I(2)–O(7)	110.8(2)
I(2)–C(14)–C(15)	125.6(5)	I(2)–C(14)–S(2)	121.2(5)
C(15)–C(14)–S(2)	113.1(5)	C(14)–C(15)–H(15)	124.5
C(14)–C(15)–C(16)	110.9(8)	H(15)–C(15)–C(16)	124.5
C(15)–C(16)–H(16)	123.7	C(15)–C(16)–C(17)	112.5(9)
H(16)–C(16)–C(17)	123.7	C(16)–C(17)–H(17)	123.9
C(16)–C(17)–S(2)	112.2(7)	H(17)–C(17)–S(2)	123.9
C(14)–S(2)–C(17)	91.2(5)	I(2)–C(18)–C(19)	119.1(5)
I(2)–C(18)–C(23)	117.3(6)	C(19)–C(18)–C(23)	123.6(6)
C(18)–C(19)–H(19)	121.2	C(18)–C(19)–C(20)	117.7(7)
H(19)–C(19)–C(20)	121.2	C(19)–C(20)–C(21)	120.3(7)
C(19)–C(20)–C(24)	117.7(6)	C(21)–C(20)–C(24)	122.0(6)
C(20)–C(21)–H(21)	119.8	C(20)–C(21)–C(22)	120.4(6)
H(21)–C(21)–C(22)	119.8	C(21)–C(22)–H(22)	120.2

C(21)–C(22)–C(23)	119.5(8)	H(22)–C(22)–C(23)	120.2
C(18)–C(23)–C(22)	118.5(8)	C(18)–C(23)–H(23)	120.8
C(22)–C(23)–H(23)	120.8	C(20)–C(24)–O(3)	124.2(6)
C(20)–C(24)–O(4)	111.7(6)	O(3)–C(24)–O(4)	124.1(7)
H(25A)–C(25)–H(25B)	108.8	H(25A)–C(25)–C(26)	110.6
H(25A)–C(25)–O(4)	110.6	H(25B)–C(25)–C(26)	110.6
H(25B)–C(25)–O(4)	110.6	C(26)–C(25)–O(4)	105.6(6)
C(25)–C(26)–H(26A)	109.5	C(25)–C(26)–H(26B)	109.5
C(25)–C(26)–H(26C)	109.5	H(26A)–C(26)–H(26B)	109.5
H(26A)–C(26)–H(26C)	109.5	H(26B)–C(26)–H(26C)	109.5
C(24)–O(4)–C(25)	115.7(6)	I(1)–O(5)–C(27)	163.2(5)
I(2)–O(6)–C(27)	110.0(4)	O(5)–C(27)–O(6)	129.4(7)
O(5)–C(27)–C(28)	115.7(6)	O(6)–C(27)–C(28)	114.9(6)
C(27)–C(28)–F(1)	108.3(7)	C(27)–C(28)–F(2)	115.8(6)
C(27)–C(28)–F(3)	111.2(7)	F(1)–C(28)–F(2)	104.0(8)
F(1)–C(28)–F(3)	104.6(7)	F(2)–C(28)–F(3)	112.0(7)
I(2)–O(7)–C(29)	160.3(9)	I(1)–O(8)–C(29)	107.5(4)
O(7)–C(29)–O(8)	125.4(8)	O(7)–C(29)–C(30)	116.7(8)
O(8)–C(29)–C(30)	117.8(7)	C(29)–C(30)–F(4)	117.6(9)
C(29)–C(30)–F(5)	117.5(7)	C(29)–C(30)–F(6)	106.1(11)
F(4)–C(30)–F(5)	110.7(10)	F(4)–C(30)–F(6)	102.1(8)
F(5)–C(30)–F(6)	99.8(9)	N–C(31)–C(32)	160(3)
C(32)–C(31')–N'	177(2)		

Table 4. Torsion angles [°] for **196**.

I(1)–C(1)–C(2)–C(3)	−176(2)	S(1)–C(1)–C(2)–C(3)	0(3)
C(2')–C(1)–C(2)–C(3)	−4(3)	S(1')–C(1)–C(2)–C(3)	142(13)
C(1)–C(2)–C(3)–C(4)	−1(5)	C(2)–C(3)–C(4)–S(1)	1(5)
I(1)–C(1)–S(1)–C(4)	176.8(14)	C(2)–C(1)–S(1)–C(4)	1(2)
C(2')–C(1)–S(1)–C(4)	42(12)	S(1')–C(1)–S(1)–C(4)	−3.9(15)
C(3)–C(4)–S(1)–C(1)	−1(3)	I(1)–C(1)–C(2')–C(3')	176(2)
C(2)–C(1)–C(2')–C(3')	5(3)	S(1)–C(1)–C(2')–C(3')	−136(14)
S(1')–C(1)–C(2')–C(3')	1(3)	C(1)–C(2')–C(3')–C(4')	1(4)
C(2')–C(3')–C(4')–S(1')	−2(4)	I(1)–C(1)–S(1')–C(4')	−177.8(12)
C(2)–C(1)–S(1')–C(4')	−37(11)	S(1)–C(1)–S(1')–C(4')	2.9(13)
C(2')–C(1)–S(1')–C(4')	−1.8(19)	C(3')–C(4')–S(1')–C(1)	2(3)
I(1)–C(5)–C(6)–C(7)	176.1(4)	C(10)–C(5)–C(6)–C(7)	−1.3(9)
C(5)–C(6)–C(7)–C(8)	−0.2(8)	C(5)–C(6)–C(7)–C(11)	178.5(5)
C(6)–C(7)–C(8)–C(9)	1.6(9)	C(11)–C(7)–C(8)–C(9)	−177.1(6)
C(7)–C(8)–C(9)–C(10)	−1.6(10)	I(1)–C(5)–C(10)–C(9)	−176.2(5)
C(6)–C(5)–C(10)–C(9)	1.3(9)	C(8)–C(9)–C(10)–C(5)	0.2(9)
C(6)–C(7)–C(11)–O(1)	−9.3(9)	C(6)–C(7)–C(11)–O(2)	171.8(5)
C(8)–C(7)–C(11)–O(1)	169.4(6)	C(8)–C(7)–C(11)–O(2)	−9.5(8)
C(7)–C(11)–O(2)–C(12)	−179.7(5)	O(1)–C(11)–O(2)–C(12)	1.3(8)
C(13)–C(12)–O(2)–C(11)	−176.9(6)	I(2)–C(14)–C(15)–C(16)	−175.9(5)
S(2)–C(14)–C(15)–C(16)	0.6(8)	C(14)–C(15)–C(16)–C(17)	0.6(9)
C(15)–C(16)–C(17)–S(2)	−1.5(9)	C(16)–C(17)–S(2)–C(14)	1.5(7)
I(2)–C(14)–S(2)–C(17)	175.5(4)	C(15)–C(14)–S(2)–C(17)	−1.2(6)
I(2)–C(18)–C(19)–C(20)	178.1(5)	C(23)–C(18)–C(19)–C(20)	−0.6(11)
C(18)–C(19)–C(20)–C(21)	0.4(9)	C(18)–C(19)–C(20)–C(24)	179.8(6)
C(19)–C(20)–C(21)–C(22)	−1.0(11)	C(24)–C(20)–C(21)–C(22)	179.7(7)
C(20)–C(21)–C(22)–C(23)	1.8(13)	I(2)–C(18)–C(23)–C(22)	−177.4(7)
C(19)–C(18)–C(23)–C(22)	1.4(14)	C(21)–C(22)–C(23)–C(18)	−1.9(14)
C(19)–C(20)–C(24)–O(3)	−10.6(9)	C(19)–C(20)–C(24)–O(4)	168.9(5)
C(21)–C(20)–C(24)–O(3)	168.7(6)	C(21)–C(20)–C(24)–O(4)	−11.7(8)
C(20)–C(24)–O(4)–C(25)	−180.0(5)	O(3)–C(24)–O(4)–C(25)	−0.4(9)
C(26)–C(25)–O(4)–C(24)	−172.4(5)	I(2)–O(6)–C(27)–O(5)	6.3(11)
I(2)–O(6)–C(27)–C(28)	−171.5(5)	I(1)–O(5)–C(27)–O(6)	88.8(18)
I(1)–O(5)–C(27)–C(28)	−93.4(18)	O(5)–C(27)–C(28)–F(1)	−103.8(8)
O(5)–C(27)–C(28)–F(2)	12.5(12)	O(5)–C(27)–C(28)–F(3)	141.9(7)
O(6)–C(27)–C(28)–F(1)	74.4(9)	O(6)–C(27)–C(28)–F(2)	−169.4(9)
O(6)–C(27)–C(28)–F(3)	−40.0(10)	I(1)–O(8)–C(29)–O(7)	6.6(12)
I(1)–O(8)–C(29)–C(30)	−170.4(7)	I(2)–O(7)–C(29)–O(8)	121.9(18)
I(2)–O(7)–C(29)–C(30)	−61(2)	O(7)–C(29)–C(30)–F(4)	−173.4(10)
O(7)–C(29)–C(30)–F(5)	−37.2(16)	O(7)–C(29)–C(30)–F(6)	73.3(11)
O(8)–C(29)–C(30)–F(4)	3.9(14)	O(8)–C(29)–C(30)–F(5)	140.1(10)
O(8)–C(29)–C(30)–F(6)	−109.4(9)	N–C(31)–C(32)–C(31')	−151(5)

Table 5. Anisotropic displacement parameters (Å^2) for **196**. The anisotropic displacement factor exponent takes the form: $-2\pi^2[h^2a^{*2}U^{11} + ...+ 2hka^*b^*U^{12}]$

	U^{11}	U^{22}	U^{33}	U^{23}	U^{13}	U^{12}
I(1)	0.0296(2)	0.0268(2)	0.0421(2)	0.00477(14)	−0.00778(15)	−0.01414(17)
C(1)	0.032(3)	0.033(3)	0.048(3)	0.008(2)	−0.009(2)	−0.019(3)
C(2)	0.042(7)	0.032(10)	0.059(7)	0.011(5)	−0.018(5)	−0.020(6)
C(3)	0.042(7)	0.040(10)	0.066(8)	0.007(8)	−0.013(5)	−0.023(6)
C(4)	0.036(6)	0.039(9)	0.064(7)	0.010(6)	−0.010(5)	−0.021(6)
S(1)	0.035(2)	0.048(3)	0.046(3)	0.003(2)	−0.0005(18)	−0.021(2)
C(2')	0.042(6)	0.047(8)	0.057(7)	0.009(6)	−0.010(5)	−0.023(5)
C(3')	0.041(6)	0.057(10)	0.067(7)	0.003(6)	−0.007(5)	−0.026(6)
C(4')	0.040(6)	0.041(7)	0.060(7)	0.016(6)	−0.012(4)	−0.029(5)
S(1')	0.043(2)	0.041(3)	0.061(2)	0.0056(17)	−0.0146(16)	−0.0284(18)
C(5)	0.028(3)	0.023(3)	0.040(3)	0.002(2)	−0.004(2)	−0.011(2)
C(6)	0.034(3)	0.024(3)	0.044(3)	0.001(2)	−0.008(2)	−0.016(3)
C(7)	0.029(3)	0.030(3)	0.039(3)	0.002(2)	−0.004(2)	−0.016(3)
C(8)	0.037(3)	0.023(3)	0.045(3)	0.003(2)	−0.007(3)	−0.011(3)
C(9)	0.050(4)	0.025(3)	0.046(3)	−0.002(2)	−0.007(3)	−0.018(3)
C(10)	0.040(3)	0.028(3)	0.040(3)	−0.001(2)	−0.005(2)	−0.017(3)
C(11)	0.034(3)	0.027(3)	0.045(3)	0.004(2)	−0.008(2)	−0.018(3)
C(12)	0.044(4)	0.042(4)	0.044(3)	0.003(3)	−0.013(3)	−0.019(3)
C(13)	0.071(6)	0.058(5)	0.045(4)	0.005(3)	−0.016(4)	−0.015(5)
O(1)	0.058(3)	0.033(2)	0.046(2)	0.0010(18)	−0.015(2)	−0.022(2)
O(2)	0.038(2)	0.030(2)	0.043(2)	0.0073(17)	−0.0141(18)	−0.013(2)
I(2)	0.0433(3)	0.0247(2)	0.0674(3)	−0.00307(19)	−0.0062(2)	−0.0100(2)
C(14)	0.036(4)	0.028(3)	0.087(5)	0.001(3)	−0.009(4)	−0.014(3)
C(15)	0.035(3)	0.024(3)	0.078(5)	0.004(3)	−0.005(3)	−0.016(3)
C(16)	0.046(5)	0.035(4)	0.123(8)	0.009(5)	0.005(5)	−0.019(4)
C(17)	0.042(4)	0.033(4)	0.162(11)	0.011(5)	−0.016(6)	−0.023(4)
S(2)	0.0791(17)	0.0381(11)	0.149(3)	0.0051(13)	−0.0616(18)	−0.0260(12)
C(18)	0.043(4)	0.018(3)	0.063(4)	0.005(3)	−0.003(3)	−0.008(3)
C(19)	0.031(3)	0.023(3)	0.065(4)	0.006(3)	−0.003(3)	−0.011(3)
C(20)	0.030(3)	0.025(3)	0.065(4)	0.003(3)	−0.002(3)	−0.012(3)
C(21)	0.044(4)	0.025(3)	0.062(4)	0.008(3)	0.004(3)	−0.013(3)
C(22)	0.088(7)	0.038(4)	0.058(4)	0.012(3)	0.002(4)	−0.021(5)
C(23)	0.079(6)	0.035(4)	0.053(4)	−0.001(3)	0.000(4)	−0.012(4)
C(24)	0.028(3)	0.020(3)	0.072(4)	0.005(3)	−0.002(3)	−0.012(3)
C(25)	0.052(4)	0.026(3)	0.070(4)	0.005(3)	−0.021(4)	−0.016(3)

C(26)	0.049(4)	0.025(3)	0.069(4)	0.004(3)	−0.013(3)	−0.013(3)
O(3)	0.055(3)	0.030(3)	0.074(3)	0.006(2)	−0.020(3)	−0.020(2)
O(4)	0.045(3)	0.022(2)	0.062(3)	0.0033(19)	−0.011(2)	−0.014(2)
O(5)	0.034(3)	0.043(3)	0.093(4)	0.004(3)	−0.010(3)	−0.024(2)
O(6)	0.048(3)	0.038(3)	0.155(7)	−0.007(3)	−0.040(4)	−0.018(3)
C(27)	0.028(3)	0.031(3)	0.060(4)	−0.004(3)	−0.008(3)	−0.011(3)
C(28)	0.035(4)	0.042(4)	0.099(6)	−0.005(4)	−0.015(4)	−0.019(4)
F(1)	0.116(6)	0.112(6)	0.117(5)	0.048(4)	−0.026(4)	−0.075(5)
F(2)	0.061(3)	0.036(3)	0.210(8)	0.011(4)	−0.052(4)	−0.019(3)
F(3)	0.074(4)	0.048(3)	0.155(6)	−0.009(3)	−0.051(4)	−0.032(3)
O(7)	0.057(4)	0.068(5)	0.159(8)	0.028(5)	0.018(5)	−0.010(4)
O(8)	0.056(4)	0.055(4)	0.074(4)	0.026(3)	−0.004(3)	−0.019(3)
C(29)	0.049(4)	0.039(4)	0.041(3)	−0.005(3)	0.001(3)	−0.018(3)
C(30)	0.088(8)	0.071(7)	0.048(4)	0.016(4)	−0.004(5)	−0.004(6)
F(4)	0.134(6)	0.064(4)	0.074(3)	0.018(3)	−0.009(3)	−0.056(4)
F(5)	0.126(6)	0.050(3)	0.081(4)	−0.007(3)	−0.007(4)	−0.029(3)
F(6)	0.123(7)	0.134(7)	0.099(5)	0.001(5)	−0.044(5)	−0.032(5)
N	0.23(2)	0.102(13)	0.29(3)	0.020(13)	0.16(2)	−0.066(13)
C(31)	0.069(8)	0.089(10)	0.096(9)	0.030(7)	−0.027(6)	−0.052(8)
C(32)	0.094(7)	0.108(9)	0.122(8)	0.014(7)	−0.010(6)	−0.061(7)
N'	0.078(11)	0.067(13)	0.081(12)	0.019(10)	−0.007(9)	−0.042(10)
C(31')	0.075(10)	0.066(14)	0.079(13)	0.019(10)	−0.002(9)	−0.041(10)

Table 6. Hydrogen coordinates and isotropic displacement parameters ($Å^2$) for **196**.

	x	y	z	U
H(2)	−0.1484	0.4155	0.2332	0.051
H(3)	−0.3729	0.4628	0.3175	0.057
H(4)	−0.4388	0.5538	0.4896	0.055
H(2')	−0.2151	0.5818	0.4994	0.058
H(3')	−0.4204	0.5780	0.5045	0.065
H(4')	−0.4002	0.4649	0.3551	0.053
H(6)	−0.0209	0.5590	0.1102	0.040
H(8)	−0.1400	0.9174	0.1118	0.044
H(9)	−0.0979	0.9158	0.2712	0.049
H(10)	−0.0209	0.7351	0.3541	0.044
H(12A)	−0.2437	0.8202	−0.1419	0.052
H(12B)	−0.1069	0.8143	−0.1941	0.052
H(13A)	−0.2637	0.9960	−0.2253	0.094
H(13B)	−0.1870	1.0189	−0.1560	0.094
H(13C)	−0.3231	1.0248	−0.1039	0.094
H(15)	0.6385	0.1903	0.0159	0.056
H(16)	0.8644	0.1480	−0.0444	0.088
H(17)	0.9579	0.1315	0.0968	0.094
H(19)	0.5239	0.0104	0.1078	0.050
H(21)	0.6385	−0.2947	0.2603	0.058
H(22)	0.6204	−0.1870	0.4039	0.082
H(23)	0.5455	0.0222	0.4006	0.077
H(25A)	0.7332	−0.3975	−0.0669	0.058
H(25B)	0.5930	−0.3866	−0.0216	0.058
H(26A)	0.7423	−0.5900	−0.0314	0.074
H(26B)	0.6696	−0.5462	0.0864	0.074
H(26C)	0.8090	−0.5570	0.0414	0.074

6 Appendix III – Results tables from microfluidic radiofluorinations

Precursor Concentration (mg/mL)	Reaction Temperature (°C)	Precursor Volume (μL)	Isotope Volume (μL)	Pump 3 Rate (μL/min)	RCY (%)
10	190	10	10	10	65.62
10	190	10	10	10	76.42
10	190	10	10	10	79.34
10	190	10	10	15	77.93
10	190	10	10	15	79.39
10	190	10	10	15	80.21
10	190	10	10	20	82.66
10	190	10	10	20	82.16
10	190	10	10	20	83.11
10	190	10	10	25	81.2
10	190	10	10	25	80.11
10	190	10	10	25	78.48
10	190	10	10	30	82.36
10	190	10	10	30	74.88
10	190	10	10	30	73.12
10	190	10	10	10	43.74
10	190	10	10	10	34.24
10	190	10	10	10	43.24
10	170	10	10	10	34.44
10	170	10	10	10	33.6
10	170	10	10	10	32.5
10	150	10	10	10	16.77
10	150	10	10	10	14.31
10	150	10	10	10	15.33
10	130	10	10	10	3.58
10	130	10	10	10	2.83
10	130	10	10	10	2.83
10	110	10	10	10	3.02
10	110	10	10	10	0.94
10	110	10	10	10	0.59
10	190	20	20	30	87.82
10	190	20	20	30	82.3
10	190	20	20	30	86.16
10	190	30	20	30	81.78
10	190	30	20	30	80.1
10	190	30	20	30	78.73
10	190	10	20	30	86.29
10	190	10	20	30	85.79
10	190	10	20	30	85.67

Table 19: Results of radiosynthesis of 4-[^{18}F]acetophenone from nitroacetophenone using [^{18}F]KF/K222 as the RFA

Precursor Concentration (mg/mL)	Reaction Temperature (°C)	Precursor Volume (μL)	Isotope Volume (μL)	Pump 3 Rate (μL/min)	RCY (%)

10	190	10	10	10	28.71
10	190	10	10	10	23.04
10	190	10	10	10	27.9
10	190	10	10	15	35.73
10	190	10	10	15	49.2
10	190	10	10	15	70.58
10	190	10	10	20	5.75
10	190	10	10	20	33.9
10	190	10	10	20	0
10	190	10	10	25	25.14
10	190	10	10	25	25.28
10	190	10	10	25	35.94
10	190	10	10	30	37.38
10	190	10	10	30	37.38
10	190	10	10	30	0
10	190	10	10	15	9.74
10	190	10	10	15	8.88
10	190	10	10	15	7.79
10	170	10	10	15	0
10	170	10	10	15	0
10	170	10	10	15	0
10	150	10	10	15	0
10	150	10	10	15	0
10	150	10	10	15	0
10	130	10	10	15	0
10	130	10	10	15	0
10	130	10	10	15	0
10	190	5	10	15	70.89
10	190	5	10	15	68.67
10	190	5	10	15	73.69
10	190	10	10	15	54.72
10	190	10	10	15	61.96
10	190	10	10	15	65.09
10	190	15	10	15	80.43
10	190	15	10	15	72.1
10	190	15	10	15	85.69
10	190	20	10	15	74.74
10	190	20	10	15	69.05
10	190	20	10	15	73.15

Table 20: Results of radiosynthesis of 4-[^{18}F]acetophenone from fluoroacetophenone using [^{18}F]KF/K222 as the RFA

Precursor Concentration (mg/mL)	Reaction Temperature (°C)	Precursor Volume (μL)	Isotope Volume (μL)	Pump 3 Rate (μL/min)	RCY (%)
10	190	10	10	10	86.78
10	190	10	10	10	84.54
10	190	10	10	10	82.9
10	190	10	10	15	86.16
10	190	10	10	15	86.87
10	190	10	10	15	89.02
10	190	10	10	20	88.41
10	190	10	10	20	85.16
10	190	10	10	20	85.32
10	190	10	10	25	81.98
10	190	10	10	25	82
10	190	10	10	25	69.61
10	190	10	10	30	77.96
10	190	10	10	30	76.66
10	190	10	10	30	68.97
10	190	10	10	15	86.16
10	190	10	10	15	86.87
10	190	10	10	15	89.02
10	170	10	10	15	66.54
10	170	10	10	15	66.99
10	170	10	10	15	67.31
10	150	10	10	15	47.15
10	150	10	10	15	43.9
10	150	10	10	15	40.98
10	130	10	10	15	14.33
10	130	10	10	15	13.76
10	130	10	10	15	11.58
10	190	10	10	15	70.59
10	190	10	10	15	69.87
10	190	10	10	15	77.19
10	190	15	10	15	81.85
10	190	15	10	15	82.17
10	190	15	10	15	82.08
10	190	5	10	15	79.65
10	190	5	10	15	81.42
10	190	5	10	15	78.45

Table 21: Results of radiosynthesis of 4-[^{18}F]acetophenone from nitroacetophenone using [^{18}F]NEt_4.F as the RFA

Precursor Concentration (mg/mL)	Reaction Temperature (°C)	Precursor Volume (μL)	Isotope Volume (μL)	Pump 3 Rate (μL/min)	RCY (%)
10	190	10	10	10	44.12
10	190	10	10	10	37.99
10	190	10	10	10	49.73
10	190	10	10	15	20.58
10	190	10	10	15	36.51
10	190	10	10	15	31.01
10	190	10	10	20	8.6
10	190	10	10	20	10.8
10	190	10	10	20	17.73
10	190	10	10	25	20.41
10	190	10	10	25	36.27
10	190	10	10	25	32.41
10	190	10	10	30	20.21
10	190	10	10	30	21.21
10	190	10	10	30	28.95
10	190	10	10	15	82.25
10	190	10	10	15	83.56
10	190	10	10	15	65.93
10	170	10	10	15	41.04
10	170	10	10	15	36.99
10	170	10	10	15	31.94
10	150	10	10	15	22.22
10	150	10	10	15	15.02
10	150	10	10	15	14.33
10	130	10	10	15	5.92
10	130	10	10	15	5.06
10	130	10	10	15	3.29
10	190	5	10	10	5.9
10	190	5	10	10	6.98
10	190	5	10	10	6.49
10	190	10	10	10	44.12
10	190	10	10	10	37.99
10	190	10	10	10	49.73
10	190	15	10	10	39
10	190	15	10	10	57.73
10	190	15	10	10	60.47
10	190	20	10	10	55.87
10	190	20	10	10	60.79
10	190	20	10	10	59.38

Table 22: Results of radiosynthesis of 4-[^{18}F]acetophenone from fluoroacetophenone using [^{18}F]NEt_4.F as the RFA

Precursor Concentration (mg/mL)	Reaction Temperature (°C)	Precursor Volume (μL)	Isotope Volume (μL)	Pump 3 Rate (μL/min)	RCY (%)
10	190	10	10	10	53.79
10	190	10	10	10	61.44
10	190	10	10	10	60.59
10	190	10	10	15	59.13
10	190	10	10	15	59.59
10	190	10	10	15	58.24
10	190	10	10	20	56.7
10	190	10	10	20	53.58
10	190	10	10	20	47.45
10	190	10	10	25	40.85
10	190	10	10	25	36.95
10	190	10	10	25	34.34
10	190	10	10	30	31.51
10	190	10	10	30	31.25
10	190	10	10	30	30.13
10	190	10	10	15	59.13
10	190	10	10	15	59.59
10	190	10	10	15	58.24
10	170	10	10	15	25.66
10	170	10	10	15	23.33
10	170	10	10	15	22.44
10	150	10	10	15	14.52
10	150	10	10	15	12.97
10	150	10	10	15	10.36
10	130	10	10	15	3.84
10	130	10	10	15	3.36
10	130	10	10	15	2.96
10	190	5	10	10	18.11
10	190	5	10	10	17.16
10	190	5	10	10	15.15
10	190	10	10	10	24.33
10	190	10	10	10	25.74
10	190	10	10	10	27.51
10	190	15	10	10	31.82
10	190	15	10	10	31.98
10	190	15	10	10	19.78
10	190	20	10	10	21.69
10	190	20	10	10	21.1
10	190	20	10	10	24.06

Table 23: Results of radiosynthesis of ethyl 4-[^{18}F]fluorobenzoate from ethyl 4-nitrobenzoate using [^{18}F]KF/K222 as the RFA

Precursor Concentration (mg/mL)	Reaction Temperature (°C)	Precursor Volume (μL)	Isotope Volume (μL)	Pump 3 Rate (μL/min)	RCY (%)
10	190	10	10	10	69.46
10	190	10	10	10	69.47
10	190	10	10	10	69.22
10	190	10	10	15	67.45
10	190	10	10	15	65.47
10	190	10	10	15	64.28
10	190	10	10	20	67.49
10	190	10	10	20	70.81
10	190	10	10	20	66.44
10	190	10	10	25	65.32
10	190	10	10	25	64.99
10	190	10	10	25	66.13
10	190	10	10	30	63.65
10	190	10	10	30	62.98
10	190	10	10	30	60.3
10	190	10	10	20	67.49
10	190	10	10	20	70.81
10	190	10	10	20	66.44
10	170	10	10	20	56.43
10	170	10	10	20	56.15
10	170	10	10	20	55.15
10	150	10	10	20	32.18
10	150	10	10	20	29.2
10	150	10	10	20	26.33
10	130	10	10	20	9.67
10	130	10	10	20	9.7
10	130	10	10	20	7.36
10	190	5	10	10	61.39
10	190	5	10	10	60.53
10	190	5	10	10	55.41
10	190	10	10	10	70.05
10	190	10	10	10	75.99
10	190	10	10	10	69.57
10	190	15	10	10	66.59
10	190	15	10	10	60.49
10	190	15	10	10	62.94
10	190	20	10	10	64.08
10	190	20	10	10	65.62
10	190	20	10	10	65.95

Table 24: Results of radiosynthesis of ethyl 4-[^{18}F]fluorobenzoate from ethyl 4-nitrobenzoate using [^{18}F]NEt_4.F as the RFA

Precursor Concentration (mg/mL)	Reaction Temperature (°C)	Precursor Volume (μL)	Isotope Volume (μL)	Pump 3 Rate (μL/min)	RCY (%)
10	190	10	10	10	71.01
10	190	10	10	10	71.22
10	190	10	10	10	71.44
10	190	10	10	15	65.07
10	190	10	10	15	69.98
10	190	10	10	15	69.41
10	190	10	10	20	68.43
10	190	10	10	20	67.31
10	190	10	10	20	63.86
10	190	10	10	25	59.6
10	190	10	10	25	59.99
10	190	10	10	25	59.61
10	190	10	10	30	51.56
10	190	10	10	30	46.09
10	190	10	10	30	41.51
10	190	10	10	10	71.01
10	190	10	10	10	69.7
10	190	10	10	10	71.22
10	190	10	10	10	71.44
10	170	10	10	10	35.59
10	170	10	10	10	33.85
10	170	10	10	10	34.12
10	150	10	10	10	20.35
10	150	10	10	10	14.33
10	150	10	10	10	13.84
10	130	10	10	10	4.08
10	130	10	10	10	4.76
10	130	10	10	10	3.06
10	190	5	10	10	16.09
10	190	5	10	10	14.96
10	190	5	10	10	16.03
10	190	10	10	10	20.69
10	190	10	10	10	20.54
10	190	10	10	10	21.58
10	190	15	10	10	21.54
10	190	15	10	10	22.61
10	190	15	10	10	23.37
10	190	20	10	10	22.59
10	190	20	10	10	22.81
10	190	20	10	10	23.74

Table 25: Results of radiosynthesis of ethyl 4-[^{18}F]fluorobenzoate from ethyl 4-[^{19}F]fluorobenzoate using [^{18}F]KF/K222 as the RFA.

Precursor Concentration (mg/mL)	Reaction Temperature (°C)	Precursor Volume (μL)	Isotope Volume (μL)	Pump 3 Rate (μL/min)	RCY (%)
10	190	10	10	10	56.42
10	190	10	10	10	45.45
10	190	10	10	10	43.16
10	190	10	10	15	42.45
10	190	10	10	15	43.44
10	190	10	10	15	47.74
10	190	10	10	20	50.06
10	190	10	10	20	49.64
10	190	10	10	20	49.53
10	190	10	10	25	48.99
10	190	10	10	25	42.55
10	190	10	10	25	45.24
10	190	10	10	30	45.39
10	190	10	10	30	44.17
10	190	10	10	30	44.13
10	190	10	10	20	50.06
10	190	10	10	20	49.64
10	190	10	10	20	49.53
10	170	10	10	20	38.96
10	170	10	10	20	34.23
10	170	10	10	20	35.36
10	150	10	10	20	15.43
10	150	10	10	20	13.49
10	150	10	10	20	13.03
10	130	10	10	20	3.06
10	130	10	10	20	3.07
10	130	10	10	20	3.69
10	190	5	10	20	34.11
10	190	5	10	20	34.04
10	190	5	10	20	36.04
10	190	10	10	20	50.06
10	190	10	10	20	49.64
10	190	10	10	20	49.53
10	190	15	10	20	44.63
10	190	15	10	20	42.81
10	190	15	10	20	46.31
10	190	20	10	20	47.2
10	190	20	10	20	46.66
10	190	20	10	20	44.88

Table 26: Results of radiosynthesis of ethyl 4-[^{18}F]fluorobenzoate from ethyl 4-[^{19}F]fluorobenzoate using [^{18}F]NEt_4.F as the RFA.

Precursor Concentration (mg/mL)	Reaction Temperature (°C)	Precursor Volume (μL)	Isotope Volume (μL)	Pump 3 Rate (μL/min)	RCY (%)
5	190	10	10	10	32.93
5	190	10	10	10	27.81
5	190	10	10	10	14.43
5	190	10	10	15	9.34
5	190	10	10	15	16.94
5	190	10	10	15	8.99
5	190	10	10	20	11.29
5	190	10	10	20	25.99
5	190	10	10	20	16.95
5	190	10	10	25	11.68
5	190	10	10	25	20.55
5	190	10	10	25	32.82
5	190	10	10	30	22.12
5	190	10	10	30	26.71
5	190	10	10	30	24.42
5	190	10	10	30	24.42
5	190	10	10	30	22.12
5	190	10	10	30	26.71
5	170	10	10	30	15.17
5	170	10	10	30	10.42
5	170	10	10	30	10.95
5	150	10	10	30	14.08
5	150	10	10	30	5.66
5	150	10	10	30	5.12
5	130	10	10	30	2.99
5	130	10	10	30	9.64
5	130	10	10	30	2.06
5	190	5	10	25	5.98
5	190	5	10	25	5.96
5	190	5	10	25	6
5	190	10	10	25	5.79
5	190	10	10	25	5.58
5	190	10	10	25	5.32
5	190	15	10	25	2.88
5	190	15	10	25	1.9
5	190	15	10	25	7.47
5	190	20	10	25	7.03
5	190	20	10	25	2.05
5	190	20	10	25	1.82

Table 27: Results of radiosynthesis of ethyl 4-[^{18}F]fluorobenzoate from trifluoroacetyl(4-ethoxycarbonylphenyl, 4-anisyl)-λ^3-iodane using [^{18}F]KF/K222 as the RFA.

Precursor Concentration (mg/mL)	Reaction Temperature (°C)	Precursor Volume (μL)	Isotope Volume (μL)	Pump 3 Rate (μL/min)	RCY (%)
10	190	10	10	10	47.19
10	190	10	10	10	38.07
10	190	10	10	10	40.65
10	190	10	10	15	29.37
10	190	10	10	15	26.34
10	190	10	10	15	26.95
10	190	10	10	20	22.91
10	190	10	10	20	23.76
10	190	10	10	20	20.05
10	190	10	10	25	16.41
10	190	10	10	25	24.88
10	190	10	10	25	19.62
10	190	10	10	30	20.05
10	190	10	10	30	20.37
10	190	10	10	30	14.34
10	190	10	10	10	22.03
10	190	10	10	10	22.27
10	190	10	10	10	21.79
10	170	10	10	10	20.02
10	170	10	10	10	18.96
10	170	10	10	10	19.54
10	150	10	10	10	13.09
10	150	10	10	10	15.34
10	150	10	10	10	17.29
10	130	10	10	10	16.34
10	130	10	10	10	14.78
10	130	10	10	10	17.43
10	190	5	10	10	10.03
10	190	5	10	10	11.63
10	190	5	10	10	12.11
10	190	10	10	10	34.71
10	190	10	10	10	31.72
10	190	10	10	10	33.05
10	190	15	10	10	23.41
10	190	15	10	10	26.55
10	190	15	10	10	27.61
10	190	20	10	10	20.65
10	190	20	10	10	17.19
10	190	20	10	10	15.52

Table 28: Results of radiosynthesis of ethyl 4-[^{18}F]fluorobenzoate from trifluoroacetyl(4-ethoxycarbonylphenyl, 4-thienyl)-λ^3-iodane using [^{18}F]NEt_4.F as the RFA.

Compound	NTR	RCY (%)
191	phenyl	56.99
191	phenyl	58.72
191	phenyl	56.97
192	4-anisyl	71.83
192	4-anisyl	54.37
192	4-anisyl	68.56
193	2-thienyl	22.07
193	2-thienyl	26.45
193	2-thienyl	25.05
194	phenyl	25.23
194	phenyl	31.25
194	phenyl	29.5
195	4-anisyl	51.27
195	4-anisyl	52.17
195	4-anisyl	43.22
196	2-thienyl	25.73
196	2-thienyl	27.9
196	2-thienyl	24.83

Table 29: Results of the radiosynthesis of ethyl 4-[^{18}F]fluorobenzoate and ethyl 3-[^{18}F]fluorobenzoate from compounds **191–196**. Optimal reaction conditions achieved were applied (*i.e.* flow rate of 10 μL/min, temperature of 190 °C, RFA to precursor ratio of 1:1). Reaction conducted in dry DMF (10mg/mL).

Compound	NTR	RCY (%)
191	phenyl	55.64
191	phenyl	52.67
191	phenyl	51.74
192	4-anisyl	58.13
192	4-anisyl	56.84
192	4-anisyl	57.9
193	2-thienyl	28.81
193	2-thienyl	21.8
193	2-thienyl	21.83
194	phenyl	22.48
194	phenyl	22.54
194	phenyl	22.88
195	4-anisyl	26.33
195	4-anisyl	29.18
195	4-anisyl	29.58
196	2-thienyl	22.53
196	2-thienyl	17.87
196	2-thienyl	17.86

Table 30: Results of the radiosynthesis of ethyl 4-[^{18}F]fluorobenzoate and ethyl 3-[^{18}F]fluorobenzoate from compounds **191–196**. Optimal reaction conditions achieved were applied (i.e. flow rate of 10 μL/min, temperature of 190 °C, RFA to precursor ratio of 1:1). Reaction conducted in DMF and H_2O (5% H_2O).

7 Appendix IIII - Publication

"Evaluation of tetraethylammonium bicarbonate as a phase-transfer agent in the formation of [^{18}F]fluoroarenes."

Journal of Fluorine Chemistry 143 (2012) 231–237

Accepted 24 July 2012

http://dx.doi.org/10.1016/j.jfluchem.2012.07.015